Cranial Morphology, Taxonomy, and Systematics of Pachycephalosaurids (Dinosauria, Ornithischia)

By

Aaron David Dyer

A thesis submitted in partial fulfillment of the requirements for the degree of

Master of Science

In

Systematics and Evolution

Department of Biological Sciences

University of Alberta

Abstract

Pachycephalosauridae (pachcycephalosaurids) were small to medium sized bipedal ornithischians, known solely from the Late Cretaceous of North America and Asia. These dinosaurs are characterised by thick, often domed frontals and parietals (frontoparietal dome), which are thought to have been used in intraspecific head-butting combat rituals. The dome, along with their thickened skull bones have a high preservation potential, particularly compared to the rest of the skeleton. Thus, the vast majority of pachycephalosaurid fossils consist of their unique skull bones, and so much research on the group has focused on these elements. The morphology of the thickened skull roof is included in the diagnosis of every species, yet the skull roof changes dramatically through ontogeny, and numerous putative species have been reidentified as juvenile or subadult representatives of other species.

In this thesis, I focus on exploring morphological variation amongst pachycephalosaurid skulls, particularly the frontoparietal dome, and address its utility in pachycephalosaurid taxonomy and phylogenetics. I begin with describing the anatomy of the only known specimen of the controversial *Gravitholus albertae*, from the Late Cretaceous of Alberta, Canada. The specimen represents a heavily fused partial skull roof, and the degree of fusion has prevented a detailed description of the specimen, thus the validity of the species has been repeatedly justified and challenged. Alternative taxonomic hypotheses suggest *Gravitholus albertae* may be synonymous with *Hanssuesia sternbergi* or *Stegoceras validum*). I utilise synchrotron μCT imaging to identify the locations of the holotype's fused contacts, which facilitates a detailed description of the specimen. *Gravitholus albertae* was then included with *Hanssuesia sternbergi* and *Stegoceras validum* in morphometric analyses, to evaluate the distinctness of these three

species. There are no ontogenetic-independent features of *"Gravitholus albertae"* that would justify a unique species. Instead, *Gravitholus albertae* and *Hanssuesia sternbergi* are morphologically consistent with mature *Stegoceras validum*. Thus, *Gravitholus albertae* and *Hanssuesia sternbergi* are synonymous with *Stegoceras validum*. Interestingly, *Stegoceras validum* appears to possess adult dimorphism in the thickness of the frontonasal boss, which is not explained by previous taxonomic hypotheses. Instances of post-traumatic injuries, consistent with head-butting, appear restricted to individuals with thicker frontonasal bosses. The dimorphism in *Stegoceras validum* is interpreted as sexual dimorphism, with the thicker bossed sex engaging in ritualistic intraspecific combat.

I then move onto assessing morphological variation in pachycephalosaurid frontoparietals by statistically testing previously proposed discrete character states used in phylogenetic analyses, attempt to identify new characters and states, and comment on the validity of *Stegoceras novomexicanum*. The use of several features previously used as structures for phylogenetic characters are supported, and the distinction of their character stares are statistically demonstrated. These states are broadly consistent with previous taxonomic assessments, although a few species in each revised character are reassessed. There is no morphological support for "*Stegoceras novomexicanum*" and is regarded as Pachycephalosauridae indeteterminate. "*Stegoceras novomexicanum* ", along with other invalidated pachycephalosaurids, were removed from a phylogenetic analysis based on a revised morphological character matrix. This phylogenetic tree of Pachycephalosauria (pachycephalosaurians) is broadly similar to pervious analyses. The main differences include recovering *Colepiocephale lambei* as a basal Pachycephalosaurinae (pachycephalosaurines), and

a polyphyletic *Sphaerotholus*. Derived pachycephalosaurines appear to be united by a cranial dome that initially develops on the parietals (as opposed to initially developing on the frontals). This distinction deserves further investigation with histological and CT methodologies to determine the developmental pathways that different pachycephalosaurid species took to grow their domes.

Preface

This thesis is an original work by Aaron David Dyer. No part of this thesis has been previously published.

Dedication

"Another world, another time, in the Age of Wonder." – Jim Henson's The Dark Crystal, 1982

"For these bones the name *Stegoceras validus* is proposed with the hope that future discoveries may aid in a clearer understanding of their affinities." – Lawrence M. Lambe 1902

To my family, blood and bound, living and late. For their endless support of my passion.

Acknowledgements

Table of Contents

List of Tables

List of Figures

List of institutional abbreviations

AMNH American Museum of Natural History, New York City NY, USA

BMNH Natural History Museum, London, United Kingdom

CCM Carter County Museum, Ekalaka MT, USA

CMN Canadian Museum of Nature, Ottawa ON, Canada

DMNH Denver Museum of Natural History, Denver CO, USA

LACM Los Angeles County Museum, Los Angeles CA, USA

MPC Paleontological and Geological Center of the Mongolian Academy of Sciences, Ulaan Baatar, Mongolia

MPM Milwaukee Public Museum, Milwaukee WI, USA

NMMNH New Mexico Museum of Natural History and Science, Albuquerque NM, USA

ROM Royal Ontario Museum, Toronto ON, Canada

TCMI The Children's Museum of Indianapolis, Indianapolis IN, USA

TMP Royal Tyrrell Museum of Palaeontology, Drumheller AB, Canada

UALVP University of Alberta Laboratory of Vertebrate Palaeontology, Edmonton AB, Canada

UAM University of Alaska Museum, Fairbanks AK, USA

UCMP University of California Museum of Paleontology, Berkeley CA, USA

UCMZ(VP) University of Calgary Museum of Zoology (Vertebrate Palaeontology), Calgary AB, Canada

UWBM; University of Washington Burke Museum, Seattle WA, USA

YPM Yale Peabody Museum, New Haven CT, USA

Z. Pal Palaeozoological Institute, Warsaw, Poland

List of anatomical abbreviations

H:N/N – height at the nasal/nasal contact

H:N/Prf – height at the nasal/prefrontal contact

H:Pl/Pso – height at the palpebral/posterior supraorbital contact

H:Prf/Pl – height at the prefrontal/palpebral contact

H:Pso/Po – height at the posterior supraorbital/postorbital contact

L:F – length of the frontal along its ventral surface

L:FP – length of the frontoparietal along its ventral surface

L:P – length of the parietal along its ventral surface

L:Pl – length of the dorsal border of the frontal/palpebral contact

L:Po – length of the dorsal border of the frontal/parietal/postorbital contact

L:Prf – length of the dorsal border of the frontal/prefrontal contact

L:Pso – length of the dorsal border of the frontal/posterior supraorbital contact

T:F/P – frontoparietal thickness

W:F/P – width of the dorsal border of the frontal/parietal contact

W:N/Prf – width across the frontals along the dorsal border of the nasal/prefrontal contact;
W:Pl/Pso – width across the frontals along the dorsal border at the palpebral/posterior supraorbital contact

W:Prf/Pl – width across the frontals along the dorsal border of the prefrontal/palpebral contact

W:post – width across the parietals at the posterior exposure of the medial extension of the parietal

W:Po/stf/Sq – width across the parietals along the dorsal border of the postorbital/squamosal contact (or at posterior extent of postorbital is the supratemporal fenestra is present)

W:Pso/Po – width across the frontals along the dorsal border of the posterior supraorbital/
postorbital contact

Chapter 1. Introduction

Pachycephalosaurids were herbivorous bipedal ornithischian dinosaurs from the Upper Cretaceous sedimentary deposits of western North America and Asia (Maryańska et al., 2004). They were typically small to medium sized (< 40 kg) however, the largest known pachycephalosaurid (AMNH 1696, *Pachycephalosaurus wyomingensis*) may have approached 480 kg (Snively and Cox, 2008). The clade name refers to their thickened, often domed skull roofs. The dome (when present) is formed by thickening (pachyostosis *sensu* (Kaiser, 1960; Sues, 1978)) and fusion of the frontals and parietals – producing a structure often termed the frontoparietal dome. The frontoparietal dome has been explained by many functional hypotheses, including species recognition (Goodwin and Horner, 2004) and thermoregulation (Landry, 1995; Rigby et al., 1987). However, the most widely discussed hypothesis is intra-specific head-butting combat (Galton, 1971). Although several studies have disagreed with this interpretation (Carpenter, 1997; Goodwin and Horner, 2004), biomechanical (Snively and Cox, 2008; Snively and Theodor, 2011; Sues, 1978), histological (Dyer et al., 2021), and pathological (Peterson et al., 2013; Peterson and Vittore, 2012) lines of evidence support the head-butting functional hypothesis.

Pachycephalosaurid skeletal remains were subject to size-selective preservational biases, which act against the preservation of small-bodied terrestrial animals (Brown et al., 2013). Luckily, their robust cranial elements have a high preservation rate; globally, hundreds of isolated cranial elements are known (Evans et al., 2013). The morphology of the skull roof is included in every pachycephalosaurid species diagnosis, and these isolated cranial elements are often diagnostic at the species level. Thus, an anatomically limited, but abundant, quantity of material that is diagnostic to species is known. The high preservation rate of these diagnostic, thick cranial elements provides a rare glimpse at small-bodied dinosaur diversity patterns leading to the Cretaceous-Paleogene mass extinction (Evans et al., 2013).

Although diagnostic, pachycephalosaurid cranial morphology can exhibit high amounts of intraspecific variation. Several species have at times synonymised as possible sexual dimorphs (*Stegoceras brevis* with *Stegoceras validum*; (Brown and Schlaikjer, 1943; Chapman et al., 1981), intraspecific variants (*Stenotholus kohleri* with *Stygimoloch spinifer* (Goodwin et al.,

1998; Sullivan, 2003), or both (*Pachycephalosaurus* spp. with *Pachycephalosaurus wyomingensis*; Galton, 1971). Pachycephalosaurid taxonomy has been revised multiple times and stating the taxonomic results of previous analyses without a reference to following taxonomic can lead to confusion. For example, Williamson and Carr (2002) considered TMP1972.027.0001 (the holotype of *Gravitholus albertae*) to represent a mature individual of an indeterminate species of *Stegoceras*. Williamson and Carr (2002) accepted four distinct species of *Stegoceras*, however, all studies following Sullivan (2003) (except for Maryańska et al., 2004) recognise these four species as distinct genera. Thus, stating Williamson and Carr's (2002) taxonomic results regarding TMP1972.027.0001 is not informative without considering subsequent taxonomic revision. A history of pachycephalosaurid taxonomic revisions – including those concluded from the results of this thesis – is provided at the end of this chapter (Fig 1.1). It should be referred to whenever the taxonomic results of previous studies are referenced.

Ontogeny has been a major focus of pachycephalosaurid research (Evans et al., 2011; Goodwin and Evans, 2016; Goodwin and Horner, 2004; Horner and Goodwin, 2009; Schott et al., 2011; Schott and Evans, 2016, 2012; Woodruff et al., 2021). Goodwin et al. (1998) suggested that the frontoparietal dome may have grow from an initial flat-headed state. Inflation of the frontoparietal dome through ontogeny has now been demonstrated in several species (*Foraminacephale brevis* Schott and Evans 2016; *Pachycephalosaurus wyomingensis*, Horner and Goodwin 2009; *Sphaerotholus buchholtzae*, Woodruff et al. 2021; *Stegoceras validum*, Schott et al. 2011), a phenomenon that has been used to invalidate some flat-headed or "partially" domed species (Horner and Goodwin, 2009; Schott et al., 2011).

The past decade has seen several studies focusing on the taxonomy of, interspecific variation, and intraspecific variation amongst pachycephalosaurids of the Belly River Group from Alberta, Canada (Schott and Evans 2012, 2016; Schott et al. 2009; 2011). These studies do not address the validity of *Gravitholus albertae* (Wall and Galton, 1979), known solely from an incomplete pachycephalosaurid skull roof (TMP1972.027.0001; Sullivan 2003). Despite the holotype representing one of the most complete pachycephalosaurids from Alberta, it has never been described in detail. The cranial elements appear indistinguishably fused (Sullivan 2003), which has prevented rigorous description and testing of taxonomic hypotheses. In chapter 2, I

utilize synchrotron μCT images of TMP1972.027.0001 to identify the boundaries between the apparent fused cranial elements, review the original diagnosis of *Gravitholus albertae*, and test the morphological distinctness of TMP1972.027.0001 from *Hanssuesia sternbergi* and *Stegoceras validum* – species which other studies have suggested are similar to or synonymous with (Sullivan, 2003; Williamson and Carr, 2002).

In chapter 3, I explore the morphological variation of pachycephalosaurid frontoparietals, and their utility in constructing phylogenetic hypotheses of pachycephalosaurid interrelationships. I statistically test the distinctness of previously constructed character states, and revise state thresholds and taxon assignments when appropriate. I perform the most taxonomically diverse morphometric analyses of frontoparietal morphology compared to previous studies (Chapman et al., 1981; Evans et al., 2013; Mallon et al., 2015; Schott and Evans 2016; Williamson and Brusatte, 2016; Woodruff et al., 2021) to construct novel morphological characters, comment on the validity of *Stegoceras novomexicanum* (Jasinski and Sullivan, 2016, 2011), and critically revise the assessments of pachycephalosaurids across the phylogenetic morphological character matrix. Crucially, I accept recent taxonomic hypotheses, and do not incorporate several invalid species in the phylogenetic analysis.

1.1 Literature cited

Baird, D., 1979. The dome-headed dinosaur *Tylosteus ornatus* Leidy 1872 (Reptilia: Ornithischia: Pachycephalosauridae). Notulae Naturae 456, 1–11.

Bakker, R.T., Sullivan, R.M., Porter, V., Larson, P., Saulsbury, S.J., 2006. *Dracorex hogwartsia* n. gen., n. so., a spiked, flat-headed pachycphalosaurid dinosaur from the Upper Cretaceous Hell Creek Formation of South Dakota, in: Lucas, S.G., Sullivan, R.M. (Eds.), Late Cretaceous Vertebrates from the Western Interior. New Mexico Museum of Natural History and Science, Bulletin 35, Albuquerque, pp. 331–345.

Brown, B., Schlaikjer, E.M., 1943. A study of the troödont dinosaurs with the description of a new genus and four new species. Bulletin of the American Museum of Natural History, 82, 115–150.

Brown, C.M., Evans, D.C., Campione, N.E., O'Brien, L.J., Eberth, D.A., 2013. Evidence for taphonomic size bias in the Dinosaur Park Formation (Campanian, Alberta), a model Mesozoic terrestrial alluvial-paralic system. Palaeogeography, Palaeoclimatology, Palaeoecology, 372, 108–122. https://doi.org/10.1016/j.palaeo.2012.06.027

Carpenter, K., 1997. Agonistic behavior in pachycephalosaurs (Ornithischia: Dinosauria): a new look at head-butting behavior. Contributions to Geology, University of Wyoming, 32, 19–25. https://pubs.geoscienceworld.org/uwyo/rmg/article-pdf/32/1/19/2953518/19.pdf

Chapman, R.E., Galton, P.M., Sepkoski, J.J., Wall, W.P., 1981. A morphometric study of the cranium of the pachycephalosaurid dinosaur *Stegoceras*. Journal of Paleontology, 55, 608–618. https://www.jstor.org/stable/1304275?seq=1&cid=pdf-reference#references_tab_contents

Dyer, A.D., LeBlanc, A.R.H., Doschak, M.R., Currie, P.J., 2021. Taking a crack at the dome: histopathology of a pachycephalosaurid (Dinosauria: Ornithischia) frontoparietal dome. Biosis: Biological Systems, 2, 248–270. https://doi.org/10.37819/biosis.002.02.0101

Evans, D.C., Brown, C.M., Ryan, M.J., Tsogtbaatar, K., 2011. Cranial ornamentation and ontogenetic status of *Homalocephale calathocercos* (Ornithischia: Pachycephalosauria)

from the Nemegt Formation, Mongolia. Journal of Vertebrate Paleontology, 31, 84–92. https://doi.org/10.1080/02724634.2011.546287

Evans, D.C., Schott, R.K., Larson, D.W., Brown, C. M., Ryan, M. J., 2013. The oldest North American pachycephalosaurid and the hidden diversity of small-bodied ornithischian dinosaurs. Nature Communications, 4, 1–10. https://doi.org/10.1038/ncomms2749

Galton, P. M., 1971. A primitive dome-headed dinosaur (Ornithischia: Pachycephalosauridae) from the Lower Cretaceous of England and the function of the dome of pachycephalosaurids. Journal of Paleontology, 45, 40–47. https://www.jstor.org/stable/1302750

Galton, P.M., Sues, H.-D., 1983. New data on pachycephalosaurid dinosaurs (Reptilia: Ornithischia) from North America. Canadian Journal of Earth Sciences 20, 462–472.

Giffin, E.B., 1989a. Pachycephalosaur paleoneurology (Archosauria: Ornithischia). Journal of Vertebrate Paleontology 9, 67–77. https://doi.org/10.1080/02724634.1989.10011739

Gilmore, C.W., 1931. A new species of Troödont dinosaur from the Lance Formation of Wyoming. Proceedings of the U.S. National Museum 79, 1–6.

Gilmore, C.W., 1924. On *Troodon validus*: an orthopodous dinosaur from the Belly River Cretaceous of Alberta. University of Alberta Department of Geology Bulletin 1, 1–43.

Goodwin, M.B., Buchholtz, E.A., Johnson, R.E., 1998. Cranial anatomy and diagnosis of *Stygimoloch spinifer* (Ornithischia: Pachycephalosauria) with comments on cranial display structures in agonistic behavior. Journal of Vertebrate Paleontology, 18, 363–375. https://doi.org/10.1080/02724634.1998.10011064

Goodwin, M.B., Evans, D.C., 2016. The early expression of squamosal horns and parietal ornamentation confirmed by new end-stage juvenile *Pachycephalosaurus* fossils from the Upper Cretaceous Hell Creek Formation, Montana. Journal of Vertebrate Paleontology, 36, e1078343. https://doi.org/10.1080/02724634.2016.1078343

Goodwin, M.B., Horner, J.R., 2004. Cranial histology of pachycephalosaurs (Ornithischia: Marginocephalia) reveals transitory structures inconsistent with head-butting behavior.

Paleobiology, 30, 253–267. https://doi.org/10.1666/0094-8373(2004)030<0253:chopom>2.0.co;2

Horner, J.R., Goodwin, M.B., 2009. Extreme cranial ontogeny in the Upper Cretaceous dinosaur *Pachycephalosaurus*. PLoS ONE, 4, e7626. https://doi.org/10.1371/journal.pone.0007626

Jasinski, S.E., Sullivan, R.M., 2011. Re-evaluation of pachycephalosaurids from the Fruitland-Kirtland transition (Kirtlandian, Late Campanian), San Juan Basin, New Mexico, with a description of a new species of *Stegoceras* and a reassessment of *Texacephale langstoni*. In R.M. Sullvian, S.G. Lucas, J.A. Spielmann (Eds.), Fossil Record 3 (pp. 202–215). New Mexico Museum of Natural History and Science, Bulletin 53.

Jasinski, S.E., Sullivan, R.M., 2016. The validity of the Late Cretaceous pachycephalosaurid *Stegoceras novomexicanum* (Dinosauria: Pachycephalosauridae). In R.M. Sullivan S.G. Lucas (Eds.), Fossil Record 5 (pp. 107–115). New Mexico Museum of Natural History and Science, Bulletin 74. https://www.researchgate.net/publication/309902536

Kaiser, H.E., 1960. Untersuchungen zur vergleichenden Osteologie der fossilen und rezenten Pachyostosen. Palaeontographica Abteilung A, 114, 113–196.

Lambe, L.M., 1918. The Cretaceous genus *Stegoceras*, typifying a new family referred provisionally to the Stegosauria. Transactions of the Royal Society of Canada 12, 23–36.

Lambe, L.M., 1902. New genera and species from the Belly River series (Mid-Cretaceous). Geological survey of Canada Contributions to Canadian Palaeontology 3, 25–81.

Landry, S.O., 1995. *Stegoceras* not a head-butter. American Zoologist, 35, 60A.

Leidy, J., 1872. Remarks on some Extinct Vertebrates. Proceedings of the Academy of Natural Sciences of Philadelphia 24, 38–40.

Longrich, N.R., Sankey, J., Tanke, D., 2010. *Texacephale langstoni*, a new genus of pachycephalosaurid (Dinosauria: Ornithischia) from the upper Campanian Aguja Formation, southern Texas, USA. Cretaceous Research 31, 274–284. https://doi.org/10.1016/j.cretres.2009.12.002

Mallon, J.C., Evans, D.C., Tokaryk, T.T., Currie, M.L., 2015. First pachycephalosaurid (Dinosauria: Ornithischia) from the Frenchman Formation (upper Maastrichtian) of Saskatchewan, Canada. Cretaceous Research 56, 426–431. https://doi.org/10.1016/j.cretres.2015.06.005

Maryańska, T., 1990. Pachycephalosauria, in: Weishampel, D.B., Dodson, P., Osmólska, H. (Eds.), The Dinosauria. University of California Press, Berkley, pp. 564–577.

Maryańska, T., Chapman, R. E., Weishampel, D. B. (2004). Pachycephalosauria. In D. B. Weishampel, P. Dodson, H. Osmólska (Eds.), The Dinosauria. University of California Press, Berkley, pp. 464–477. http://ebookcentral.proquest.com/lib/ualberta/detail.action?docID=470900.

Peterson, J.E., Dischler, C., Longrich, N.R., 2013. Distributions of cranial pathologies provide evidence for head-butting in dome-headed dinosaurs (Pachycephalosauridae). PLoS ONE, 8, e68620. https://doi.org/10.1371/journal.pone.0068620

Peterson, J.E., Vittore, C.P., 2012. Cranial pathologies in a specimen of *Pachycephalosaurus*. PLoS ONE, 7, e36227. https://doi.org/10.1371/journal.pone.0036227

Rigby, J.K.Jr., Rice, A., Currie, P.J., 1987. Dinosaur thermoregulatory Cretaceous/Tertiary survival strategies. Geological Society of America Abstracts with Programs, 19, 820.

Ryan, M.J., Evans, D.C., 2005. Ornithischian dinosaurs, in: Currie, P.J., Koppelhus, E. (Eds.), Dinosaur Provincial Park: A Spectacular Ancient Ecosystem Revealed. Indiana University Press, Bloomington, pp. 313–348.

Schott, R.K., Evans, D.C., 2012. Squamosal ontogeny and variation in the pachycephalosaurian dinosaur *Stegoceras validum* Lambe, 1902, from the Dinosaur Park Formation, Alberta. Journal of Vertebrate Palaeontology, 32, 903–913.

Schott, R.K., Evans, D.C., 2016. Cranial variation and systematics of *Foraminacephale brevis* gen. nov. and the diversity of pachycephalosaurid dinosaurs (Ornithischia: Cerapoda) in the Belly River Group of Alberta, Canada. Zoological Journal of the Linnean Society, 179, 865–906. https://doi.org/10.1111/zoj.12465

Schott, R.K., Evans, D.C., Goodwin, M.B., Horner, J.R., Brown, C.M., Longrich, N.R., 2011. Cranial ontogeny in *Stegoceras validum* (Dinosauria: Pachycephalosauria): A quantitative model of pachycephalosaur dome growth and variation. PLoS ONE, 6, e21092. https://doi.org/10.1371/journal.pone.0021092

Schott, R.K., Evans, D.C., Williamson, T.E., Carr, T.D., Goodwin, M.B., 2009. The anatomy and systematics of *Colepiocephale lambei* (Dinosauria: Pachycephalosauridae). Journal of Vertebrate Paleontology 29, 771–786. https://doi.org/10.1671/039.029.0329

Snively, E., Cox, A., 2008. Structural mechanics of pachycephalosaur crania permitted head-butting behavior. Palaeontologia Electronica, 11, 1–17. http://palaeo-electronica.orghttp://palaeo-electronica.org/2008_1/140/index.html

Snively, E., Theodor, J.M., 2011. Common functional correlates of head-strike behavior in the pachycephalosaur *Stegoceras validum* (Ornithischia, Dinosauria) and combative artiodactyls. PLoS ONE, 6, e21422. https://doi.org/10.1371/journal.pone.0021422

Sternberg, C.M., 1945. Pachycephalosauridae proposed for dome-headed dinosaurs, *Stegoceras lambei* n. sp., described. Source: Journal of Paleontology 19, 534–538.

Sues, H.-D., (1978). Functional morphology of the dome in pachycephalosaurid dinosaurs. Neues Jahrbuch Für Geologie Und Paläontologie Monatshefte, 8, 489–472.

Sues, H.-D., Galton, P.M., 1987. Anatomy and classification of the North American Pachycephalosauria (Dinosauria: Ornithischia). Paleontographica Abteilung A 198, 1–40.

Sullivan, R.M., 2006. A taxonomic review of the Pachycephalosauridae (Dinosauria: Ornithischia), in: Lucas, S.G., Sullivan, R.M. (Eds.), Late Cretaceous Vertebrates from the Western Interior. New Mexico Museum of Natural History and Science, Bulletin 35, Albuquerque, pp. 347–365.

Sullivan, R.M., 2003. Revision of the dinosaur *Stegoceras* Lambe (Ornithischia, Pachycephalosauridae). Journal of Vertebrate Paleontology, 23, 181–207. https://doi.org/10.1671/0272-4634(2003)23[181:ROTDSL]2.0.CO;2

Sullivan, R.M., 2000. *Prenocephale edmontonensis* (Brown and Schlaikjer) new comb. and *P. brevis* (Lambe) new comb. (Dinosauria: Ornithischia: Pachycephalosauria) from the upper Cretaceous of North America, in: Lucas, S.G., Heckert, A.B. (Eds.), Dinosaurs of New Mexico. New Mexico Museum of Natural History and Science, Bulletin 17, Albuquerque, pp. 117–190.

Wall, W.P., Galton, P.M., 1979. Notes on pachycephalosaurid dinosaurs (Reptilia: Ornithischia) from North America, with comments on their status as ornithopods. Canadian Journal of Earth Sciences, 16, 1176–1186. https://doi.org/10.1139/e79-104

Watabe, M., Tsogtbaatar, K., Sullivan, R.M., 2011. A new pachycephalosaurid from the Baynshire Fromation (Cenomanian-Late Santonian), Gobi Desert, Mongolia, in: Sullivan, R.M., Lucas, S.G., Spielmann, J.A. (Eds.), Fossil Record 3. New Mexico Museum of Natural History and Science, Bulletin 53, Albuquerque, pp. 489–497.

Williamson, T.E., Brusatte, S.L., 2016. Pachycephalosaurs (Dinosauria: Ornithischia) from the Upper Cretaceous (upper Campanian) of New Mexico: A reassessment of *Stegoceras novomexicanum*. Cretaceous Research 62, 29–43. https://doi.org/10.1016/j.cretres.2016.01.012

Williamson, T.E., Carr, T.D., 2002. A new genus of derived pachycephalosaurian from western North America. Journal of Vertebrate Paleontology, 22, 779–801. https://doi.org/10.1671/0272-4634(2002)022[0779:ANGODP]2.0.CO;2

Woodruff, D.C., Goodwin, M.B., Lyson, T.R., Evans, D.C., 2021. Ontogeny and variation of the pachycephalosaurine dinosaur *Sphaerotholus buchholtzae*, and its systematics within the genus. Zoological Journal of the Linnean Society, 193, 563–601. https://academic.oup.com/zoolinnean/article/193/2/563/6125117

Table 1.1 History of pachycephalosaurid taxonomic revisions. Columns represent groups of specimens and their taxonomic assignments.

Reference													
Leidy 1872									*Tylosteus ornatus*				
Lambe 1902		*Stegoceras validus*											
Lambe 1918		*Stegoceras validus*	*Stegoceras brevis*										
Gilmore 1924		*Troodon validus*											
Gilmore 1931									*Troodon wyomingensis*				
Brown and Schlaikjer 1943	*Troodon validus*		*Troodon sternbergi*	*Troodon edmontonensis*					*Pachycephalosaurus wyomingensis*	*Pachycephalosaurus grangeri*	*Pachycephalosaurus reinheimeri*	*Pachycephalosaurus sp.*	
Sternberg 1945	*Stegoceras validus*	*Stegoceras brevis*	*Stegoceras lambei*	*Stegoceras sternbergi*	*Stegoceras edmontonensis*								
Baird 1979								*Pachycephalosaurus wyomingensis*					
Galton 1971	*Stegoceras validus*			*Stegoceras edmontonensis*									
Wall and Galton 1979	*Gravitholus albertae*	*Stegoceras browni*	*Stegoceras validus*	*Stegoceras brevis?*	*Stegoceras lambei?*	*Stegoceras sternbergi?*	*Stegoceras edmontonensis*	*Stegoceras sp.*	*Pachycephalosaurus wyomingensis*				
Chapman et al 1981	*Gravitholus albertae*	*Stegoceras browni*	*Stegoceras validus*	*Stegoceras edmontonensis*	*Stegoceras sp.*								

Galton and Sues 1983	Sues and Galton 1987	Giffin et al. 1988	Giffin 1989a	Maryańska 1990	Sullivan 2000	Williamson and Carr 2002	Sullivan 2003	Maryańska et al. 2004	Ryan and Evans (2005)	Bakker et al. 2006
				Pachycephalosaurus wyomingensis	Pachycephalosaurus wyomingensis	Pachycephalosaurus wyomingensis	Pachycephalosaurus wyomingensis	Pachycephalosaurus wyomingensis	Pachycephalosaurus wyomingensis	Pachycephalosaurus wyomingensis
Stygimoloch spinifer	Stygimoloch spinifer	Stenotholus kohleri	Stenotholus kohleri	Stygimoloch spinifer	Stygimoloch spinifer	Stygimoloch spinifer	Stygimoloch spinifer	Stygimoloch spinifer	Stygimoloch spinifer	Stygimoloch spinifer
										Dracorex hogwartsia
						Sphaerotholus goodwini	Prenocephale goodwini	Sphaerotholus goodwini		
	Stegoceras sp.					Sphaerotholus buchholtzae	Prenocephale edmontonensis	Sphaerotholus buchholtzae		
Stegoceras edmontonense	Stegoceras edmontonense			Stegoceras edmontonense	Prenocephale edmontonensis	Incertae sedis		Stegoceras edmontonense		
					Stegoceras sternbergi?	Stegoceras sternbergi	Hanssuesia sternbergi		Stegoceras sternbergi	
						Stegoceras breve			Stegoceras breve	
					Stegoceras lambei?	Stegoceras lambei	Colepiocephale lambei			
					Prenocephale brevis	Prenocephale brevis	Prenocephale brevis			
Stegoceras validus	Stegoceras validum			Stegoceras validum	Stegoceras validum	Stegoceras validum	Stegoceras validum	Stegoceras validum	Stegoceras validum	Stegoceras validum
Ornatotholus browni	Ornatotholus browni			Ornatotholus browni	Ornatotholus browni	Stegoceras validum?	Stegoceras validum	Ornatotholus browni	Stegoceras validum	Stegoceras validum
Gravitholus albertae	Gravitholus albertae			Gravitholus albertae	Gravitholus albertae?	Incertae sedis; Stegoceras validum?	Pachycephalosauridae indet.	Gravitholus albertae	Stegoceras sp. or Pachycephalosauridae indet.	Stegoceras validum

Study	Taxa (top to bottom)
Sullivan 2006	Dracorex hogwartsia; Stygimoloch spinifer; Pachycephalosaurus wyomingensis; Prenocephale goodwini; Prenocephale edmontonensis; Hanssuesia sternbergi; Colepiocephale lambei; Prenocephale brevis; Stegoceras validum; Pachycephalosauridae indet.
Horner and Goodwin 2009	Pachycephalosaurus wyomingensis
Schott et al. 2009	Stygimoloch spinifer; Pachycephalosaurus wyomingensis; Prenocephale goodwini; Prenocephale edmontonensis; Prenocephale brevis
Longrich et al. 2010	Dracorex hogwartsia; Stygimoloch spinifer; Pachycephalosaurus wyomingensis; Texacephale langstoni; Sphaerotholus goodwini; Sphaerotholus buchholtzae; Sphaerotholus edmontonensis; Sphaerotholus brevis; Gravitholus albertae
Jasinski and Sullivan 2011	Dracorex hogwartsia; Stygimoloch spinifer; Pachycephalosaurus wyomingensis; Prenocephale goodwini; Pachycephalosauridae indet; Stegoceras novomexicanum; Pachycephalosauridae indet.
Watabe et al 2011	Dracorex hogwartsia; Stygimoloch spinifer; Pachycephalosaurus wyomingensis; Prenocephale edmontonensis
Schott et al. 2011	Pachycephalosaurus wyomingensis
Evans et al. 2013	Stegoceras novomexicanum; Sphaerotholus buchholtzae; Sphaerotholus edmontonense; Colepiocephale lambei; Hanssuesia sternbergi; Prenocephale brevis; Stegoceras validum
Mallon et al. 2015	Pachycephalosaurus wyomingensis; Stegoceras novomexicanum; Sphaerotholus goodwini; Sphaerotholus buchholtzae
Williamson and Brusatte 2016	Pachycephalosaurus wyomingensis; Pachycephalosauridae indet; Sphaerotholus buchholtzae

Jasinski and Sullivan 2016	Schott and Evans 2016	Goodwin and Evans 2016	Woodruff et al 2021	Dyer (This Thesis)
	Pachycephalosaurus wyomingensis?	*Pachycephalosaurus wyomingensis*	*Dracorex hogwartsia*	*Pachycephalosaurus wyomingensis*
			Stygimoloch spinifer	
			Pachycephalosaurus wyomingensis	
Stegoceras novomexicanum		*Stegoceras novomexicanum*	*Stegoceras novomexicanum*	Pachycephalosauridae indet
				Pachycephalosauridae indet
Sphaerotholus goodwini	*Sphaerotholus goodwini*		*Sphaerotholus goodwini*	*Sphaerotholus goodwini*
Sphaerotholus buchholtzae	*Sphaerotholus buchholtzae*		*Sphaerotholus buchholtzae*	*"Sphaerotholus" buchholtzae*
			Sphaerotholus edmontonensis	*"Sphaerotholus" edmontonensis*
Hanssuesia sternbergi	*Hanssuesia sternbergi*		*Hanssuesia sternbergi*	*Stegoceras validum*
Colepiocephale lambei	*Colepiocephale lambei*		*Colepiocephale lambei*	*Colepiocephale lambei*
	Foraminacephale brevis		*Foraminacephale brevis*	*Foraminacephale brevis*
Stegoceras validum	*Stegoceras validum*		*Stegoceras validum*	*Stegoceras validum*

13

Chapter 2. Anatomy and taxonomic validity of the pachycephalosaurid *Gravitholus albertae* from the Belly River Group (Campanian) of Alberta, Canada

2.1 Introduction

Wall and Galton (1979) named and described the pachycephalosaurid *Gravitholus albertae* based on TMP 1972.027.0001, which they described as a frontoparietal. Their diagnosis included a dome larger and wider than any known specimen of *Stegoceras* (which then included what would become *Colepiocephale lambei,* Sullivan, 2003; *Foraminacephale brevis,* Schott and Evans, 2016; *Hanssuesia sternbergi,* Sullivan 2003; and *Sphaerotholus edmontonensis,* Woodruff et al., 2021), a large depression and pits on the parietal, a relatively small braincase, and absence of node-like ornamentation. Wall and Galton (1979) incompletely described the type locality and horizon of *Gravitholus albertae*. They reported TMP1972.027.0001 was donated to the then Provincial Museum of Alberta by Mr. Ted Malach, that it was collected from the Oldman Formation (prior to the recognition of the Dinosaur Park Formation; Eberth and Hamblin, 1993) near Jenner Ferry in Alberta, Canada, and reported latitude and longitude coordinates. However, those coordinates are 43 km south of the modern Jenner Bridge. Sullivan (2003) reported a personal communication from Dr. David Eberth (TMP) confirming TMP1972.027.0001 came from the Oldman Formation; however, Dr. Eberth has since forgotten where the type locality is (pers. comm., 2019).

The validity of *Gravitholus albertae* was supported in subsequent publications (e.g., Sues and Galton, 1987). Chapman et al. (1981) performed a Principal Component Analysis on various linear measurements of North American pachycephalosaurid domes. They recovered *Gravitholus albertae* separated from a cluster of *Stegoceras* (which then included specimens currently referred to *Colepiocephale lambei*, *Foraminacephale brevis*, *Hanssuesia sternbergi*, *Sphaerotholus buchholtzae*, and *Stegoceras validum*). However, the measurements used in that analysis were not based on homologous landmarks (Goodwin, 1990). Giffin (1989a) reported braincase (endocranial) measurements for TMP1972.027.0001 and supported Wall and Galton's (1979) claim that it had a relatively small endocast compared to other pachycephalosaurid specimens (namely CMN138 and UALVP 8501; *Stegoceras validum* and *Foraminacephale brevis*).

Maryańska (1990) suggested the unique frontoparietal shape of *Gravitholus albertae* was due to pathology, a conclusion supported by Peterson et al. (2013). Sullivan (2000) recognised that TMP1972.027.0001 was not solely a frontoparietal (as described by Wall and Galton, 1979) and suggested it included both fused postorbital + postfrontals and parts of both supraorbital IIs. They suggested that these peripheral elements were not fully incorporated into the dome, resulting in an apparently posteriorly wide frontoparietal, and stated (without reporting any measurements) that TMP1972.027.0001 is similar in size to the holotypes of *Colepiocephale lambei* and *Hanssuesia sternbergi* (CMN8818 and CMN8817 respectively, then still considered specimens of *Stegoceras*). Despite recognising that the description and diagnosis presented by Wall and Galton (1979) for *Gravitholus albertae* were incomplete, Sullivan (2000) did not reject the taxon, but suggested it was similar to *Stegoceras sternbergi* (currently *Hanssuesia sternbergi*)

Williamson and Carr (2002) hypothesised TMP1972.027.0001 was referable to *Stegoceras* sp. (at the time, *Stegoceras* included what would become *Colepiocephale lambei, Foraminacephale brevis*, *Hanssuesia sternbergi*, and *Stegoceras validum*) and tested this by including TMP1972.027.0001 in a specimen level pachycephalosaurian cladistic analysis. TMP1972.027.0001 was recovered in a polytomy that included (what would later be named) *Colepiocephale lambei*, *Hanssuesia sternbergi*, and *Stegoceras validum*. TMP1972.027.0001 and *Stegoceras* "unambiguously" shared grooved frontals, a pear-shaped dome, a tall and convex frontonasal boss, and a posterior dome margin perpendicular to a parietosquamosal shelf rather than forming a down-turned parietal. They concluded that *Gravitholus albertae* was a *nomen dubium* and that TMP1972.027.0001 represented an adult *Stegoceras* sp.

Sullivan (2003) elaborated on the incomplete description and diagnosis provided by Wall and Galton (1979). Sullivan identified both postorbitals and a right posterior supraorbital, then speculated on the preservation of the right anterior supraorbital (palpebral) and prefrontal. Sullivan (2003) argued that dome size was a poor defining character, and that the parietal depression was an artifact of pathology or weathering (in part citing Maryańska, 1990). Sullivan regarded the endocranial cavity of *Gravitholus albertae* was similarly sized to specimens of *Hanssuesia sternbergi* (without providing any measurements or specimen numbers). Sullivan

observed TMP1972.027.0001 shared peripheral elements (postorbital, posterior supraorbital, and palpebral (anterior supraorbital)) not incorporated into the dome with *Colepiocephale lambei*, and a broad frontonasal boss with *Hanssuesia sternbergi*. He interpreted that there was a posteriorly directed extension of the parietals, uninflated anterolateral regions of the frontal, and that it lacked a parietosquamosal shelf. He noted minor ornamentation on the posteromedial extension of the parietal. Sullivan (2003) agreed with Williamson and Carr (2002) in regarding *Gravitholus albertae* as *nomen dubium*, but considered TMP1972.027.0001 as Pachycephalosauridae indet., although noted its similarity to *Hanssuesia sternbergi*.

Sullivan (2006) and Jasinski and Sullivan (2011) followed Sullivan's (2003) referral of TMP1972.027.0001 without adding any additional comments. However numerous papers continued to consider *Gravitholus albertae* valid (Lehman, 2010; Longrich et al., 2010; Peterson et al., 2013). Schott and Evans (2016) excluded TMP1972.027.0001 when discussing pachycephalosaurid diversity in the Belly River Group due to the fusion of cranial elements, which precluded identifying the homologous landmarks necessary for morphometric analysis (pers. comm. David Evans ROM 2020).

The goal of this chapter is to resolve the anatomical and taxonomic problems posed by TMP1972.027.0001 by utilizing synchrotron imaging technologies to study its osteology and discern sutural contacts among the skull roof elements (which appear to be heavily fused, Sullivan, 2003). This will allow for a thorough comparison of the TMP1972.027.0001 to other pachycephalosaurids and the identification of homologous landmarks used in bivariate and multivariate morphometric analyses. These will be used to test the validity of *Gravitholus albertae*, with a particular focus on its possible synonymy with *Hanssuesia sternbergi* or *Stegoceras validum*.

2.2 Materials and methods

2.2.1 Synchrotron μCT imaging and segmentation

TMP1972.027.0001 was photographed with a Canon T4i rebel camera (Fig. 2.1). Photographs were touched up using Adobe Lightroom Classic. TMP1972.027.0001 was

additionally scanned using a LMI Technologies 3D scanner. Models were created in FlexScan 3D (Fig. 2.2), then imported into Geomagic Design X for imaging.

TMP1972.027.0001 was subjected to synchrotron radiation μ-CT imaging at the Canada Light Source facility at the University of Saskatchewan in Saskatoon, Canada. Scanning was performed on the BMIT 05ID-2 beamline at 80 KeV with a Wiggler field of 3.8T and 3.0 mm filters of aluminum and copper respectively (mounded at an angle to the beam; actual transverse distance of 3.31 mm). Images were captured with a DALSA Shad-o-box detector (115 mm by 65mm field of view; pixel size = 50 μm) with 100 ms exposure. Three thousand projection images were captured over a 180º rotation per vertical step. Seventeen vertical steps were performed with 1 mm overlap between adjacent steps. To obtain adequate transmission, both high energy photons and the highest possible photon flux were required due to the high degree of absorption of TMP1972.027.0001. A combination of glass microspheres (packed around TMP1972.027.0001 within a 150 mm diameter PVC tube) and an aluminum U-shaped profiler (the "U" shape matched the dimensions of the PVC tube) were used to normalize absorption and prevent detector oversaturation. This also required the use of a D-shaped absorber when collecting flat images, whereby the combined absorption of the D-shaped absorber and the U-shaped profiler was exactly the combined absorption of the U-shaped profiler and the PVC tube filled with glass microspheres. The amount of available glass microspheres was insufficient to completely immerse TMP1972.027.0001. Several aluminum bars were used to fill additional space. However, this was still insufficient to immerse the entire specimen. The most posterior position of TMP1972.027.0001 was left exposed and was not scanned. The horizontal field of view of the detector was too small to capture the entire width of TMP1972.027.0001. Therefore, it was positioned such that the more complete (right) side fit in the field of view. Cranial elements of TMP1972.027.0001 were then manually segmented in Dragonfly v.4.0 (Object Research Systems (ORS) INC, Montreal, Canada, 2020; software available at http://www.theobjects.com/dragonfly). The ROI Painter 3D mode was used in combination with range thresholding to segment each individual element. The slab average and slab minimum intensity projection functions were occasionally used to better visualise sutural contacts (Fig. 2.3B', D', E'). Some contacts were open ventrally and internally, but dorsally fused. In these cases, the dorsal direction of the contact was continued to the surface, following the direction of

vasculature when observable. The frontoparietal of ROM53555 was also segmented from CT images (see Schott et al., 2011 for imaging methods) to increase the sample of large *Stegoceras validum* in morphometric analyses performed in this study. ROIs created in Dragonfly v4.0 were converted into mesh objects, then imported into Geomagic Design X and underwent the fix normal and smooth functions. These and a segmented frontoparietal model of UALVP 2 (http://n2t.net/ark:/87602/m4/M43121) were measured and imaged in Geomagic Design X.

2.2.3 Morphometrics

2.2.3.1 Specimens and measurements

Most of the specimens and their measurements used in the morphometric analyses performed in this study were taken from Schott and Evans (2016). A total of 24 new specimens (including TMP1972.027.0001, 21 *Stegoceras validum* specimens, and two "*Hanssuesia sternbergi*"; Appendix A1.1) from the AMNH, TMP, and UALVP were measured first-hand. Linear measurements were taken using a traditional digital caliper, utilising proportional caliper when the traditional caliper could not be fit to the landmarks (frontoparietal thickness, heights from articulated specimens). Some measurements were estimated based on published photographs (e.g., AMNH 5388; Brown and Schlaikjer, 1943). These measurements are based on homologous landmarks at the contacts between cranial elements (Fig. 2.4), initially proposed by Goodwin (1990).

Schott et al. (2011) and Schott and Evans (2016) reported measuring widths from isolated frontals, doubling the width of the preserved frontals to estimate the width across both frontals. However, width measurements in those studies were not taken from numerous available fused frontoparietals that only preserved one of the bilateral width landmarks. These are as complete as isolated frontals, for which width measurements were recorded (by doubling the preserved widths on the isolated frontals). Frontoparietal width measurements were estimated from several specimens, including fused ones that preserved either the left or the right landmark.

Schott et al. (2011) and Schott and Evans (2016) did not address bilateral measurements – the heights and lengths of the peripheral element contacts with the frontoparietal – but instead reported single measurements when two could have been measured for each. In this study, left

and right measurements (when preserved) were measured from new specimens, and some previously studied specimens were remeasured. Left and right measurements, when both are preserved, were then averaged. These averages were used in morphometric analyses.

Although not specified in Schott and Evans (2016), the landmarks identified in their Figure 17 imply that endocranial length was measured ventrally along the midline from the contact of the frontals and parietals to the division between the olfactory bulbs. This is shorter than the endocranial length used by Giffin (1989a), who measured from the pit for the cartilaginous portion of the supraoccipital to the anterior extent of the olfactory bulbs. However, examination of published photographs revealed that endocranial length for some specimens was likely measured using the total preserved portion of the endocranium, extending posteriorly beyond the midline frontal-parietal contact (e.g., CMN138, CMN 8817, CMN9148, Sullivan 2003; CMN1108A, Brown and Schlaikjer 1943). Unfortunately, not all the specimens reported in Schott and Evans (2016) could be re-examined, so morphometric analyses were not performed on endocranial measurements. See Appendix A1.2 for additional specimens with corrected measurements.

Taxonomic treatment: TMP2000.026.0001 and TMP2017.012.0019

TMP2000.026.0001 has been inconsistently referred to *Stegoceras validum* and *Hanssuesia sternbergi*. Sullivan (2003) figured and discussed the specimen as *Stegoceras validum*, but included TMP2000.026.0001 in the lists for both *Stegoceras validum* and *Hanssuesia sternbergi* in his appendix. Schott et al. (2011) regarded TMP2000.026.0001 as *Stegoceras validum*, citing Ryan and Evans (2005) and Sullivan (2006; although they likely meant to cite Sullivan 2003). Evans et al. (2013) referred TMP2000.026.0001 to *Hanssuesia sternbergi*. Finally, Schott and Evans (2016) referred TMP2000.026.0001 to *Stegoceras validum*.

The domes of both TMP2000.026.0001 and TMP2017.012.0019 appear to preserve depressed (or shallow) parietal portions of the dome compared to the frontals, and the latter preserves an apparent broad frontonasal boss. Both features were considered diagnostic of *Hanssuesia sternbergi* (Sullivan 2003). These specimens are included in a cohort of specimens historically referred to "*Hanssuesia sternbergi*" for morphometric analyses.

2.2.3.2 Principal Component Analysis

Four Principal Component Analyses (PCA) were performed on 24 frontoparietal specimens (18 *Stegoceras validum*, 5 *Hanssuesia sternbergi*, and TMP1972.027.0001; Appendix A1.3) that all preserved 16 linear measurements (excluding L:FP, L:P, W:post, L:Prf due to low sample sizes; Appendix A1.1) in the statistical program PAST 4.04 (Hammer et al., 2001) using a variance-covariance matrix. Each PCA differed in the standardization of the linear measurements. The first was a non-transformed analysis. The second used logarithmically transformed linear measurements; previous studies have only performed PCA on logarithmically transformed linear frontoparietal measurements (Evans et al., 2013; Schott and Evans, 2016; Williamson and Brusatte, 2016). The third and fourth used size standardized linear measurements, where each measurement was divided by the length of the frontal or the width of the frontoparietal respectively, as both are strong statistical predictors of other linear frontoparietal measurements based on Reduced Major Axis (RMA) regression analyses, and typically used as standard (x) variables these regressions (Schott and Evans 2016; Schott et al. 2011). Given that six of the 16 linear measurements are width measurements, size standardising based on the length of the frontal may recover the purported diagnostic frontoparietal width of *Hanssuesia sternbergi* (Sullivan, 2003).

2.2.3.3 Frontoparietal bivariate and allometric analyses

Most of the diagnosis for *Hanssuesia sternbergi* (Sullivan 2003) can be demonstrated in bivariate analyses, and used to test its validity, and referral of TMP1972.027.0001 to *Hanssuesia sternbergi*. The purported diagnostic width should be observable in biplots comparing frontoparietal widths to frontal length. Frontoparietal length may be a more appropriate baseline for comparing frontoparietal widths. However, only two "*Hanssuesia sternbergi*" specimens preserve complete parietals, compared to six that preserve complete frontal lengths. Additionally, five of the seven frontoparietal width measurements occur on the frontal, therefore frontal length is an appropriate measurement to assess relative frontoparietal width. Reduced Major Axis regressions of log-transformed measurements were used to compare the relative width of "*Hanssuesia sternbergi*", *Stegoceras validum,* and TMP1972.027.0001. RMA regressions account for error in both the y and x variables (appropriate given the inclusion of estimated linear

measurements in this dataset) and is an appropriate method to interpret patterns of allometry (Smith, 2009). Specimens of *Colepiocephale lambei* were included in width biplots to compare intraspecific width variance in another closely related species. RMA regressions of log-transformed measurements were also used to compare supraorbital heights on the frontoparietal to examine the diagnostic "inflated supraorbital lobes" of *Hanssuesia sternbergi*.

PC 2 of the non-transformed and L:F proportionate PCA, and PC 3 of the log-transformed PCA appeared to separate large frontoparietal specimens into two clusters, but were not separated based on previous taxonomic referrals. Following taxonomic revisions, these clusters were hypothesised to represent adult sexual dimorphs of *Stegoceras validum*. To further test this hypothesis, RMA regressions were performed in Past 4.04 using the linear measurements that strongly loaded positively and negatively respectfully (*y* and *x* variables) on the PCs that appeared to capture sexual dimorphism, which included additional specimens that were too incomplete for PCA. RMA regressions including frontoparietal height and thickness measurements excluded specimens with frontoparietal thickness ≤ TMP1984.005.0001 due to discontinuous allometry (see subsequent discussion). Sexual dimorphism was tested following the methods outlined by Mallon (2017). Normality of PC scores and residuals (from the previously mentioned RMA regressions) of large (W:F/P > 80 mm) presumed adult individuals (Schott et al., 2011) were tested with the Shapiro-Wilk and Anderson-Darling tests (performed in PAST 4.04). Hartigan's Dip test, using 10000 iterations, were used to test for unimodality (performed in R v1.4.1103). Mixture analyses were performed to determine if the data (PC scores and residuals) were a better fit to a single (unimodal) or two normal distributions (bimodal) (performed in PAST 4.04). Akaike information criterion (AIC) values were used to determine the best-fitting distribution. Lower AIC values indicate a better fitting model, with differences of at least 2 indicating a significantly better-fitting model.

Following taxonomic revisions, frontoparietal allometric patterns in *Stegoceras validum* were re-examined. Frontoparietal width is the strongest statistical predictor of other frontoparietal measurements (Schott et al., 2011; Schott and Evans 2016) and was used as the standard variable (x) to assess allometry. RMA regressions were performed on log-transformed linear measurements. Allometry was identified in regressions where the 95% confidence interval

around the slope excluded 1 (positive if above 1, negative if below), and isometry if it encompassed 1.

Schott et al. (2011) recognised that frontoparietal thickness scaled isometrically with respect to frontoparietal width in *Stegoceras validum* when flat-headed and partly domed specimens were removed from RMA regression, and scaled with positive allometry (with respect to frontoparietal width) when those specimens were included with fully domed specimens. They hypothesised this could be due having few large specimens in their analysis, or a change in growth rate with size. With a substantial increase in the number of available large *Stegoceras validum* after taxonomic revisions, discontinuous allometry can be tested. Discontinuous allometry of frontoparietal thickness was tested by comparing the allometric slopes of frontoparietal width vs thickness amongst specimens thinner and thicker than TMP1984.005.0001 respectively (Appendix A1.4). Frontoparietal width significantly correlates with frontoparietal thickness for specimens thinner then TMP1984.005.0001 and thicker than TMP1984.005.0001 respectively. Their 95% confidence slope intervals are exclusive of each other, with the thinner specimens displaying high positive allometry (slope 95% CI = 1.97-4.86), and thicker specimens displaying isometry (slope 95% CI = 0.92-1.13). Thus, frontoparietal thickness exhibits discontinuous allometry with respect to frontoparietal width. Non-linear regressions can incorporate discontinuous allometry, and therefore were performed on non-transformed linear frontoparietal measurements, using frontoparietal width as the standard variable. AIC values were used to identify the best-fitting function for each pairing.

2.3 Systematic Palaeontology

Dinosauria Owen 1842

Ornithischia Seeley 1887

Pachycephalosauria Maryańska and Osmólska 1974

Pachycephalosauridae Sternberg 1945

Stegoceras Lambe 1902

Stegoceras validum Lambe 1902

Lectotype: CMN 515, frontoparietal

Type locality and horizon: Upper Belly River Group (likely the Dinosaur Park Formation)

Synonymy: *Troodon validus* Gilmore 1924; *Troodon sternbergi* Brown and Schlaikjer 1943; *Stegoceras sternbergi* Sternberg 1945; *Gravitholus albertae* Wall and Galton 1979; *Stegoceras browni* Wall and Galton 1979; *Ornatotholus browni* Galton and Sues 1983; *Hanssuesia sternbergi* Sullivan 2003

Referred Material: TMP1972.027.0001, incomplete skull roof. See Appendix A1.1 for additional referred material.

Emended diagnosis: A medium-sized pachycephalosaurid differing from all other pachycephalosaurs, where known, by possessing six or more nodes in the primary parietosquamosal node row without a ventral corner node, and a row of small, keel-shaped nodes on lateral margins of postorbitals and squamosal, numerous minute tubercles on lateral and posterior sides of the postorbitals and squamosals, no nasal ornamentation, a greatly reduced maxillary-premaxillary diastema, and a pubic peduncle of the ilium that is mediolaterally compressed and platelike. Differs from all other domed pachycephalosaurids (except possibly *Colepiocephale lambei*), where known, in possessing a parietosquamosal shelf throughout ontogeny (may be obliterated in mature individuals). The palpebral and prefrontal are not incorporated into the dome, as in *Acrotholus audeti*, *Pachycephalosaurus wyomingensis*, *Prenocephale prenes*, and *Sphaerotholus*. Modified from Schott et al. (2011).

Comments: This chapter continues to demonstrate that *Stegoceras validum* is a highly morphologically variable animal. The parietosquamosal shelf, which has been a crucial diagnostic feature, is known to decrease in relative size through ontogeny (Schott et al., 2011). Here the ontogenetic end stage of that reduction is identified, with posterior progression of the dome (reducing the parietosquamosal shelf) reaching the posterior extent of the parietal, which forms a "downturned" medial extension of the parietal. Adult *Stegoceras validum* are also identified with large posterior parietal shelves with no sign of being incorporated to the dome, which forms the previously diagnostic "depressed parietal region" of *Hanssuesia sternbergi*.

2.4 Description

General overview

TMP1972.027.0001 is an incomplete pachycephalosaurid skull roof with a preserved length of 130.73 mm and a maximum skull width of 133.50 mm (Figs. 2.1-2.2). It includes a damaged frontoparietal, partial right nasal, right prefrontal, right palpebral, posterior supraorbitals, nearly complete postorbitals, and fragments of the left prefrontal and squamosal (Fig. 2.5). Nearly all the bones appear indistinguishably fused to each other; however, their sutures are observable in synchrotron μCT images (Fig. 2.3) except for the interfrontal, frontoparietal, and right posterior supraorbital-postorbital sutures. Most of the dorsal surface of the specimen forms a massive "pear-shaped" cranial dome (narrowing anteriorly), typical of *Stegoceras validum* and *Colepiocephale lambei* (Schott et al., 2009). This excludes the prefrontal and palpebral from the dome, which are incorporated in "derived" pachycephalosaurid domes (e.g., *Sphaerotholus* and *Pachycephalosaurus,* Evans et al., 2013)

The frontoparietal and interfrontal sutures are externally fused, although a faint trace of the frontoparietal contact is observable within the cerebellar fossa (Fig. 2.2B, 2.6A). The frontoparietal suture is unobservable in synchrotron μCT images (Fig. 2.3E). An internal fracture occurs where the interfrontal suture is expected (Fig. 2.3A, E), thus the state of internal interfrontal fusion is unknown (cracks may form along fused interfrontal sutures; Dyer et al., 2021). The peripheral elements are more completely fused with each other than each are to the frontoparietal. The nasal-prefrontal suture is an exception; it remains mostly open. This unfused contact extends through to the prefrontal – frontal suture. The prefrontal – palpebral suture is heavily fused. The entire right posterior supraorbital – postorbital suture is indistinguishably fused. The frontal-nasal and right frontoparietal-postorbital sutures are indistinguishably fused dorsally. The left squamosal appears to have been more fused to the postorbital and parietal than the right, as indicated by attached chunks of the left squamosal (particularly on the postorbital) and the clean sutural surface for the right squamosal (Figs. 2.1D, 2.2D). Otherwise, the left peripheral elements appear less fused to each other and to the frontoparietal than the right elements. The sutural surface for the left palpebral on the frontal is clean, without any remnant of the palpebral or damage to the frontal. The same is true for most of the left sutural surface for the prefrontal. Part of the left prefrontal remains attached, although its suture with the frontal

remains unfused. The left posterior supraorbital and postorbital appear to have broken and been reattached along their sutures with the frontoparietal. The most medial portion of the left posterior supraorbital – postorbital suture remains internally open, although its lateral extent was not imaged during synchrotron µCt scanning.

Nasal

TMP1972.027.0001 preserves a fragmentary posterior portion (~ 20 mm anteroposterior) of the right nasal. The medial portion, which formed the internasal suture, is missing. The nasal contacts the frontal posteromedially and the prefrontal posterolaterally. The contact with the frontal is slightly concave anteriorly in dorsal view (Fig. 2.5), so that the nasal slightly surrounds the anterior boss of the frontal. The contact with the prefrontal is broadly directed anterolaterally. It is slightly concave on the lateral surface of the nasal, such that the dorsal portion of the contact overhangs laterally.

The nasal is dorsoventrally thick, both at the midline (H:N/N = 35.13 mm) and laterally (H:N/Prf = 26.79 mm). It contributes to a distinct frontonasal boss. The dorsal surface is smooth, lacking the tesserate (Williamson and Carr, 2002; Woodruff et al. 2021; "tuberculate", Schott et al., 2011) texture seen in *Stegoceras validum* (UALVP 2, Gilmore, 1924), aside from a groove (positioned at the lateral margin of the boss) that extends anterodorsally to the prefrontal, like the grooves that occur on the surface on the frontals near the contact with the palpebral and prefrontal.

The contact area for the frontal on the ventral surface is broadly 'v' shaped, which corresponds to the anteroventral flange of the frontal (Fig. 2.7). The ventral surface of the nasal is slightly depressed, forming part of the roof of the nasal cavity. Within this surface, the nasal preserves a facet for the anteroventral projection of the frontal (Fig. 2.7D-E). Two posteriorly directed ridges on this facet (Fig. 2.7D-E) correspond to the anteroventrally directed grooves on the dorsal surface of the anteroventral projection of the frontal (Fig. 2.7B-C). Lateral to the facet is a short (~ 3 mm) posteriorly directed process, positioned at the ventral base of the nasal between the contacts with the frontal and prefrontal. A ventrolateral ridge extends anteriorly from this posterior projection. It contacts the prefrontal dorsally and anteroventrally, and the

frontal posteroventrally. A shallow anteroposteriorly directed groove rests on the dorsal surface of this ridge.

Prefrontal

Most of the right prefrontal is preserved, with only the most anterior portion missing (Fig. 2.5). A fragmentary posteromedial portion of the left prefrontal is preserved. The prefrontal contacts the nasal anteromedially, the frontal medially and posteriorly (which forms a "L" shaped notch on the frontal in dorsal view), and the palpebral laterally. The prefrontal is incipiently incorporated into the frontonasal boss (Fig. 2.5C), a unique feature amongst known pachycephalosaurs. This portion is smoothed; the remainder of the dorsal surface is rugose. Anteriorly and medially (aside from the frontonasal boss), the rugosity resembles the tuberculate ornamentation seen in uninflated cranial roof elements of *Stegoceras validum* (Schott et al. 2011). Laterally and posteriorly, the rugosity appears coalesced compared to the surrounding tubercules, and along with the palpebral, contributes to a larger supraorbital boss (Figs. 2.1A, 2.5D). The prefrontal is not incorporated into the frontoparietal dome.

The ventral surface of the prefrontal contributes to the rooves of the orbit and nasal cavity. These surfaces are separated by an anterolaterally directed ridge that extends from the frontal (Fig. 2.5B). Several vessels enter the orbital roof on the prefrontal. Medioventrally the prefrontal receives the ventrolateral ridge of the nasal and most of the anteroventral projection of the frontal (Fig. 2.7C). The contact with the palpebral is nearly straight, except for a shallow horizontal ridge that extends along the ventral margin of the contact.

Palpebral (anterior supraorbital) (See Appendix A1.5 for revised nomenclature)

The palpebral contacts the prefrontal medially, frontal posteromedially, and posterior supraorbital posteriorly (Fig. 2.5). The contacts with the frontal and posterior supraorbital are straight. The contact with the frontal appears extensive, unlike the restricted contact described in derived pachycephalosaurids (*Acrotholus audeti, Prenocephale prenes,* and *Sphaerotholus*; Evans et al., 2013).

The dorsal surface of the palpebral is convex and rugose, and forms most of a supraorbital boss (Figs. 2.1A, 2.5D) like in *Prenocephale prenes* (Maryańska and Osmólska,

1974, although they mention each peripheral element is separated from each other, there is no discernible diastema between the contacts of the prefrontal and palpebral in *Prenocephale prenes*). This rugosity is shallow and more irregular than the typical tesserate rugosity of uninflated cranial roof bones (such as the palpebral of UALVP 2). This rugosity extends onto the lateral surface, such that the lateral ridge does not extend onto the palpebral (Fig. 2.2F; Schott et al., 2011; Schott and Evans, 2012), whereas a lateral ridge is retained in the holotype of *Prenocephale prenes*. *Pachycephalosaurus wyomingensis* (AMNH 1696, Brown and Schlaikjer, 1943) and *Sphaerotholus buchholtzae* (DMNH EPV.97077, Woodruff et al., 2021) do not appear to have a supraorbital boss, and the dorsal surfaces for the supraorbital elements are smooth and continuous with each other and the frontal.

The preserved ventral surface of the palpebral contributes to the orbital roof, which is slightly depressed from the rounded orbital rim. The ventral surface is pierced by numerous canals (Fig. 2.8B). These enter the palpebral at shallow angles and are oriented perpendicular to the palpebral-frontal contact. Some canals rest in furrows that extend onto (and then enter) the frontal.

Posterior supraorbital

The posterior supraorbital contacts the palpebral anteriorly, the frontal medially, and the postorbital posteriorly (Fig. 2.5). Although the right posterior supraorbital-postorbital suture appears obliterated, the respective contacts of these two bones with the frontal are identifiable and are separated by a diastema (both have a dorsally arched contact with the frontoparietal). The left posterior supraorbital appears to have been reattached to the frontoparietal, with the break running along the frontal-posterior supraorbital suture (Figs. 2.1B, 2.2B).

The dorsal margin of the posterior supraorbital that contacts the frontal is strongly arched, with the maximum height of the contact skewed posteriorly (Fig. 2.5C; unique to TMP1972.027.0001). The dorsal surface extending perpendicular from the middle of the frontal contact is smooth. The dorsal surface becomes rugose towards the contact with the palpebral and postorbital, and towards the lateral margin. The dorsal inflation extends to the lateral margin, but a slight anteroposterior ridge may represent the remnants of a dorsolateral ridge. The left posterior supraorbital is not incorporated into the dome, although this may be due to a

pathological depression that also affects the postorbital and frontoparietal (Fig. 2.8C). The lateral surfaces of the posterior supraorbitals are rugose, developed by bumps rather than depressions.

The ventral surface of the posterior supraorbital contributes to most of the posterodorsal region of the orbital roof. Vascular canals are oriented perpendicular to the posterior supraorbital – frontal contact, some resting in furrows, like on the prefrontal and palpebral (Fig. 2.8B). A possible muscle scar is marked by a small peg-like rugosity resting in a shallow depression in the posterolateral corner of the orbit roof (Fig. 2.8A-B). The orbital rim on the posterior supraorbital is sharper than that on the palpebral.

Postorbital

Both postorbitals are nearly complete, although the ventrolateral margins of both are weathered. The temporal rooves remain intact, but not the ventral surface of either postorbital bar. The postorbital contacts the posterior supraorbital anteriorly, the frontoparietal medially, and the squamosal posteriorly. The sutural surface for the squamosal is continuous from the postorbital onto the parietal (Figs. 2.2, 2.5), eliminating the supratemporal fenestrae.

The postorbital is completely incorporated into the frontoparietal dome (Fig. 2.5), contra Sullivan (2003). The dome continuously extends from the frontoparietal to the lateral edge of the postorbital, such that there is no lateral shelf. The postorbital contribution to the dome slightly overhangs the lateral surface of the postorbital-squamosal bar, and forms the maximum width of the skull (Figs. 2.1C, 2.2C). The dorsal surface is extremely smooth, but rugose towards the anterior, lateral, and posterior margins. Chunks of the left squamosal appear fused onto the postorbital. A deep pathological depression exposes an open frontoparietal-postorbital suture on the left side (Fig. 2.8C).

The preserved ventral surface forms part of the temporal roof. The temporal roof contains two shallow mediolateral depressions, which extend onto the parietals. Vascular canals rest in furrows, cross the parietal-postorbital contact and enter each element. The surface for the squamosal tongue is preserved on the right postorbital (Fig. 2.2B).

Frontoparietal

The frontoparietal (fused frontals and parietals) is nearly complete but is dorsally and ventrally damaged. Two large holes along the dorsal surface extend through most of the frontoparietal (Figs. 2.1A-B, 2.2A-B). Ventrally, the frontoparietal is damaged along the left anterolateral corner of the frontonasal boss (missing the anteroventral flange, Fig. 2.5C). Many of the posterior neurocranial contacts are damaged, including the left posterior portion of the cerebral fossa, the contacts for the supraoccipital and left laterosphenoid, and the right sutural surface for the prootic and opisthotic (Figs. 2.1B, 2.2B, 2.6A). Missing portions are inferred from the neurocranial arrangement described by Giffin (1989a). The ventral and posterior portion of the occipital surface of the parietal, including the ventral and posterior sutural surfaces for the right squamosal, are damaged.

TMP1972.027.0001 preserves the absolutely and proportionally widest frontoparietal of any unquestionable known Belly River Group pachycephalosaurid (108.99 mm (W:F/P)/51.62 mm (L:F) = 2.11; see Sullivan, 2003 for discussion on the provenance of BMNH R 8648, an incomplete skull roof of *Pachycephalosaurus wyomingensis* originally reported from the Oldman formation). Despite its great width, the frontoparietal is only 6.24 mm longer than in UALVP 2 (121.24 mm, 115.18 mm respectively; W:F/P = 80.98mm), and is 15.7 mm shorter than the longest known Belly River Group pachycephalosaurid frontoparietal (TMP2017.012.0019; L:FP = 137.12 mm).

The dorsal surface forms a massive dome, which is continuous with the frontonasal boss, the posterior supraorbital and the postorbital, and which extends to the posterior margin of the parietal (Figs. 2.1-2.2, 2.5). The dome apex is relatively flat and broad where unaltered by pathologies (Figs. 2.1C-D, 2.2C-D). The largest lesion is situated on the left side of the parietal and is 24 mm by 30 mm, and 16 mm at its deepest. It has a terraced appearance, with smaller depressions lying inside larger ones. The broad frontonasal boss is posterolaterally separated from the supraorbital lobes by a distinct groove on either side (the left groove is dorsally bifurcated; 2.2 E-F). The frontonasal boss of TMP1972.027.0001 is anteroposteriorly distinct, similar to UALVP 2, whereas "*Hanssuesia sternbergi*" typically possesses anteroposteriorly short frontonasal bosses (see figs. 4-5 in Sullivan, 2003). The anteroposterior extent of the frontonasal boss varies in *Colepiocephale lambei* (e.g., short in TMP1992.088.0001; Schott et

al., 2009), *Foraminacephale brevis* (e.g., TMP1985.036.0292, small; TMP1987.050.0029, enlarged; Schott and Evans, 2016) and *Sphaerotholus buchholtzae* (UCMP 186026 – nasal process of the frontal 17% frontoparietal length; UWBM 89701 most anterior frontals (most anterior frontal process) 18% frontoparietal length; ROM 53584 – frontal projection 12% frontoparietal length; Woodruff et al., 2021).

The peripheral margins of the supraorbital lobes are quite rugose but smooth posteromedially into the dome. The dome is steep towards the supraorbital lobes (134º along the palpebral contact) but does reach the dorsal margins of the supraorbital elements (prefrontal, palpebral, and posterior supraorbital; Fig. 2.5). The sutural surface for the right posterior supraorbital is concave in dorsal view. The posterior extent of the supraorbital lobe is greater in *Colepiocephale lambei,* and is marked by an indentation in the lateral surface of the frontoparietal at the contact between the posterior supraorbital and postorbital (Sternberg, 1945; Sullivan, 2003), an apomorphy of the taxon (Schott et al., 2009). In dorsal view, the frontoparietal of TMP1972.027.0001 is not indented between the sutural surfaces for the posterior supraorbital and postorbital.

The posterior medial extension of the parietal of TMP1972.027.0001 is not visible in lateral view photographs of previous publications (Wall and Galton, 1979; Sullivan, 2003), although it is visible in a figured lateral line drawing in Wall and Galton (1979, fig. 1). It is more distinct in orthographic views of the laser model (Fig. 2.2E-F) compared to photographs (Fig. 2.1E-F). The posterior medial extension of the parietal is confluent with the dome, eliminating a posterior shelf (the parietosquamosal shelf; contra to Williamson and Carr, 2002) and instead forming a "down-turned" parietal (Sternberg 1945), a unique feature amongst specimens of *Stegoceras validum*. Otherwise, a dome extending to the posterior margin of the parietal is restricted to other domed pachycephalosaurids, except for *Colepiocephale lambei* (which presumably has a narrow posterior projection portion of the parietal in-between the supratemporal fenestrae; Schott et al., 2009). The medial extension of the parietal preserves a shallow sagittal node (also present in UALVP 2, although Evans et al., 2021 described this as a ridge) that is laterally and ventrally bordered by a tuberculate rugosity. There is no indication that a primary node row extended on the parietal, although the right side of the medial extension

of the parietals that contacts the squamosal is damaged, and possibly could have otherwise preserved a coalescing medial node. *Stegoceras validum* variably preserves a coalescing node or the medial node is completely positioned on the squamosal (Schott and Evans, 2012). This state was historically unknown for "*Hanssuesia sternbergi*". However, TMP2017.012.0019 preserves a coalescing node on the right side of the medial extension of the parietal. The ventral surface of the medial extension of the parietal in TMP1972.027.0001 preserves a shallow groove that follows the posterior border of the parietal (Figs. 2.1B, 2.2B).

The ventral surface is divided into five fossae: the endocranial fossa (which includes the olfactory bulbs and the cerebellar fossa), the orbital fossae, and the temporal rooves. The relative length of the endocranial fossa (from the anterior extent of the olfactory bulbs to the pit for the supraoccipital cartilage – L:olf/soc; see Giffin, 1989a) is similar to large *Stegoceras validum* and "*Hanssuesia sternbergi*" (Table 2.1). TMP1972.027.0001 does have the shortest L:olf/soc (32.41 mm) amongst these large specimens, although it is ~ 1.6 mm shorter than UALVP 2 (Fig 2.6). TMP2017.012.0019 preserves the longest L:olf/soc (46.03 mm) amongst the examined specimens. Compared to frontoparietal length (as in Giffin, 1989a), the L:olf/soc of UALVP 2 (29.7%) is indistinct from TMP1972.027.001 (26.7%) and TMP2017.012.0019 (33.6%)

The orbital fossae are separated from the endocranial fossa by thick sutures for the accessory orbital ossifications, orbitosphenoid, and laterosphenoid (see Giffin, 1989b for neurocranial anatomy), as in "*Hanssuesia sternbergi*" (Brown and Schlaikjer, 1943) and large *Stegoceras validum* (e.g., UALVP 2, Fig. 2.6). The medial border of the orbital fossa is pierced by numerous vascular canals, some of which are situated within furrows that extend onto the supraorbital elements.

The parietal portion of the temporal chamber is extremely narrow, and the roof is horizontal as in *Stegoceras validum*, "*Hanssuesia sternbergi*", *Foraminacephale brevis* (see chapter 3 for quantification and recharacterization of *Colepiocephale lambei*). The temporal rooves preserve a pair of deep furrows on each side. These cross the parietal-postorbital suture and lead to vascular foramina. Similar vascular furrows were described from the parietals of *Colepiocephale lambei* (Schott et al., 2009).

2.5 Results

2.5.1 Principal component analyses results

2.5.1.1 Iteration loadings

Table 2.2 summarises the PC variances and loadings for all PCA iterations. Variable loadings in PC 1 of all iterations were positive (aside from H:N/N and T:F/P in the W:F/P proportionate iteration). PC 1 in the non-transformed, LOG transformed, and L:F proportionate explain > 80% of the total variance, whereas it explains 48.4% in the W:F/P proportionate matrix. The amount of total variance that each PC 1 explained in each iteration seems to result from the total range of the variables used in each analysis (in descending PC 1 variance: non-transformed PC 1 = 92.0% total variance, range of variables = 104.98, min = 4.01, maximum = 108.99; L:F proportionate PC 1 = 82.9% total variance, range of variables = 2.02, minimum = 0.09, maximum = 2.11; log-transformed PC 1 = 82.0% total variance, range of variables = 1.44, minimum = 0.60, maximum = 2.04; W:F/P proportionate PC 1 = 48.4 % total variance, range of variables = 1.07, minimum = 0.09, maximum = 1.16). Variables with the largest range also had the highest loadings on PC 1 of all iterations (Appendix 1.5). PC 1 in previous PCA analyses of linear frontoparietal measurements explained frontoparietal size (Evans et al., 2013; Schott and Evans, 2016) in the non-transformed and L:F proportionate iterations are both strongly loaded by W:F/P, W:Pso/Po, W:Pl/Pso, and T:F/P. W:F/P has the strongest loading amongst these. PC 1 in the LOG-transformed iteration was strongly loaded by H:N/N and H:Pso/Po. PC 1 in the W:F/P proportionate iteration was very strongly loaded by L:F (0.72), but also strongly loaded by W:Pl/Pso.

PC 2 in the non-transformed and L:F proportionate iterations explained 2.38% and 4.58% of the total variance respectively. They were both strongly positively loaded by the heights of the frontonasal boss (H:N/N and H:N/Prf), and strongly negatively loaded by an anterior and posterior frontoparietal width (W:Prf/Pl and W:Po/stf/Sq). PC 2 in the LOG-transformed iteration explained 4.62% of the variance. It was strongly negatively loaded by thickens of the frontal-palpebral contact (H:Pl/Pso and H:Prf/Pl). W:Prf/Pl had the strongest positive loading, but this was less than 0.3. PC 2 explained 16.0% of the variance in the W:F/P proportionate iteration. All frontoparietal heights, including T:F/P, strongly positively loaded in PC 2. L:F had the strongest negative loading, but was greater than -0.3.

PC 3 explained 1.3% of the total variance in the non-transformed iteration. It was strongly positively loaded by L:Pl, and strongly negatively loaded by T:F/P and L:Po. PC 3 explained 4.2% of the total variance in the LOG-transformed iteration. It was strongly positively loaded by L:Pl, and strongly negatively loaded by H:N/Prf. PC 3 in the L:F proportionate and W:F/P iterations explained 3.2% and 10.5% of the total variance respectively. It was strongly positively loaded by W:N/Prf and strongly negatively loaded by T:F/P in both iterations.

2.5.1.2 Iteration Scoring

TMP1972.027.0001 and "*Hanssuesia sternbergi*" show little or no distinction from *Stegoceras validum* (Fig. 2.9). TMP1972.027.0001 has the highest score of any specimen in PC 1 of the LOG-transformed, L:F proportionate, and W:F/P proportionate iterations. Only one specimen of *Stegoceras validum* overlaps in the range of "*Hanssuesia sternbergi*" in the L:F proportionate iteration. Otherwise, multiple *Stegoceras validum* (particularity ROM53555, which preserves squamosal ornamentation consistent with other *Stegoceras validum*; pers. comm. David Evans ROM 2020) fall within or encompass "*Hanssuesia sternbergi*" PC 1 range in the other iterations. TMP1972.027.0001 falls within the range of *Stegoceras validum* in PC 2 and 3 in all iterations. It also falls within the range of "*Hanssuesia sternbergi*" in PC 2 of the L:F proportionate and W:F/P proportionate iterations, and within PC 3 in all iterations except for the LOG-transformed iteration. Some specimens of "*Hanssuesia sternbergi*" fall outside the range of *Stegoceras validum* in PC 2 of the non-transformed iteration, in PC 3 of the LOG-transformed iteration, and PC 2 of the L:F proportionate iteration.

There appeared to be two clusters of large frontoparietal specimens distributions were noted in PC 2 of the non-transformed iteration and the L:F proportionate iteration, and in PC 3 of the LOG-transformed iteration. This separation is restricted to large specimens, which all score strongly positively in PC 1 of these iterations. It does not reflect previous taxonomic distinctions. Specimens of *Stegoceras validum* and "*Hanssuesia sternbergi*" occur on both sides of the divide, except in PC 3 of the LOG-transformed iteration. Here, three specimens of "*Hanssuesia sternbergi*" score together (positively in PC 3), whereas two specimens of "*Hanssuesia sternbergi*", three specimens of *Stegoceras validum*, and TMP1972.027.0001 score negatively.

2.5.2 Diagnostic morphometrics of *Hanssuesia sternbergi*

L:F positively correlated with all widths in *Stegoceras validum*, but did not significantly correlate with width measurements in "*Hanssuesia sternbergi*" (Table 2.3; Fig. 2.10). W:N/Prf, W:F/P, and W:Po/stf/Sq scale with positive allometry relative to L:F in *Stegoceras validum*. The other two widths scaled isometrically relative to L:F. There is considerable overlap between similarly sized frontoparietals of "*Hanssuesia sternbergi*" and *Stegoceras validum* in the biplots comparing L:F to W:N/Prf, W:Prf/Pl, and W:Pl/Pso. For the other three widths (W:Pso/Po, W:F/P, and W:Po/stf/sq), specimens of "*Hanssuesia sternbergi*" are typically wider than similarly sized specimens of *Stegoceras validum*, except for TMP1972.027.0001. Furthermore, specimens of *Colepiocephale lambei* exhibit similar or greater variance in proportionate width to the combined sample of *Stegoceras validum* + "*Hanssuesia sternbergi*" + TMP1972.027.0001 (except for W:N/Prf; Fig. 2.10A). Furthermore, some specimens of *C. lambei* are proportionately wider than "*Hanssuesia sternbergi*" (Fig. 2.10B-C, E-F). The combined variance of "*Hanssuesia sternbergi*" and large *Stegoceras validum* is similar to the variance amongst smaller *Stegoceras validum*. The inclusion of "*Hanssuesia sternbergi*" and TMP1972.027.0001 with *Stegoceras validum* when correlating L:F to each width measurement increases r values and tightens 95% confidence intervals around slopes (Table 2.3) compared to when *Stegoceras validum* is analyzed separately. All widths scale with positive allometry relative to frontal length in this combined sample.

All frontoparietal heights significantly positively correlated with, and were positively allometric to W:F/P, in *Stegoceras validum* (Table 2.4, Fig. 2.11). H:Pso/Po may weakly positively correlate with W:F/P in "*Hanssuesia sternbergi*" (p = 0.057), otherwise no frontoparietal height significantly correlated with W:F/P in "*Hanssuesia sternbergi*". Specimens of "*Hanssuesia sternbergi*" show similar frontoparietal height to large *Stegoceras validum*. "*Hanssuesia sternbergi*" specimens almost always fall below the best fit line for *Stegoceras validum*. Frontoparietal heights of TMP1972.027.0001 are indistinct from both *Stegoceras validum* and "*Hanssuesia sternbergi*" except perhaps H:Pso/Po, although it also falls below the best fit line for *Stegoceras validum*. The inclusion of "*Hanssuesia sternbergi*" and TMP1972.027.0001 with *Stegoceras validum* increases r values and tightens 95% confidence intervals around slopes compared to when *Stegoceras validum* is analyzed separately.

2.5.3. Dimorphism

The distribution of large frontoparietals (W:F/P > 80 mm) across PC 2 scores from the non-transformed PCA iteration were indistinct from normal distributions (W = 0.89, p = 0.2; A = 0.48, p = 0.17; Fig. 2.12A), and was best-fit to unimodal distributions (AIC = 57.18; bimodal AIC = 60.45) in the mixture analysis (Fig. 2.12A). However, the Hartigan's dip test suggested a weak bimodal distribution. The average PC 2 score of pathological specimens may be slightly larger than that of non-pathological specimens (t = 1.89, p = 0.07).

The distribution of large frontoparietals across PC 3 in scores from the LOG-transformed PCA iteration was not normal (W = 0.83, p = 0.04; A = 0.74, p = 0.03; Fig. 2.12B), and was best-fit to a bimodal distribution (AIC = -27.03, unimodal AIC = -23.81) in the mixture analysis. Specimen group assignments are summarised in Table 2.5. However, the Hartigan's dip test did not indicate a bimodal distribution (p = 0.12). The average PC 3 score of pathological specimens was significantly lower than non-pathological specimens (t = 2.14, p = 0.04).

Five antagonistic relationships were identified from these three principal components. Four of these are identical from PC 2 of the non-transformed and L:F proportionate iterations (Fig 2.13A-D; positive: H:N/N, H:N/Prf; negative W:Prf/Pl, W:Po/stf/Sq). The fifth is from PC 3 of the LOG-transformed iteration (Fig. 2.13E; positive: L:Pl; negative: H:N/Prf). Exclusion of flat and low domed frontoparietals (T:F/P ≤ TMP1984.005.0001) increased r values and tightened slope confidence intervals when frontonasal boss heights were compared to W:Prf/Pl (Table 2.6). However, excluding these specimens decreased r values and increased slope confidence intervals when frontonasal boss heights were compared to W:Po/stf/Sq and L:Pl respectively.

Residuals from RMA regressions of H:N/N (vs. W:Prf/Pl) and H:N/Prf (vs. W:Prf/Pl; vs. W:Po/stf/Sq) amongst large specimens (W:F/P > 80 mm) were significantly or weakly non-normally distributed (Fig. 2.14A, C-D). Inclusion of the next largest frontoparietal (TMP1984.121.0021; W:F/P = 71.08) results in a significantly non-normal distribution of the residuals for H:N/N (vs. W:Prf/Pl). The distribution of residuals of the H:N/N (vs. W:Prf/Pl) amongst large specimens was significantly multi-modal (D = 0.16, p = 0.009), and was best fit by a bimodal distribution based on the mixture analysis (bimodal AIC = -30.58; unimodal AIC =

-25.06). Specimen groupings were nearly identical to the LOG-transformed PC 3 groups, except for ROM53555 (Table 2.5). The residuals of the H:N/Prf contact (vs. W:Po/stf/Sq) amongst large specimens were also best-fit by a bimodal distribution (bimodal AIC = -21.25, unimodal AIC = -17.48). Specimen groupings were identical to the LOG-transformed PC 3 groups. However, this distribution was significantly unimodal (D = 0.12, p = 0.22). Neither a unimodal nor bimodal distribution significantly better-fit the distribution of large specimens' residuals of the H:N/N (vs. W:Po/stf/Sq) (AIC = -22.63 and -22.39 respectively). Residuals of the H:N/Prf (vs. W:Prf/Pl; vs. L:Pl) amongst large specimens showed no statistical division (Fig. 2.14B, E). The average residual for the H:N/N and the H:N/Prf (vs. W:Po/stf/Sq) amongst pathological specimens was weakly larger than non-pathological specimens (t = 1.78, p = 0.089; t = 1.83, p = 0.081).

2.5.4 Frontoparietal allometry and non-linear relationships in *Stegoceras validum* (= *Gravitholus albertae* and *Hanssuesia sternbergi*)

Table 2.7 summarises the RMA regression results for bivariate regressions of *Stegoceras validum* (inclusive of "*Hanssuesia sternbergi*" and "*Gravitholus albertae*"). All log-transformed linear measurements significantly positively correlated with W:F/P. The r values ranged from 0.77 (L:F) to 0.98 (W:Pso/Po). Frontoparietal widths show the highest r values, followed by frontoparietal lengths (aside from L:F and L:Prf, although the latter had a small sample size of 10), then frontoparietal heights (including frontoparietal thickness).

All frontoparietal heights (including frontoparietal thickness) scale with positive allometry relative to W:F/P. The 95% confidence interval (CI) around the slopes of T:F/P and H:Pso/Po are exclusive, and the CI of T:F/P overlaps with H:N/Prf by 0.01. In both instances, T:F/P has a steeper slope (more strongly positively allometric). Otherwise, CI around slopes of frontoparietal heights all overlap each other. Frontoparietal thickness is strongly positively allometric amongst thin (T:F/P < TMP1984.005.0001, a reference specimen for "partly" and "fully" domed *Stegoceras validum*; Schott et al., 2011) frontoparietals (CI around slope = 1.97 to 4.86) relative to W:F/P, whereas it is isometric relative to W:F/P amongst thicker specimens (T:F/P > TMP1984.005.0001; CI around slope = 0.92 to 1.13; Appendix A1.4).

All frontoparietal lengths scale with negative allometry with respect to W:F/P, with the exceptions of L:Prf and L:Po, which scale isometrically relative to W:F/P. The 95% CI around the slope of L:Pso is higher and excludes the 95% CI of L:F. Otherwise, 95% CI around the slopes of linear measurements of the same allometric state overlap each other.

The W:N/Prf is the only width that scales isometrically with respect to W:F/P. All other widths are negatively allometric with respect to W:F/P. The 95% CI around the slope of W:Pso/Po overlap the same CI of W:Pl/Pso by 0.01, and with W:Prf/Pl by 0.02 (both of which have smaller slopes than W:Pso/Po. Otherwise, the 95% Ci around the slopes of the four posterior widths all overlap with each other.

Nearly all bivariate relationships of non-transformed linear measurements are best explained by non-linear functions, with the exception of H:Pl/Pso vs. W:F/P (Table 2.8, Fig. 2.15). Numerous best-fit functions are within two AIC of other functions. Allometric relationships appear to be independent of the best fitting non-linear functions. H:Pl/Pso, L:Prf, L:Po, are non-asymptotic. Otherwise, all other variables approach or would eventually reach an asymptote.

2.6 Discussion

2.6.1 Validity of *Gravitholus albertae*

Some of the previous anatomical interpretations of TMP1972.027.0001 were clearly influenced by the fusion of the peripheral elements to the frontoparietal (e.g., degree that the postorbitals are incorporated into the dome; misidentification of the nasal, prefrontals, left posterior supraorbital). However, other misinterpretations are apparent without a segmented model (specimen described as a frontoparietal, absence of squamosal nodes (Wall and Galton, 1979; Longrich et al., 2010), presence of a parietosquamosal shelf (Williamson and Carr, 2002)).

Sullivan (2003) correctly noted that the dome width and thickness, as well as the pathological depression of TMP1972.027.0001 should not be considered as diagnostic features. The dome is as thick as in some specimens of *Colepiocephale lambei* (e.g., TMP2000.057.0001), *"Hanssuesia sternbergi"* (CMN 9148), and *Stegoceras validum* (ROM 53555). The extreme dome width of TMP.1972.027.0001 (complete incorporation of the postorbitals) while unique, is

consistent with ontogenetic trends in *Stegoceras validum*, where the postorbital lateral shelf is reduced as the postorbital is incorporated into the dome (Schott et al., 2011).

Giffin (1989a) presented endocranial measurements for numerous pachycephalosaurid specimens. In her text, she compared TMP1972.027.0001 (W:F/P = 108.99 mm) to CMN 138 and UALVP 8501 (W:F/P = 53.1 mm and 38.81 mm respectively; the latter is currently regarded as *Foraminacephale brevis*; Sullivan, 2003; Schott and Evans, 2016). Giffin concluded that TMP1972.027.0001 preserved a remarkably small endocranium (L:olf/soc = 34 mm, compared to 39 mm – CMN 138 and an estimates 29 mm – UALVP 8501 (which does not preserve the olfactory bulbs)) and supported the validity of "*Gravitholus albertae*". Interestingly, Giffin presented but did not discuss endocranial measurements of AMNH 5388 (*Stegoceras validum*; W:F/P = 82 mm) which preserved a L:olf/soc of 34 mm (41% W:F/P, 59% L:F), more similar to TMP1972.027.0001 (30% W:F/P; 63% L:F), in fact proportionately smaller than TMP1972.027.0001 when compared to the length of the frontal. This study demonstrates that TMP1972.027.0001 preserves an endocranium that is proportionately sized (to frontoparietal length) like in large specimens of "*Hanssuesia sternbergi*" (TMP2017.012.0019) and *Stegoceras validum* (UALVP 2). Giffin (1989a) suggested that endocranial size in *Pachycephalosaurus wyomingensis* scaled with negative allometry relative to frontoparietal length. Negative allometry of the endocranium may be widespread amongst pachycephalosaurids and would explain the relatively small endocranium of TMP1972.027.0001 and other large *Stegoceras validum* (including "*Hanssuesia sternbergi*"). This should be further examined with LOG-transformed linear regressions of linear measurements based on standardized homologous landmarks (e.g., L:olf/soc; Giffin, 1989a).

TMP1972.027.0001 is morphologically consistent with a mature "end-stage" *Stegoceras validum,* and so is referred to this species. Unique features of TMP1972.027.0001, such as a down-turned parietal and a dome that laterally extends beyond the lateral ridge are the logical end stages (or continuations) of previously recognised ontogenetic trends in *Stegoceras validum* – which include the reduction of the lateral and posterior shelves (Schott et al., 2011; Sternberg, 1945 phrased the down-turned parietal as the opposite state of having a horizontal parietal

shelf)). Additionally, the smooth dorsal surface of the nasals is consistent with maturity, where the immature texture on the nasal (e.g., UALVP 2) has become smooth.

2.6.2. Validity of *Hanssuesia sternbergi*

Much of the revised diagnosis for *Hanssuesia sternbergi* proposed by Sullivan (2003), if valid, can be tested by morphometric analyses. The relative width of the frontoparietal dome must have been extremely unusual to Sullivan (2003), as it is referenced three times in the diagnosis (anterior portion wide, posterior portion wide, and frontonasal boss broad). Sullivan (2003) described the disproportionate width of *Hanssuesia sternbergi* as being unique amongst all known pachycephalosaurids. However, specimens of *Hanssuesia sternbergi* display a range of relative widths, some of which are consistent with specimens previously assigned to *Stegoceras validum*. TMP1972.027.0001 and ROM53555 (*Stegoceras validum*; the latter additionally preserves squamosal ornamentation diagnostic of *Stegoceras validum*) are proportionately as wide as many *Hanssuesia sternbergi* specimens. The combined variation in width amongst *Hanssuesia sternbergi* + *Stegoceras validum* is similar to that in *Colepiocephale lambei*, of which some specimens are relatively wider than *Hanssuesia sternbergi*. Therefore, the relative width of the frontoparietal is not diagnostic for *Hanssuesia sternbergi*.

Similarly, the "more inflated" supraorbital lobes supposedly diagnostic of *Hanssuesia sternbergi* (Sullivan, 2003) are not corroborated by the RMA regressions. Supraorbital heights of *Hanssuesia sternbergi* are consistent with *Stegoceras validum* (including TMP1972.027.0001). Sullivan (2003) did not qualify the shape of a "reduced" supraorbital lobe, although he described the supraorbital lobes (lateral or lateral prefrontal lobes in their text) as "not well developed" and positioned posterior to the frontonasal boss. This description may refer in part to the variation in the anteroposterior prominence of the frontonasal boss, as well as allometric variation of frontoparietal widths. The supraorbital widths are negatively allometric with respect to W:F/P in *Stegoceras validum*, whereas growth of the frontonasal boss is isometric (Schott et al., 2011). This results in a frontonasal boss that that is proportionately wider compared to supraorbital widths in larger specimens and results in smaller, indistinct supraorbital lobes, which do not extend as medially as they do in smaller individuals. Furthermore, growth in the most posterior supraorbital width (W:Pso/Po) is likely less negatively allometric than the other two supraorbital

39

widths. Thus, the posterior portion of the supraorbital lobes widens quicker, and blends the posterior extend of the supraorbital lobes with the posterior portion of the frontoparietal dome. In *Colepiocephale lambei*, the frontoparietal possesses a medial indentation along the most anterior portion of the sutural surface for the postorbital. This indentation is retained through ontogeny and maintains the appearance of a well-developed supraorbital lobe in the taxon.

The final purported diagnostic features of *Hanssuesia sternbergi* include the depressed parietal and reduced parieto-squamosal shelf. Only two referred specimens of *Hanssuesia sternbergi* preserve a complete parietal, which makes assessing this state in most specimens difficult. The apex of the dome is positioned on the frontals in CMN8817, TMP 1987.036.0363, and TMP2017.012.0019, which results in the parietal being more shallowly anteriorly inclined than in *Stegoceras validum* (e.g., UALVP 2). The parietal of CMN 9148 (*Hanssuesia sternbergi*) however, is steeply inclined, and the supraorbital lobes are almost indistinct (Fig 5A-C in Sullivan, 2003). Conversely, the parietal of CMN38079 (*Hanssuesia stenbergi*) appears shallowly inclined, although the supraorbital lobes are more distinct than they are in UALVP 2 (Fig 5G-I in Sullivan, 2003.

The cranial dome of *Stegoceras validum* initially inflates in the either the frontals and anterior portion of the parietals (Schott et al., 2011) or solely in the frontals (Goodwin et al., 2016). Regardless, it progressively incorporates more of the parietal (and posterior shelf) and postorbital through ontogeny (Schott et al., 2011), expanding anteroposteriorly and mediolaterally respectively. TMP1972.027.0001 exemplifies the end-stage of these trends, whereby the posterior and lateral shelves are completely incorporated into the dome. Thus, a reduced parieto-squamosal shelf is a feature of mature *Stegoceras validum* (as hypothesised by Williamson and Carr, 2002), and not diagnostic to *Hanssuesia sternbergi*. Variation in the timing or degree to which the parietal is incorporated into the dome may explain the "depressed" parietal, where delayed incorporation results in a disproportionately inflated frontal, compared to the parietal. Similar variation occurs in the extent that the postorbital and posterior supraorbital is incorporated into the dome. ROM 53555, the largest historically referred *Stegoceras validum*, possesses a postorbital and posterior supraorbital that are ventrally restricted on the dome. These characteristics are shared with TMP2017.012.0019 but are unlike UALVP 2 and

TMP1972.027.0001, where these bones are dorsally arched and incorporated into the dome (Fig. 2.16). Alternatively, a depressed parietal and ventrally restricted posterior supraorbitals and postorbitals may represent healed pathologies. TMP1992.002.0003, preserves a large resorptive pathology that covers nearly the entire dorsal surface of the parietal. If that individual had survived and to continued growing, the resulting morphology would result in a "depressed" parietal relative to the (mostly) unaffected frontals.

Sullivan (2003) referred UCMP 130051, a complete pachycephalosaurid skull roof from the Judith River Formation of Montana (Goodwin 1990), to *Hanssuesia sternbergi*, but there is no reason not to refer it to *Stegoceras validum* (see Schott and Evans, 2012), except perhaps the apparent straight (but damaged) dorsal surface of the nasals. Future studies ofhis specimen, among numerous large, fused pachycephalosaurid skulls, would greatly benefit from a similar synchrotron μCT study as was performed on TMP1972.027.0001.

2.6.3 Frontoparietal allometry of *Stegoceras validum* (= *Hanssuesia sternbergi* + *Gravitholus albertae*)

Inclusion of TMP1972.027.0001 and "*Hanssuesia sternbergi*" with other *Stegoceras validum* (including 24 new specimens) in this analysis increased r values for all variables from the more restricted sample in Schott et al. (2011). Including TMP1972.027.0001 and *"Hanssuesia sternbergi"* lowers slope for frontoparietal thickness, all heights, and all widths (except for the width of the frontonasal boss) from the slopes from RMA calculated in Schott et al. (2011). Slopes for the lengths for the palpebral, posterior supraorbital, and parietal all decreased, whereas slopes for the contact length of the postorbital and the length of the frontal both increased. Despite these differences, the 95% confidence interval around these slopes did overlap with those in Schott et al. (2011). Patterns of allometry were identical, except for W:Po/stf/Sq and the L:Pso, which were found to be negatively allometric with respect to W:F/P (isometric in Schott et al. 2011).

Lower r values (< 0.9) in RMA regressions comparing frontoparietal heights to frontoparietal width may be indicative of discontinuous allometry, similar to frontoparietal thickness. The low r values associated with some frontoparietal contact lengths may be more

indicative of ontogenetically independent intraspecific variation (or small sample size for the length of the prefrontal contact).

2.6.4 Frontoparietal linear measurement transformations for PCA

Previous PCAs of linear frontoparietal measurement typically exclude a variable from the analysis to test if each resulting Principal Component correlated with frontoparietal size. Evans et al. (2013) excluded L:F/P, whereas Schott and Evans (2016) excluded W:F/P (Williamson and Brusatte (2016) did not exclude any measurements). Schott and Evans (2016) report that W:F/P was the strongest statistical predictor in bivariate analyses of *Foraminacephale brevis* (perhaps due to a larger sample size), which presumably lead them to exclude this variable from PCA. Schott et al. (2011) also found W:F/P to be the strongest statistical predictor in *Stegoceras validum* (although this sample excluded "*Hanssuesia sternbergi*"). No variables were excluded in the PCA analyses of this study. W:F/P was the strongest variable to load on PC 1 of the non-transformed and L:F proportionate iterations, thus PC 1 in these iterations explain frontoparietal size. Conversely L:F was the strongest variable to load in the W:F/P proportionate iteration, and thus PC 1 in this iteration also explained frontoparietal size. W:F/P did not strongly load on any of the first 3 PCs in the LOG-transformed iteration; however, PC 1 in this iteration as well as in Schott and Evans (2016) was most strongly loaded by H:N/N. PC 1 positively correlated with W:F/P in Schott and Evans (2016), which lead them to conclude that PC 1 explained frontoparietal size. Thus, PC 1 in all four iterations appear to be broadly explained by size. PC 1 is the only axis in the PCAs that shows any potential separation amongst specimens of "*Hanssuesia sternbergi*", *Stegoceras validum,* and TMP1972.027.0001, which suggests that frontoparietals assigned to *Gravitholus albertae* and *Hanssuesia sternbergi* are best distinguished (but not completely) from frontoparietals of *Stegoceras validum* only in their size.

The variables mainly explaining frontoparietal size (PC1) in each iteration appear to be directly related to their ranges (maximum-minimum). In the non-transformed and L:F proportionate iterations, W:F/P had the largest range, followed by the two posterior supraorbital widths and frontoparietal thickness (Appendix A1.5). Frontoparietal heights have the largest ranges in the LOG-transformed matrix (L:Pl has the absolute largest range, but a single outlier specimen nearly doubles this range). The range of H:N/N is 27.1 mm (9.9 mm – 37.0 mm) when

not transformed, and 0.574 (0.996 – 1.570) after LOG transformation; W:F/P ranges 69.8 mm (39.2 mm – 109 mm) and 0.45 (1.59 – 2.04) respectively. Given that the total range from the smallest variable (4.01 mm – L:Pl) to the largest (109 mm – W:F/P) is less than two orders of magnitude, the non-transformed PCA iteration is more appropriate than the LOG-transformed iteration for assessing frontoparietal variation in *Stegoceras validum*. Furthermore size-standardising the linear measurements with L:F recovers nearly identical variable loadings in the first three axes. The W:F/P proportionate PCA iteration recovered variable loadings different from the non-transformed and L:F proportionate PCA iterations.

Schott and Evans (2016) and Williamson and Brusatte (2016) did not include *Stegoceras validum* frontoparietals wider than 57.5 mm (W:F/P) in PCA, whereas the specimens of "*Hanssuesia sternbergi*" they included were much larger (W:F/P ranged 88.9 – 102.5 mm). This hindered direct comparisons between the purported taxa in multivariate analyses (although large *Stegoceras validum* were included in bivariate analyses). In addition to TMP1972.027.0001, this study included three other large (W:F/P > 80 mm) *Stegoceras validum* frontoparietals in PCA analyses, which allowed for a more direct comparison to "*Hanssuesia sternbergi*".

2.6.5 Frontoparietal dimorphism in large *Stegoceras validum*

Most PC 2 and 3 axes from the various PCA iterations show complete overlap between TMP1972.027.0001, "*Hanssuesia sternbergi*", and *Stegoceras validum*. Two principal components appear to divide large frontoparietals, but not solely along purported taxonomic divisions. Interestingly, the RMA regression of the H:N/Prf vs. L:Pl (which strongly antagonistically load on PC 3 of the LOG-transformed iteration), does not indicate dimorphism amongst large frontoparietals. Instead, the RMA regressions of antagonistic variables strongly loading in PC 2 of the non-transformed and L:F proportionate iterations demonstrate dimorphism in the height of the frontonasal boss amongst large *Stegoceras validum*. However, ROM 53555 is recovered as a "tall morph" based on the H:N/Prf, and a "short morph" based on H:N/N (the latter consistent with its PC 2 score, although those scores were not bimodal). A larger sample of large *Stegoceras validum* frontoparietals may clear up the inconsistencies between PC scores and antagonistic loading variable pairs, particularly with the PC 2 scores in the non-transformed iteration.

Although large, presumable adult specimens of *Stegoceras validum* can consistently be divided (aside from ROM53555) into "tall" bossed and "short" bossed morphologies (Table 2.5), juvenile specimens and subadult specimens cannot be divided into distinct clusters. Thus, the juvenile and subadult morphologies of "tall" bossed and "short" bossed adult morphologies are currently indistinguishable. Pathologies show some restriction to specimens with taller frontonasal bosses throughout ontogeny, despite there being no apparent dimorphism amongst juveniles and subadults. Amongst the cohort of examined adult *Stegoceras validum*, the only pathological specimens (TMP1972.027.0001 and TMP1979.014.0853) preserve unambiguously "tall" bossed morphologies. Although absent from flat-headed specimens (Peterson et al., 2013) pathologies appear on frontoparietal domes spanning nearly the entire ontogenetic series of *Stegoceras validum*, ranging from W:F/P of 46.07 mm (TMP1992.002.0003) to 108.99 mm (TMP1972.027.0001). Throughout the entire ontogenetic series, pathologies are only ever present on relatively taller bossed individuals, including juveniles and subadults that do not show distinct frontonasal boss dimorphism. The average PC 3 score (LOG-transformed iteration; which is largely explained by the lateral height of the frontonasal boss) of pathological specimens is lower than non-pathological specimens, and average PC 2 scores (non-transformed iteration; largely explained by both frontonasal boss heights) of pathological specimens may be weakly larger than non-pathological specimens. Average residuals of pathological specimens may also be weakly larger than non-pathological specimens in some RMA regressions based on the non-transformed and L:F proportionate PC 2 antagonistically loadings variables. In all these cases, the sample of pathological specimens is low (n = 4 - 6). An increased sample of pathological specimens would likely strengthen the statistical distinction of pathologies on "taller" bossed *Stegoceras validum*.

The pathologies observed on pachycephalosaurid frontoparietals are consistent with post-traumatic lesions resulting from intraspecific combat (Peterson and Vittore, 2012; Dyer et al., 2021) and do not show significant differences in their occurrences across genera (Peterson et al., 2013). If the apparent dimorphism in frontonasal boss heights was taxonomic, by contrast, pathologies should occur on both short bossed and tall bossed specimens.

The frontoparietal dome is hypothesised to have evolved by sexual selection, as it served as weapon during intraspecific combat for mate or territory acquisition, as occurs in modern animals, such as bovids (Geist, 1966; Peterson et al., 2013). Several studies have attempted to demonstrate dimorphism in pachycephalosaurid domes (Brown and Schlaikjer, 1943; Galton, 1971; Chapman et al. 1981; Galton and Sues 1983; Giffin 1989b). Previously proposed dimorphism in *Stegoceras validum* based on morphometric analyses (Chapman et al., 1981) has been reinterpreted as taxonomic division (*Stegoceras validum* and *Foraminacephale brevis*; Sullivan, 2000; Sullivan, 2003). Dimorphism in *Pachycephalosaurus wyomingensis* was hypothesised based on varying degrees of dome inflation but has not been discussed since the publication of Giffin (1989b). Dome inflation begins in the frontals in *Stegoceras validum* (Goodwin et al. 2016; but possibly the anterior part of the parietals as well, Schott et al., 2011), and expands to the parietals, postorbitals, posterior supraorbitals, and nasals (forming the frontonasal boss) to varying degrees. The heights of the frontonasal bosses, when compared to frontoparietal widths, show some statistically significant dimorphism amongst large *Stegoceras validum*. This can be explained by dimorphism in the extent that the dome progresses from the frontal to include the posterior portion of the nasals (like the variation in the ontogenetic anterior-posterior progression of the dome). The apparent restriction of pathologies to these "taller bossed" frontoparietals is consistent with sexual dimorphism, whereby sexes differ in the extent that the anterior portion of the dome inflates, with the thicker domed sex engaging in ritualistic intraspecific combat.

Frontoparietals of *Stegoceras validum* may also be sexually dimorphic in the extent that they incorporate the parietals into the dome. This is highly speculative, as there are only three large *Stegoceras validum* that preserve complete parietals. However, the degree that the parietal is incorporated into the dome does seem mirror the development of the frontonasal boss. TMP2017.012.0019 consistently groups as a "short bossed" *Stegoceras validum* and preserves a dome that is largely restricted to the frontals, with a shallow parietal portion of the dome, and a flat posterior parietal shelf. TMP1972.027.0001 and UALVP 2 consistently group as "tall bossed" *Stegoceras validum*, and preserve domes that incorporate more of the parietal, with the dome apex near the frontoparietal contact, and reduced (thickened) or obliterated posterior parietal shelves.

2.7 Conclusions

Synchrotron μCT imaging is suitable for identifying the fused contacts in TMP1972.027.0001 and may be an appropriate method for future studies of large, fused pachycephalosaurid skulls. *Gravitholus albertae* cannot be distinguished from *Stegoceras validum* based on its original diagnosis. Morphological differences between TMP1972.027.0001, "*Hanssuesia sternbergi*" and historically identified *Stegoceras validum* are explained by ontogenetic patterns and allometry. Thus, *Gravitholus albertae* and *Hanssuesia sternbergi* are synonyms with *Stegoceras validum*. Potential dimorphism is apparent in the heights of the frontonasal bosses (compared to anterior and posterior frontoparietal widths) and does not strictly divide specimens based on their historical taxonomic assignments. Pathologies appear to be restricted to "taller morphs", and suggest this dimorphism is sexual. A larger sample size of large and pathological *Stegoceras validum* are required to confirm this sexual dimorphism.

2.8 Literature cited

Brown, B., Schlaikjer, E.M., 1943. A study of the troödont dinosaurs with the description of a new genus and four new species. Bulletin of the American Museum of Natural History 82, 115–150.

Chapman, R.E., Galton, P.M., Sepkoski, J.J., Wall, W.P., 1981. A morphometric study of the cranium of the pachycephalosaurid dinosaur *Stegoceras*. Journal of Paleontology 55, 608–618.

Dyer, A.D., LeBlanc, A.R.H., Doschak, M.R., Currie, P.J., 2021. Taking a crack at the dome: histopathology of a pachycephalosaurid (Dinosauria: Ornithischia) frontoparietal dome. Biosis: Biological Systems 2, 248–270. https://doi.org/10.37819/biosis.002.02.0101

Eberth, D.A., Hamblin, A.P., 1993. Tectonic, stratigraphic, and sedimentologic significance of a regional discontinuity in the upper Judith River Group (Belly River wedge) of southern Alberta, Saskatchewan, and northern Montana. Canadian Journal of Earth Sciences 30, 174–200.

Evans, D.C., Brown, C.M., You, H., Campione, N.E., 2021. Description and revised diagnosis of Asia's first recorded pachycephalosaurid, *Sinocephale bexelli* gen. nov., from the Upper Cretaceous of Inner Mongolia, China. Canadian Journal of Earth Sciences 58, 981–992. https://doi.org/10.1139/cjes-2020-0190

Evans, D.C., Schott, R.K., Larson, D.W., Brown, C.M., Ryan, M.J., 2013. The oldest North American pachycephalosaurid and the hidden diversity of small-bodied ornithischian dinosaurs. Nature Communications 4, 1–10. https://doi.org/10.1038/ncomms2749

Galton, P.M., 1971. A primitive dome-headed dinosaur (Ornithischia: Pachycephalosauridae) from the Lower Cretaceous of England and the function of the dome of pachycephalosaurids. Journal of Paleontology 45, 40–47.

Galton, P.M., Sues, H.-D., 1983. New data on pachycephalosaurid dinosaurs (Reptilia: Ornithischia) from North America. Canadian Journal of Earth Sciences 20, 462–472.

Geist, V., 1966. The evolution of horn-like organs. Behaviour 27, 175–214.

Giffin, E.B., 1989a. Pachycephalosaur paleoneurology (Archosauria: Ornithischia). Journal of Vertebrate Paleontology 9, 67–77. https://doi.org/10.1080/02724634.1989.10011739

Giffin, E.B., 1989b. Notes on pachycephalosaurs (Ornithischia). Journal of Paleontology 63, 525–529. https://doi.org/10.1017/S0022336000019739

Gilmore, C.W., 1924. On *Troodon validus*: an orthopodous dinosaur from the Belly River Cretaceous of Alberta. University of Alberta Department of Geology Bulletin 1, 1–43.

Goodwin, M.B., 1990. Morphometric landmarks of pachycephalosaurid cranial material from the Judith River Formation of northcentral Montana, in: Carpenter, K., Currie, P.J. (Eds.), Dinosaur Systematics: Approaches and Perspectives. Cambridge University Press, Cambridge, pp. 189–201. https://doi.org/10.1017/cbo9780511608377.017

Goodwin, M.M., Nirody, J.A., Huynh, T., Horner, J.R., Parkinson, D.Y., Schott, R.C., Evans, D.C., 2016. Mapping and visualizing the complex internal anatomy of pachycephalosaur domes, in: Farke, A., MacKenzie, A., Miller-Camp, J. (Eds.), Society of Vertebrate Paleontology October 2016 Abstracts of Papers 76th Annual Meeting. Society of Vertebrate Paleontology, Salt Lake City, p. 145.

Hammer, Ø., Harper, D.A.T., Ryan, P.D., 2001. Past: paleontological statistics software package for education and data analysis. Palaeontologia Electronica 4, 1–9.

Jasinski, S.E., Sullivan, R.M., 2011. Re-evaluation of pachycephalosaurids from the Fruitland-Kirtland transition (Kirtlandian, Late Campanian), San Juan Basin, New Mexico, with a description of a new species of *Stegoceras* and a reassessment of *Texacephale langstoni*, in: Sullvian, R.M., Lucas, S.G., Spielmann, J.A. (Eds.), Fossil Record 3. New Mexico Museum of Natural History and Science, Bulletin 53, Albuquerque, pp. 202–215.

Lambe, L.M., 1902. New genera and species from the Belly River series (Mid-Cretaceous). Geological survey of Canada Contributions to Canadian Palaeontology 3, 25–81.

Lehman, T.M., 2010. Pachycephalosauridae from the San Carlos and Aguja formations (upper Cretaceous) of West Texas, and observations of the frontoparietal dome. Journal of Vertebrate Paleontology 30, 786–798. https://doi.org/10.1080/02724631003763532

Longrich, N.R., Sankey, J., Tanke, D., 2010. *Texacephale langstoni*, a new genus of pachycephalosaurid (Dinosauria: Ornithischia) from the upper Campanian Aguja Formation, southern Texas, USA. Cretaceous Research 31, 274–284. https://doi.org/10.1016/j.cretres.2009.12.002

Mallon, J.C., 2017. Recognizing sexual dimorphism in the fossil record: lessons from nonavian dinosaurs. Paleobiology 43, 495–507. https://doi.org/10.5061/dryad.8f6d2

Maryańska, T., 1990. Pachycephalosauria, in: Weishampel, D.B., Dodson, P., Osmólska, H. (Eds.), The Dinosauria. University of California Press, Berkley, pp. 564–577.

Maryańska, T., Chapman, R.E., Weishampel, D.B., 2004. Pachycephalosauria, in: Weishampel, D.B., Dodson, P., Osmólska, H. (Eds.), The Dinosauria. University of California Press, Berkley, pp. 464–477.

Maryańska, T., Osmólska, H., 1974. Pachycephalosauria, a new suborder of ornithischian dinosaurs. Palaeontologica Polonica 30, 45–120.

Owen, R., 1842. Report of British fossil reptiles, Pt II. Report of the British Association for the Advancement of Science 11, 60–204.

Peterson, J.E., Dischler, C., Longrich, N.R., 2013. Distributions of cranial pathologies provide evidence for head-butting in dome-headed dinosaurs (Pachycephalosauridae). PLoS ONE 8. https://doi.org/10.1371/journal.pone.0068620

Peterson, J.E., Vittore, C.P., 2012. Cranial pathologies in a specimen of *Pachycephalosaurus*. PLoS ONE 7, e36227. https://doi.org/10.1371/journal.pone.0036227

Ryan, M.J., Evans, D.C., 2005. Ornithischian dinosaurs, in: Currie, P.J., Koppelhus, E. (Eds.), Dinosaur Provincial Park: A Spectacular Ancient Ecosystem Revealed. Indiana University Press, Bloomington, pp. 313–348.

Schott, R.K., Evans, D.C., 2016. Cranial variation and systematics of *Foraminacephale brevis* gen. nov. and the diversity of pachycephalosaurid dinosaurs (Ornithischia: Cerapoda) in the Belly River Group of Alberta, Canada. Zoological Journal of the Linnean Society 179, 865–906. https://doi.org/10.1111/zoj.12465

Schott, R.K., Evans, D.C., 2012. Squamosal ontogeny and variation in the pachycephalosaurian dinosaur *Stegoceras validum* Lambe, 1902, from the Dinosaur Park Formation, Alberta. Journal of Vertebrate Palaeontology 32, 903–913.

Schott, R.K., Evans, D.C., Goodwin, M.B., Horner, J.R., Brown, C.M., Longrich, N.R., 2011. Cranial ontogeny in *Stegoceras validum* (Dinosauria: Pachycephalosauria): A quantitative model of pachycephalosaur dome growth and variation. PLoS ONE 6, e21092. https://doi.org/10.1371/journal.pone.0021092

Schott, R.K., Evans, D.C., Williamson, T.E., Carr, T.D., Goodwin, M.B., 2009. The anatomy and systematics of *Colepiocephale lambei* (Dinosauria: Pachycephalosauridae). Journal of Vertebrate Paleontology 29, 771–786. https://doi.org/10.1671/039.029.0329

Seeley, H.G., 1887. On the classification of the fossil animals commonly named Dinosauria. Proceedings of the Royal Society of London 43, 165–171.

Smith, R.J., 2009. Use and misuse of the Reduced Major Axis for line-fitting. American Journal of Physical Anthropology 140, 476–486. https://doi.org/10.1002/ajpa.21090

Sternberg, C.M., 1945. Pachycephalosauridae proposed for dome-headed dinosaurs, *Stegoceras lambei* n. sp., described. Source: Journal of Paleontology 19, 534–538.

Sues, H.-D., Galton, P.M., 1987. Anatomy and classification of the North American Pachycephalosauria (Dinosauria: Ornithischia). Paleontographica Abteilung A 198, 1–40.

Sullivan, R.M., 2006. A taxonomic review of the Pachycephalosauridae (Dinosauria: Ornithischia), in: Lucas, S.G., Sullivan, R.M. (Eds.), Late Cretaceous Vertebrates from the Western Interior. New Mexico Museum of Natural History and Science, Bulletin 35, Albuquerque, pp. 347–365.

Sullivan, R.M., 2003. Revision of the dinosaur *Stegoceras* Lambe (Ornithischia, Pachycephalosauridae). Journal of Vertebrate Paleontology 23, 181–207. https://doi.org/10.1671/0272-4634(2003)23[181:ROTDSL]2.0.CO;2

Sullivan, R.M., 2000. *Prenocephale edmontonensis* (Brown and Schlaikjer) new comb. and *P. brevis* (Lambe) new comb. (Dinosauria: Ornithischia: Pachycephalosauria) from the

upper Cretaceous of North America, in: Lucas, S.G., Heckert, A.B. (Eds.), Dinosaurs of New Mexico. New Mexico Museum of Natural History and Science, Bulletin 17, Albuquerque, pp. 117–190.

Wall, W.P., Galton, P.M., 1979. Notes on pachycephalosaurid dinosaurs (Reptilia: Ornithischia) from North America, with comments on their status as ornithopods. Canadian Journal of Earth Sciences 16, 1176–1186. https://doi.org/10.1139/e79-104

Williamson, T.E., Brusatte, S.L., 2016. Pachycephalosaurs (Dinosauria: Ornithischia) from the Upper Cretaceous (upper Campanian) of New Mexico: A reassessment of *Stegoceras novomexicanum*. Cretaceous Research 62, 29–43. https://doi.org/10.1016/j.cretres.2016.01.012

Williamson, T.E., Carr, T.D., 2002. A new genus of derived pachycephalosaurian from western North America. Journal of Vertebrate Paleontology 22, 779–801. https://doi.org/10.1671/0272-4634(2002)022[0779:ANGODP]2.0.CO;2

Woodruff, D.C., Goodwin, M.B., Lyson, T.R., Evans, D.C., 2021. Ontogeny and variation of the pachycephalosaurine dinosaur *Sphaerotholus buchholtzae*, and its systematics within the genus. Zoological Journal of the Linnean Society 193, 563–601.

2.9 Tables and Figures

Table 2.1. Endocranial measuremtents of large *Hanssuesia sternbergi*, *Stegoceras validum*, and TMP1972.027.0001. Measurements in mm

Specimen	Taxon	W:F/P	L:F	L:Olf/Soc	W:endo
TMP1972.027.0001	*"Gravitholus albertae"*	108.99	51.62	32.41 29.7% W:F/P 62.8% L:F	17.38 15.9% W:F/P 33.7% L:F
TMP2000.026.0001	*"Hanssuesia sternbergi"*	102.50	–	35.85 35.0% W:F/P	19.46 19.0% W:F/P
TMP2017.012.0019	*"Hanssuesia sternbergi"*	88.54	52.72	46.03 52.0% W:F/P 87.3% L:F	–
AMNH5388	*Stegoceras validum*	82.00	57.98	34.00 41.5% W:F/P 58.6% L:F	–
ROM53555	*Stegoceras validum*	107.93	58.00	37.07 34.3% W:F/P 63.9% L:F	20.77 19.2% W:F/P 35.8% L:F
UALVP 2	*Stegoceras validum*	80.98	52.02	34.20 42.2% W:F/P 65.7% L:F	21.00 25.9% W:F/P

Table 2.2. Loadings for PCA analyses of frontoparietal linear measurements.

Measurement's loading >|0.30| are bolded.

	Non-transformed			LOG-transformed			Scaled to L:F			Scaled to W:F/P		
	PC 1	PC 2	PC 3	PC 1	PC 2	PC 3	PC 1	PC 2	PC 3	PC 1	PC 2	PC 3
	92.0%	2.38%	1.20%	82.0%	4.62%	4.24%	82.9%	4.58%	3.16%	48.4%	16.0%	10.5%
H:n/n	0.16048	**0.45984**	0.15906	**0.32976**	0.013993	-0.26655	0.18434	**0.47183**	0.023842	-0.02673	**0.41585**	0.11443
H:n/prf	0.11258	**0.4625**	-0.0403	0.27923	-0.16853	**-0.6008**	0.12355	**0.4708**	-0.1478	0.024788	**0.30056**	-0.08007
H:pfr/pl	0.11656	0.24742	0.28239	0.28676	**-0.30724**	0.017972	0.1175	0.29777	0.17857	0.098374	**0.35223**	0.10761
H:pl/pso	0.10507	0.14057	0.045447	**0.31099**	**-0.66856**	0.20084	0.12212	0.15281	0.13547	0.06235	**0.32122**	0.067709
H:pso/po	0.11422	0.22138	0.033067	0.23633	-0.24957	-0.07766	0.11737	0.24928	0.069222	0.13073	0.21888	-0.02208
W:n/pfr	0.15698	0.081494	0.58689	0.22431	0.21549	0.15057	0.14008	0.11956	**0.67662**	0.18039	-0.07767	**0.78883**
W:pfr/pl	0.24132	**-0.34176**	-0.09083	0.19598	0.27982	0.002274	0.20664	**-0.32424**	-0.13925	0.28319	-0.15066	-0.23865
W:pl/pso	**0.36612**	-0.29166	0.19718	0.22312	0.1336	0.15394	**0.34115**	-0.25588	0.22851	**0.36789**	0.17577	0.0525
W:pso/po	**0.43801**	0.10582	-0.03898	0.23729	0.13746	0.045046	**0.44529**	0.052939	0.058169	0.26106	0.28322	0.038886
W:f/p	**0.48221**	-0.10908	-0.26645	0.26603	0.26474	-0.00878	**0.51061**	-0.19221	-0.13006		NA	
W:po/stf/sq	0.2937	**-0.33875**	0.25067	0.22889	0.22552	0.18	0.26639	**-0.30986**	0.21918	0.27169	0.000849	0.129
L:pl	0.088145	0.051352	**0.3108**	0.28227	-0.03482	**0.62451**	0.09012	0.070216	0.27068	0.094096	0.20782	0.21596
L:pso	0.096294	0.060137	0.003736	0.18241	0.10498	-0.10763	0.071932	0.076956	-0.09213	0.18652	0.07097	-0.14697
L:po	0.24325	-0.0074	**-0.32745**	0.23189	0.15516	-0.06591	0.24492	-0.07974	-0.23183	0.10752	-0.01359	-0.23379
L:f	0.12781	-0.10221	0.21464	0.10528	0.13659	0.002929		NA		**0.72032**	-0.22726	-0.18634
T:f/p	**0.32217**	0.28556	**-0.33667**	0.28761	0.17424	-0.18565	**0.35537**	0.20901	**-0.43508**	-0.06248	**0.47082**	**-0.32573**

Table 2.3. RMA results of frontoparietal widths vs L:F. p values < 0.05 are bolded.

		n	r	slope	ci	incercept	ci	p	allometry
W:N/Prf	*Stegoceras validum*	31	0.70	1.55	1.19, 1.89	-1.15	- 1.70, -0.56	**1.03E-5**	+
	Hanssuesia sternbergi	6	0.42	2.88	-0.50, 9.48	-3.42	-14.7, 2.44	0.41	NA
	Total	38	0.78	1.70	1.36, 2.03	-1.38	-1.94, -0.82	**6.68E-9**	+
W:Prf/Pl	*Stegoceras validum*	33	0.73	1.20	0.89, 1.46	-0.35	-0.78, 0.14	**1.34E-6**	Iso
	Hanssuesia sternbergi	6	0.38	1.91	-0.43, 7.07	-1.54	-10.4, 2.51	0.46	NA
	Total	40	0.80	1.34	1.07, 1.59	-0.58	-0.99, -0.13	**8.05E-10**	+
W:Pl/Pso	*Stegoceras validum*	32	0.72	1.16	0.84, 1.46	-0.16	-0.63, 0.37	**4.03E-6**	Iso
	Hanssuesia sternbergi	6	0.71	1.22	0.12, 2.01	-0.18	-1.54, 1.72	0.11	NA
	Total	38	0.78	1.37	1.07, 1.63	-0.49	-0.92, 0.02	**5.90E-9**	+
W:Pso/Po	*Stegoceras validum*	32	0.71	1.13	0.85, 1.39	-0.07	-0.49, 0.40	**5.79E-6**	Iso
	Hanssuesia sternbergi	6	0.56	1.49	-0.34, 4.17	-0.58	-5.18, 2.61	0.25	NA
	Total	39	0.77	1.47	1.14, 1.75	-0.61	-1.06, -0.05	**7.91E-9**	+
W:F/P	*Stegoceras validum*	33	0.69	1.48	1.12, 1.82	-0.67	-1.22, -0.08	**7.6E-5**	+
	Hanssuesia sternbergi	6	0.65	1.20	0.03, 3.03	-0.10	-3.22, 1.94	0.16	NA
	Total	40	0.77	1.79	1.43, 2.10	-1.16	-1.64, -0.55	**5.88E-9**	+
W:Po/stf/Sq	*Stegoceras validum*	19	0.83	1.48	1.00, 1.80	-0.81	-1.35, 0.00	**8.89E-6**	+
	Hanssuesia sternbergi	6	0.77	2.17	0.35, 5.94	-1.92	-8.42, 1.26	0.12	NA
	Total	25	0.86	1.85	1.32, 2.23	-1.4	-2.04, -0.50	**2.81E-8**	+

Table 2.4. RMA results of frontoparietal heights vs W:F/P. p values < 0.05 are bolded.

		n	r	slope	ci	incercept	ci	p	allometry
H:N/N	*Stegoceras validum*	32	0.80	2.01	1.34, 2.59	-2.32	-3.35, -1.18	**3.45E-8**	+
	Hanssuesia sternbergi	6	0.36	4.92	-6.84, 13.6	-8.25	-25.5, 14.7	0.48	NA
	Total	39	0.83	1.70	1.28, 2.10	-1.81	-2.53, -1.07	**6.03E-11**	+
H:N/Prf	*Stegoceras validum*	31	0.83	1.73	1.26, 2.16	-1.94	-2.70, -1.11	**1.07E-8**	+
	Hanssuesia sternbergi	6	0.10	7.82	-12.3, 25.2	-14.1	-48.3, 25.0	0.84	NA
	Total	38	0.83	1.55	1.23, 1.89	-1.65	-2.24, -1.08	**1.81E-10**	+
H:Prf/Pl	*Stegoceras validum*	39	0.78	2.09	1.56, 2.56	-2.54	-3.35, -1.65	**4.71E-9**	+
	Hanssuesia sternbergi	8	0.40	4.49	-0.65, 13.3	-7.49	-25.1, 2.51	0.33	NA
	Total	48	0.84	1.74	1.44, 2.07	-1.97	-2.57, -1.44	**1.57E-13**	+
H:Pl/Pso	*Stegoceras validum*	38	0.73	1.97	1.45, 2.37	-2.43	-3.15, -1.54	**1.55E-7**	+
	Hanssuesia sternbergi	9	0.20	3.55	1.26, 13.0	-5.71	-24.3, -1.27	0.61	NA
	Total	48	0.84	1.71	1.43, 1.99	-2.01	-2.53, -1.52	**7.12E-14**	+
H:Pso/Po	*Stegoceras validum*	39	0.80	1.67	1.20, 1.98	-1.74	-2.29, -0.96	**1.09E-9**	+
	Hanssuesia sternbergi	9	0.65	5.29	1.42, 13.3	-9.02	-25, -1.48	0.057	+?
	Total	49	0.87	1.48	1.28, 1.68	-1.45	-1.80, -1.09	**4.23E-16**	+

Table 2.5. Mixture analysis group assignments based on LOG-transformed PC 3 scores of large (W:F/P > 80 mm) *Stegoceras validum.* Holotypes designated with asterisk.

Specimen	Previous taxonomic assignment	Reference	LOG PCA (PC 3)	H:N/N vs W:Prf/Pl residuals	H:N/Prf vs W:Po/stf/Sq residuals
AMNH 5388	*Stegoceras validum*	Brown and Schlaikjer (1943)	Taller	Taller	Taller
CMN 192	*Hanssuesia sternbergi*	Brown and Schlaikjer (1943)	NA	Taller	NA
CMN 8817*	*Hanssuesia sternbergi*	Sullivan (2003)	Shorter	Shorter	Shorter
CMN 9148	*Hanssuesia sternbergi*	Sullivan (2003)	Taller	Taller	Taller
ROM 53555	*Stegoceras validum*	Schott et al. (2011)	Taller	Shorter	Taller
TMP1972.027.0001*	*Gravitholus albertae*	Wall and Galton (1979)	Taller	Taller	Taller
TMP1979.014.0853	*Hanssuesia sternbergi*	Sullivan (2003)	Taller	Taller	Taller
TMP1987.036.0363	*Hanssuesia sternbergi*	Sullivan (2003)	Shorter	Shorter	Shorter
TMP2017.012.0019	*Hanssuesia sternbergi*	This study	Shorter	Shorter	Shorter
UALVP 2	*Stegoceras validum*	Gilmore 1924; Schott et al. (2011)	Taller	Taller	Taller

Table 2.6. RMA results for linear frontoparietal measurements vs frontoparietal width amongst *Stegoceras validum*. Thin specimens preserve frontoparietal thicknesses ≤ TMP1984.005.0001.

	Group	n	r	slope	ci	incercept	ci	p	allometry
H:N/N vs.	All	39	0.68	2.44	1.67, 3.09	-2.77	-3.85, -1.47	1.96E-6	+
W:Prf/Pl	Excluding thin	31	0.74	1.66	1.21, 1.98	-1.44	-1.95, -0.71	2.41E-6	+
H:N/Prf vs.	All	40	0.63	2.33	1.59, 2.88	-2.68	-3.60, -1.48	1.38 E-5	+
W:Prf/Pl	Excluding thin	30	0.64	1.78	1.12, 2.27	-1.74	-2.56, -0.66	1.43 E-4	+
H:N/N vs.	All	26	0.87	1.43	1.10, 1.73	-1.12	-1.62, -0.59	1.03E-7	+
W:Po/stf/Sq	Excluding thin	24	0.82	1.36	1.05, 1.66	-1.01	-1.49, -0.48	7.48E-7	+
H:N/Prf vs.	All	26	0.70	1.32	0.94, 1.68	-1.32	-1.62, -0.41	7.62E-5	ISO
W:Po/stf/Sq	Excluding thin	24	0.67	1.26	0.87, 1.63	-0.93	-1.52, -0.29	3.75E-4	ISO
H:N/Prf vs.	All	40	0.76	1.43	1.06, 1.77	-0.47	-0.87, -0.04	1.09E-8	+
L:Pl	Excluding thin	30	0.71	1.12	0.65, 1.48	-0.09	-0.50, 0.45	1.32E-5	ISO

Table 2.7. RMA results for linear frontoparietal measurements vs frontoparietal width
Stegoceras validum

	n	r	slope	ci	incercept	ci	p	allometry
H:N/N	39	0.83	1.70	1.28, 2.08	-1.81	-2.50, -1.06	6.03E-11	+
H:N/Prf	38	0.83	1.55	1.24, 1.87	-1.65	-2.22, -1.11	1.82E-10	+
H:Prf/Pl	48	0.84	1.74	1.44, 2.05	-1.97	-2.54, -1.44	1.57E-13	+
H:Pl/Pso	48	0.84	1.71	1.44, 1.97	-2.01	-2.49, -1.55	7.12E-14	+
H:Pso/Po	49	0.87	1.48	1.28, 1.68	-1.45	-1.80, -1.10	4.23E-16	+
T:F/P	67	0.86	2.14	1.86, 2.40	-2.28	-2.79, -1.80	6.44E-21	+
L:Prf	10	0.79	0.72	0.48, 0.97	-0.12	-0.53, 0.29	6.47E-3	_
L:Pl	50	0.83	1.08	0.82, 1.28	-0.80	-1.18, -0.33	1.02E-13	Iso
L:Pso	50	0.91	0.74	0.66, 0.83	-0.04	-0.21, 0.11	4.00E-20	_
L:Po	34	0.89	1.03	0.83, 1.21	-0.31	-0.65, 0.07	2.41E-12	Iso
L:F	40	0.77	0.56	0.44, 0.65	0.65	0.48, 0.86	5.88E-9	_
L:P	24	0.93	0.72	0.58, 0.83	0.44	0.25, 0.68	8.05E-11	_
W:N/Prf	42	0.91	0.91	0.79, 1.02	-0.21	-0.42, -0.01	7.84E-17	Iso
W:Prf/Pl	49	0.92	0.74	0.66, 0.82	0.31	0.17, 0.45	2.87E-21	_
W:Pl/Pso	51	0.96	0.76	0.71, 0.81	0.42	0.33, 0.50	7.44E-30	_
W:Pso/Po	52	0.98	0.83	0.80, 0.87	0.33	0.26, 0.39	1.05E-38	_
W:Po/stf/Sq	32	0.96	0.85	0.74, 0.96	0.14	-0.06, 0.34	2.01E-17	_

Table 2.8. Non-linear relationships of linear frontoparietal measurements vs. W:F/P.
Smallest AIC are bolded.

	Allometry	Linear	Power	Exponential	Von Bertalanffy	Michaelis	Logistic	Gompertz	Hill
H:N/N	+	925.66	866.59	929.41	858.33	956.24	883.62	870.43	**858.31**
H:N/Prf	+	767.19	**764.88**	770.16	764.9	779.24	767.74	765.99	767.39
H:Prf/Pl	+	689.79	657.25	693.21	**656.89**	720.31	671.12	663.84	658.61
H:Pl/Pso	+	**511.5**	513.58	514.03	513.66	521.84	516.87	515.8	516.01
H:Pso/Po	+	713.18	**712.64**	716.24	713.44	726.49	731.5	721.71	715.21
T:F/P	+	3592	2921.3	3608.3	**2837.2**	4484	3117.1	2933.7	2838.3
L:Prf	_	44.3	**43.4**	43.6	48.6	51.2	45.0	45.5	44.6
L:Pl	Iso	282.9	279.5	285.6	276.5	277.1	263.1	269.5	**248.4**
L:Pso	_	214.8	208.1	217.6	207.2	**205.2**	205.5	206.1	207.4
L:Po	Iso	657.6	655.2	**653.3**	661.2	664.4	656.7	655.3	657.8
L:F	_	1024	980.7	1027.1	977.7	**975.2**	979.1	978.3	980.0
L:P	_	659.1	655.2	663.2	647.9	667.2	607.8	628.2	**468.2**
W:N/Prf	Iso	367.0	367.0	369.9	367.4	**365.9**	373.8	370.5	369.3
W:Prf/Pl	_	833.4	**829.7**	837.1	830.9	847.9	840.9	835.4	832.4
W:Pl/Pso	_	925.9	**924.4**	930.6	924.5	965.1	925.9	924.9	926.9
W:Pso/Po	_	588.7	591.0	592.9	590.7	631.1	**560.0**	574.3	565.8
W:Po/stf/Sq	_	593.8	575.3	599.4	566.9	567.5	532.9	548.7	**499.2**
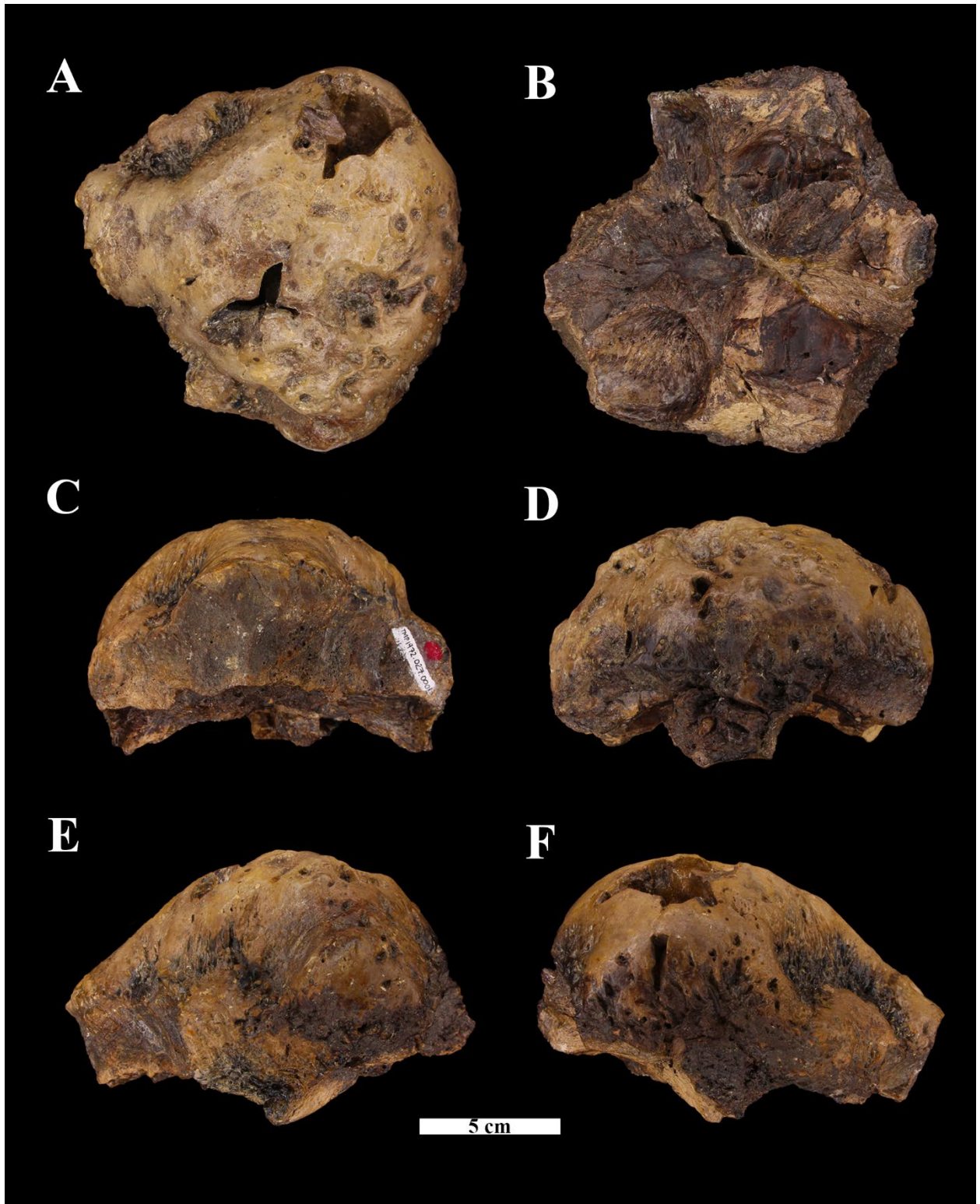
Figure 2.1. TMP1972.027.0001, the holotype of "*Gravitholus albertae*" Wall and Galton 1979. Photographs of the skull roof in dorsal (A), ventral (B), anterior (C), posterior (D), left lateral (E), and right lateral (F) views.
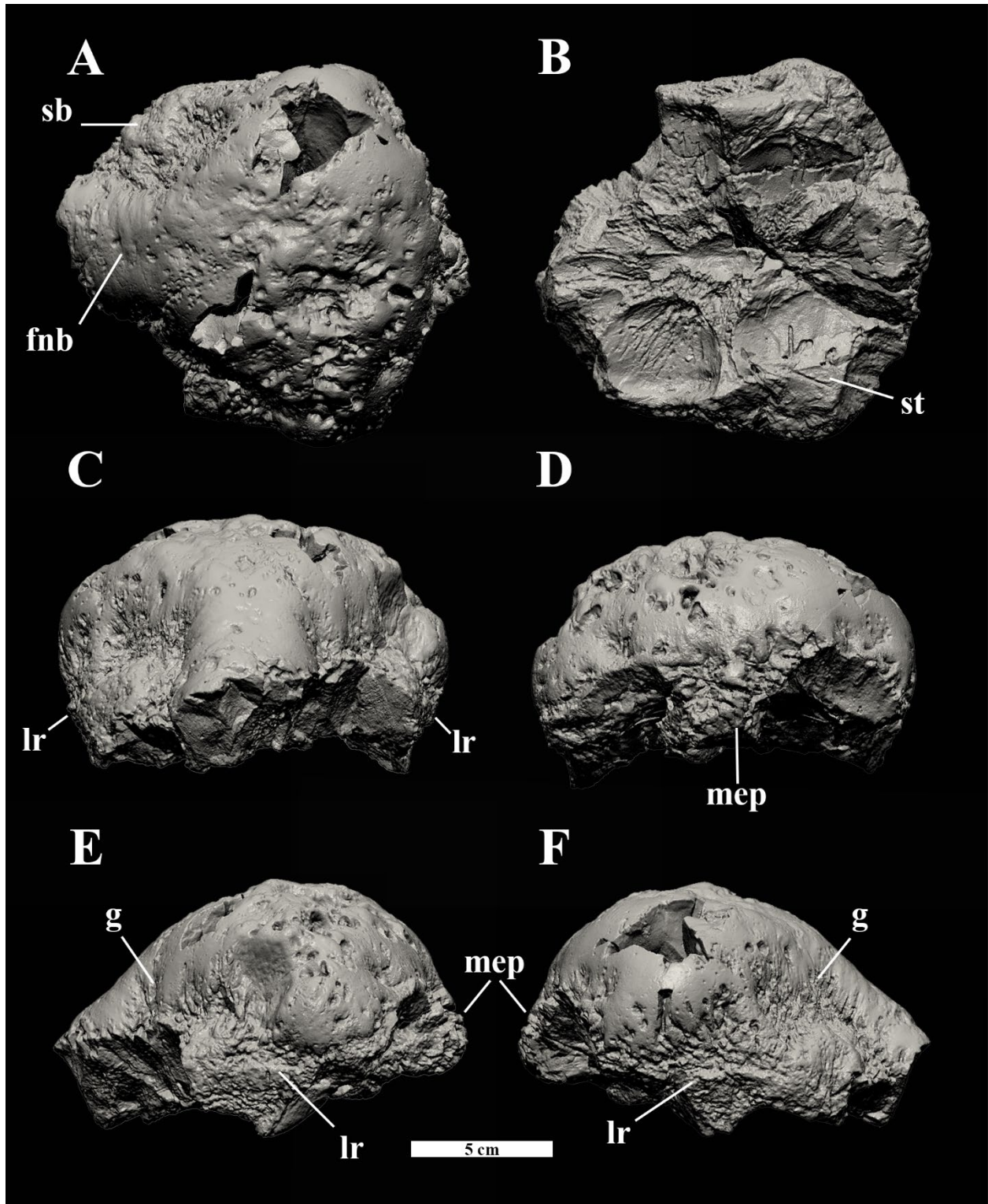
Figure 2.2. Orthographic projections of TMP1972.027.0001. Images of 3-D Surface scan images? Laser scan images in dorsal (A), ventral (B), anterior (C), posterior (D), left lateral (E),

and right lateral (F) views. Abbreviations: **fnb** – frontonasal boss; **g** – groove; **lr** – lateral ridge; **mep** – medial extension of the parietal; **sb** – supraorbital boss; **st** – groove for the squamosal tongue.
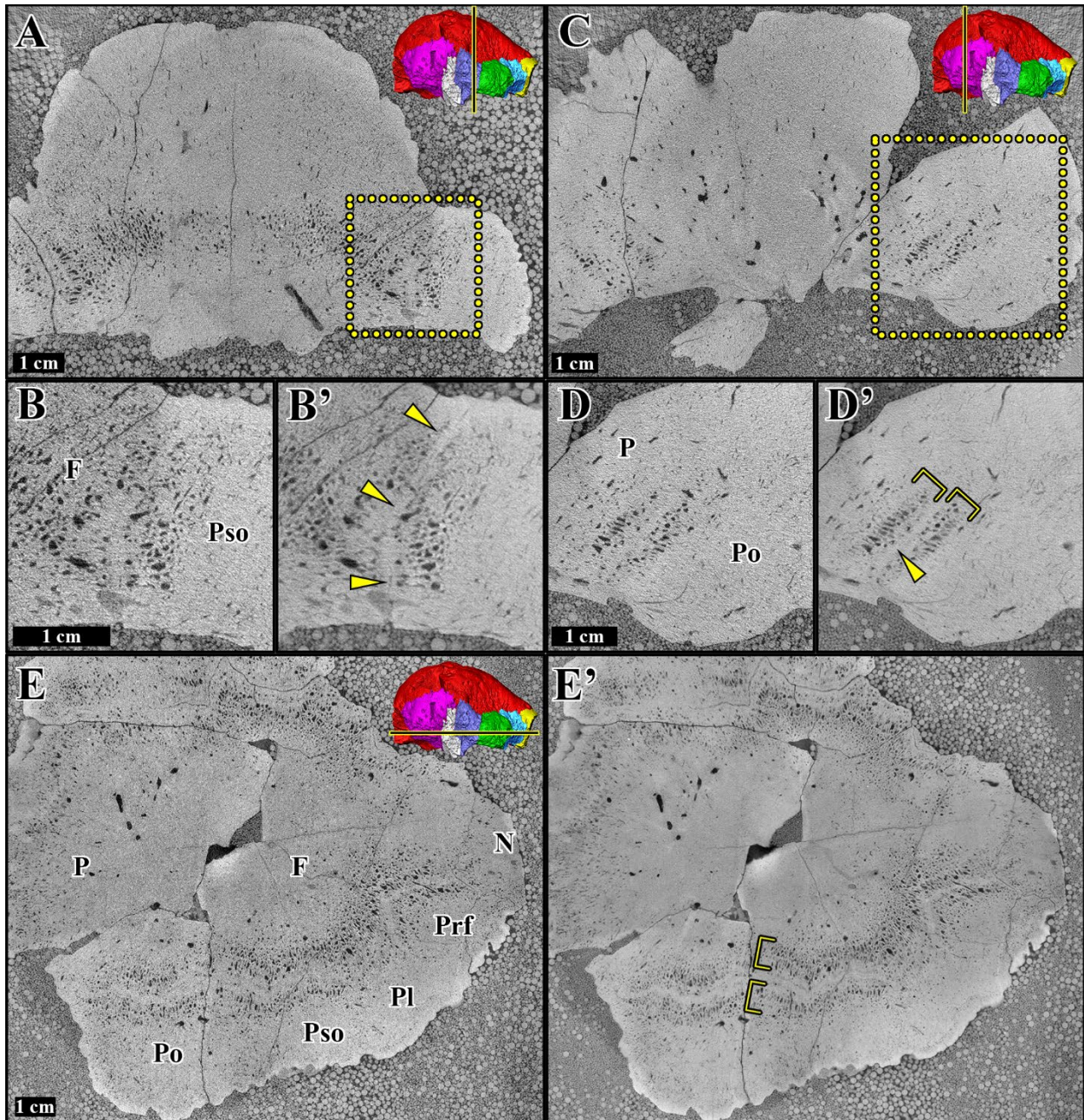
Figure 2.3. Synchrotron-CT images of TMP 1972.027.0001. A) Coronal plane across the frontal-posterior supraorbital sutures in posterior view. B) Enlarged area around the right frontal-posterior supraorbital suture. B') Same area, averaged from a five 50 μm thick slices. Arrows identify the frontal-posterior supraorbital suture. C) Coronal plane across the parietal-postorbital sutures in posterior view. D) Enlarged area around the right parietal-postorbital suture. D') Same area, averaged from a five 50 μm thick slices. Arrow identifies the parietal-postorbital suture.

Brackets identify the vascularized area adjacent to the suture. E) Horizontal plane across the lower half of the peripheral element contacts in dorsal view. E') Same area, averaged from a five 50 μm thick slices. Brackets identify the vascularized area adjacent to the sutures.
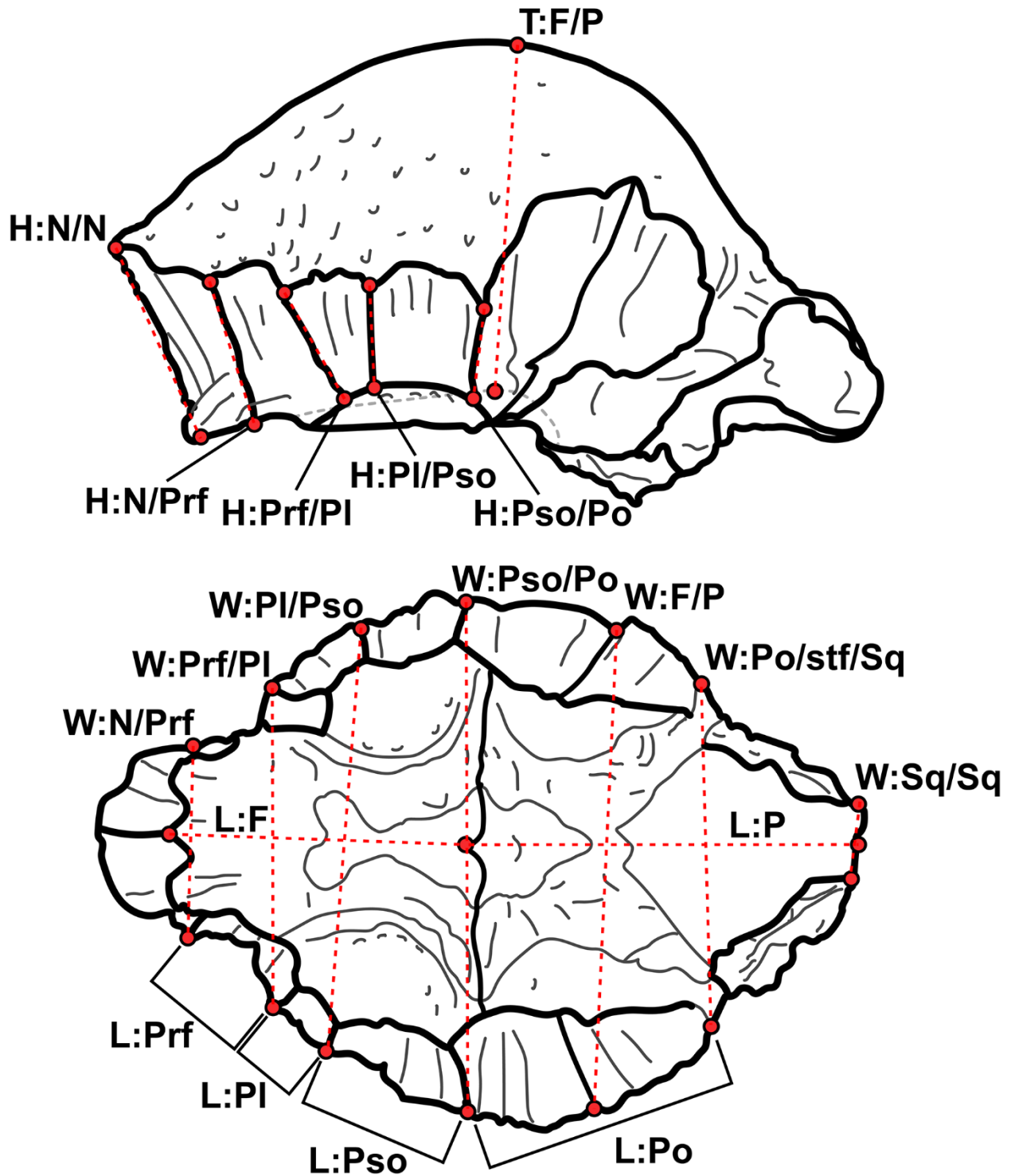
Figure 2.4. Linear measurements used in morphometric analyses. Line drawings based on UALVP 2. H:N/N – Height at the nasal/nasal contact; H:N/Prf – height at the nasal/prefrontal contact; H:Prf/Pl – height at the prefrontal/palpebral contact; H:Pl/Pso – height at the

palpebral/posterior supraorbital contact; H:Pso/Po – height at the posterior supraorbital/postorbital contact; T:F/P – frontoparietal thickness; W:N/Prf – width at the nasal/prefrontal contact; W:Prf/Pl – width at the prefrontal/palpebral contact; W:Pl/Pso – width at the palpebral/posterior supraorbital contact; W:Pso/Po – width at the posterior supraorbital/postorbital contact; W:F/P – Width at the frontal/parietal contact. W:Po/stf/Sq – Width at the postorbital/squamosal contact (or at posterior extent of postorbital is the supratemporal fenestra is present; L:F – length of the frontal; L:P – length of the parietal; L:Prf – length of the prefrontal; L:Pl – length of the palpebral; L:Pso – length of the posterior supraorbital; L:Po – length of the postorbital.
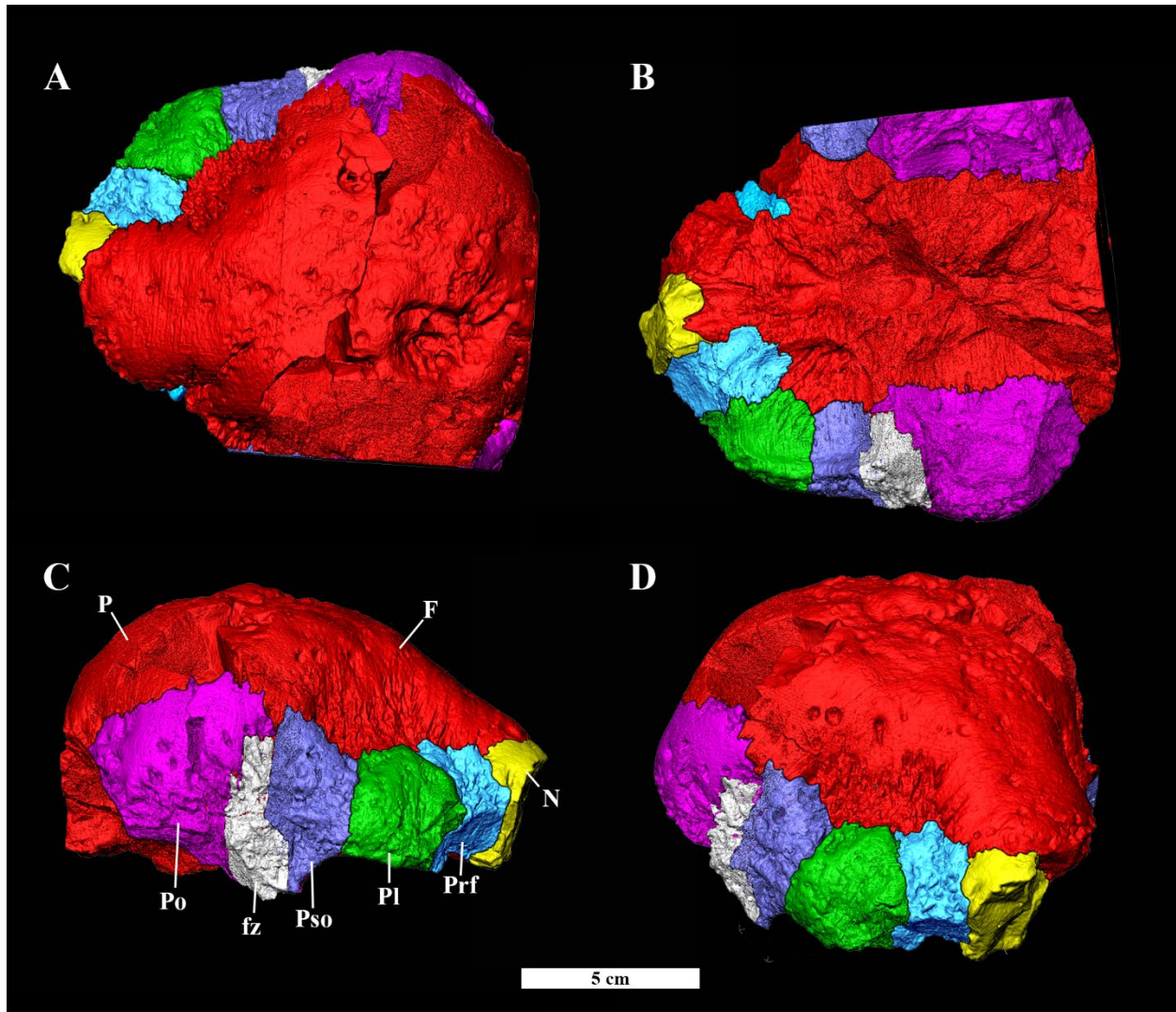
Figure 2.5. Segmented model of TMP1972.027.0001. Skull roof in dorsal (A), ventral (B), right lateral (C), and right anterodorsal (oblique) views (D). **F,** frontal; **fz,** fused zone containing postorbital-posterior supraorbital contact, **N,** nasal, **P,** parietal, **Pl,** palpebral, **Prf,** prefrontal, **Pso,** posterior supraorbital.

A) TMP1972.027.0001
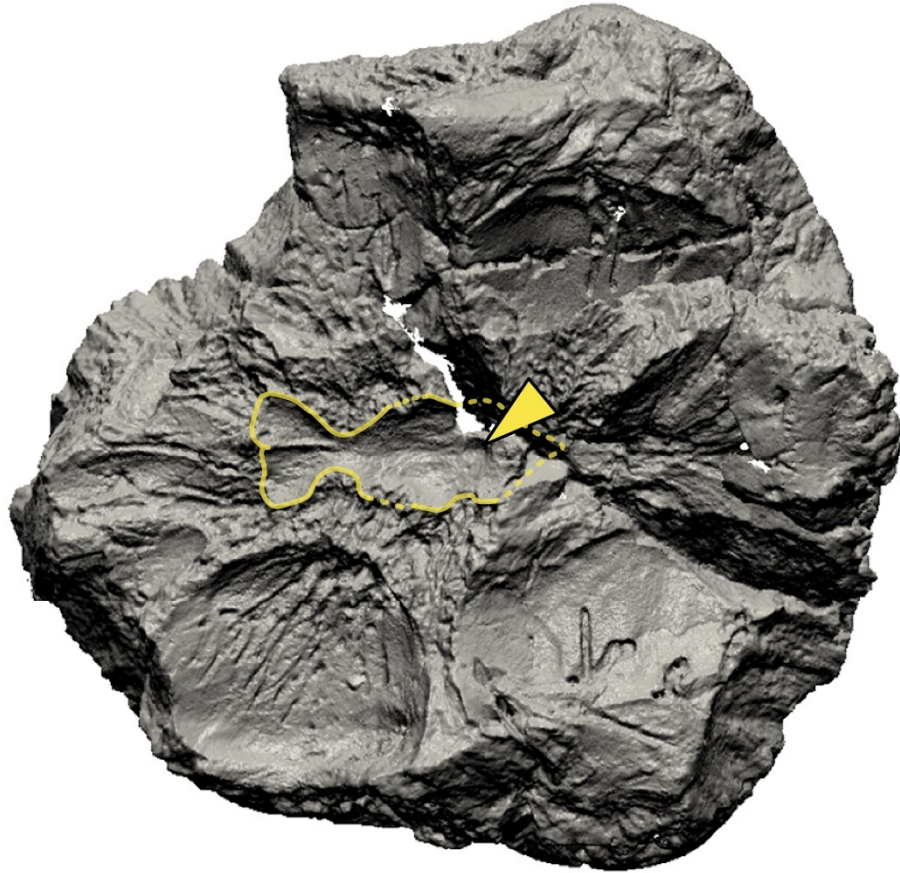
B) UALVP 2

5 cm
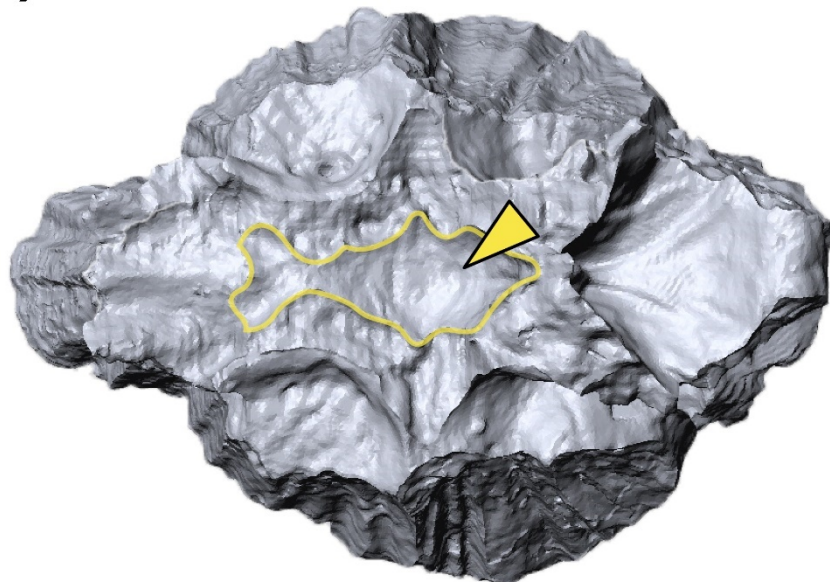
Figure 2.6. Endocranial outlines of TMP1972.027.0001 and UALVP 2. Computer model of TMP1972.027.0001 (A) and a segmented model of the frontoparietal model of UALVP 2 (B). Arrows indicates the pit for the supraoccipital cartilage.
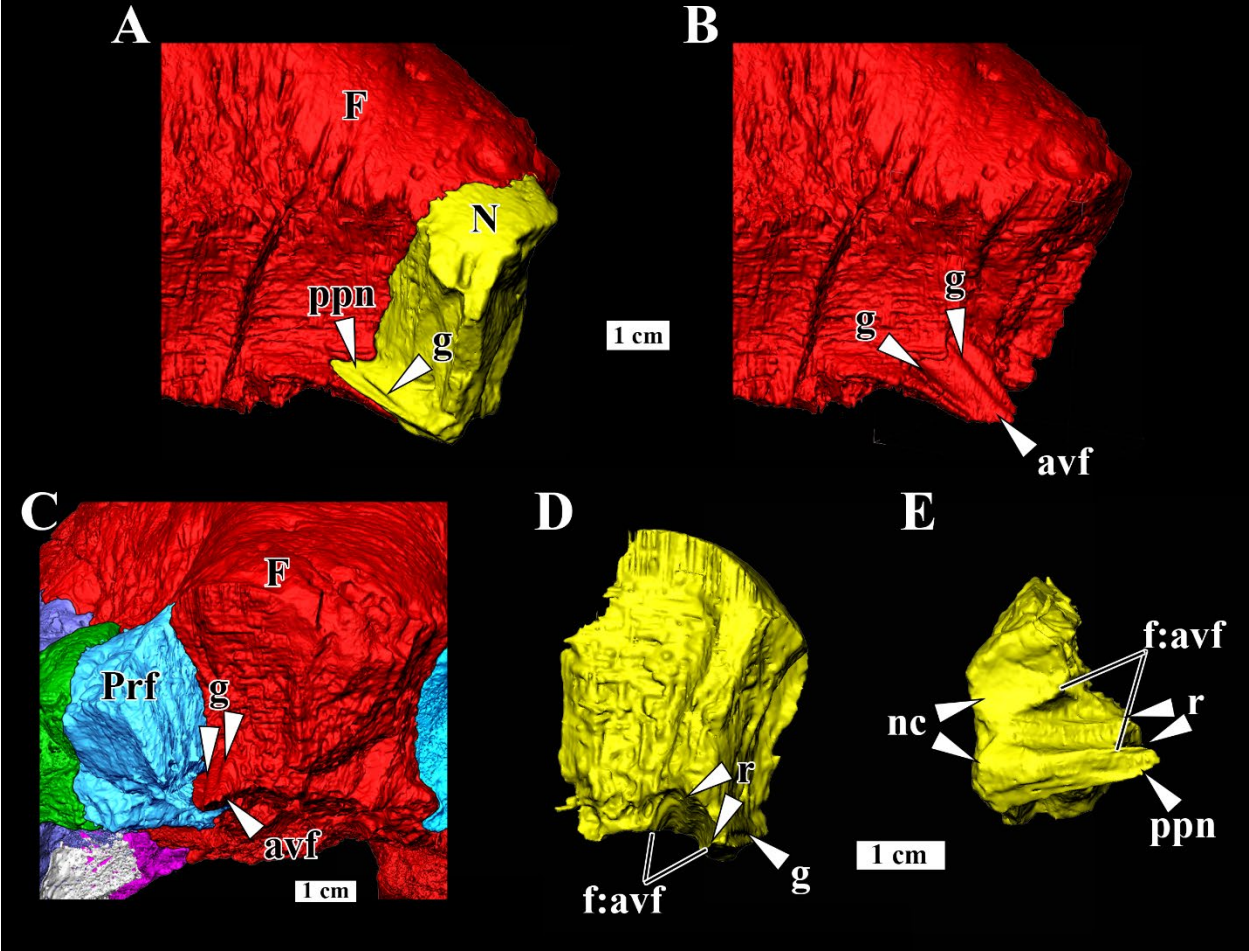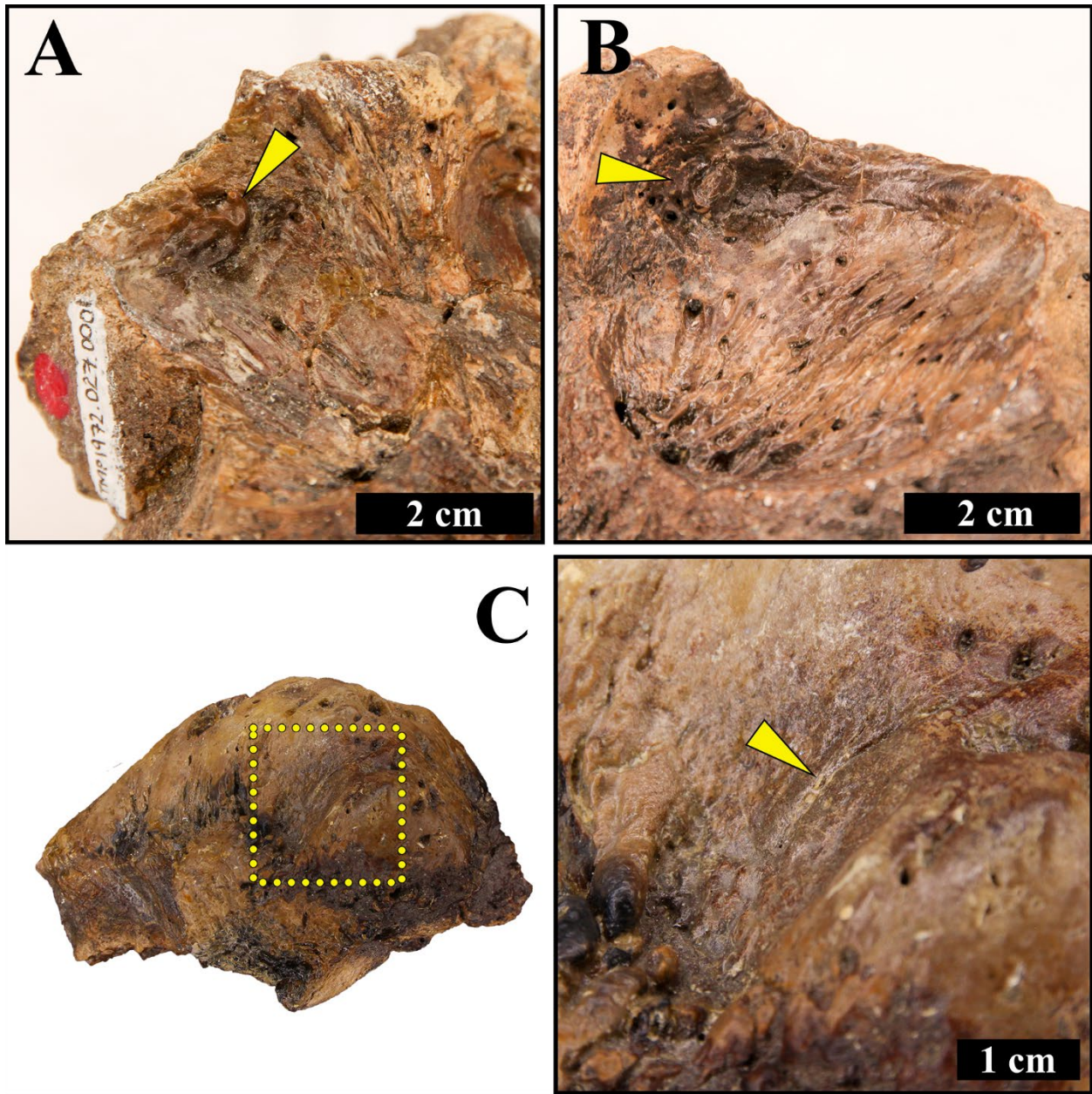
Figure 2.8. Additional photographs of TMP1972.027.0001. Posterodorsal muscle scars (arrows) on the left (A) and right (B) orbital roof. C) An open frontoparietal/postorbital suture (arrow) situated within a depressed lesion. Dashed box on large image indicates position of image C.

74
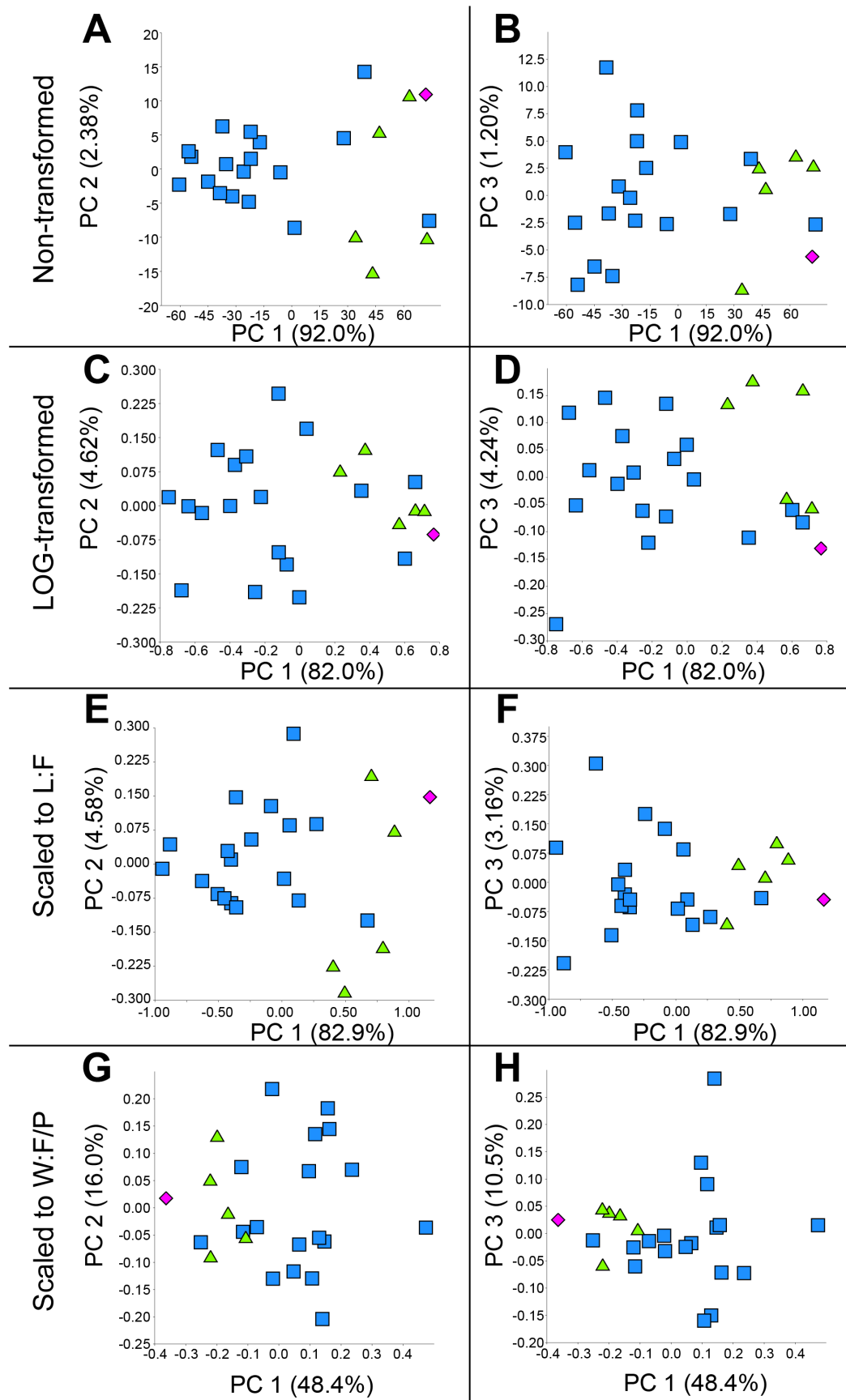
Figure 2.9. Frontoparietal Principal Component Analysis of TMP1972.027.0001, "*Hanssuesia sternbergi*", and *Stegoceras validum*. TMP1972.027.0001 – purple diamond; "*Hanssuesia sternbergi*" – green triangles; *Stegoceras validum* – blue squares. A and B) Non-transformed linear measurement results. C and D) LOG-transformed linear measurement results. E and F) Frontal length proportionate transformed linear measurement results. G and H) Frontoparietal Width proportionate transformed linear measurement results.
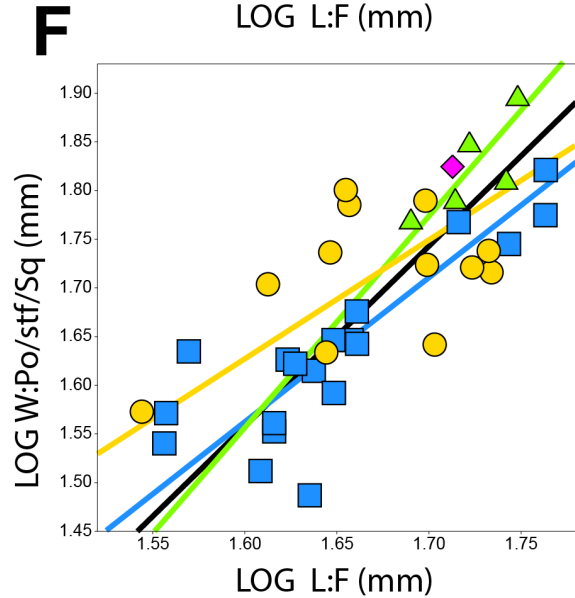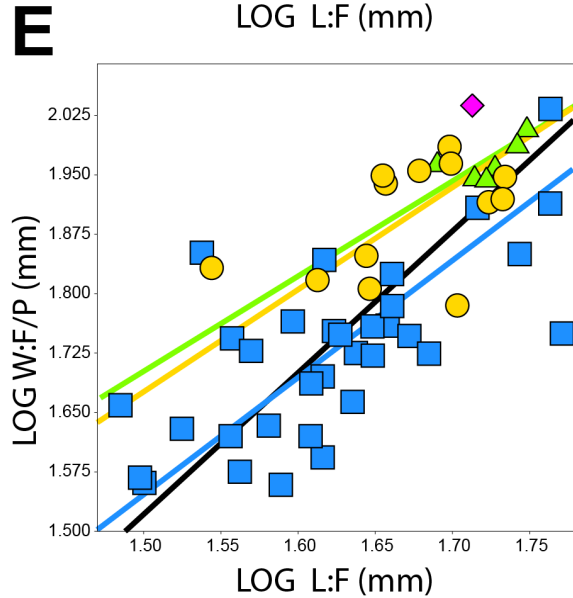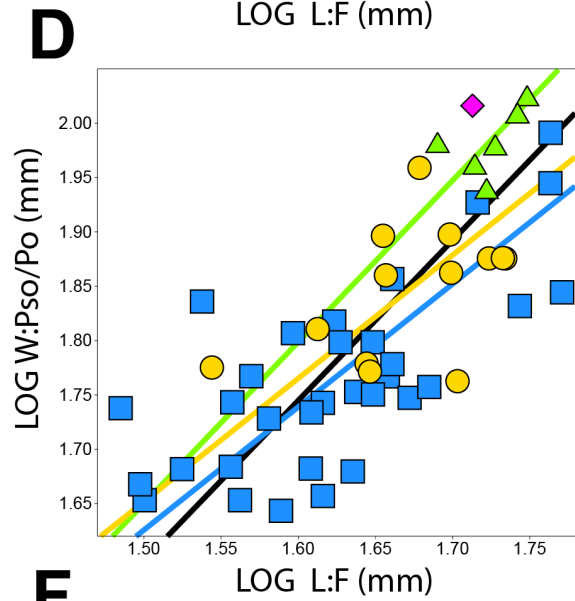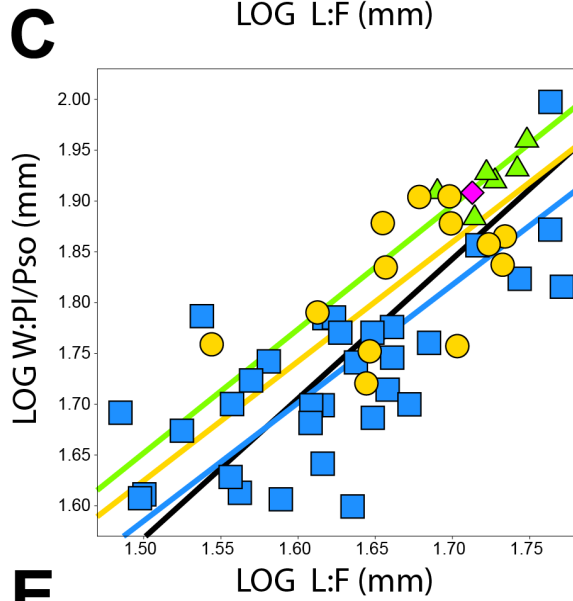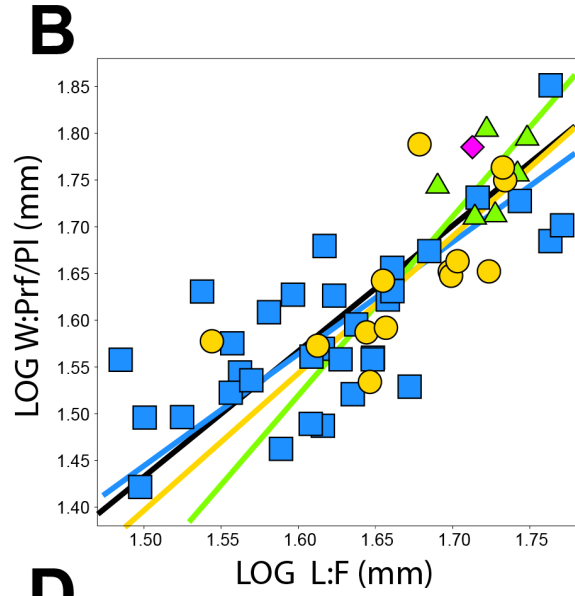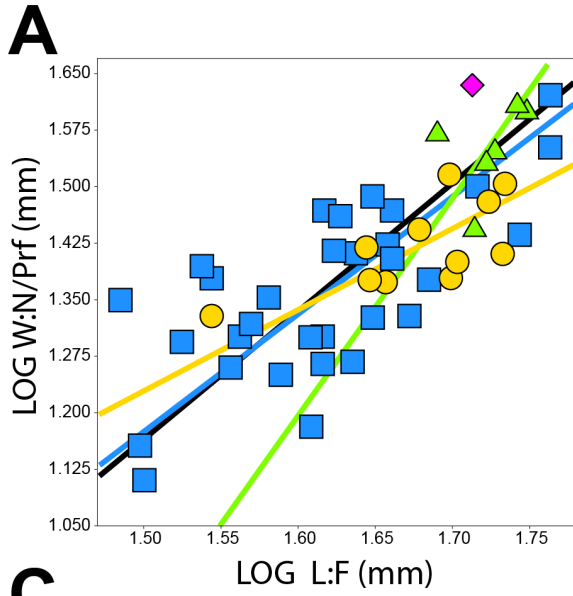
Figure 2.10. RMA regressions of various frontoparietal widths vs. frontal length. Purple Diamond – TMP1972.027.0001; blue squares – *Stegoceras validum*; green triangles – *Hanssuesia sternbergi*; yellow circles – *Colepiocephale lambei*; black line – TMP1972.027.0001 + *Hanssuesia sternbergi* + *Stegoceras validum*. A) LOG width at the contacts of the nasals and prefrontals (**W:N/Prf**; mm) vs. LOG frontal length (**L:F**; mm). B) LOG width at the contacts of the prefrontals and palpebrals (**W:Prf/Pl**; mm) vs. LOG frontal length (mm). C) LOG width at the contacts of the palpebrals and posterior supraorbitals (**W:Pl/Pso**; mm) vs. LOG frontal length (mm). D) LOG width at the contacts of the posterior supraorbitals and postorbitals (**W:Pso/Po**; mm) vs. LOG frontal length (mm). E) LOG width at the contacts of the frontal and parietal (**W:F/P; mm**) vs. LOG frontal length (mm). LOG temporal (**W:Po/stf/Sq**; mm) vs. LOG frontal length.
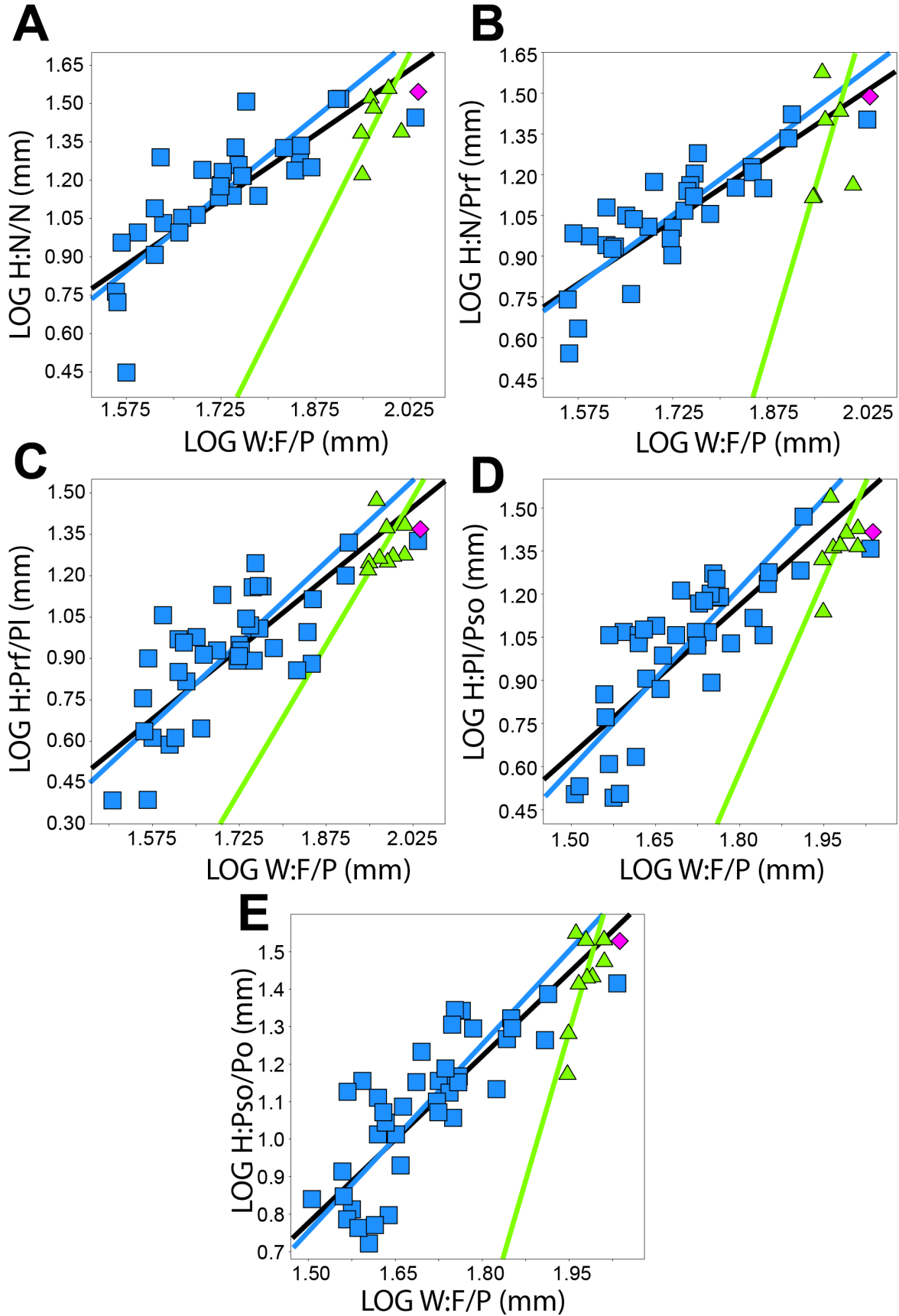
Figure 2.11. RMA regressions of various frontoparietal heights vs. frontoparietal width. Purple diamond – TMP1972.027.0001; blue squares – *Stegoceras validum*; green triangles – *Hanssuesia sternbergi*; black line – TMP1972.027.0001 + *Hanssuesia sternbergi* + *Stegoceras validum*. A) LOG height at the contacts of the nasals (**H:N/N**; mm) vs. LOG frontoparietal width (**W:F/P**; mm). B) LOG height at the contacts of the nasal and prefrontal (**H:N/Prf**; mm) vs. LOG frontoparietal width (**W:F/P**; mm). C) LOG height at the contacts of the prefrontal and palpebral (**H:Prf/Pl**; mm) vs. LOG frontoparietal width (**W:F/P**; mm). D) LOG height at the contacts of the palpebral and posterior supraorbital (**H:Pl/Pso**; mm) vs. LOG frontoparietal width (**W:F/P**; mm). A) LOG height at the contacts of the posterior supraorbital and postorbital (**H:Pso/Po**; mm) vs. LOG frontoparietal width (**W:F/P**; mm).

A Non-transformed

W:F/P > 80mm

W=0.89	A=0.48	D=0.14	AIC	Pathology
p=0.20	p=0.17	p=0.092	Uni=**57.18**	t=1.89
			Bi=60.45	p=0.072

PC2 / PC1 / Frequency

B LOG-transformed

W:F/P > 80mm

W=0.83	A=0.74	D=0.13	AIC	Pathology
p=**0.040**	p=**0.033**	p=0.12	Uni=-23.81	t=2.14
			Bi=**-27.03**	p=**0.044**

PC3 / PC1 / Frequency

80
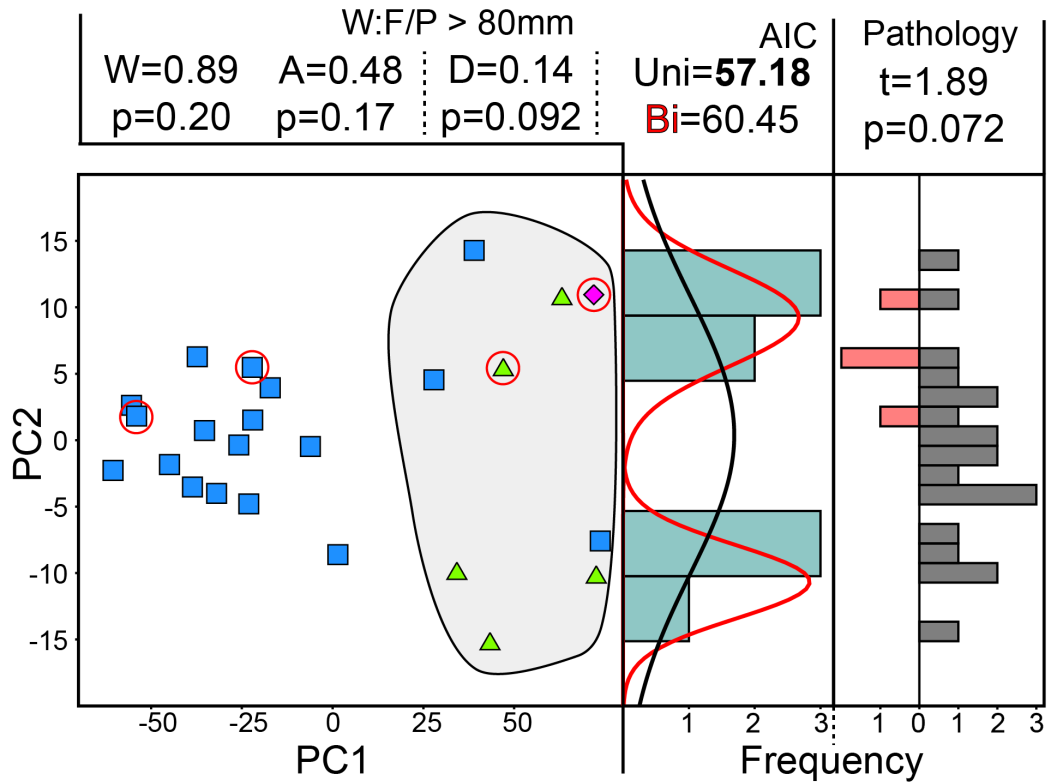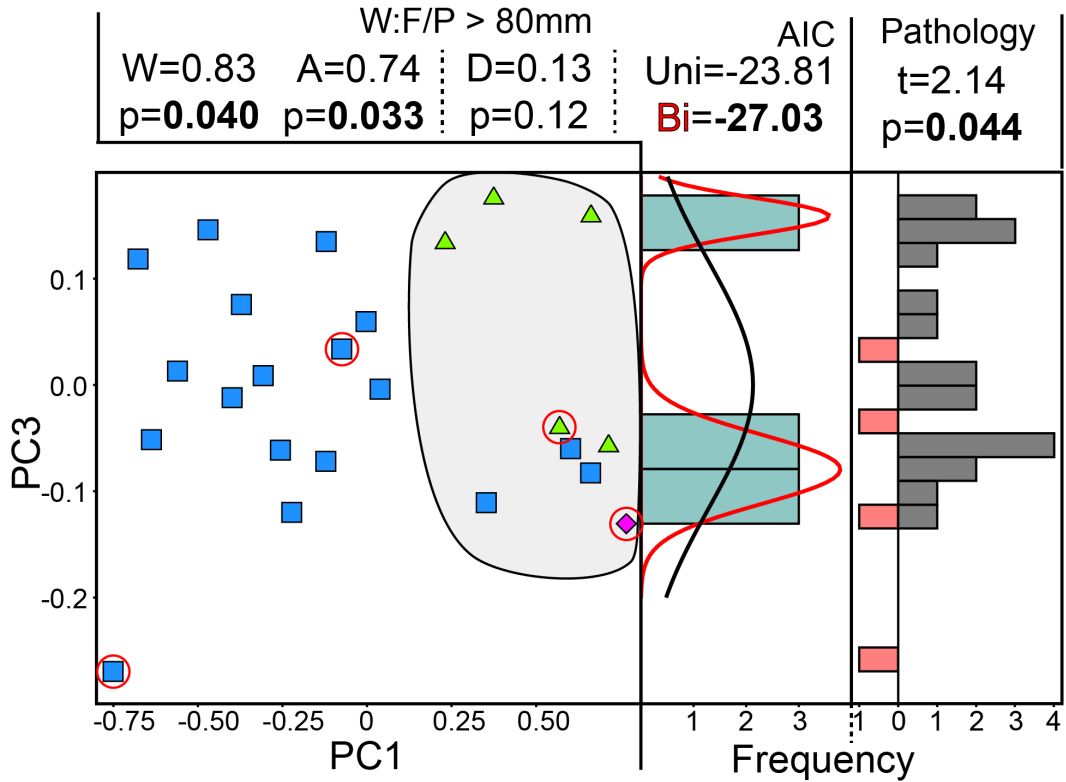
Figure 2.12 Statistical tests of dimorphism from PCA amongst large (W:F/P > 80 mm) *Stegoceras validum.* A) Non-transformed PCA iteration. B) LOG-transformed iteration. Purple diamond – TMP1972.027.0001; blue squares – *Stegoceras validum*; green triangles – *Hanssuesia sternbergi*; Grey outline – large *Stegoceras validum* (W:F/P > 80 mm); Red circles – pathological specimens. Left histogram: distribution of large *Stegoceras validum* across PC 2 (non-transformed) and PC 3 (LOG-transformed) respecively. Black line = best fitting unimodal distribtiotion; red lines = best fitting bimodal distribution (based on mixture analysis). W: Shapiro-Wilk statistic; A: Anderson-Darling statistic; D: Hartigan's Dip statistic. AIC values from mixture analysis; AIC values of significantly "better fitting" distributaions bolded (smallest AIC = best fit; significant difference is > 2). Right (bi) histogram: distribution of pathological and non-pathological *Stegoceras validum* across across PC 2 (non-transformed) and PC 3 (LOG-transformed) respecively. t = Student's t statistic (assuming equal variance). p values < 0.05 are bolded.
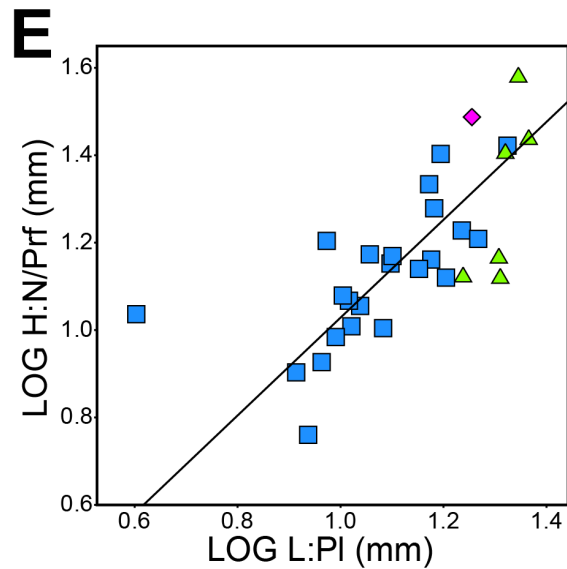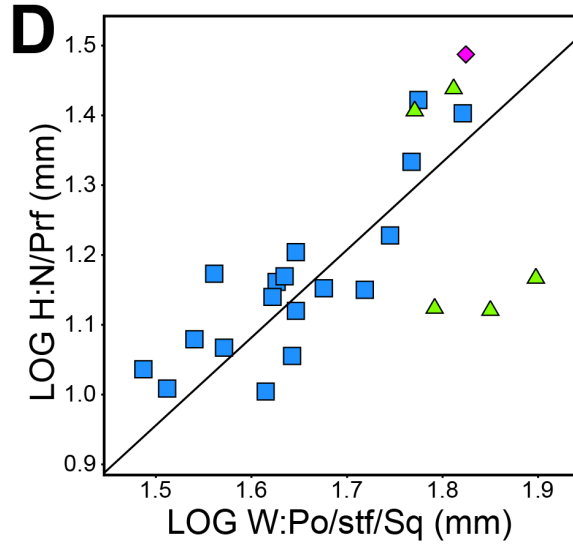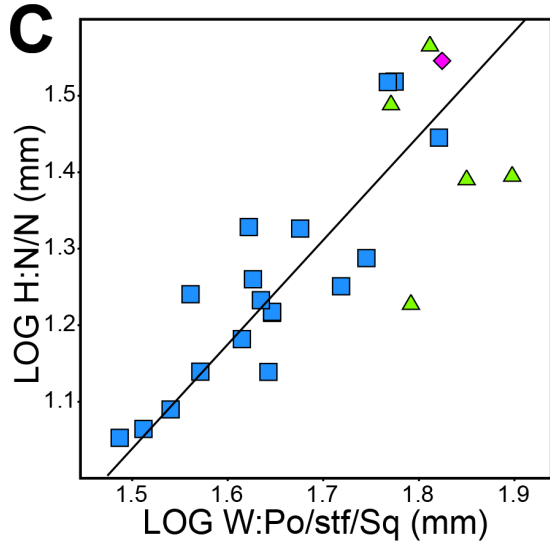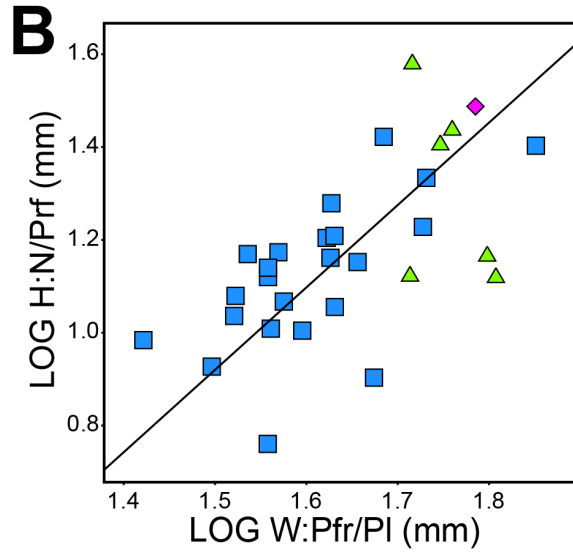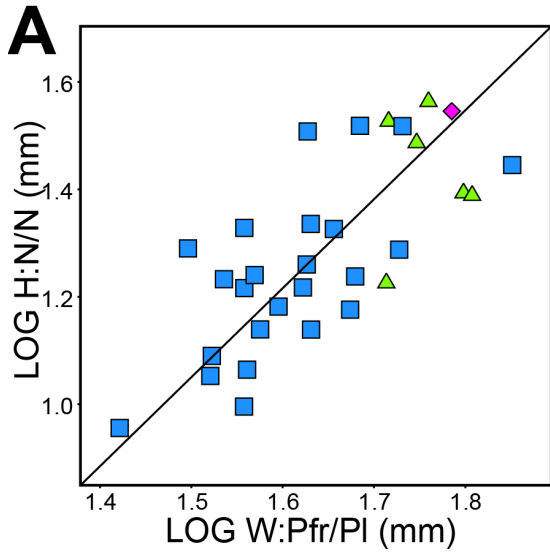
Figure 2.13. RMA regressions of measurements that loaded strongly and antagonistically in PCA. Purple diamond – TMP1972.027.0001; blue squares – *Stegoceras validum*; green triangles – *Hanssuesia sternbergi*; black line – best fit line. A) Height at the nasal – nasal contact (**H:N/N**; mm) vs. width at the prefrontal – palpebral contact (**W:Prf/Pl**; mm). B) Height at the nasal – prefrontal contact (**H:N/Prf**; mm) vs. width at the prefrontal – palpebral contact. C) Height at the nasal – nasal contact vs. temporal width (**W:Po/stf/Sq**; mm). D) height at the nasal – prefrontal contact vs. temporal width. E) Height at the nasal – prefrontal contact vs. palpebral length (**L:Pl**; mm).
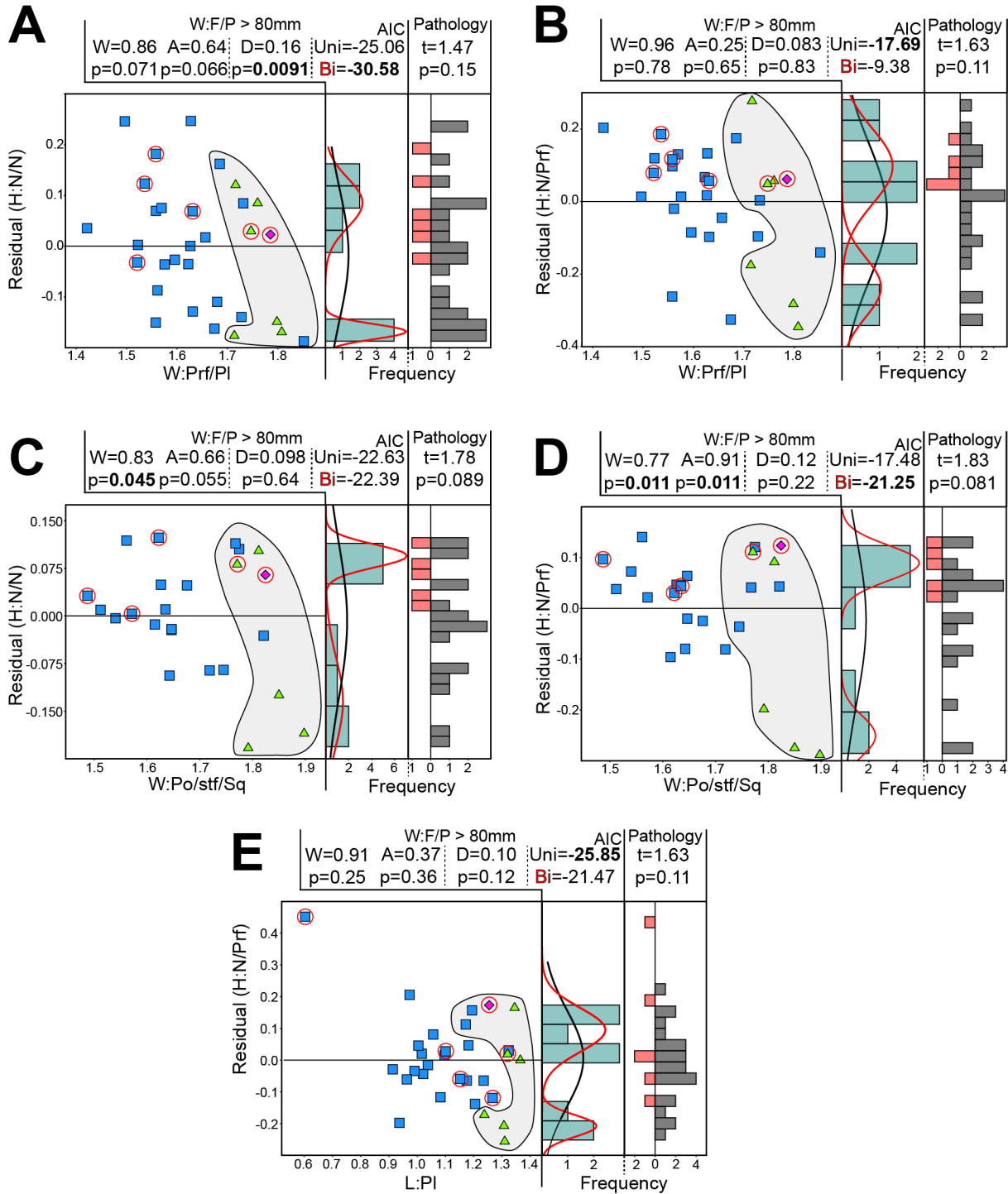
Figure 2.14. Statistical tests of dimorphism from RMA residuals amongst large (W:F/P > 80 mm) *Stegoceras validum.* A) Height at the nasal – nasal contact (LOG **H:N/N**; mm) vs. width at the prefrontal – palpebral contact (LOG **W:Prf/Pl**; mm). B) Height at the nasal –

prefrontal contact (LOG **H:N/Prf**; mm) vs. width at the prefrontal – palpebral contact. C) Height at the nasal – nasal contact vs. temporal width (LOG **W:Po/stf/S**q; mm). D) height at the nasal – prefrontal contact vs. temporal width. E) Height at the nasal – prefrontal contact vs. palpebral length (LOG **L:Pl**; mm). Purple diamond – TMP1972.027.0001; blue squares – *Stegoceras validum*; green triangles – *Hanssuesia sternbergi*; Grey outline – large *Stegoceras validum* (W:F/P > 80mm); Red circles – pathological specimens. Left histogram: distribution of large *Stegoceras validum* across RMA residuals. Black line = best fitting unimodal distribtiotion; red lines = best fitting bimodal distribution (based on mixture analysis). **W**: Shapiro-Wilk statistic; **A**: Anderson-Darling statistic; **D**: Hartigan's Dip statistic. AIC values from mixture analysis; AIC values of significantly "better fitting" distributaions bolded (smallest AIC = best fit; significant difference is > 2). Right (bi) histogram: distribution of pathological and non-pathological *Stegoceras validum* across across RMA residuals. **t** = Student's t statistic (assuming equal variance). p values < 0.05 are bolded.
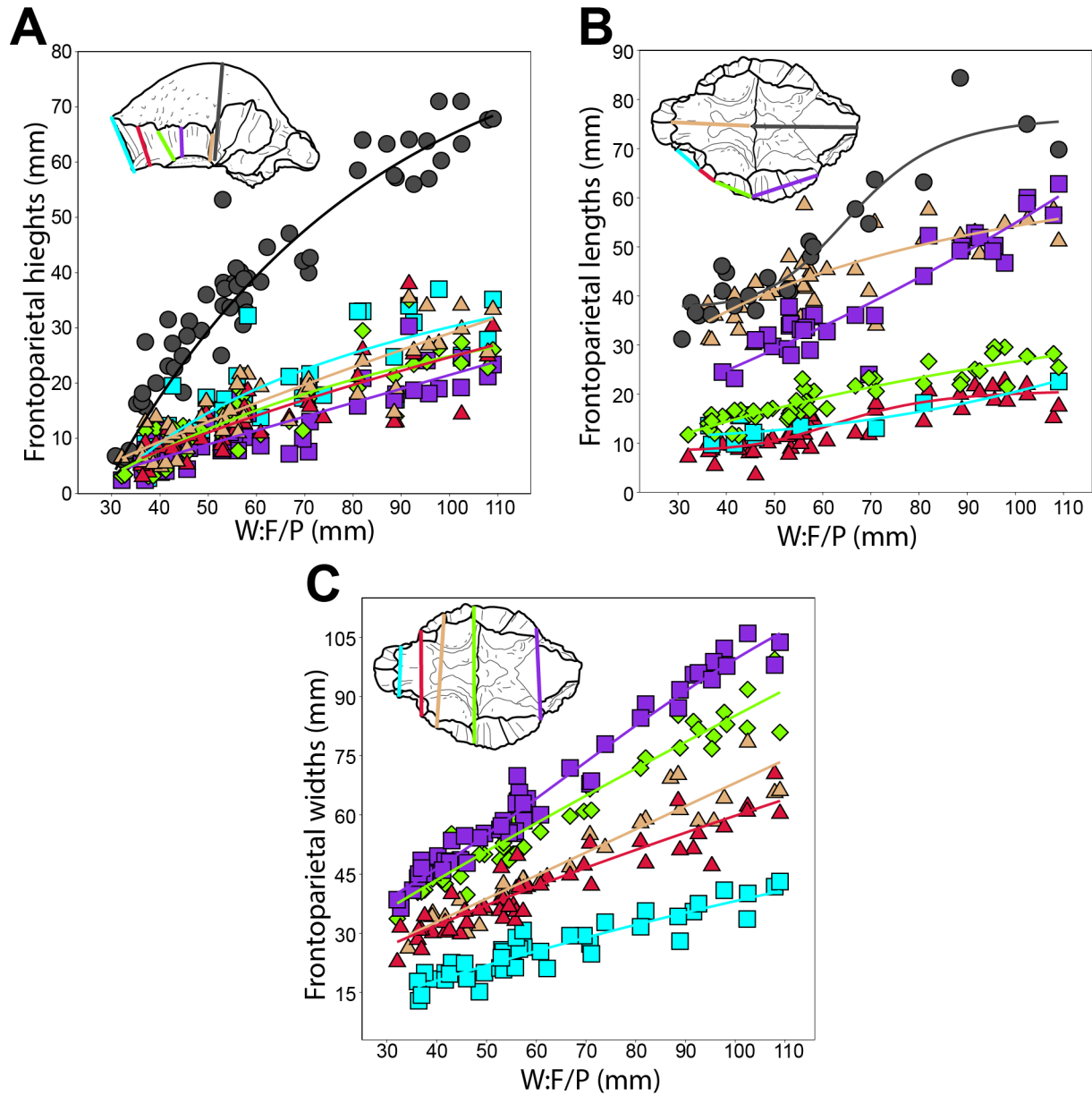
Figure 2.15. Non-linear relationships of linear frontoparietal measurements to W:F/P in *Stegoceras validum* (including *Hanssuesia sternbergi* and *Gravitholus albertae*). "Best-fit" non-linear functions used have the lowest AIC (Table 2.X). A) Frontoparietal heights vs frontoparietal width (W:F/P). Blue squares – nasal/nasal height; red triangles – nasal/prefrontal height; green diamonds – prefrontal/palpebral height; purple squares – palpebral/posterior supraorbital height; brown triangles – posterior supraorbital/postorbital height; black circles – frontoparietal thickness. B) Frontoparietal lengths vs. frontoparietal width. Blue squares –

86

prefrontal length; red triangles – palpebral length; green diamonds – posterior supraorbital length; purple squares – postorbital length; brown triangles – frontal length; black circles – parietal length. C) Frontal and parietal widths vs. frontoparietal width. Blue squares – nasal/prefrontal width; red triangles – prefrontal/palpebral width; brown triangles – palpebral/posterior supraorbital width; green diamonds – posterior supraorbital/postorbital width; purple squares – width at the postorbital/supratemporal fenestra contact (squamosal if closed).

A) TMP2017.012.0019
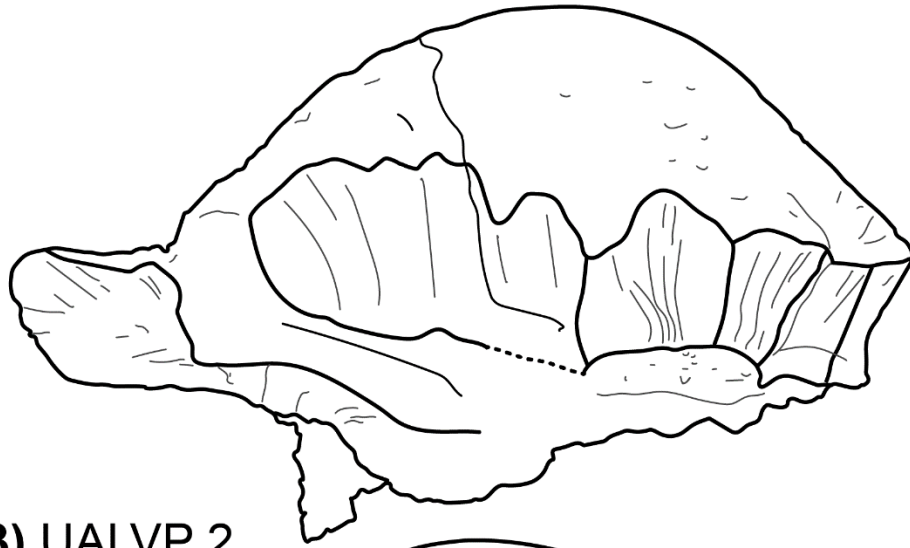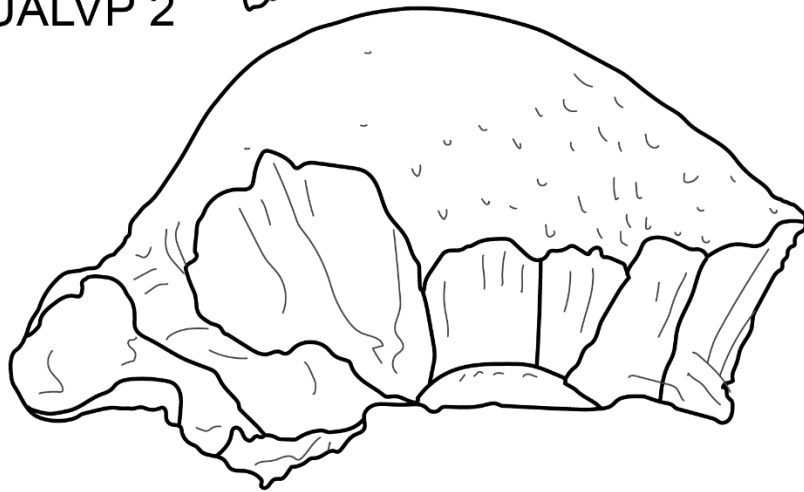
B) UALVP 2

C) TMP1972.027.0001
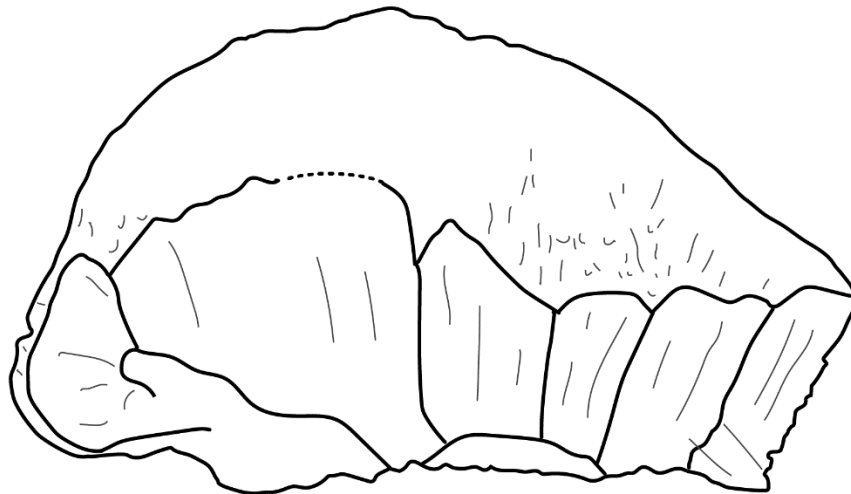
5cm

Figure 2.16. Frontoparietal variation in adult *Stegoceras validum*. Lateral line drawings of A) TMP2017.012.0019. B) UALVP 2 (mirrored). C) TMP1972.027.0001.

Chapter 3. Diagnostic value of pachycephalosaurid frontoparietal domes; phylogenetic character re-evaluation, construction, and phylogenetic analyses

3.1 Introduction

Pachycephalosaurian interrelationships and phylogenetics have been problematic. Brown and Schlaikjer (1943) proposed the first "phylogeny" of pachycephalosaurids (then Troodontidae). This was based on six species, which have now been revised into three species: *Stegoceras validum*, *Sphaerotholus edmontonensis,* and *Pachycephalosaurus wyomingensis* (the former two then referred to *Troodon*). *Stegoceras validum* was proposed as an ancestral species for which *Sphaerotholus edmontonensis* and *Pachycephalosaurus wyomingensis* separately arose.

Dong (1978) proposed a second pachycephalosaurian family – Homalocephaleridae – in the description of *Micropachycephalosaurus hongtuyanensis* (which is now regarded as Cerapoda incertae sedis; Butler and Zhao, 2009). The homalocephalerids included pachycephalosaurians with thickened skull roofs but no cranial dome (*Homalocephale calathocercos*, *Goyocephale lattimorei*, and *Wannanosaurus yansiensis*). Perle et al. (1982) corrected the name to Homalocephalidae and supported its distinction with the description of *Goyocephale lattimorei*. Sues and Galton (1987) and Longrich et al. (2010) are the only phylogenetic analyses that recovered a monophyletic "Homalocephalidae" (although the flat-headed *Dracorex hogwartsia* was not recovered in this clade). Most analyses recover a "Homalocephalidae" consisting of a basal pachycephalosaurian paraphyly (Maryańska et al., 2004; Schott et al., 2009; Sereno, 1986, 2000; Sullivan, 2003; Watabe et al., 2011; Williamson and Carr, 2002), although recent analyses recover a polyphyletic "Homalocephalidae" (Evans et al., 2013; Schott and Evans, 2016; Williamson and Brusatte, 2016; Woodruff et al., 2021). Furthermore, most flat-headed pachycephalosaurids are regarded as juveniles (Butler and Zhao, 2009; Evans et al., 2011), for which unknown adult specimens may develop a cranial dome, as is known to occur in *Foraminacephale brevis* (Schott and Evans, 2016)*, Pachycephalosaurus wyomingensis* (Goodwin and Evans, 2016; Horner and Goodwin, 2009) and *Stegoceras validum* (Schott et al., 2011).

Most analyses agree on a derived position of *Pachycephalosaurus wyomingensis*, *Prenocephale prenes*, *Sphaerotholus* spp. (Evans et al., 2021, 2013; Longrich et al., 2010; Maryańska et al., 2004; Schott et al., 2009; Sullivan, 2003; Williamson and Carr, 2002). Recent pachycephalosaurian phylogenetic analyses recover a basal pachycephalosaurid clade containing *Colepiocephale lambei*, *Hanssuesia sternbergi*, and *Stegoceras* spp. (Evans et al., 2021, 2013; Schott and Evans, 2016; Woodruff et al., 2021).

The most recent suite of pachycephalosaurian phylogenetic analyses have been based on the character matrix assembled by Evans et al. (2013), with little to no re-examination or re-assessment of character states (see Williamson and Brusatte, 2016 and Evans et al., 2021 for some exceptions) unless describing new material (e.g., Schott and Evans 2016). Their results have been largely congruent, however differ in their resolution (highly resolved in Schott and Evans 2016, largely unresolved in Williamson and Brusatte, 2016 and Woodruff et al. 2021). Errors exist in the character matrix such as the coding for *Alaskacephale gangloffi* (Williamson and Brusatte 2016), however, successive analyses have not referenced or included these corrections (Woodruff et al., 2021; unclear if they were included in Evans et al. 2021). Furthermore, inconsistencies exist in the results of some analyses (e.g., character 52 referenced in figure 14 of Woodruff et al. 2021, despite the analysis only including 51 characters). Thus, a careful re-examination of the working pachycephalosaurian character matrix and state assignments is warranted.

Recently, several pachycephalosaurid species have been proposed to be invalid, such as *Dracorex hogwartsia*, *Stegoceras novomexicanum*, and *Stygimoloch spinifer* (Horner and Goodwin, 2009; Goodwin and Evans, 2016; Williamson and Brusatte, 2016). Additionally, *Hanssuesia sternbergi* is synonymous with *Stegoceras validum* (see chapter 2). Removing these taxa from phylogenetic analyses reduces the diversity of two relatively stable clades over the past decade of pachycephalosaurid phylogenetics – the basal "*Stegoceras*" like clade, and reduces Pachycephalosaurini to solely *Pachycephalosaurus wyomingensis* (Sullivan, 2006). Removing these taxa from phylogenetic analyses has the potential to influence tree topology and requires examination. For example, the revision of seven character states and removal of *Dracorex hogwartsia* and *Stygimoloch spinifer* in Williamson and Brusatte (2016) resulted in a largely

unresolved Pachycephalosauridae. The construction of two novel characters and removal of the same species (and *Stegoceras novomexicanum*) in Schott and Evans (2016) appeared to reinforce a resolved topology. Addition of *Sphaerotholus edmontonensis* to the dataset used by Schott and Evans (2016) resulted in a largely unresolved Pachycephalosauridae (Woodruff et al., 2021; two new characters were apparently added; however, one is reworded to a previously constructed character, and the other only serves to score a purported apomorphic feature of *Sphaerotholus buchholtzae*, so neither of which would affect tree topology). Inclusion of *Sinocephale bexelli*, *Stegoceras novomexicanum*, *Stygimoloch spinifer*, but not *Dracorex hogwartsia* recovered a tree topology more consistent with Schott and Evans (2016), but less resolved. The goals of this chapter are to briefly review diagnostic morphometrics of some pachycephalosaurids, revise the working pachycephalosaurian phylogenetic morphological character matrix, test for statistical grouping and distinctness of previously proposed morphological character states, and to identify novel morphometric distinctions amongst pachycephalosaurid frontoparietals that are phylogenetically informative.

3.2 Materials and Methods

3.2.1 Specimens and measurements

Linear measurements based on homologous landmarks (Fig. 2.4) of 151 pachycephalosaurid frontoparietals (Appendix A1.1**)** were mainly acquired from published literature (Evans et al., 2011, 2013; Schott and Evans 2016; Schott et al., 2011; Williamson and Brusatte, 2016; Woodruff et al., 2021). Revised measurements for NMMNH P-27403 (*Sphaerotholus goodwini*) were accepted from Williamson and Brusatte (2016). This sample included 13 valid pachycephalosaurid species. New specimens were measured first-hand using digital callipers, and a proportionate caliper when necessary (e.g., T:F/P). Some measurements were supplemented from published photographs (e.g., L:F when only L:FP was reported; L:Prf; see Appendix A1.1 for measurement revisions). Measurements of photographs were taken in Adobe Photoshop v22.1.1. Newley measured specimens had bilateral measurements treated as in chapter 2. The frontoparietals of two articulated skulls (DMNH EPV.97077, *Sphaerotholus buchholtzae*; MPC-D 100/1204, *Prenocephale prenes*) were segmented from CT data in Dragonfly v.4.0 (Object Research Systems (ORS) INC, Montreal, Canada, 2020; software

available at http://www.theobjects.com/dragonfly) and measured in Geomagic Design X, following the steps performed on TMP1972.027.0001 (see Chapter 2.2.1). CT data for DMNH EPV.97077 was accessed from http://n2t.net/ark:/87602/m4/M18280. CT parameters for DMNH EPV.97077 and MPC-D 100/1204 were reported in Bourke et al. (2014) and Snively and Theodore (2011) respectively.

3.2.2 Purported diagnostic morphometrics

I follow the regression analysis methods of Schott et al., (2011), Evans et al., (2013), and Schott and Evans (2016). All regression analyses were performed on log-transformed linear measurements and calculated using reduced major axis (RMA) regressions.

Morphometric features thought to be diagnostic of *Amtocephale gobiensis* (relatively short length of the frontal compared to the parietal) and *Stegoceras novomexicanum* (elongate contact between the frontal and prefrontal) were tested. Length of the frontal (L:F; x) was plotted against L:P (y), and residuals amongst specimens were compared. If the L:F of *Amtocephale gobiensis* (MPC-D 100/1203) is distinctly elongate, it should have a residual distinct from other pachycephalosaurids. Jasinski and Sullivan (2016) included an elongate frontal-prefrontal contact in their revised diagnosis of *Stegoceras novomexicanum.* To test this, L:Prf (y) was plotted against L:F and W:F/P respectively (x). If *Stegoceras novomexicanum* has a distinctly elongate L:Prf, it's residuals (NMMNH P-33898) will be distinct from specimens of *Stegoceras validum*.

3.2.3 Phylogenetic matrix assessment and character construction

Three characters from the Woodruff et al. (2021) character matrix were selected for statistical testing of discrete states within a continuous character: Woodruff et al. (2021) characters (Wch) 29, 31, and 37. RMA regressions of L:Pl and W:post (Wch 31 and 37 respectively) were both compared to W:F/P (x; which is a standard size variable in pachycephalosaurid morphometrics; Schott and Evans, 2016; Schott et al. 2011), with L:Pl also being compared to W:Prf/Pl and W:Po/stf/Sq (based on antagonistic PC loadings). Distinct character states were assessed using Jenks natural breaks optimisation (e.g., Powers et al., 2020) and mixture analyses on the distribution of residuals from these regressions. The Jenks natural

breaks optimizations were performed in R v1.4.1103, using the plotJenks function in the GmAMisc package. A goodness of fit (GVF) of at least 0.68 was used to identify statistically distinct cohorts. Mixture analyses of residuals were performed in PAST 4.04 (Hammer et al., 2001). The model (number of normal distributions) with the lowest AIC was regarded as the best fitting distribution, and was accepted as significantly better than the alternatives if the AIC difference was at least 2 (as long as the distributions are mutually exclusive of one another). For Wch 29, statistical tests were performed on the anterior angle of the temporal roof in lateral view on the parietal. A horizontal plane was standardised from the respective ventral points of H:N/N and H:Pso/Po. Angles were measured from lateral photographs. Two specimens of each species were selected for angle measurements, except for *Acrotholus audeti, Amtocephale gobiensis, Prenocephale* prenes, *Sphaerotholus edmontonensis, Sphaerotholus goodwini,* for each of which only a specimen is known to preserve the required landmarks (at least in easily observable form).

Four PCA iterations were performed on 16 homologous linear measurements (same as in chapter 2) of 52 pachycephalosaurid frontoparietals. Each iteration differed in how the data were or were not standardised, following the same methods as in chapter 2. Variables that strongly antagonistically loaded (positive and negative respectively) in each PC were identified. These antagonistically loading variables were then log-transformed and subjected to RMA regressions. The distribution of residuals was examined for taxonomic separation and possible coding for phylogenetic analyses. The results of these tests were used to construct new characters and define states for them.

The initial character matrix for this analysis was acquired from Woodruff et al. (2021). *Hanssuesia sternbergi* was removed from the character matrix, following the results of chapter 2. After morphometric analyses, Williamson and Brusatte (2016) was followed in regarding *Stegoceras novomexicanum* as a *nomen dubium*, and it was removed from the phylogenetic analysis. *Dracorex hogwartsia* and *Stygimoloch spinifer* are regarded as ontogimorphs of *Pachycephalosaurus wyomingensis* (Goodwin and Evans, 2016; Goodwin and Horner, 2009), and excluded from the phylogenetic analysis. Fowler (2017) proposed stratigraphic separation of *Pachycephalosaurus wyomingensis* and *Stygimoloch spinifer* in the Hell Creek Formation, largely based on AMNH 1696 (*Pachycephalosaurus wyomingensis*; stratigraphically lower),

TCMI 2004.17.1 (holotype of *Dracorex hogwartsia*, considered *Stygimoloch spinifer* by Fowler 2017), and MPM 8111 (*Stygimoloch spinifer*; the later two both from the upper two thirds of the formation), and apparent congruence of unspecified additional specimens. This led Evans et al. (2021) to retain *Stygimoloch spinifer* in a phylogenetic analysis. This stratigraphic separation requires much more investigation. Until strong support for this stratigraphic separation is demonstrated, *Dracorex hogwartsia* and *Stygimoloch spinifer* are considered as synonyms of *Pachycephalosaurus wyomingensis*.

Revisions to character states not statistically tested largely relied on published photographs. Codings for synonymised taxa were merged, with any incongruence treated as polymorphism. Characters that only scored for the presence/absence of apomorphic states were removed (Wch 24, 26, 32, 46, 47, and 51). Revised taxon scorings proposed by Williamson and Brusatte (2016) were included, unless otherwise tested in this study. Squamosal character states for *Colepiocephale lambei* were assessed based on the referral of squamosals described by Goodwin (1990) and Schott and Evans (2011). Additional character wording revisions and character state revisions, and character removals are supplied in the Appendix 2.1**.**

3.2.4 Phylogenetics

The initial character matrix used in this study came from Woodruff et al. (2021). This character matrix and its revisions (Appendix 2.2-3) were assembled in Mesquite V3.6 (Maddison and Maddison, 2021). This matrix consisted of 18 taxa (16 pachycephalosaurians) and 46 characters. This matrix was then exported into TNT V1.5 (Goloboff and Catalano, 2016) and analysed using a New Technology search parsimony analysis. Parameters included using 10000 replicates with ten rounds of ratcheting, five rounds of tree fusing, and five rounds of drifting. *Psittacosaurus mongoliensis* was set as the outgroup taxon. A strict and a separate 50% majority consensus tree were constructed from the resulting group of most parsimonious trees. The 50% majority consensus tree was exported, then imported into Mesquite V3.6, where the consistency index and retention index were calculated. Character state changes were identified using the Trace Character History function using the Parsimony Ancestral States method.

3.3 Results

3.3.1 Diagnostic morphometrics

Amtocephale gobiensis frontal length – parietal length

Watabe et al. (2011) diagnosed *Amtocephale gobiensis* in part by the ratio between the length of the frontal and the length of the frontoparietal. L:P scales with positive allometry against L:F (slope c_i = 1.23 – 1.83; Table 3.1) amongst 11 pachycephalosaurid species (Fig 3.1). The residual for MPC-D 100/1203 (*Amtocephale gobiensis*) is not unique, but scored like specimens of *Goyocephale lattimorei*, *Homalocephale calathocercos*, *Sphaerotholus buchholtzae*, *Sphaerotholus goodwini*, and *Stegoceras validum*. The residual for MPC-D 100/1201 (*Homalocephale calathocercos*) is more extreme than *Amtocephale gobiensis*.

Stegoceras novomexicanum frontal – prefrontal contact

Jasinski and Sullivan (2016) revised the diagnosis of *Stegoceras novomexicanum* to include a relatively elongate contact between the frontal and the prefrontal. L:Prf (y) significantly correlated with W:F/P and L:F amongst *Stegoceras validum* and NMMNH P-33898 (*Stegoceras novomexicanum*). The W:F/P regression had a higher r value than the L:F regression (Table 3.1; Fig 3.2). L:Prf scales with isometry with respect to L:F, and with negative allometry compared to W:F/P. NMMNH P-33898 has a relatively more extreme residual when L:Prf is compared to W:F/P, but was still equivalent to some specimens of *Stegoceras validum* from the Dinosaur Park Formation (TMP1990.066.0002 and TMP2006.012.0241).

3.3.2 Previously constructed characters

Wch 29: Roof of temporal chamber as manifest on parietal in lateral view: absent (0); small, roof horizontal (1); enlarged, dorsally arched (2).

This character is problematic, as it describes multiple character-state variables (problematic character type I A.6; Simões et al., 2017): size and shape of the temporal roof. Here, the size component of the character is removed (which can be examined in future analyses), and the shape of arching, or angle of the temporal roof is examined. Williamson and Carr (2002) originally created this character and defined its character states as absent [0], horizontal [1], and inclined dorsocaudally [2]. Evans et al. (2013) revised the character states to reflect size, and degree of arching.

After standardizing a horizontal line, the Jenks natural break analysis identified a single natural break in the distribution of the anterior angles of the temporal roof amongst 15 pachycephalosaurids, with a GOF of 0.71 (Table 3.2). The natural break occurs between 22 and 26º. The distribution of the anterior angle of the temporal roofs (Fig 3.3) was best fit to a unimodal distribution in the mixture analysis (Table 3.3). The threshold for character states is assigned based on the lower and upper bounds of natural gap identified in the Jenks natural break analysis (absent [0], anterior angle < 22º [1], anterior angle > 26º [2]). *Amtocephale gobiensis*, *Foraminacephale brevis*, *Sphaerotholus goodwini*, and *Stegoceras validum* are assigned [1]. *Acrotholus audeti*, *Colepiocephale lambei*, *Pachycephalosaurus wyomingensis*, *Sphaerotholus buchholtzae*, and *Sphaerotholus edmontonensis* are assigned [2]. *Alaskacephale gangloffi, Homalocephale calathocercos*, *Goyocephale lattimorei*, *Sinocephale bexelli*, *Tylocephale gilmorei*, and *Wannanosaurus yansiensis* assigned as "[?]", due to the available material lacking required landmarks, or due to obstruction of the landmarks (articulated skulls). This character is revised as character 27 in this analysis (Appendix A2.2).

Wch 31 (character 30 of this analysis): Contact of anterior supraorbital with frontal: absent (0); restricted (1); extensive (2).

This character does not define the threshold between a restricted and extensive frontal-palpebral contact (problematic character type V, Simões et al., 2017). L:Pl antagonistically loaded against W:Po/stf/Sq in PC 2 of the log-transformed PCA iteration (Table 3.4), as well as W:Prf/Pl in PC 4 of the W:F/P proportionate iteration (Table 3.5). L:Pl correlated with W:F/P, however, did not correlate with either W:Prf/Pl or W:Po/stf/Sq (Table 3.1; Fig. 3.3). The Jenks natural break analyses identified a natural break in the distribution of residuals in three RMA regressions of the length of the frontal-palpebral contact (y), all against frontoparietal widths (x) (W:Prf/Pl, W:F/P, and W:Po/stf/Sq; Table 3.2). The distribution of these residuals in each regression were best fit to bimodal distributions (Table 3.3). The boundary between groups in the mixture analysis occurred above the natural break in the W:Prf/Pl and W:F/P regressions. The boundary between groups in the mixture analysis in the W:Po/stf/Sq regression was congruent with the natural break in the distribution of the residuals. Taxonomic distributions between the natural breaks and the bimodal distributions were least congruent in the W:Prf/Pl regression, and

most congruent in the W:Po/stf/Sq regression. The W:Po/stf/Sq regression was chosen for the state assessment reference due to the congruence between the Jenks natural break analysis and the Mixture analysis. *Acrotholus audeti*, *Goyocephale lattimorei*, *Pachycephalosaurus wyomingensis*, *Prenocephale prenes*, and *Sphaerotholus buchholtzae* are assessed as restricted [1]. *Amtocephale gobiensis*, *Colepiocephale lambei*, *Foraminacephale brevis*, *Sphaerotholus edmontonensis*, and *Sphaerotholus goodwini* are assessed as extensive [2]. *Stegoceras validum* is also assessed as extensive [2], although this requires the exclusion of a single "outlier" specimen (TMP1992.002.0003) from the other 26 specimens. All other pachycephalosaurians assigned "[?]" pending discovery of additional material.

Wch 37 (in part character 35 of this analysis): Exposure of posteromedian (intersquamosal) process between squamosals: caudolateral wings well developed (0); restricted (1); broad (2).

The width of the posterior exposure of the parietal is weakly correlated (r = 0.58) with, and scales isometrically against, W:F/P amongst pachycephalosaurids (Table 3.1; Fig 3.5). The Jenks natural break analysis identified a single natural break in the distribution of residuals with a GOF of 0.69 (Table 3.2). A bimodal distribution was the best fitting model (compared to alternatives) that explained the distribution of the residuals, however, was not a significantly better fit than a unimodal distribution (Table 3.3). The suggested bimodal distributions were not exclusive, with a smaller distribution occurring within the larger distribution). The threshold for "restricted" and "broad" exposure is defined at the lower and upper bounds of the natural break. *Amtocephale gobiensis*, *Goyocephale lattimorei*, *Homalocephale calathocercos*, *Sinocephale bexelli*, *Sphaerotholus buchholtzae*, and *Sphaerotholus edmontonensis* are assigned broad posterior exposures of the parietal [1]. *Acrotholus audeti*, *Pachycephalosaurus wyomingensis*, *Prenocephale prenes*, and *Sphaerotholus goodwini* are assigned narrow posterior exposures of the parietal [2]. Five of six specimens of *Foraminacephale brevis* occur above the natural break (TMP2003.012.0252 occurs below the natural break), so it is assigned [1/2]. Most *Stegoceras validum* plot below the break, except for three specimens (UCMZ(VP)2008.002, TMP1972.027.0001, TMP2019.012.0022), and the species is also assigned [1/2].

Wch 38 codes the presence or absence of an intersquamosal contact posterior to the parietal. This is herein interpreted as part of the transitional series of the medial extension of the

parietal; the presence of an intersquamosal contact restricts the medial extension of the parietal from being posteriorly exposed. Wch 37 and 38 violate the principle of logical independence (character splitting, Type I B characters; Simões et al. 2017). All taxa that are scored for the presence of an extensive intersquamosal contact were also be scored for a restricted exposure of the medial extension of the parietal. Wch 38 was removed from the character matrix of this analysis, and a fourth character state added to Wch 37 (character 35 of this analysis). Therefore, final assignments of [1/2/3] and [2/3] are given to *Stegoceras validum* and *Pachycephalosaurus wyomingensis*, respectively (Goodwin et al., 1998; Sullivan, 2003).

3.3.3 PCA

PC Variance and Loadings

Tables 3.4-3.7 summarise the PC variance and loadings for all four PCA iterations. PC 1 accounts for > 65% of the total variance in the non-transformed, LOG-transformed, and the L:F proportionate iteration, whereas PC 1 explains 34.9% of the total variance in the W:F/P proportionate iteration. All variables positively loaded on PC 1 in all four iterations, except for W:Po/stf/Sq, H:Pso/Po, and L:Pso in the W:F/P proportionate iteration. The variables that had the highest loadings in PC 1 of each iteration also had the largest ranges (after transformations, if performed). W:Pso/Po, W:F/P, and W:Po/stf/Sq all strongly positively loaded on PC 1 of the non-transformed and L:F proportionate iteration, with T:F/P also strongly positively loading in the non-transformed iteration. H:N/N, H:N/Prf, and H:Pl/Pso all strongly positively loaded on PC 1 of the LOG-transformed iteration. W:Prf/Pl, W:Pl/Pso, L:Po, and L:F all strongly positively loaded on PC 1 of the W:F/P proportionate iteration.

PC 2 of the non-transformed iteration explained 4.3% of the total variance, and was strongly positively loaded by L:Po, and strongly negatively loaded by W:Po/stf/Sq. PC 2 of the L:F proportionate iteration explained 12.0% of the total variance, and was strongly loaded by the same variables, as well as being strongly positively loaded by H:N/N and T:F/P. PC 2 of the W:F/P proportionate iteration explained 20.0% of the total variance, was strongly positively loaded by W:Po/stf/Sq, and strongly negatively loaded by T:F/P. PC 2 of the LOG-transformed iteration explained 7.9% of the total variance, and was strongly positively loaded by L:Pl.

PC 3 of the non-transformed iteration explained 2.2% of the total variance and was strongly positively loaded by W:N/Prf, W:Pl/Pso, and W:Pso/Po, and strongly negatively loaded by L:F and T:F/P. PC 3 of the LOG-transformed iteration explained 5.2% of the total variance, was strongly positively loaded by H:Pso/Po, W:Po/stf/Sq, L:Pl, and L:Pso, and strongly negatively loaded by H:N/N. PC 3 of the L:F proportionate iteration explained 6.4% of the total variance, was strongly positively loaded by W:Pl/Pso and L:Pl, and strongly negatively loaded by T:F/P. PC 3 of the W:F/P proportionate iteration explained 14.6% of the total variation, and was strongly positively loaded by H:Pso.Po, W:Po/stf/Sq, and T:F/P.

PC 4 of the non-transformed iteration explained 1.2% of the total variance, was strongly positively loaded by H:N/N, H:N/Prf, and H:Pso/Po, and strongly negatively loaded by W:Prf/Pl. PC 4 of the LOG-transformed iteration explained 3.9% of the variance, and was strongly negatively loaded by H:N/Prf and H:Pso/Po. PC 4 of the L:F proportionate iteration explained 3.9% of the total variance, was strongly positively loaded by W:Prf/Pl, and strongly negatively loaded by T:F/P. PC 4 of the W:F/P proportionate iteration explained 10.0% of the total variance, was strongly positively loaded by H:N/N, W:N/Prf, and L:Pl, and strongly negatively loaded by W:Prf/Pl, and L:F.

PC 5 of the non-transformed iteration explained 1.0% of the total variance, was strongly positively loaded by H:Pso/Po, and strongly negatively loaded by W:F/P and T:F/P. PC 5 of the LOG-transformed iteration explained 2.1% of the total variance, and was strongly negatively loaded by H:Pl/Pso. PC 5 of the L:F proportionate iteration explained 3.4% of the total variance, was strongly positively loaded by H:N/Prf and H:Pso/Po, and strongly negatively loaded by W:Prf.Pl.

Iteration scorings

PC 1

Pachycephalosaurus wyomingensis and *Prenocephale prenes* are broadly positively separated from all other pachycephalosaurids on PC 1 in the non-transformed iteration but overlap with each other (Fig 3.6). PC 1 scores in the LOG-transformed iteration are broadly similar, however, *Pachycephalosaurus wyomingensis* score like some *Stegoceras validum* and

like *Sphaerotholus goodwini* (Fig 3.7). All pachycephalosaurids overlap in PC 1 of the L:F proportionate iteration, except for *P. prenes*, which is positively separated (Fig 3.8). *Acrotholus audeti, "Stegoceras novomexicanum"* and smaller specimens of both *Colepiocephale lambei* and *Stegoceras validum* are positively separated from other pachycephalosaurids in PC 1 of the W:F/P proportionate iteration (Fig 3.9).

PC 2

Prenocephale prenes* is negatively separated from other pachycephalosaurids in PC 2 of the non-transformed iteration. *Foraminacephale brevis* is also negatively separated from most pachycephalosaurids, but overlaps with *Sphaerotholus buchholtzae*. *Sphaerotholus buchholtzae* and *Sphaerotholus edmontonensis* overlap with *Pachycephalosaurus wyomingensis,* small *Stegoceras validum* and *"Stegoceras novomexicanum"*. *Acrotholus audeti* and *Sphaerotholus goodwini* overlap with *Colepiocephale lambei* and *Stegoceras validum*. *Colepiocephale lambei* completely overlaps with *Stegoceras validum* in PC 2 of the non-transformed iteration.

Acrotholus audeti, Pachycephalosaurus wyomingensis, Sphaerotholus buchholtzae*, and a single specimen of *Stegoceras validum* are negatively separated from all other pachycephalosaurids in PC 2 of the log-transformed iteration. *Colepiocephale lambei, Foraminacephale brevis, Sphaerotholus edmontonensis, Sphaerotholus goodwini, "Stegoceras novomexicanum"* and all other *Stegoceras validum* overlap with each other in the LOG-transformed iteration.

Foraminacephale brevis* and *Prenocephale prenes* overlap and are negatively separated from all other pachycephalosaurids (except *Sphaerotholus buchholtzae*) in PC 2 of the L:F proportionate iteration. All other species overlap in PC 2 of the L:F proportionate iteration. PC 2 scores in the W:F/P proportionate iteration are broadly similar, but inverted to the PC 2 of the L:F proportionate iteration. However, *"Stegoceras novomexicanum"* and small specimens of *Stegoceras validum* overlap with *Foraminacephale brevis* and *Prenocephale prenes*.

PC 3

Pachycephalosaurus wyomingensis* is negatively separated from all other pachycephalosaurids in PC 3 of both the non-transformed and L:F proportionate iterations.

101

Foraminacephale brevis and *Prenocephale prenes* are positively separated from all other pachycephalosaurids (which all otherwise overlap) in PC 3 of the LOG-transformed iteration. *Foraminacephale brevis* is positively separated form *Acrotholus audeti*, *Prenocephale prenes*, and *Sphaerotholus* spp., in PC 3 of the L:F proportionate iteration, but overlaps with *Colepiocephale lambei* and *Stegoceras validum*. *Acrotholus audeti* and *Pachycephalosaurus wyomingensis* are positively separated from all other pachycephalosaurids in the W:F/P proportionate iteration.

PC 4

Pachycephalosaurid species show little separation on PC 4 of the non-transformed iteration. *Colepiocephale lambei*, *Pachycephalosaurus wyomingensis*, and *Stegoceras validum* cover nearly the entire range of all specimens in this axis. *Foraminacephale brevis* has a relatively restricted range. Specimens of *Stegoceras validum* show a divergent trend from smaller to larger specimens in PC 4 scores. There is no taxonomic separation in PC 4 of the LOG-transformed iteration. *Acrotholus audeti* and one specimen of *Sphaerotholus buchholtzae* are positively separated from other pachycephalosaurids in PC 4 of the L:F proportionate iteration. *Prenocephale prenes* is positively separated from *Pachycephalosaurus wyomingensis* in this axis, otherwise all other taxa overlap with each other. Pachycephalosaurids show little separation in PC 4 of the W:F/P proportionate iteration. *Pachycephalosaurus wyomingensis* is negatively separated from *Prenocephale prenes*, and *Foraminacephale brevis* is positively separated from *Sphaerotholus buchholtzae.*

PC 5

Acrotholus audeti is positively distinct from all other pachycephalosaurids in PC 5 of the non-transformed iteration. Some specimens of *Colepiocephale lambei* are negatively separated from all other pachycephalosaurids in this axis. *Pachycephalosaurus wyomingensis* and *Prenocephale prenes* overlap with each other and are positively separated from *Colepiocephale lambei* and *Foraminacephale brevis*. *Colepiocephale lambei* is negatively separated from *Sphaerotholus buchholtzae* and only overlaps with a single specimen of *Stegoceras validum*. Pachycephalosaurids show no taxonomic separation in PC 5 of the LOG-transformed and L:F proportionate iterations. *Prenocephale prenes* is negatively separated from *Colepiocephale*

lambei, *Foraminacephale brevis*, and *Pachycephalosaurus wyomingensis* PC 5 of the W:F/P proportionate iteration. *Colepiocephale lambei* and *Pachycephalosaurus wyomingensis* are also positively separated from *Sphaerotholus buchholtzae*.

3.3.4 New character assessments

Character 29 (new): Height of the frontal-nasal contact compared to the length of the frontal-posterior supraorbital contact: tall (0); short (1). Requires replication for novel assessments.

H:N/N and L:Pso strongly antagonistically loaded in PC 3 of the LOG-transformed PCA (Table 3.4). The log height at the frontal-nasal contact was weakly correlated with log L:Pso (r = 0.58; Table 3.1; Figure 3.10). It scales with positive allometry relative to L:Pso (slope 95% confidence = 1.44 – 2.4). The Jenks natural break analysis identified a single natural break in the distribution of the residuals (GOF = 0.73; Table 3.2). The distribution of residuals was best fit to a bimodal distribution (Table 3.3). The Jenks natural break analysis and Mixture analysis differed on the assignments of three specimens. A new character was created to code for H:N/N relative to L:Pso (character 29). The Jenks natural break analysis had better taxonomic separation and was used as the threshold between character states. *Foraminacephale brevis*, *Pachycephalosaurus wyomingensis*, *Prenocephale prenes*, and *Sphaerotholus goodwini* are assigned a short H:N/N relative to L:Pso [0]. *Acrotholus audeti*, *Sphaerotholus buchholtzae*, and *Sphaerotholus edmontonensis* are assigned a tall H:N/N relative to L:Pso [1]. *Stegoceras validum* is also assigned [1], however, this requires the exclusion of one outlier specimen (TMP1981.041.0102) from the other 35 used in the regression analysis. *Colepiocephale lambei* is assigned [0/1] as specimens belonging to this taxon are nearly evenly split by the natural break. All other taxa in the analysis are assigned [?].

Character 32 (completely revised): Doming of the skull roof: Initiates overtop of the frontals (0); initiates overtop of the parietals (1)

W:Po/stf/Sq antagonistically loaded against L:Po in PC 2 of the non-transformed PCA (Table 3.6) and the L:F proportionate PCA (Table 3.7). W:Po/stf/Sq and W:Pl/Pso antagonistically loaded in PC 3 of the L:F proportionate PCA (Table 3.7), and in PC 3 of the W:F/P proportionate PCA (Table 3.5). However, in the last two pairs, only one variable loaded

103

>|0.3| (all loaded >|0.2|). L:Po correlated with W:Po/stf /Sq, and W:Po/stf/Sq correlated with both W:Pl/Pso and W:F/P (Table 3.1; Fig 3.11).

The Jenks natural break analysis identified a single natural gap in the residuals from RMA regressions of L:Po (y) against W:Po/stf/Sq (x) (Table 3.2). The distribution of the residuals was best fit to a trimodal distribution (Table 3.3). However, these distributions were not mutually exclusive, with one distribution residing within another. A bimodal distribution was a significantly better fit than a unimodal distribution. The boundary between these distributions is more negative than the natural break, with seven specimens incongruent between the two methods. The natural break in the distribution of residuals better separates taxa than the mixture analysis, although several taxa still fall on either side of the natural break (*Colepiocephale lambei*, *Foraminacephale brevis*, *Pachycephalosaurus wyomingensis*, *Prenocephale prenes*, and *Sphaerotholus buchholtzae*).

The Jenks natural break analysis identified a single natural break in the distribution of the residuals in the W:Po/stf/Sq (y) vs W:Pl/Pso (x) RMA regression. The distribution of residuals was best (but not significantly better than alternatives) fit by a trimodal distribution. However, these distributions were not mutually exclusive. A bimodal distribution was a significantly better fitting model than a unimodal distribution. The Jenks natural break analysis and mixture analysis disagree on the assignment of four specimens. The Jenks natural break separates taxa better. *Acrotholus audeti*, *Goyocephale lattimorei*, *Homalocephale calathocercos, Sphaerotholus goodwini*, *Stegoceras validum* all occur below the natural gap. All but one specimen of *Colepiocephale lambei*, occur below the gap. *Amtocephale gobiensis*, *Prenocephale prenes*, *Sphaerotholus buchholtzae* and *Sphaerotholus edmontonensis* all occur above the gap, and all but one specimen of *Foraminacephale brevis* and *Pachycephalosaurus wyomingensis* (TCMI 2004.17.1) fall above the gap.

Character states are assigned based broadly on the natural gap in the distributions of residuals in the W:Po/stf/Sq vs. W:Pl/Pso RMA regression, with some exceptions where ontogeny is concerned. *Amtocephale gobiensis*, *Prenocephale prenes, Sphaerotholus buchholtzae*, and *Sphaerotholus edmontonensis* are assigned [1]. *Foraminacephale brevis* and *Pachycephalosaurus wyomingensis* are also assigned [1], however, this requires the exclusion of

a single outlier specimen from each. For *Pachycephalosaurus wyomingensis*, the outlier is the flatheaded holotype of "*Dracorex hogwartsia*" (TCMI 2004.17.1), and there appears to be a positive trend in the residuals of this species though ontogeny. *Acrotholus audeti*, *Sphaerotholus goodwini*, and *Stegoceras validum* are all assigned [0]. *Colepiocephale lambei* is assigned [0], although this requires the exclusion of a single outlier specimen. *Goyocephale lattimorei*, *Homalocephale calathocercos*, and *Wannanosaurus yansiensis* are assigned [?] as mature, domed specimens for these species are unknown, and it is possible they would never develop a dome. The only known specimen of *Sinocephale bexelli* does not preserve the frontal. However, it is tentatively assigned [0] based on its residuals in the W:Po/stf/Sq vs W:F/P RMA regression (Fig 3.11). *Alaskacephale gangloffi* and *Tylocephale gilmorei* are scored as [?] due to absent or damaged material. *Psittacosaurus mongoliensis* and *Yinlong downsi* are assessed as [?].

This character replaces Wch 34, which codes for the presence/absence of a parietosquamosal shelf, due to the interpretation that the codings reflect the relative origination center of dome development. The parietosquamosal shelf results from dome inflation beginning in the frontals in *Stegoceras validum*, progressing posteriorly through ontogeny, and potentially resulting in obliteration of the parietosquamosal shelf (Williamson and Carr, 2002; Chapter 2). *Colepiocephale lambei* possesses a narrow, uninflated medial extension of the parietal, which would have closely resembled *Stegoceras validum* (Schott et al. 2009). In *Foraminacephale brevis*, dome inflation begins over the entire dorsal surface of the parietals, and never results in the formation of a parietosquamosal shelf. Thus, rather than coding for the presence or absence of the parietosquamosal shelf, which may be lost in fully mature individuals, this new character codes for differences in frontal and parietal widths. This appears congruent with initial areas of dome development, whereby when the middle parietal width (W:Po/stf/sq) is compared to the middle frontal width (W:Pl/Pso), pachycephalosaurids that dome their parietals first have disproportionately wider parietals, compared to pachycephalosaurids that dome their frontals first, and *vice versa*.

W:Po/stf/Sq scales with negative allometry relative to W:F/P in *Stegoceras validum* (Schott et al. 2011; Appendix A2.4), but with positive allometry in *Foraminacephale brevis* (Schott and Evans, 2016), *Prenocephale prenes*, and *Sphaerotholus buchholtzae* (Appendix

A2.4). The scaling relationship between W:Po/stf/Sq and W:F/P in *Colepiocephale lambei* is statistically isometric (Appendix A2.4), however, the 95% confidence interval around the slope was large (range = 0.9; 0.49 to 1.39) compared to the other four species (ranges from 0.19 to 0.53). W:Po/stf/Sq scaled with negative allometry relative to W:F/P when *Colepiocephale lambei* was combined with *Stegoceras validum* (r = 0.94), but with positive allometry when *Foraminacephale brevis*, *Prenocephale prenes*, and *Sphaerotholus buchholtzae* were combined (r = 0.98).

H:N/N and W:Po/stf/Sq are strongly antagonistically loaded in PC 3 of the LOG-transformed PCA and PC 2 of the L:F proportionate PCA (Tables 3.4, 3.7). H:N/N weakly correlate with W:Po/stf/Sq (r = 0.62, Table 3.1). H:N/N scaled isometrically against W:Po/stf/Sq (slope 95% confidence = 0.91–1.98). The Jenks natural break analysis identified a single natural break in the distribution of residuals (GOF = 0.76; Table 3.2). The distribution of the residual was best fit by a bimodal distribution in the mixture analysis (Table 3.3). The Jenks natural break analysis and mixture analysis differ in the assignment of three specimens. The Jenks natural break analysis had better taxonomic separation, however, did not significantly differ from the mixture analysis. Residuals for *Foraminacephale brevis*, *Homalocephale calathocercos*, *Pachycephalosaurus wyomingensis*, *Prenocephale prenes*, and *Sphaerotholus* spp. fall below the gap. *Acrotholus audeti* falls above the gap, along with most specimens of *Colepiocephale lambei* and *Stegoceras validum*. The taxonomic division in the residuals of this regression was not selected for character construction but is used to support the assignments for character 32.

3.3.6 Phylogenetic analysis

The New Technologies search in TNT recovered seven equally most parsimonious trees (MPTs), each with a tree length of 73. The strict consensus of these trees recovered a largely unresolved Pachycephalosauridae (Figure 3.12). *Wannanosaurus yansiensis* was recovered as the basal-most pachycephalosaurian, consistent with recent phylogenetic analyses (Evans et al. 2013; Schott and Evans; Woodruff et al. 2021; Evans et al. 2021). The sister taxon to *Wannanosaurus yansiensis* is Pachycephalosauridae (*sensu* Sereno, 1998). *Stegoceras validum* is recovered as the basal-most pachycephalosaurid. Pachycephalosauridae is united by a broad exposure of the squamosal on the occiput [character 17(1)], and a broad, dorsally ornamented parietal septum

[20(1)]. *Stegoceras validum* is the sister taxon to Pachycephalosaurinae. Pachycephalosaurines are united by a marked lateral deflection of the preacetabular process [9(1)], an arched premaxillary-maxillary diastema [15(1)], enlarged nodes ventral to the primary squamosal node row (corner nodes) [38(1)], rostral nodes [43(1)], and a convex posterolateral margin of the skull roof [45(1)] (postorbital-squamosal contact; straight in *Pachycephalosaurus wyomingensis* and *Tylocephale gilmorei*). *Colepiocephale lambei* is recovered as a basal pachycephalosaurine. It forms a clade with *Goyocephale lattimorei*, the two species being united by the presence of a node row dorsal to the primary squamosal node row [46(1)] (also present in *Alaskacephale gangloffi* and *Pachycephalosaurus wyomingensis*).

Sister to *Colepiocephale lambei* + *Goyocephale lattimorei* is a polytomy of all other pachycephalosaurines. Pachycephalosaurines more derived than *Colepiocephale lambei* and *Goyocephale lattimorei* are united by a distally downturned post-acetabular process of the ilium [11(1)], dorsally restricted depressions for the atlanto-occipital capsular membrane/ligament [25(2)] (except for *Homalocephale calathocercos*), closed supratemporal fenestrae at maturity [26(1)], the absence of a groove separating the frontonasal boss from the supraorbital lobes [28(1)] (except for *Foraminacephale brevis*), a cranial dome that initially inflates from the parietal [32(1)] (except *Sphaerotholus goodwini*), five or fewer nodes in the primary squamosal node row [37(0)] (except for *Foraminacephale brevis*; also present in *Goyocephale lattimorei*), and a medial node of the primary squamosal node row equally sized to the other primary nodes [40(1)] (except for *Alaskacephale gangloffi* and *Homalocephale calathocercos*). Within this polytomy, "*Sphaerotholus*" *buchholtzae* and "*Sphaerotholus*" *edmontonensis* are recovered as a clade, united by a tall H:N/N relative to L:Pso [29(0)] (also present in *Acrotholus* audeti, *Colepiocephale lambei*, *Stegoceras validum*), a continuous border between the contacts for the posterior supraorbital and postorbital on the frontoparietal [31(2)] (also present in *Pachycephalosaurus wyomingensis* and *Sphaerotholus goodwini*), and a medial-most node of the primary squamosal node row that straddles the parieto-squamosal suture [39(1)] (also present in *Foraminacephale brevis*, *Homalocephale calathocercos*, and *Stegoceras validum*)

A 50% majority rule consensus tree was constructed from the 7 MPTs (Fig 3.12). The 50% majority consensus tree has a consistency index of 0.72 and retention index of 0.75.

Amtocephale gobiensis, *Foraminacephale brevis*, *Pachycephalosaurus wyomingensis*, *Prenocephale prenes*, *Sphaerotholus buchholtzae*, *Sphaerotholus edmontonensis*, *Sphaerotholus goodwini*, and *Tylocephale gilmorei* form a clade within the large pachycephalosaurine polytomy.

"*Sphaerotholus*" *buchholtzae* and "*Sphaerotholus*" *edmontonensis* form a clade that is sister to a clade consisting of *Amtocephale gobiensis, Foraminacephale brevis*, *Pachycephalosaurus wyomingensis*, *Prenocephale prenes*, *Sphaerotholus goodwini* and *Tylocephale gilmorei. Amtocephale gobiensis*, and *Foraminacephale brevis* are unresolved within this clade. *Sphaerotholus goodwini* and *Prenocephale prenes* are successively more derived. *Pachycephalosaurus wyomingensis* and *Tylocephale gilmorei* are the most derived pachycephalosaurines.

A dome that begins inflating on the parietal [29(1)] (aside from *Sphaerotholus goodwini*) and the similar size of the medial node to the remaining nodes in the primary node row [40(0)] unites the large clade within the large pachycephalosaurine polytomy in the 50% majority consensus. A relatively short H:N/N compared to L:Pso [29(1)], and a single node (corner node) ventral to the primary squamosal node row temporal roof angled < 22º [27(1)] unites pachycephalosaurines more derived than "*Sphaerotholus*" *buchholtzae* and "*Sphaerotholus*" *edmontonensis* (although a reversal to a temporal roof angle > 26º unites *Pachycephalosaurus wyomingensis*, and *Prenocephale prenes*; this character state is unknown for *Tylocephale gilmorei*). *Pachycephalosaurus wyomingensis*, *Prenocephale prenes*, *Sphaerotholus goodwini* and *Tylocephale gilmorei* are united by the dorsal position of two main depressions for the atlanto-occipital capsular membrane/ligament [25(2)] (see Tsuihiji, 2010, for soft tissue correlates), by a restrictive posterior exposure of the mesial extension of the parietal [35(2)] (also present in *Acrotholus audeti*, *Foraminacephale brevis*, and *Stegoceras validum*), and the placement of the medial node of the primary squamosal node row on the squamosal [39(0)] (also present in *Goyocephale lattimorei* and *Stegoceras validum*). *Pachycephalosaurus wyomingensis* and *Tylocephale gilmorei* are united by a straight dorsolateral contact between the postorbital and squamosal in dorsal view [45(0)], but this is also pleomorphic for Pachycephalosauridae.

3.4 Discussion

Contrary to Williamson and Carr (2016) and Jasinski and Sullivan (2016) NMMNH P-33898 ("*Stegoceras novomexicanum*") does not possess an elongate frontal-prefrontal contact compared to *Stegoceras validum*. Furthermore, additional purported diagnostic features are intraspecifically or ontogenetically variable in other taxa. The tapered frontal-nasal contact purportedly diagnostic for "*Stegoceras novomexicanum*" is variably present in both *Colepiocephale lambei* (Schott et al., 2009) and in *Stegoceras validum* (TMP1992.002.0003). Frontal domes that flatten laterally near the supraorbital elements represent an ontogenetically ephemeral feature in *Stegoceras validum* (e.g., UALVP 8502) as the frontal dome tends to expand mediolaterally. The angle between the parietal-squamosal contacts appears to include a dorsoventral component in Jasinski and Sullivan (2016). The measured angle does not appear to follow the dorsal, more complete border, but is measured from a posterior landmark at the ventral margin of the contact to an anterior point along the dorsal margin. Measuring continuously along the dorsal margin of the contact results in a steeper angle, more like specimens of *Stegoceras validum*. The purported relatively medial position of the supratemporal fenestrae can be demonstrated by measuring the inter-fenestral width of the parietal. This width is essentially the same in both NMMNH P-33898 (10.9 mm) and TMP1982.020.0189 (12.7 mm), which only differ by 4mm in W:F/P. Finally, frontoparietal sutural fusion is highly variable ontogenetically in *Stegoceras validum* (fused in TMP1992.002.0003, W:F/P = 46.07 mm; unfused in TMP2017.012.0019, W:F/P = 88.54 mm), thus is not a diagnostic feature of "*Stegoceras novomexicanum*", nor is it a consistent indicator of maturity. Finally, size is not a valid species diagnosis for pachycephalosaurids (Sullivan 2003). Thus, Williamson and Brusatte (2016) are correct to invalidate *Stegoceras novomexicanum*.

Amongst pachycephalosaurids, the length of the parietal scales with positive allometry relative to the length of the frontal. Thus, smaller frontoparietals should have relatively elongate frontals, compared to the parietals, which likely contributed to the putatively but not substantively diagnostic frontal length of *Amtocephale gobiensis* (Watabe et al., 2011). The length of the frontal compared to the parietal does distinguish *Amtocephale gobiensis* from some species (*Acrotholus audeti*, *Foraminacephale brevis*, *Pachycephalosaur*us *wyomingensis, Prenocephale prenes*, and *Sphaerotholus edmontonensis*). However, this feature alone is not diagnostic of *Amtocephale gobiensis*.

Ratios should only be used in diagnoses if the two compared features isometrically scale. Most linear measurements of pachycephalosaurid frontoparietals allometrically scale with respect to frontoparietal lengths and widths (Evans et al., 2013; Schott and Evans 2016; Schott et al. 2011), and thus ratios will not be maintained though growth. For example, that the length of the frontal scales with negative allometry relative to the length of the parietal.

The anatomy of the fused frontoparietal is included in the diagnosis of nearly every pachycephalosaurid species. Despite this, even large morphometric analyses of pachycephalosaurids have typically been restricted to four to six species (Evans et al. 2013; Schott and Evans 2016; Williamson and Brusatte 2016; Woodruff et al. 2021). The PCA of pachycephalosaurid frontoparietals presented in this chapter has the highest taxonomic diversity of any analysis so far performed, and includes *Pachycephalosaurus wyomingensis* and *Prenocephale prenes* for the first time. PCA analyses reflect broad taxonomic distinctions. Individual species are sometimes completely distinct in a PC (e.g., *Pachycephalosaurus wyomingensis* in PC 3 of the non-transformed iteration). Typically at least two PCs are required to isolate a given species (e.g. PC's 1 and 2 in the W:F/P proportionate iteration). Despite this, only a few antagonistically loading variables were able to sufficiently divide pachycephalosaurid species into discrete character states for phylogenetic analyses.

Statistically significant separation of features in previously identified characters were recovered. However, these did not always separate taxa based on their previous assignments. *Acrotholus audeti* and *Colepiocephale lambei* possess steeply angled anterior portions of the temporal roof ("arched" temporal roof of previous studies), whereas *Sphaerotholus goodwini* is reassessed as having a shallowly angled anterior portion of the temporal roof ("horizontal" temporal roof of previous analyses). It should be noted that pachycephalosaurids also appear to vary in the posterior inclination of the parietal, compared to the frontal. How this relates to scoring of the temporal roof morphology is unknown, but should be considered in future analyses, perhaps using the posteroventral extent of the parietal as the posterior "horizontal" landmark.

"*Sphaerotholus*" *edmontonensis* and *Sphaerotholus goodwini* were reassessed as each possess a broad frontal-palpebral contact, contrary to previous assessments (Longrich et al.,

2010). *Stegoceras validum* is polymorphic for the posterior exposure of the medial extension of the parietal and includes specimens with broad and narrow exposures, as well as no exposure (inter-squamosal contact). *Pachycephalosaurus wyomingensis* is also reassessed as polymorphic, with specimens possessing a narrow exposure of the medial extension of the parietal or inter-squamosal contact.

These revised codings emphasise the importance of statistically testing for distinct character states. Both Jenks natural breaks and mixture analyses were used to assess statistical groupings of residuals from RMA, but Jenks natural breaks typically outperformed mixture analyses by separating specimens more consistently in taxonomic terms, whereas mixture analyses tended to divide specimens of a single species between groups (polymorphism). Future studies will have to replicate RMA regressions and statistical testing of residuals when assessing new material, as placement and orientation (slope and intercept) of the regression will change as new information is added and would not be comparable to the gaps identified in this analysis.

The relationship between the width of the frontal and the width of the parietal appears to be phylogenetically informative (particularly the width of the parietal; W:Po/stf/Sq) and likely predicts the location of initial dome inflation. The parietal is proportionally wider in species where the dome developed initially on the parietals (eg. *Foraminacphele brevis*, *Pachycephalosaurus wyomingensis*), compared to species where the dome initially developed on the frontals (e.g., *Stegoceras validum*). Regarding species for which a large ontogenetic sample is known, the allometric relationship of W:Po/stf/Sq to W:F/P is congruent with differences in initial areas of dome development. In *Stegoceras validum*, dome inflation initiates in the frontals (Goodwin et al. 2016; and possibly the anterior portion of the parietals, Schott et al., 2011), then progresses posteriorly to incorporate the posterior parietal shelf. *Colepiocephale lambei* would have preserved posterior medial extension of the parietal that was not inflated, resulting in a posterior shelf to the dome. Although the allometric relationship between W:Po/stf/Sq and W:F/P is statistically isometric, the 95% confidence intervals were large compared to other species. This may be due to a smaller sample size, or a large amount of individual variation. When *Colepiocephale lambei* was combined with *Stegoceras validum*, W:Po/stf/Sq scaled with negative allometry relative to W:F/P (more so than when *Stegoceras validum* was analysed

alone). Species where the middle width of the parietal (W:Po/stf/Sq) scales quicker than the anterior width (W:F/P) also have domes that expand anteriorly through ontogeny (where known). Species where the middle width of the parietal scales slower than the anterior width have domes that are anteriorly restricted and/or progress posteriorly though ontogeny. Thus, frontoparietal widths (particularly parietal widths) can provide information on the origin and ontogenetic progression of the dome.

Additionally, almost the exact same taxonomic separation is observed when H:N/N is compared to W:Po/stf/Sq, with parietal first species possessing proportionately shorter H:N/N. The cranial dome of *Foraminacephale brevis* begins inflating via the entire parietal, then progresses anteriorly, incorporating more and more of the frontals through ontogeny. This results in an ephemeral anterior frontal shelf as the frontal is incorporated into the dome, which also occurs in *Pachycephalosaurus wyomingensis* (e.g., MPM8111). By inflating the frontals and anterior portion of the parietals first, the height of the frontal-nasal contact increases earlier in dome development of *Stegoceras validum*, whereas it is delayed in *Foraminacephale brevis* and *Pachycephalosaurus wyomingensis,* resulting in the shorter condition.

Many characters in the working pachycephalosaurid matrix are located on the frontoparietal dome. The dome is known to develop from flat-headed juveniles in several species (*Foraminacephale brevis*, *Pachycephalosaurus wyomingensis*, and *Stegoceras validum*; Schott and Evans 2016; Goodwin and Horner 2009; Schott et al. 2011). Yet, taxa known only from juvenile remains have until now remained coded as if they are or would never develop a dome. For example, *Goyocephale lattimorei* and *Homalocephale calathocercos* have historically been scored as not possessing a groove separating the frontonasal boss from the supraorbital lobes [28(0)]. However, both *Foraminacephale brevis* and *Stegoceras validum,* which possess this groove in developed adults, do not possess the groove as flat-headed juveniles. In these instances, unless the feature is known to be ontogenetically independent, taxa known solely from juvenile specimens should be scored as inapplicable for features that develop in maturity (Prieto-Márquez, 2014).

The 50% majority consensus recovered in this analysis is largely incongruent with previous analyses. Major differences include recovering *Colepiocephale lambei* as a

pachycephalosaurine, a polyphyletic *Sphaerotholus,* more derived placements for *Prenocephale prenes* and *Tylocephale gilmorei*, and the basal positions of *Alaskacephale gangloffi*, *"Sphaerotholus" buchholtzae,* and *"Sphaerotholus" edmontonensis* within Pachycephalosaurinae. Following the rule of monophyly, *"Sphaerotholus" buchholtzae* and *"Sphaerotholus" edmontonensis* cannot be referred to *Sphaerotholus* and require a new generic name. However, given the strict consensus tree did not resolve an immediate sister-group to pachycephalosaurid relationships other than *"Sphaerotholus" buchholtzae* and *"Sphaerotholus" edmontonensis* and that all the character states uniting *"Sphaerotholus" buchholtzae* and *"Sphaerotholus" edmontonensis* are converged upon in other pachycephalosaurids, taxonomic revisions should be withheld until the entire character matrix is reviewed, and a more resolved phylogenetic tree is recovered. A monophyletic *Sphaerotholus* is typically recovered close to Pachycephalosaurini (*Dracorex hogwartsia*, *Pachycephalosaurus wyomingensis*, and *Stygimoloch spinifer*; Evans et al. 2013, 2021, Schott and Evans 2016, Williamson and Brusatte 2016; Woodruff et al. 2021). A basal position of *"Sphaerotholus" buchholtzae* and *"Sphaerotholus" edmontonensis* within Pachycephalosaurinae is more consistent with the topology recovered by Longrich et al. (2010), where *Prenocephale prenes* and *Tylocephale gilmorei* were more closely related to *Pachycephalosaurus wyomingensis* than *"Sphaerotholus" buchholtzae* and *"Sphaerotholus" edmontonensis* were.

Only a few characters in the working pachycephalosaurid character matrix were selected for re-examination in this study but the entire matrix should be re-examined. However, the total number of characters is very low (~2.8 characters/pachycephalosaurian) for the number of taxa in the analysis. Of the 46 characters analysed, 15 code for synapomorphies of Pachycephalosauria, and do not provide any information on pachycephalosaurian interrelationships. Most pachycephalosaurians are known from very incomplete material and can often not be scored, resulting in 54% of the character matrix scored as [?]. A much broader understanding of pachycephalosaurian anatomy is likely required to have a robust understanding of their interrelationships. The dearth of pachycephalosaurian material may become an unexpected advantage in some regards for future studies. There are relatively few characters to critically re-evaluate, compared to other smaller bodied dinosaurs (e.g. dromaeosaurids; Powers et al., 2020)

3.5 Conclusions

Numerous errors in the pachycephalosaurian character matrix likely had a strong effect on previously purported interrelationships. Removing invalid species, revising character states and taxon assessments, and creating novel phylogenetic characters resulted in a novel, but largely unresolved Pachycephalosauridae. Pachycephalosaurine interrelationships are largely unknown. Strong hypotheses of pachycephalosaurian interrelationships will require a large amount of osteological anatomy, which is currently unknown for most pachycephalosaurians. Character matrices for phylogenetic analyses should be periodically reviewed, especially when initially coding taxa for continuous morphological characters.

3.6 Literature Cited

Bourke, J.M., Porter, W.R., Ridgely, R.C., Lyson, T.R., Schachner, E.R., Bell, P.R., Witmer, L.M., 2014. Breathing life into dinosaurs: tackling challenges of soft-tissue restoration and nasal airflow in extinct species. Anatomical Record 297, 2148–2186. https://doi.org/10.1002/ar.23046

Brown, B., Schlaikjer, E.M., 1943. A study of the troödont dinosaurs with the description of a new genus and four new species. Bulletin of the American Museum of Natural History 82, 115–150.

Butler, R.J., Zhao, Q., 2009. The small-bodied ornithischian dinosaurs *Micropachycephalosaurus hongtuyanensis* and *Wannanosaurus yansiensis* from the Late Cretaceous of China. Cretaceous Research 30, 63–77. https://doi.org/10.1016/j.cretres.2008.03.002

Dong, Z., 1978. A new genus of Pachycephalosauria from Laiyang, Shantung. Vertebrata PalAsiatica 16, 225–229.

Evans, D.C., Brown, C.M., Ryan, M.J., Tsogtbaatar, K., 2011. Cranial ornamentation and ontogenetic status of *Homalocephale calathocercos* (Ornithischia: Pachycephalosauria) from the Nemegt Formation, Mongolia. Journal of Vertebrate Paleontology 31, 84–92. https://doi.org/10.1080/02724634.2011.546287

Evans, D.C., Brown, C.M., You, H., Campione, N.E., 2021. Description and revised diagnosis of Asia's first recorded pachycephalosaurid, *Sinocephale bexelli* gen. nov., from the Upper Cretaceous of Inner Mongolia, China. Canadian Journal of Earth Sciences 58, 981–992. https://doi.org/10.1139/cjes-2020-0190

Evans, D.C., Hayashi, S., Chiba, K., Watabe, M., Ryan, M.J., Lee, Y.N., Currie, P.J., Tsogtbaatar, K., Barsbold, R., 2018. Morphology and histology of new cranial specimens of Pachycephalosauridae (Dinosauria: Ornithischia) from the Nemegt Formation, Mongolia. Palaeogeography, Palaeoclimatology, Palaeoecology 494, 121–134. https://doi.org/10.1016/j.palaeo.2017.11.029

Evans, D.C., Schott, R.K., Larson, D.W., Brown, C.M., Ryan, M.J., 2013. The oldest North American pachycephalosaurid and the hidden diversity of small-bodied ornithischian dinosaurs. Nature Communications 4, 1–10. https://doi.org/10.1038/ncomms2749

Fowler, D.W., 2017. Revised geochronology, correlation, and dinosaur stratigraphic ranges of the Santonian-Maastrichtian (Late Cretaceous) formations of the Western Interior of North America. PLoS ONE 12, e0188426. https://doi.org/10.1371/journal.pone.0188426

Giffin, E.B., 1989. Notes on pachycephalosaurs (Ornithischia). Journal of Paleontology 63, 525–529. https://doi.org/10.1017/S0022336000019739

Gilmore, C.W., 1931. A new species of Troödont dinosaur from the Lance Formation of Wyoming. Proceedings of the U.S. National Museum 79, 1–6.

Goloboff, P.A., Catalano, S.A., 2016. TNT version 1.5, including a full implementation of phylogenetic morphometrics. Cladistics 32, 221–238. https://doi.org/10.1111/cla.12160

Goodwin, M.B., Buchholtz, E.A., Johnson, R.E., 1998. Cranial anatomy and diagnosis of *Stygimoloch spinifer* (Ornithischia: Pachycephalosauria) with comments on cranial display structures in agonistic behavior. Journal of Vertebrate Paleontology 18, 363–375. https://doi.org/10.1080/02724634.1998.10011064

Goodwin, M.B., Evans, D.C., 2016. The early expression of squamosal horns and parietal ornamentation confirmed by new end-stage juvenile *Pachycephalosaurus* fossils from the Upper Cretaceous Hell Creek Formation, Montana. Journal of Vertebrate Paleontology 36, e1078343. https://doi.org/10.1080/02724634.2016.1078343

Hammer, Ø., Harper, D.A.T., Ryan, P.D., 2001. Past: paleontological statistics software package for education and data analysis. Palaeontologia Electronica 4, 1–9.

Horner, J.R., Goodwin, M.B., 2009. Extreme cranial ontogeny in the upper cretaceous dinosaur *Pachycephalosaurus*. PLoS ONE 4, e7626. https://doi.org/10.1371/journal.pone.0007626

Jasinski, S.E., Sullivan, R.M., 2016. The validity of the Late Cretaceous pachycephalosaurid *Stegoceras novomexicanum* (Dinosauria: Pachycephalosauridae), in: Sullivan, R.M.,

Lucas, S.G. (Eds.), Fossil Record 5. New Mexico Museum of Natural History and Science, Bulletin 74, Albuquerque, pp. 107–115.

Longrich, N.R., Sankey, J., Tanke, D., 2010. *Texacephale langstoni*, a new genus of pachycephalosaurid (Dinosauria: Ornithischia) from the upper Campanian Aguja Formation, southern Texas, USA. Cretaceous Research 31, 274–284. https://doi.org/10.1016/j.cretres.2009.12.002

Maddison, W.P., Maddison, D.R., 2021. Mesquite: a modular system for evolutionary analysis.

Maryańska, T., Chapman, R.E., Weishampel, D.B., 2004. Pachycephalosauria, in: Weishampel, D.B., Dodson, P., Osmólska, H. (Eds.), The Dinosauria. University of California Press, Berkley, pp. 464–477.

Maryańska, T., Osmólska, H., 1974. Pachycephalosauria, a new suborder of ornithischian dinosaurs. Palaeontologica Polonica 30, 45–120.

Perle, A., Maryańska, T., Osmólska, H., 1982. *Goyocephale lattimorei* gen. et sp. n., a new flat-headed pachycephalosaur (Ornithischia, Dinosauria) from the Upper Cretaceous of Mongolia. Acta Palaeontologica Polonica 27, 8–45.

Powers, M.J., Sullivan, C., Currie, P.J., 2020. Re-examining ratio based premaxillary and maxillary characters in Eudromaeosauria (Dinosauria: Theropoda): Divergent trends in snout morphology between Asian and North American taxa. Palaeogeography, Palaeoclimatology, Palaeoecology 547, 109704. https://doi.org/10.1016/j.palaeo.2020.109704

Prieto-Márquez, A., 2014. A juvenile *Edmontosaurus* from the late Maastrichtian (Cretaceous) of North America: Implications for ontogeny and phylogenetic inference in saurolophine dinosaurs. Cretaceous Research 50, 282–303. https://doi.org/10.1016/j.cretres.2014.05.003

Schott, R., Evans, D., 2011. New information on pachycephalosaurid dinosaur diversity in the Foremost Formation (Campanian) of Alberta, in: Society of Vertebrate Paleontology

Abstracts of Papers Seventy-First Annual Meeting. Society of Vertebrate Paleontology, Las Vegas, p. 189.

Schott, R.K., Evans, D.C., 2016. Cranial variation and systematics of *Foraminacephale brevis* gen. nov. and the diversity of pachycephalosaurid dinosaurs (Ornithischia: Cerapoda) in the Belly River Group of Alberta, Canada. Zoological Journal of the Linnean Society 179, 865–906. https://doi.org/10.1111/zoj.12465

Schott, R.K., Evans, D.C., Goodwin, M.B., Horner, J.R., Brown, C.M., Longrich, N.R., 2011. Cranial ontogeny in *Stegoceras validum* (Dinosauria: Pachycephalosauria): A quantitative model of pachycephalosaur dome growth and variation. PLoS ONE 6, e21092. https://doi.org/10.1371/journal.pone.0021092

Schott, R.K., Evans, D.C., Williamson, T.E., Carr, T.D., Goodwin, M.B., 2009. The anatomy and systematics of *Colepiocephale lambei* (Dinosauria: Pachycephalosauridae). Journal of Vertebrate Paleontology 29, 771–786. https://doi.org/10.1671/039.029.0329

Sereno, P.C., 2000. The fossil record, systematics and evolution of pachycephalosaurs and ceratopsians from Asia, in: Benton, M.J., Shishkin, M.A., Unwin, D.M., Kurochkin, E.N. (Eds.), The Age of Dinosaurs in Russia and Mongolia. Cambridge University Press, Cambridge, pp. 480–516.

Sereno, P.C., 1998. A rationale for phylogenetic definitions, with application to the higher-level taxonomy of Dinosauria. Neues Jahrbuch fur Geologie und Palaontologie - Abhandlungen 210, 41–83. https://doi.org/10.1127/njgpa/210/1998/41

Sereno, P.C., 1986. Phylogeny of the bird-hipped dinosaurs (Order Ornithischia). National Geographic Research 2, 234–256.

Simões, T.R., Caldwell, M.W., Palci, A., Nydam, R.L., 2017. Giant taxon-character matrices: quality of character constructions remains critical regardless of size. Cladistics 33, 198–219. https://doi.org/10.1111/cla.12163

Snively, E., Theodor, J.M., 2011. Common functional correlates of head-strike behavior in the pachycephalosaur *Stegoceras validum* (Ornithischia, Dinosauria) and combative artiodactyls. PLoS ONE 6, e21422. https://doi.org/10.1371/journal.pone.0021422

Sternberg, C.M., 1945. Pachycephalosauridae proposed for dome-headed dinosaurs, *Stegoceras lambei* n. sp., described. Source: Journal of Paleontology 19, 534–538.

Sues, H.-D., Galton, P.M., 1987. Anatomy and classification of the North American Pachycephalosauria (Dinosauria: Ornithischia). Paleontographica Abteilung A 198, 1–40.

Sullivan, R.M., 2006. A taxonomic review of the Pachycephalosauridae (Dinosauria: Ornithischia), in: Lucas, S.G., Sullivan, R.M. (Eds.), Late Cretaceous Vertebrates from the Western Interior. New Mexico Museum of Natural History and Science, Bulletin 35, Albuquerque, pp. 347–365.

Sullivan, R.M., 2003. Revision of the dinosaur *Stegoceras* Lambe (Ornithischia, Pachycephalosauridae). Journal of Vertebrate Paleontology 23, 181–207. https://doi.org/10.1671/0272-4634(2003)23[181:ROTDSL]2.0.CO;2

Tsuihiji, T., 2010. Reconstructions of the axial muscle insertions in the occipital region of dinosaurs: Evaluations of past hypotheses on Marginocephalia and Tyrannosauridae using the extant phylogenetic bracket approach. Anatomical Record 293, 1360–1386. https://doi.org/10.1002/ar.21191

Watabe, M., Tsogtbaatar, K., Sullivan, R.M., 2011. A new pachycephalosaurid from the Baynshire Fromation (Cenomanian-Late Santonian), Gobi Desert, Mongolia, in: Sullivan, R.M., Lucas, S.G., Spielmann, J.A. (Eds.), Fossil Record 3. New Mexico Museum of Natural History and Science, Bulletin 53, Albuquerque, pp. 489–497.

Williamson, T.E., Brusatte, S.L., 2016. Pachycephalosaurs (Dinosauria: Ornithischia) from the Upper Cretaceous (upper Campanian) of New Mexico: A reassessment of *Stegoceras novomexicanum*. Cretaceous Research 62, 29–43. https://doi.org/10.1016/j.cretres.2016.01.012

Williamson, T.E., Carr, T.D., 2002. A new genus of derived pachycephalosaurian from western North America. Journal of Vertebrate Paleontology 22, 779–801. https://doi.org/10.1671/0272-4634(2002)022[0779:ANGODP]2.0.CO;2

Woodruff, D.C., Goodwin, M.B., Lyson, T.R., Evans, D.C., 2021. Ontogeny and variation of the pachycephalosaurine dinosaur *Sphaerotholus buchholtzae*, and its systematics within the genus. Zoological Journal of the Linnean Society 193, 563–601.

3.7 Tables and Figures

Table 3.1. Results from RMA regressions of log-transformed homologous linear measuremnts of pachycephalosaurid frontopareital domes.

y vs. x	n	r	slope	ci	incercept	ci	p
L:P vs. L:F	32	0.86	1.51	1.23 – 1.84	-0.79	-1.34 – -0.32	4.44E-10
L:Prf vs. L:F	14	0.66	1.33	0.88 – 1.8	-0.97	-1.89 – -0.19	0.0095
L:Prf vs. W:F/P	14	0.75	0.72	0.44 – 0.92	-0.10	-0.46 – 0.39	0.0019
L:Pl vs. W:Prf/Pl	105	0.09	1.23	1.02 – 3.83	-0.93	-5.14 – -0.59	0.38
L:Pl vs. W:F/P	108	0.39	1.09	0.90 – 1.27	-0.90	-1.23 – -0.54	3.82E-5
L:Pl vs. W:Po/stf/Sq	73	0.10	1.14	0.79 – 3.66	-0.91	-5.25 – -0.31	0.41
W:post vs. WFP	34	0.64	1.31	0.99 – 1.57	-1.26	-1.74 – -0.65	4.21E-4
H:N/N vs. L:Pso	76	0.58	1.99	1.44 – 2.40	-1.48	-2.05 – -0.74	2.28 E-8
L:Po vs. W:Po/stf/Sq	83	0.68	1.11	0.85 – 1.29	-0.41	-0.73 – 0.05	1.79E-12
W:Pl/Pso vs. W:Po/stf/Sq	75	0.85	1.32	1.15 – 1.53	-0.64	-0.99 – -0.32	7.58E-22
W:Po/stf/Sq vs. W:F/P	93	0.92	0.99	0.90 – 1.09	-0.07	-0.26 – 0.08	2.52E-38

Table 3.2. Results from Jenks natural break analyses.

Distribution	GOF	Range of natural gap
Anterior angle of the temporal roof	0.7088	21.28º – 26.14º
Residuals (L:Pl vs. W:Prf/Pl)	0.7032	-0.12 – -0.15
Residuals (L:Pl vs. W:F/P)	0.7412	-0.13 – -0.18
Residuals (L:Pl vs. W:Po/stf/Sq	0.7996	-0.18 – -0.7
Residuals (W:post vs. W:FP)	0.6865	-0.05 – 0.015
Residuals (H:N/N vs. L:Pso)	0.7343	-0.07 – 0.11
Residuals (W:Po/stf/Sq vs. W:Pl:Pso)	0.7527	0.17 – 0.31
Residuals (H:N/N vs. W:Po/stf/Sq)	0.7551	-0.03 – 0.01

Table 3.3. Results from Mixture Analyses. AIC values reported. Best fitting models are bolded. An asertix identifies significantly better best fitting models.

Variable	1 Group	2 Groups	3 Groups
Anterior angle of the temporal roof	**80.99***	83.98	90.26
Residuals (L:Pl vs. W:Prf/Pl)	-192.4	**-223.1**	-222
Residuals (L:Pl vs. W:F/P)	-244	-304.3	**-308.5***
Residuals (L:Pl vs. W:Po/stf/Sq)	-126.9	**-179.8**	-178.1
Residuals (W:post vs. W:FP)	-70.95	**-72.92** (distributions not exclusive)	-69.63 (distributions not exclusive)
Residuals (H:N/N vs. L:Pso)	-127.5	**-142.9***	-138.2
Residuals (L:Po vs. W:Po/stf/Sq)	-238.6	-253.4	**-256.5*** (distributions not exclusive)
Residuals (W:Po/stf/PSq vs. W:Pl/Pso)	-285.8	-294.6	**-295.2** (distributions not exclusive)
Residuals H:N/N vs. W:Po/stf/Sq	-108.4	**-123.2***	NA

Table 3.4. Loadings for the LOG-transformed PCA of frontoparietal linear measurements.
Measurement's loading >|0.30| are bolded.

	PC 1 (76.5%)	PC 2 (7.89%)	PC 3 (5.20%)	PC 4 (3.85%)	PC 5 (2.09%)
H:n/n	**0.35945**	0.22585	**-0.45811**	0.036861	0.10845
H:n/prf	**0.33384**	0.030359	-0.27447	**-0.71318**	0.28266
H:pfr/pl	0.29941	0.051247	-0.06823	0.012434	-0.28256
H:pl/pso	**0.31337**	-0.05001	-0.03522	0.045716	**-0.78905**
H:pso/po	0.26845	-0.24499	**0.33575**	**-0.44685**	-0.1793
W:n/pfr	0.22577	0.24733	-0.04404	0.20721	0.045198
W:pfr/pl	0.21411	-0.17112	-0.08141	0.21853	0.099813
W:pl/pso	0.19017	0.040245	0.10929	0.14832	0.028041
W:pso/po	0.21541	-0.02717	0.11287	0.065589	0.084795
W:f/p	0.23679	-0.05843	0.1508	0.14367	0.23901
W:po/stf/sq	0.2401	-0.25797	**0.3977**	-0.0048	0.15393
L:pl	0.10418	**0.83697**	**0.38252**	-0.06676	-0.00696
L:pso	0.19282	-0.07256	**0.4146**	0.11294	0.12144
L:po	0.23699	-0.02734	-0.23531	0.192	0.003538
L:f	0.14865	-0.06241	-0.09158	0.19057	0.052637
T:f/p	0.28291	-0.09863	-0.00603	0.24503	0.23531

Table 3.5. Loadings for the W:F/P proportionate PCA of frontoparietal linear measurements. Measurement's loading >|0.30| are bolded.

	PC 1 (34.9%)	PC 2 (20.0%)	PC 3 (14.6%)	PC 4 (9.99%)	PC 5 (5.48%)
H:n/n	0.16134	-0.279	0.23997	**0.34673**	-0.03731
H:n/prf	0.063878	-0.08756	0.27168	0.26868	-0.1797
H:pfr/pl	0.12528	-0.04336	0.24086	0.23169	0.11593
H:pl/pso	0.10806	0.006736	0.24208	0.16034	0.035279
H:pso/po	-0.00916	0.25405	**0.35487**	0.25336	-0.05113
W:n/pfr	0.29742	-0.03406	-0.12599	**0.34979**	-0.20448
W:pfr/pl	**0.32509**	0.0993	0.23555	**-0.37434**	**-0.33964**
W:pl/pso	**0.37808**	0.21509	-0.22175	0.17215	0.22004
W:pso/po	0.29496	0.2398	0.016654	0.23321	-0.11586
W:po/stf/sq	-0.2603	**0.67965**	**0.38627**	0.008935	-0.0114
L:pl	0.12284	0.062823	-0.28137	**0.33826**	0.3057
L:pso	-0.00303	0.24901	-0.03392	0.061134	**0.44817**
L:po	**0.33593**	-0.18979	0.19759	-0.10846	-0.17565
L:f	**0.56713**	0.22576	-0.02834	**-0.40794**	0.21477
T:f/p	0.03165	**-0.34406**	**0.48567**	-0.14522	**0.59882**

Table 3.6. Loadings for the non-transformed PCA of frontoparietal linear measurements.

Measurement's loading >|0.30| are bolded.

	PC 1 (88.9%)	PC 2 (4.32%)	PC 3 (2.19%)	PC 4 (1.22%)	PC 5 (1.03%)
H:n/n	0.13245	0.26779	0.036576	**0.34146**	0.11352
H:n/prf	0.11621	0.06393	0.050941	**0.41406**	0.27021
H:pfr/pl	0.111	0.11496	-0.05842	0.23356	0.16633
H:pl/pso	0.10659	0.048878	-0.04668	0.073255	0.21138
H:pso/po	0.17345	-0.2179	-0.02641	**0.30485**	**0.40123**
W:n/pfr	0.13455	0.18578	**0.32685**	0.049492	0.1726
W:pfr/pl	0.25239	0.0523	-0.09943	**-0.56892**	0.28908
W:pl/pso	0.28718	0.19705	**0.37046**	-0.23289	-0.16613
W:pso/po	**0.39253**	0.035888	**0.36243**	-0.0389	0.14097
W:f/p	**0.43927**	0.066945	0.1631	-0.04176	**-0.40885**
W:po/stf/sq	**0.45388**	**-0.71763**	-0.10321	0.012853	0.014049
L:pl	0.020981	0.15424	0.28117	0.23548	-0.1959
L:pso	0.13957	-0.14822	-0.01446	0.17753	-0.20528
L:po	0.19645	**0.35493**	-0.23162	-0.08493	0.28806
L:f	0.16023	0.17298	**-0.32292**	-0.19537	0.15744
T:f/p	**0.33717**	0.25026	**-0.57447**	0.20733	**-0.40534**

Table 3.7. Loadings for the L:F proportionate PCA of frontoparietal linear measurements.
Measurement's loading >|0.30| are bolded.

	PC 1 (67.5%)	PC 2 (12.0%)	PC 3 (6.42%)	PC 4 (3.92%)	PC 5 (3.40%)
H:n/n	0.12803	**0.39191**	-0.07794	0.023154	0.28829
H:n/prf	0.12262	0.17345	-0.13825	0.10646	**0.37789**
H:pfr/pl	0.10647	0.16486	-0.0632	0.042708	0.28296
H:pl/pso	0.10615	0.1182	-0.07823	0.15797	0.17187
H:pso/po	0.20843	-0.12187	-0.13179	0.24091	**0.40159**
W:n/pfr	0.10612	0.21769	0.24792	0.17313	0.25218
W:pfr/pl	0.20648	0.10336	-0.17762	**0.51575**	**-0.46468**
W:pl/pso	0.28141	0.097244	**0.5362**	0.007442	-0.19155
W:pso/po	**0.39513**	0.046078	0.29268	0.21083	0.015568
W:f/p	**0.46154**	0.08319	0.096914	-0.29085	-0.28794
W:po/stf/sq	**0.52**	**-0.62599**	-0.22415	0.044044	0.097596
L:pl	0.02805	0.058202	**0.43388**	-0.24541	0.20711
L:pso	0.1532	-0.19297	0.13584	-0.27408	0.14482
L:po	0.12921	**0.36879**	-0.10004	0.20064	-0.1543
T:f/p	0.29822	**0.33949**	**-0.45255**	**-0.54836**	-0.08148
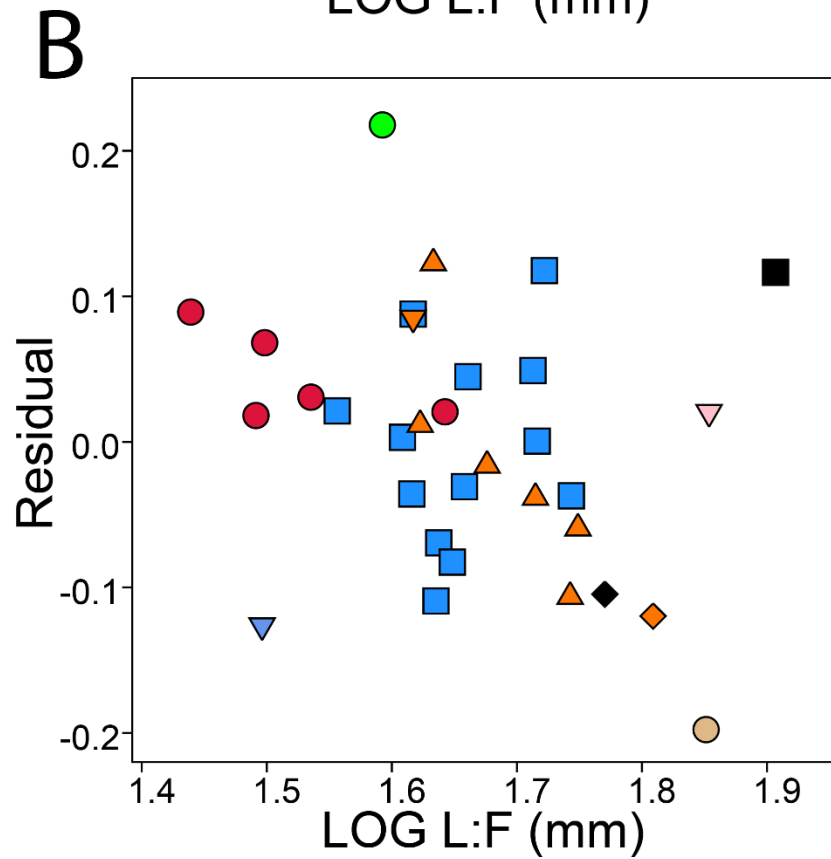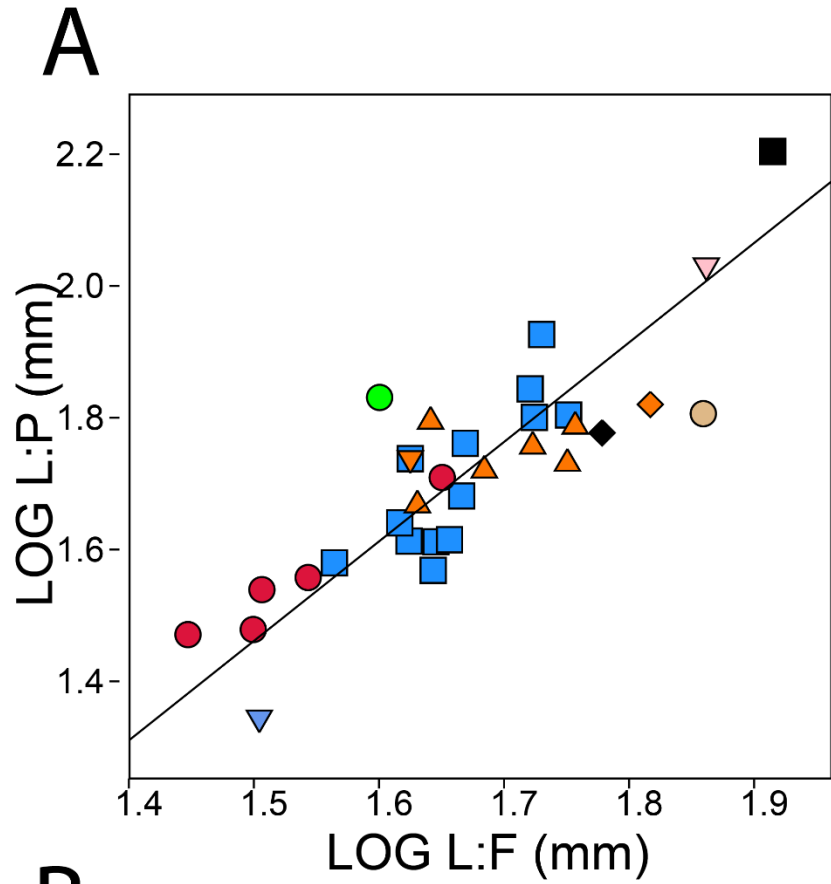
Figure 3.1. RMA regression of L:P vs. L:F amongst pachycephalosaurids. A) RMA regression. B) Residuals ploted against L:F. *Amotocephale gobiensis* – blue inverted triangle, *Acrotholus audeti* – green circle, *Foraminacphale brevis* – red circles, *Goyocephale lattimorei* – black diamond, *Homalocephale calathocercos* – brown circle, *Pachycephalosaurus wyomingensis* – black square, *Prenocephale prenes* – pink inverted triangle, *Sphaerotholus buchhotlzae* – orange triangles, *Sphaerotholus edmontonensis* – orange inverted triangle, *Sphaerotholus goodwini* – orange diamond, *Stegoceras valdium* – blue squares.

A

r=0.66
slope = 1.33 (0.88-1.80)
p = 0.0095

LOG L:Prf (mm)

1.35

1.20

1.05

1.5   1.6   1.7

LOG L:F (mm)

B

r=0.75
slope = 0.72 (0.44-0.92)
p = 0.0019

LOG L:Prf (mm)

1.35

1.20

1.05

1.65   1.80   1.95

LOG W:F/P (mm)

131
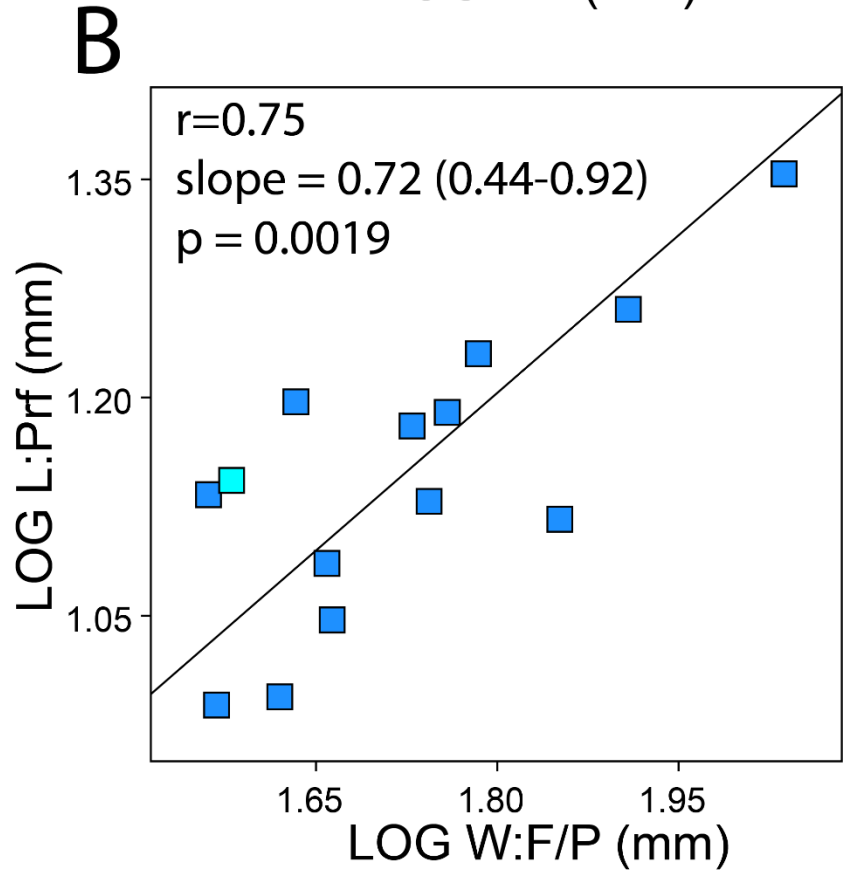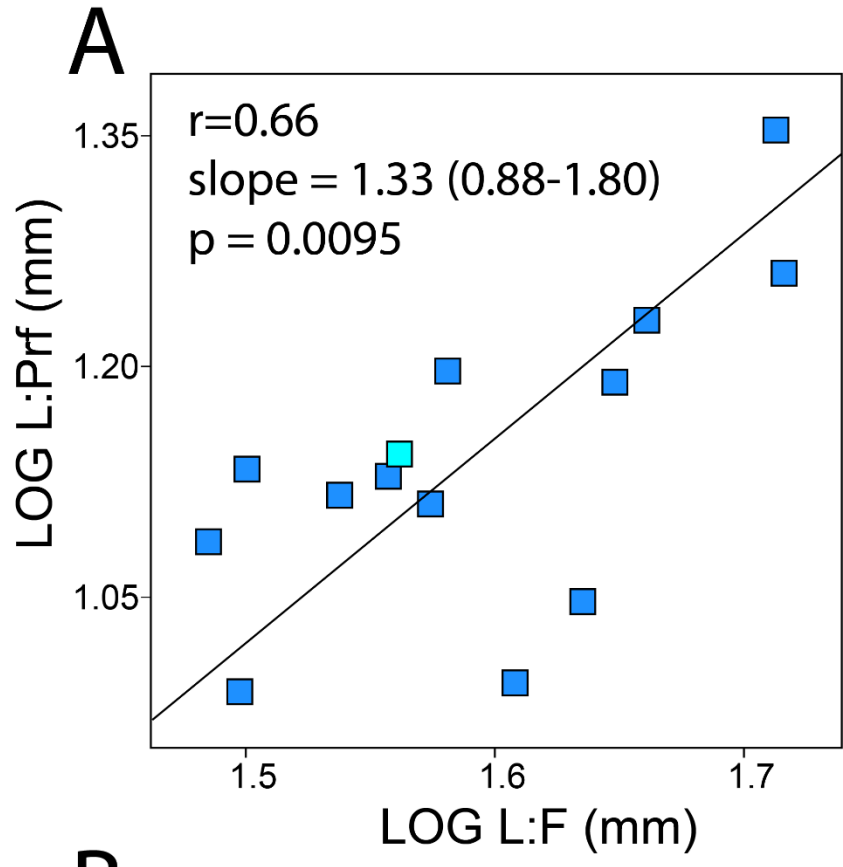
Figure 3.2. Purported diagnostic Prefrontal – Frontal contact length of *Stegoceras novomexicanum* compared to *Stegoceras validum*. A) RMA regression of L:Prf vs. L:F. B) RMA regression of L:Prf vs. W:F/P. *Stegoceras novomexicanum* – light blue square, *Stegoceras validum* – dark blue squares.

A) UALVP 2
14.0°
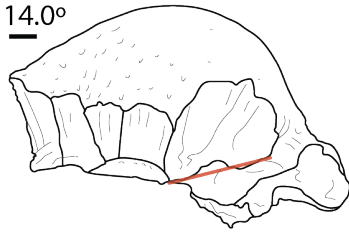
B) TMP1972.027.0001
16.2°
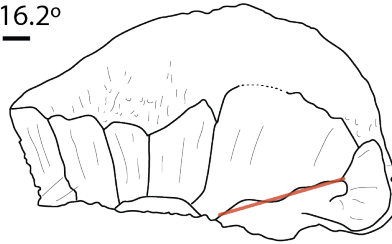
C) UALVP 47278
17.0°
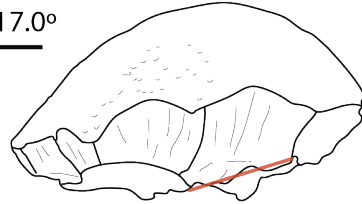
D) TMP1987.050.0029
13.8°
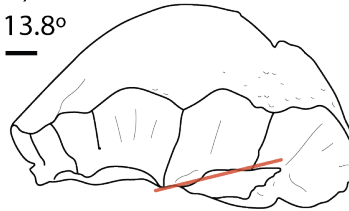
E) NMMNH P-27403
21.0°
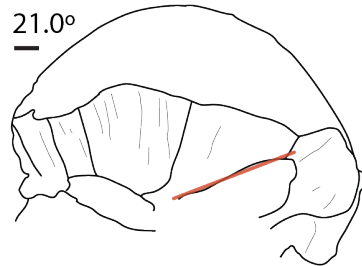
F) MPC-D 100/1203
21.3°
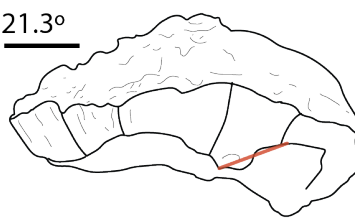
G) CMM V-87-1
27.2°
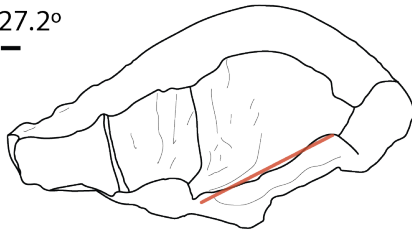
H) ROM68290
36.0°
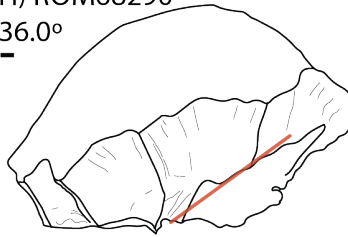
I) MPC-D 100/1207
26.8°
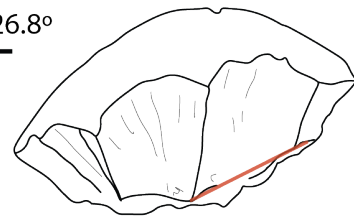
J) TMP1987.113.0003
29.0°
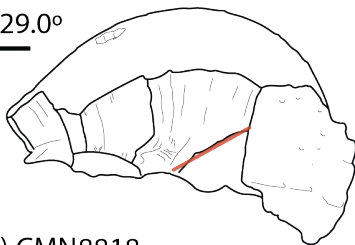
K) USNM PAL 537766
26.1°
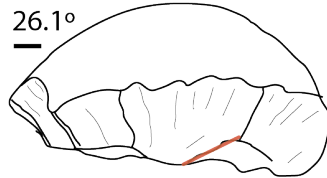
L) CMN8830
40.9°
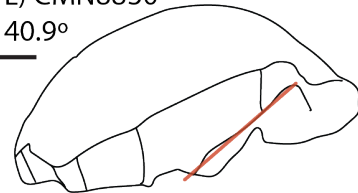
M) CMN8818
27.0°
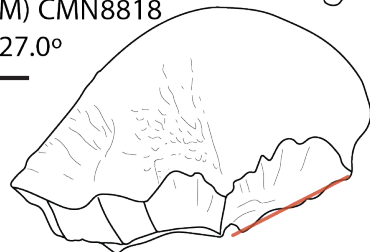
N) TMP1990.002.0001
31.4°
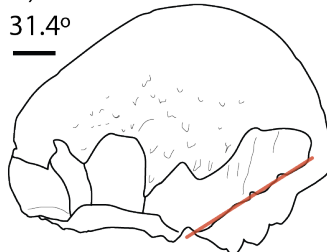
O) TMP2008.045.0001
28.7°

133
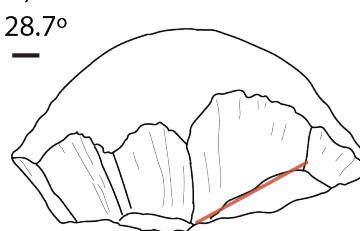
Figure 3.3. Variation in the anterior angles of the temporal roof amongst pachycephalosaurids. References are for published lateral figures. A) UALVP 2 – *Stegoceras validum*. B) TMP1972.027.0001 (mirrored) – *Stegoceras validum* C) UALVP 47278 (mirrored) – *Foraminacephale brevis*. D) TMP1987.050.0029 – *Foraminacephale brevis* (Schott and Evans, 2016). E) NMMNH P-27403 – *Sphaerotholus goodwini* (Williamson and Carr, 2002). F) MPC-D 100/1203 – *Amtocephale gobiensis* (Watabe et al., 2011). A-F represent [27(1)]. G) CMM V-87-1 – *Pachycephalosaurus wyomingensis*. ROM68290 – *Pachycephalosaurus wyomingensis* (photograph acquired from the ROM online collections (https://collections.rom.on.ca/start/12953). I) MPC-D 100/1207 – *Prenocephale prenes* (Evans et al., 2018). J) TMP1987.113.0003 – *Sphaerotholus buchholtzae*. K) USNM PAL 537766 – *Sphaerotholus buchholtzae* (Woodruff et al., 2021). L) CMN8830 – *Sphaerotholus edmontonensis* (Woodruff et al., 2021). M) CMN8818 – *Colepiocephale lambei* (mirrored) (Sternberg, 1945). N) TMP1990.002.0001 – *Colepiocephale lambei* (mirrored). O) TMP2008.045.0001 – *Acrotholus audeti* (Evans et al., 2013). G-O represent [27(2)]. Scale bars = 1 cm.
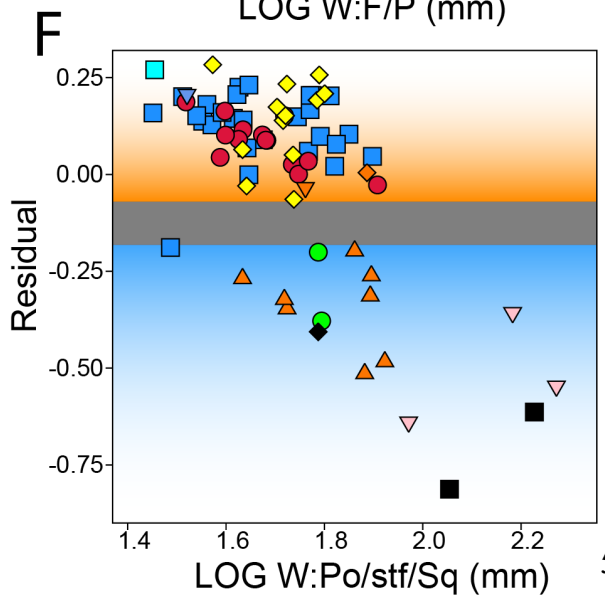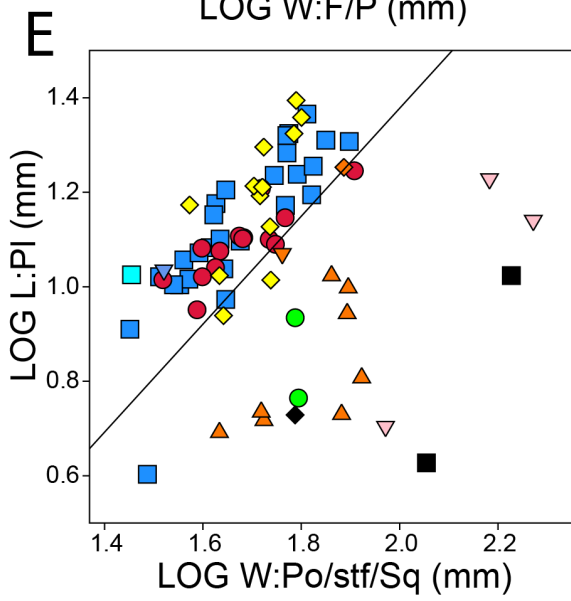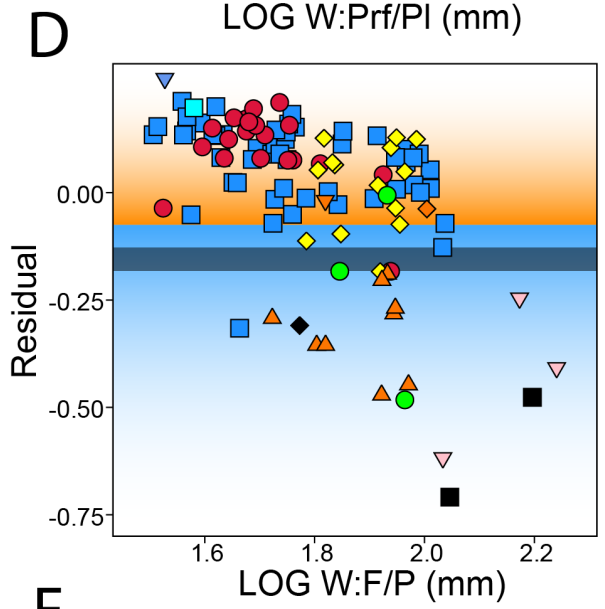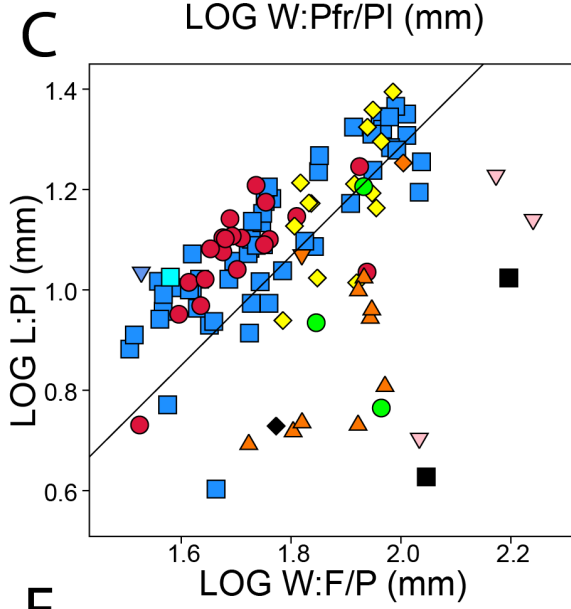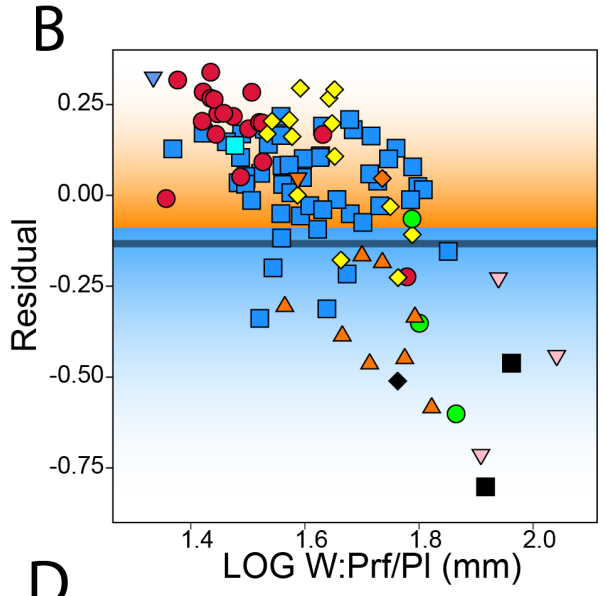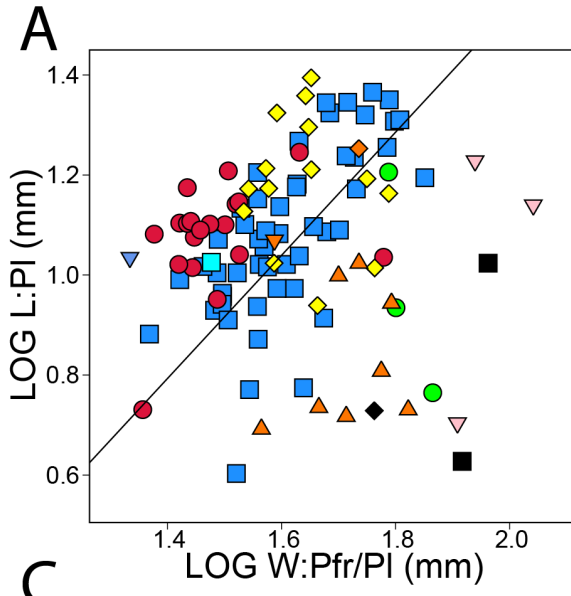
Figure 3.4. Statistical testing for discrete broad and restrictive frontal-palpebral contacts amongst pachycephalosaurids. A) RMA regression of L:Pl vs. W:Prf/Pl. B) Residuals of L:Pl vs. W:Prf/Pl. C) RMA regression of L:Pl vs. W:F/P. D) Residuals of L:Pl vs. W:F/P. E) RMA regression of L:Pl vs. W:Po/stf/Sq. F) Residuals of L:Pl vs. W:F/P. Grey boxes mark the natural gap identified in Jenks natural break analyses of the distribution of residuals. Blue and orange shading identify the bimodal groups identified in Mixture Analyses. *Amotocephale gobiensis* – blue inverted triangle, *Acrotholus audeti* – green circle, *Colepiocephale lambei* – yellow diamonds. *Foraminacphale brevis* – red circles, *Goyocephale lattimorei* – black diamond, *Pachycephalosaurus wyomingensis* – black square, *Prenocephale prenes* – pink inverted triangle, *Sphaerotholus buchhotlzae* – orange triangles, *Sphaerotholus edmontonensis* – orange inverted triangle, *Sphaerotholus goodwini* – orange diamond, *Stegoceras novomexicanum* – light blue square, *Stegoceras valdium* – dark blue squares.

A

B

137
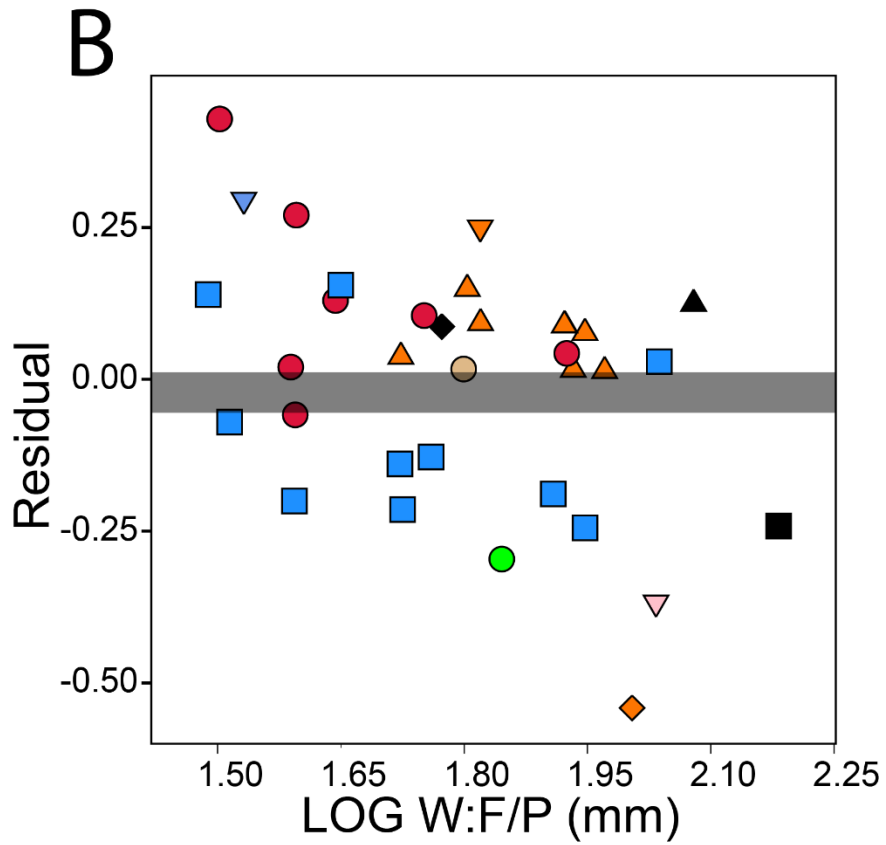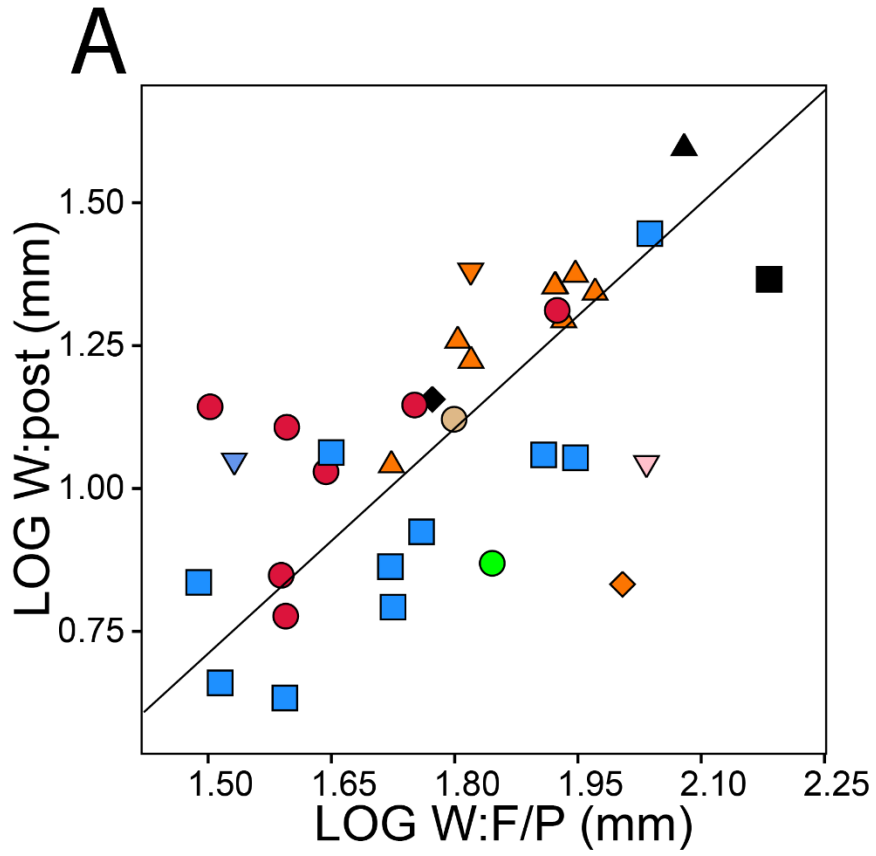
Figure 3.5. Statistical testing of discrete "broad" and "narrow" posterior exposures of the medial extension of the parietal. A) RMA regression of W:post vs. W:F/P. B) residuals form that RMA. Grey bar identifies the natural gap in the distribution of residuals. *Amotocephale gobiensis* – blue inverted triangle, *Acrotholus audeti* – green circle, *Foraminacphale brevis* – red circles, *Goyocephale lattimorei* – black diamond, *Homalocephale calathocercos* – brown circle *Pachycephalosaurus wyomingensis* – black square, *Prenocephale prenes* – pink inverted triangle, *Sinocephale bexelli* – black triangle, *Sphaerotholus buchhotlzae* – orange triangles, *Sphaerotholus edmontonensis* – orange inverted triangle, *Sphaerotholus goodwini* – orange diamond, *Stegoceras valdium* – dark blue squares.
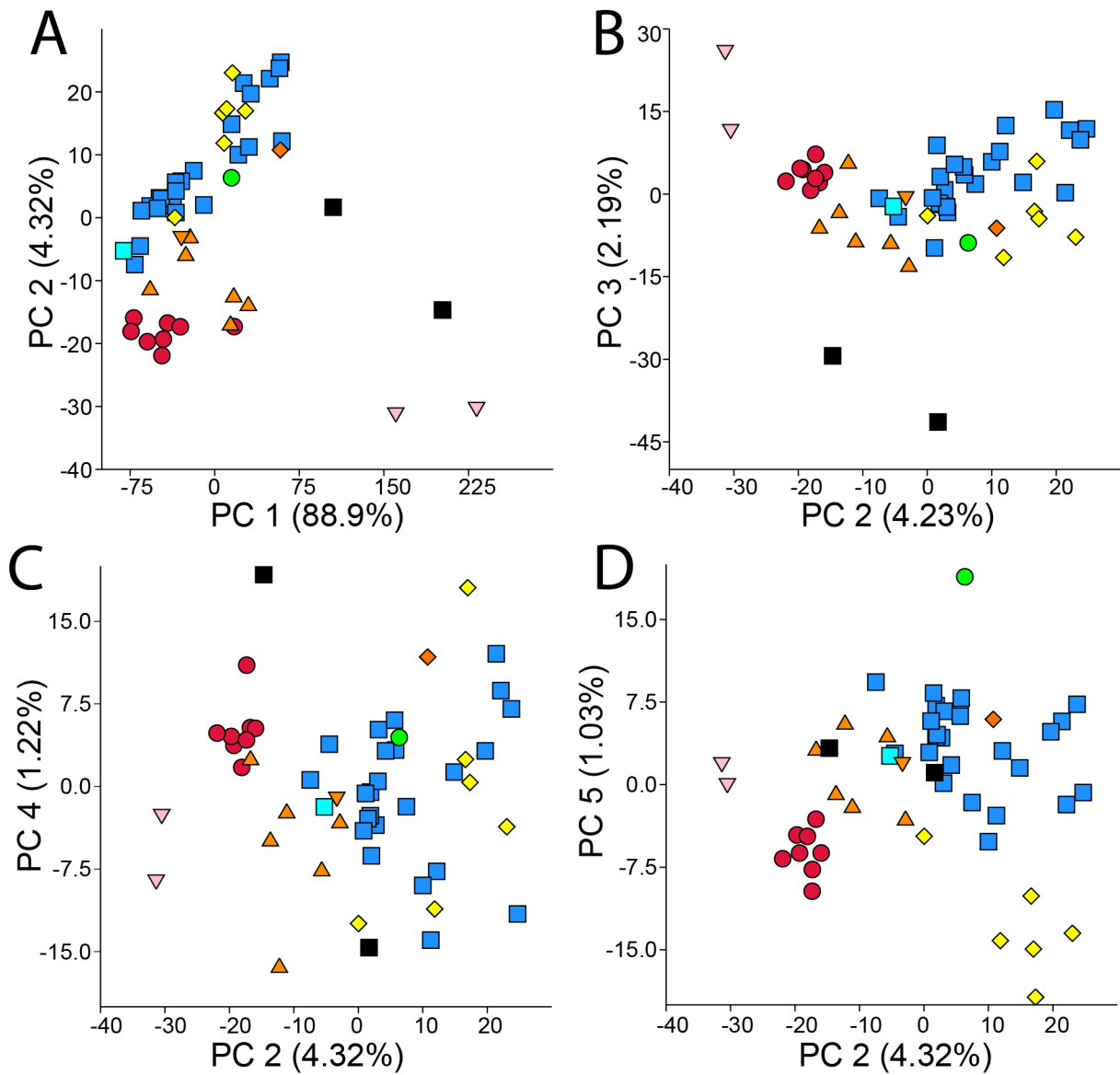
Figure 3.6. PCA of pachycephalosaurid frontoparietal non-transformed linear measurements. *Acrotholus audeti* – green circle, *Foraminacphale brevis* – red circles, *Pachycephalosaurus wyomingensis* – black square, *Prenocephale prenes* – pink inverted triangle, *Sphaerotholus buchhotlzae* – orange triangles, *Sphaerotholus edmontonensis* – orange inverted triangle, *Sphaerotholus goodwini* – orange diamond, *Stegoceras novomexicanum* – light blue square, *Stegoceras valdium* – dark blue squares.
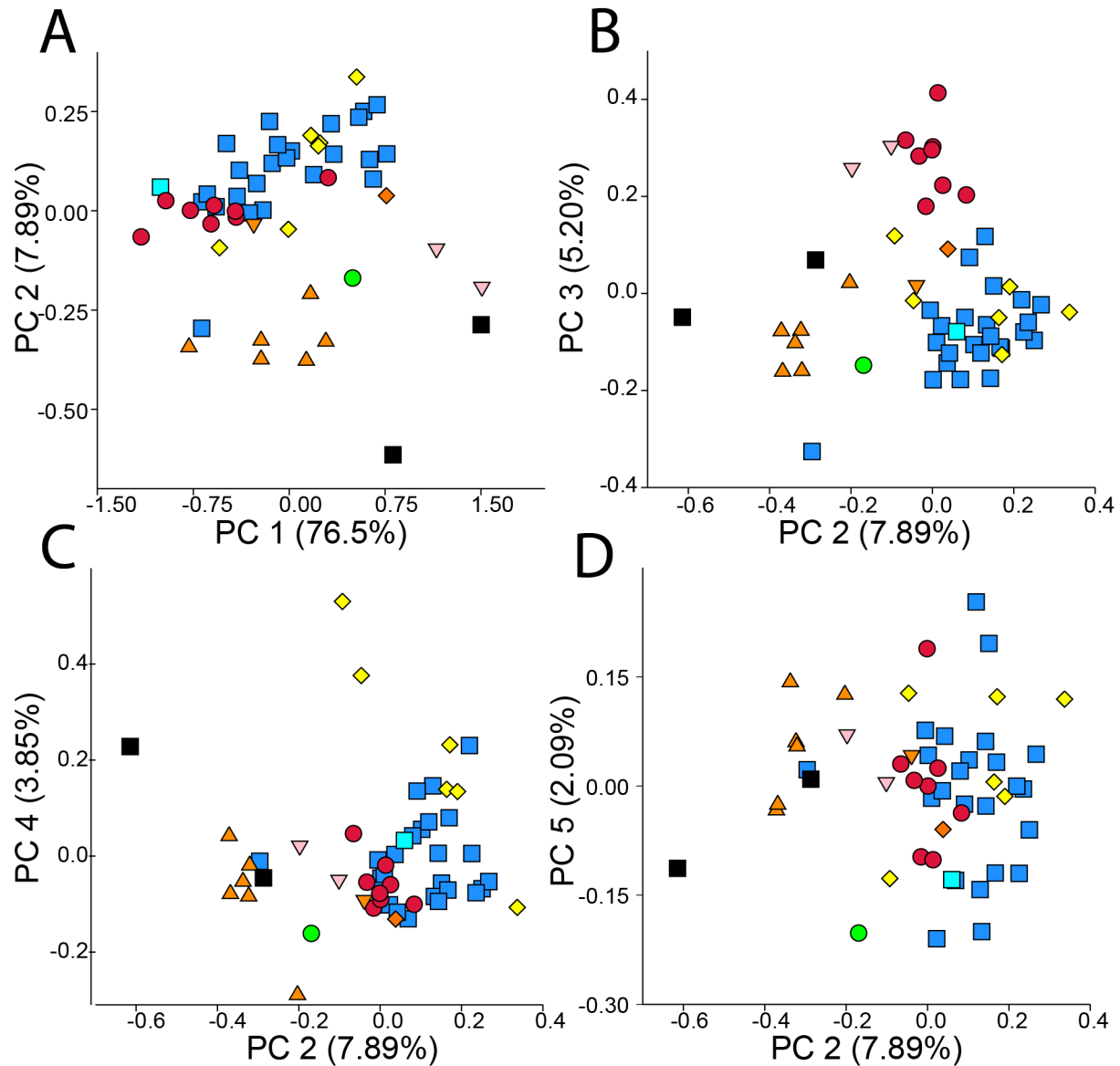
Figure 3.7 PCA of pachycephalosaurid frontoparietal LOG-transformed linear measurements. *Acrotholus audeti* – green circle, *Foraminacphale brevis* – red circles, *Pachycephalosaurus wyomingensis* – black square, *Prenocephale prenes* – pink inverted triangle, *Sphaerotholus buchhotlzae* – orange triangles, *Sphaerotholus edmontonensis* – orange inverted triangle, *Sphaerotholus goodwini* – orange diamond, *Stegoceras novomexicanum* – light blue square, *Stegoceras valdium* – dark blue squares.
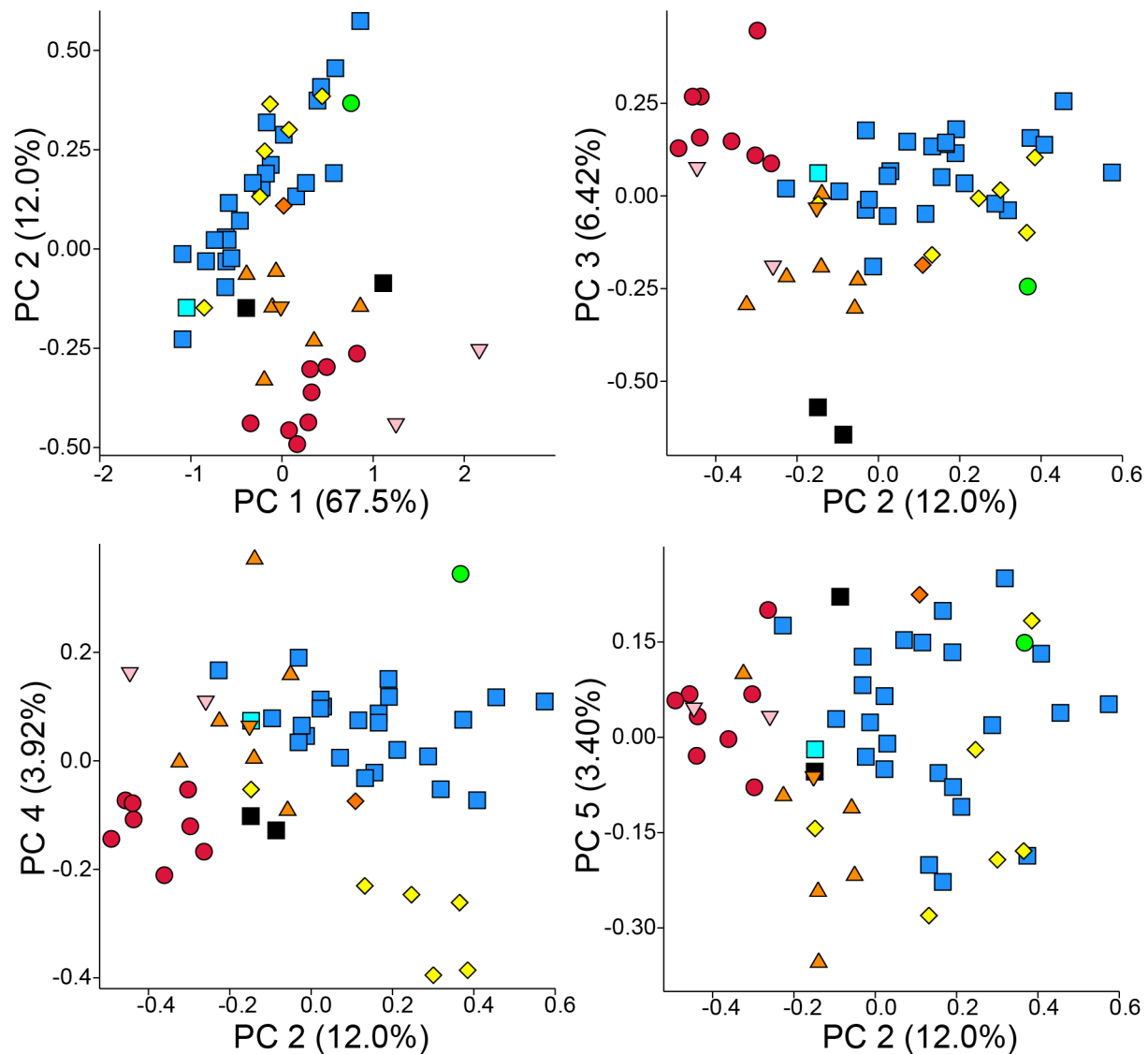
Figure 3.8. PCA of pachycephalosaurid frontoparietal L:F proportionate linear measurements. *Acrotholus audeti* – green circle, *Foraminacphale brevis* – red circles, *Pachycephalosaurus wyomingensis* – black square, *Prenocephale prenes* – pink inverted triangle, *Sphaerotholus buchhotlzae* – orange triangles, *Sphaerotholus edmontonensis* – orange inverted triangle, *Sphaerotholus goodwini* – orange diamond, *Stegoceras novomexicanum* – light blue square, *Stegoceras valdium* – dark blue squares.
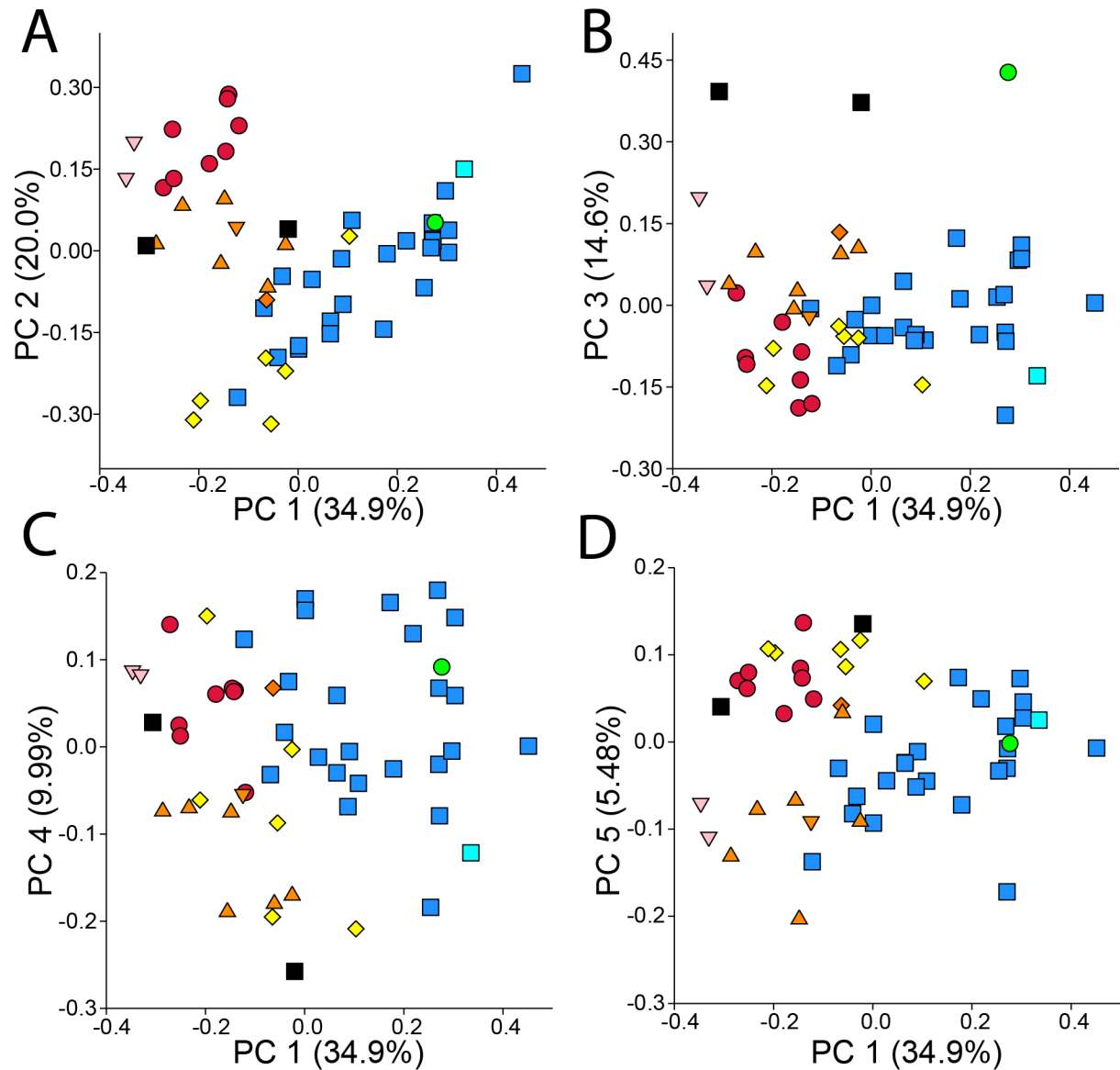
Figure 3.9. PCA of pachycephalosaurid frontoparietal W:F/P proportionate linear measurements. *Acrotholus audeti* – green circle, *Foraminacphale brevis* – red circles, *Pachycephalosaurus wyomingensis* – black square, *Prenocephale prenes* – pink inverted triangle, *Sphaerotholus buchhotlzae* – orange triangles, *Sphaerotholus edmontonensis* – orange inverted triangle, *Sphaerotholus goodwini* – orange diamond, *Stegoceras novomexicanum* – light blue square, *Stegoceras valdium* – dark blue squares.
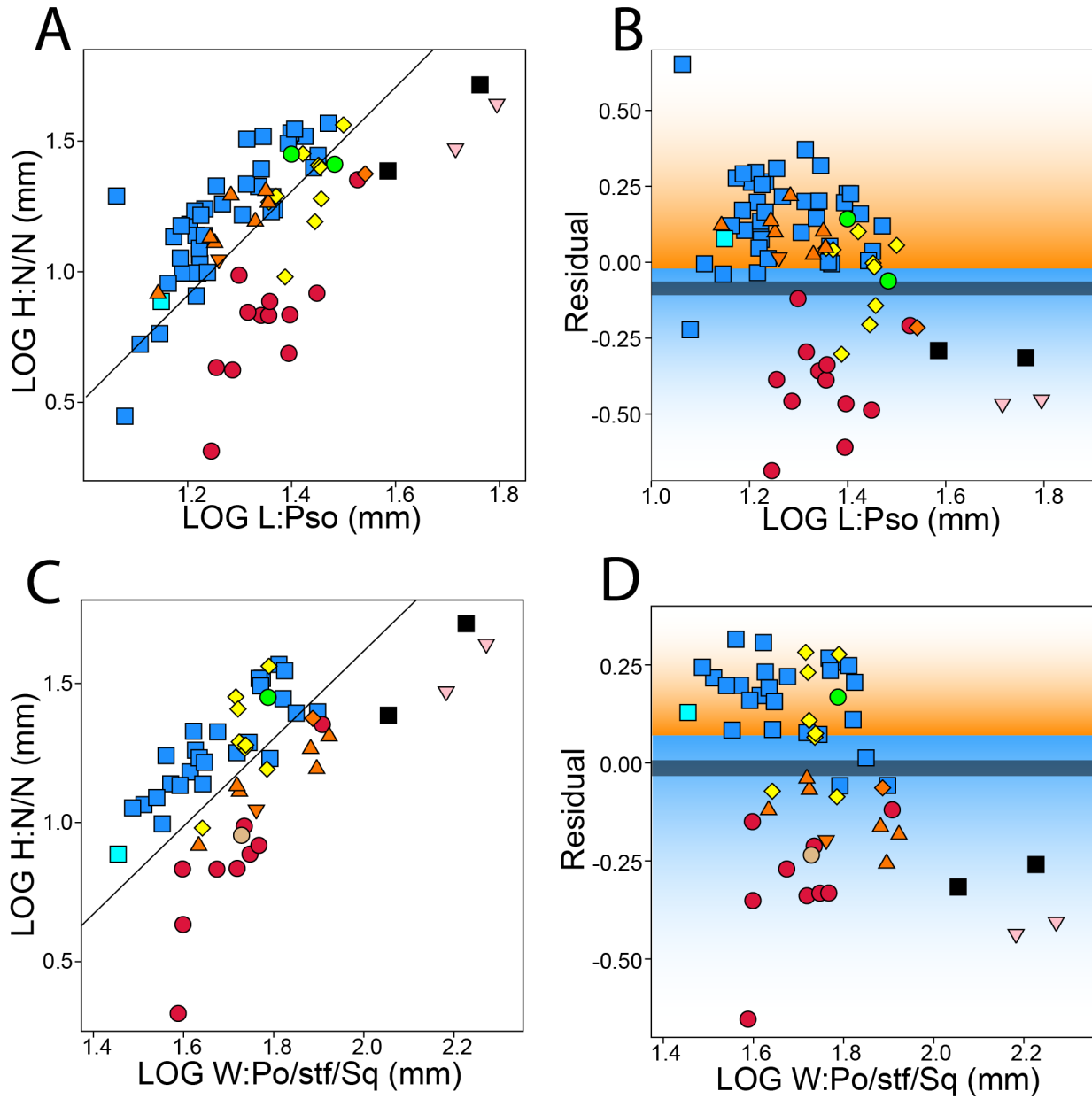
Figure 3.10. RMA regressions of linear measurements that strongly antagonistically loaded in PC 3 of the LOG-transformed PCA and in PC 2 of the L:F proportionate PCA. A) RMA regression of H:N/N vs. L:Pso. B) Residuals of that RMA regression. C) RMA regression of H:N/N vs. W:Po/stf/Sq. D) Residual of that regression. Grey boxes mark the natural gap identified in Jenks natural break analyses of the distribution of residuals. Blue and orange shading identify the bimodal groups identified in Mixture Analyses. *Acrotholus audeti* – green circle, *Foraminacphale brevis* – red circles, *Homalocephale calathocercos* – brown circle

Pachycephalosaurus wyomingensis – black square, *Prenocephale prenes* – pink inverted triangle, *Sphaerotholus buchhotlzae* – orange triangles, *Sphaerotholus edmontonensis* – orange inverted triangle, *Sphaerotholus goodwini* – orange diamond, *Stegoceras novomexicanum* – light blue square, *Stegoceras valdium* – dark blue squares.

145
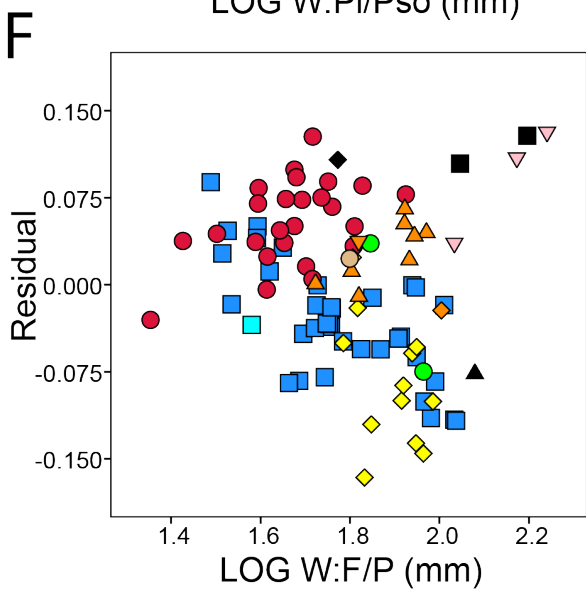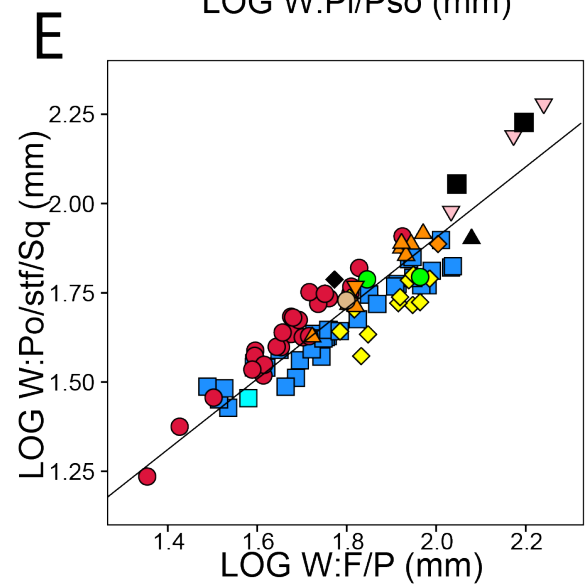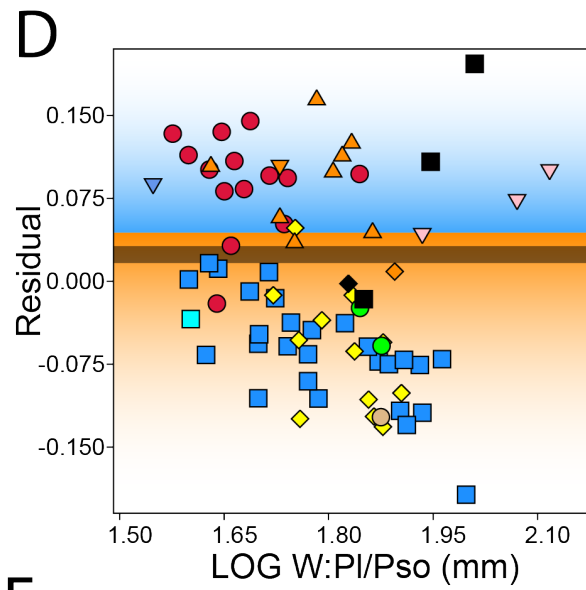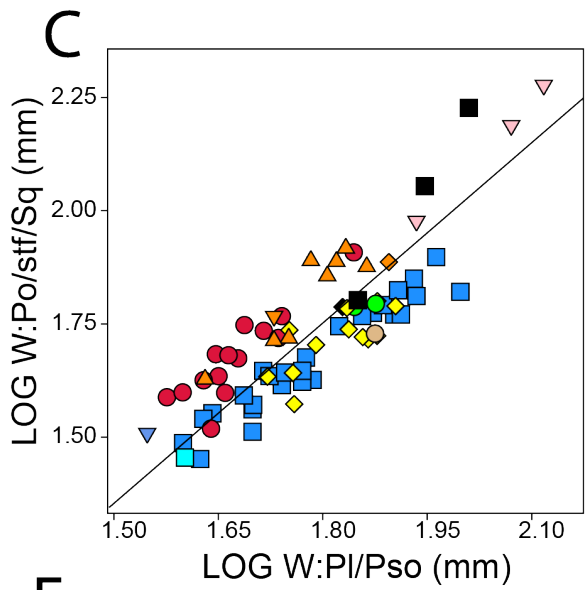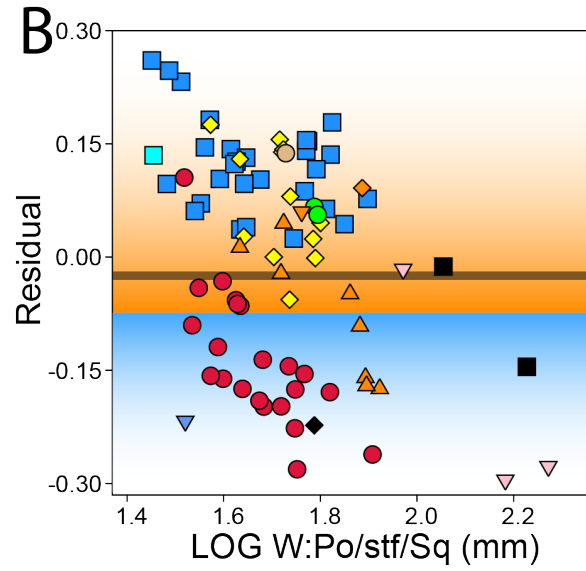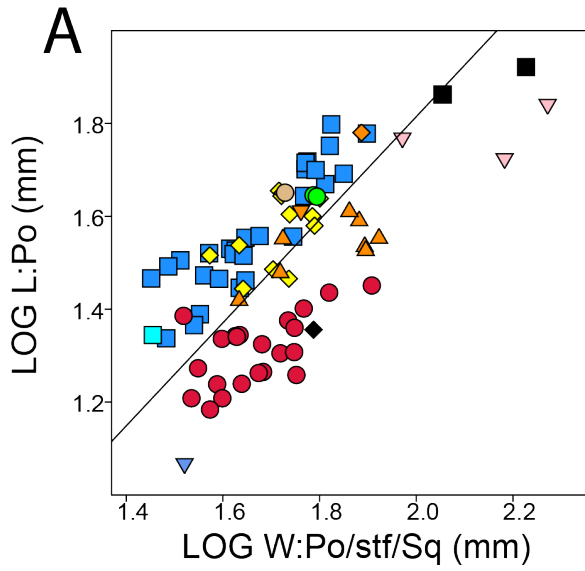
Figure 3.11. RMA regressions of linear measurements that strongly antagonistically loaded in PC 2 of the non-transformed and L:F proportionate PCAs, and in PC 3 of the W:F/P proportionate PCA. A) RMA regression of L:Po vs. W:Po/stf/Sq. B) Residuals of that RMA regression. C) RMA regression of W:Po/stf/Sq vs. W:Pl/Pso. D) Residual of that regression. E) RMA regression of W:Po/stf/Sq vs. W:F/P. F) Residuals for that regression. Blue and orange shading identify the bimodal groups identified in Mixture Analyses. *Acrotholus audeti* – green circle, *Colepiocephale lambei* – yellow diamonds; *Foraminacphale brevis* – red circles, *Homalocephale calathocercos* – brown circle *Pachycephalosaurus wyomingensis* – black square, *Prenocephale prenes* – pink inverted triangle, *Sinocpehale bexelli* – black inverted triangle, *Sphaerotholus buchhotlzae* – orange triangles, *Sphaerotholus edmontonensis* – orange inverted triangle, *Sphaerotholus goodwini* – orange diamond, *Stegoceras novomexicanum* – light blue square, *Stegoceras valdium* – dark blue squares.
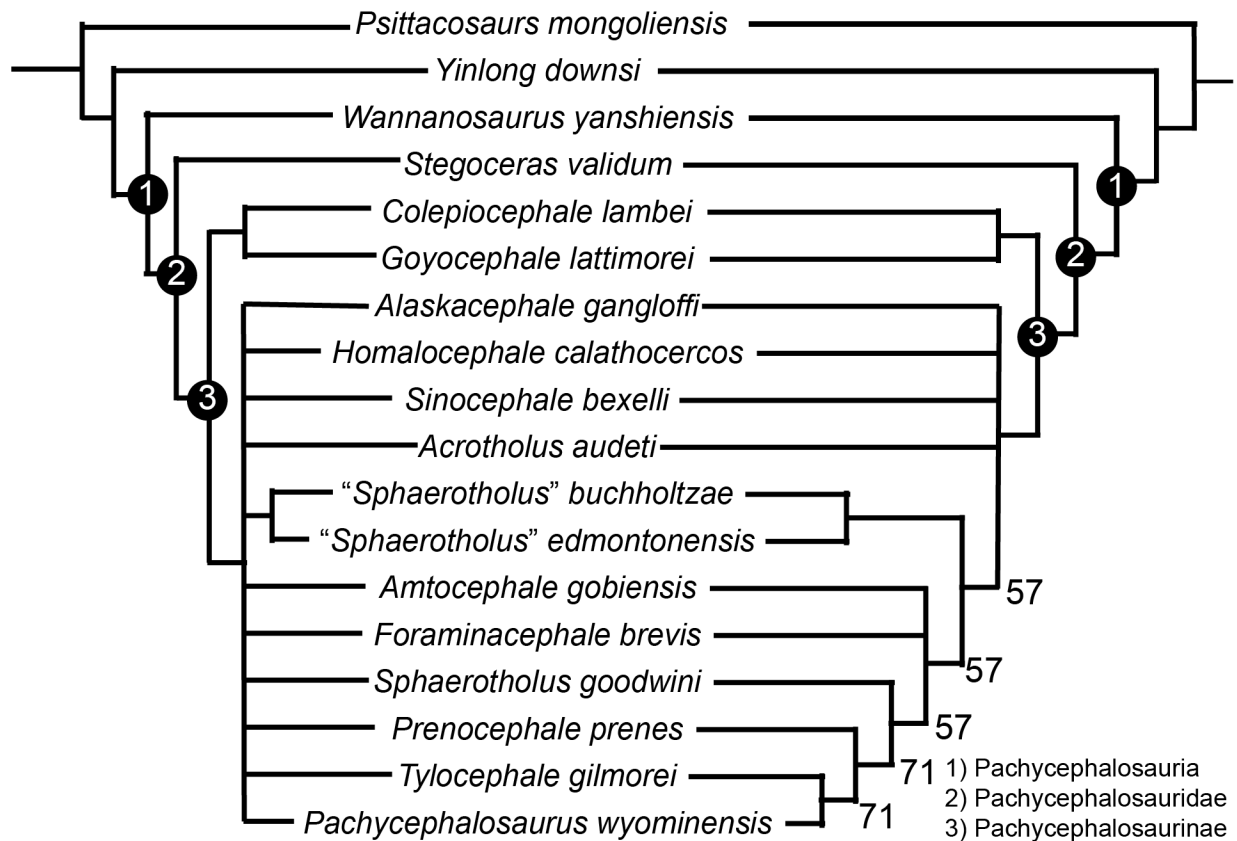
Figure 3.12. Revised phylogenetic tree of pachycephalosaurians. Left – strict consensus of the seven MPT's that resulted from a New Technologies search in TNT, using 10000 replicates, ten rounds of ratcheting and five rounds of tree fusing and drifting respectively. Right – 50% majority consensus of the seven MPT's. Numbers next to branches in the 50% majority consensus identify the percentage of MPT's that recovered that clade.

Chapter 4. Conclusions

I've advanced our understanding of ontogenetic, intraspecific, and interspecific variation in pachycephalosaurids. The knowledge presented in this thesis revised our understanding, perhaps confidence (or lack of) in recognising pachycephalosaurid species.

I utilised synchrotron µCT technologies to describe the anatomy of a controversial pachycephalosaurid specimen (TMP1972.027.0001) and taxon (*Gravitholus albertae*). The extreme fusion of the relatively complete skull roof had until now prevented a detailed description of the specimen. I described the morphology of TMP1972.027.0001, but could not identify any morphological unique features that would support it as a distinct species. Instead, 1972.027.0001 preserves end-stage ontogenetic features of *Stegoceras validum*.

I included TMP1972.027.0001 in morphometric analyses to compare it to pachycephalosaurid species that have been proposed to share close taxonomic affinities – *Hanssuesia sternbergi* and *Stegoceras validum*. These revealed no morphological distinction between any of these species. Like the end stage ontogenetic features of TMP1972.027.0001, the diagnosis of *Hanssuesia sternbergi* can be explained by allometric growth patterns already known for *Stegoceras validum*. Therefore, I synonymise *Gravitholus albertae* and *Hanssuesia sternbergi* with *Stegoceras validum*.

PCA and bivariate analyses of homologous linear measurements of frontoparietals are an appropriate method for testing pachycephalosaurid species hypotheses, particularly when large ontogenetic and allometric patterns are of concern (Schott and Evans, 2016; Chapters 2-3). Previous PCA's of linear frontoparietal measurements were performed on log-transformed measurements (Evans et al., 2013; Schott and Evans 2016; Williamson and Brusatte 2016). Log-transformation methods, including those of this thesis result in were used in this thesis, as well as non-transformed and size-standardised methods. PCA of log-transformed linear measurement did recover patterns of adult dimorphism in *Stegoceras validum*, but the measurements that strongly loaded on that PC axis did not. Patterns of frontoparietal width indicative of the elements that initially inflate to form the dome (frontals or parietals) were not identified in PCA of log-transformed linear measurements but were identified in PCA of non-transformed and size standardized linear measurements. PCA of log-transformed measurements did identify some

potentially phylogenetically informative relationships. Future studies may benefit from performing multiple iterations of PCA analyses that differ on the standardization of the data, and further investigate the utility of each standardization method. These methods have yet to be used to test the synonymy of *Dracorex hogwartsia* and *Stygimoloch spinifer* with *Pachycephalosaurus wyomingensis*, which is currently supported by qualitative assessments (Horner and Goodwin, 2009; Goodwin and Evans, 2016). Three dimensional geometric morphometrics also seems a promising and appropriate method (Woodruff et al., 2021), but should also be performed alongside traditional linear measurement PCA to compare the power of these methods.

Four genera have been proposed to be synonymous with *Pachycephalosaurus*: *Dracorex*, *Stenotholus*, *Stygimoloch*, and *Tylosteus*. A similar number of genera have now been synonymised with *Stegoceras*: *Gravitholus*, *Hanssuesia*, and *Ornatotholus*. Ignoring ontogeny, particularly in well sampled systems results in erroneously overestimated pachycephalosaurid diversity – possibly by a factor of three or four. Despite this, pachycephalosaurids still offer a unique glimpse into small-bodied dinosaur diversity, that is less obscured by size-selective preservational biases.

I identify novel adult dimorphism in the thickness of the frontonasal boss amongst *Stegoceras validum*, which is not explained by previous taxonomic hypotheses (*Gravitholus albertae* and *Hanssuesia sternbergi*). Instances of post-traumatic pathologies are restricted to specimens with relatively thicker frontonasal bosses. Thus, I propose that the variation in frontonasal boss thickness is sexually dimorphic, with the sex possessing the anteriorly thicker domes engaging in intraspecific combat, possibly for mate or territory acquisition (Peterson et al. 2013). Sexual dome dimorphism may exist posterolaterally as well in that the lateral and posterior shelves are incorporated into the dome. However, this requires a larger sample of complete adult frontoparietals for rigorous testing.

Interestingly, the same variables that explain dimorphism in *Stegoceras validum* also explain morphological variation amongst several pachycephalosaurid species in PCA of the largest suite of pachycephalosaurids ever analysed. *Colepiocephale lambei*, *Pachycephalosaurus wyomingensis*, and "*Sphaerotholus*" *buchholtzae* have an extensive range in PC 4 of the non-

transformed PCA iteration, like *Stegoceras validum*. Amongst these four species, the average PC 4 scores of pathological specimens is significantly larger than non-pathological specimens, which scores in the same direction as taller frontonasal bosses (t = 3.03, p = 0.018; Appendix A3.1). Thus, sexual dimorphism in the thickness of the frontonasal boss may be widespread amongst pachycephalosaurids. This in turn supports the intrasexual head-butting combat hypothesis (Galton 1971; Peterson et al. 2013) and that dome evolution was in response to sexual selection. However, a relatively large sample of *Foraminacephale brevis* (n = 8) does not strongly vary in PC 4 of the non-transformed PCA. *Foraminacephale brevis* may not have had sexually dimorphic frontonasal bosses.

Careful re-examination of the working pachycephalosaurid phylogenetic character matrix (Evans et al., 2013) identified numerous errors in the previous scoring of taxa. Statistical testing of discrete character states of three select continuous characters revealed discrete character states, and character state assignments for several species shifted. Many characters describe features and states of mature, developed individuals. However, species known solely from juvenile material have previously been scored for these ontogeny-dependant characters, which likely influenced previous phylogenetic results. Although the entire character matrix likely requires further examination and statistical testing of discrete character states, more complete skeletal material will likely be required to construct strong pachycephalosaurian phylogenetic relationships. Additionally, including heterodontosaurids with pachycephalosaurids in phylogenetic analyses may help polarize characters in pachycephalosaurids, and help resolve their interrelationships. However, the inclusion of heterodontosaurids as basal pachycephalosaurians (Dieudonné et al., 2020) should be further examined.

One apparently strong dividing feature amongst pachycephalosaurids is whether the dome initially inflates in the frontals or the parietals. Frontoparietal widths and their allometric relationships appear to reflect where the dome initially developed and were used to assess species that currently lack large ontogenetic samples. Modes of development are amongst the most important criteria of homology (Nelson, 1978), and thus synapomorphy (Patterson, 1982). I hypothesis that that the distinction between frontal first and parietal first doming modes is a strong divide amongst pachycephalosaurids, and are crucial for understanding their evolution.

Histological methods may be an appropriate method for identifying where domes initially inflate. Domes preserve growth lines (Lehman 2010; Dyer et al., 2021), which reflect the morphology of the dome at the time the growth lines formed. Features such as a posterior parietal shelf should be observable along growth lines of frontal first doming pachycephalosaurids even if the parietal is completely incorporated in fully mature individuals. These growth lines can also be observed in CT images (Goodwin et al., 2016), which would be more appropriate to assess species only know from limited samples.

5.1 Literature Cited

Dieudonné, P.E., Cruzado-Caballero, P., Godefroit, P., Tortosa, T., 2020. A new phylogeny of cerapodan dinosaurs. Historical Biology 33, 2335–2355. https://doi.org/10.1080/08912963.2020.1793979

Dyer, A.D., LeBlanc, A.R.H., Doschak, M.R., Currie, P.J., 2021. Taking a crack at the dome: histopathology of a pachycephalosaurid (Dinosauria: Ornithischia) frontoparietal dome. Biosis: Biological Systems 2, 248–270. https://doi.org/10.37819/biosis.002.02.0101

Evans, D.C., Schott, R.K., Larson, D.W., Brown, C.M., Ryan, M.J., 2013. The oldest North American pachycephalosaurid and the hidden diversity of small-bodied ornithischian dinosaurs. Nature Communications 4, 1–10. https://doi.org/10.1038/ncomms2749

Galton, P.M., 1971. A primitive dome-headed dinosaur (Ornithischia: Pachycephalosauridae) from the Lower Cretaceous of England and the function of the dome of pachycephalosaurids. Journal of Paleontology 45, 40–47.

Goodwin, M.B., Evans, D.C., 2016. The early expression of squamosal horns and parietal ornamentation confirmed by new end-stage juvenile *Pachycephalosaurus* fossils from the Upper Cretaceous Hell Creek Formation, Montana. Journal of Vertebrate Paleontology 36, e1078343. https://doi.org/10.1080/02724634.2016.1078343

Goodwin, M.M., Nirody, J.A., Huynh, T., Horner, J.R., Parkinson, D.Y., Schott, R.C., Evans, D.C., 2016. Mapping and visualizing the complex internal anatomy of pachycephalosaur domes, in: Farke, A., MacKenzie, A., Miller-Camp, J. (Eds.), Society of Vertebrate Paleontology October 2016 Abstracts of Papers 76th Annual Meeting. Society of Vertebrate Paleontology, Salt Lake City, p. 145

Horner, J.R., Goodwin, M.B., 2009. Extreme cranial ontogeny in the Upper Cretaceous dinosaur *Pachycephalosaurus*. PLoS ONE 4, e7626. https://doi.org/10.1371/journal.pone.0007626

Lehman, T.M., 2010. Pachycephalosauridae from the San Carlos and Aguja formations (upper Cretaceous) of West Texas, and observations of the frontoparietal dome. Journal of Vertebrate Paleontology 30, 786–798. https://doi.org/10.1080/02724631003763532

Nelson, G., 1978. Ontogeny, phylogeny, paleontology, and the biogenetic law. Systematic Zoology 19, 324–345.

Patterson, C., 1982. Morphological characters and homology, in: Joysey, K.A., Friday, A.E. (Eds.), Problems of Phylogenetic Reconstruction. Academic Press, London and New York, pp. 21–74.

Peterson, J.E., Dischler, C., Longrich, N.R., 2013. Distributions of cranial pathologies provide evidence for head-butting in dome-headed dinosaurs (Pachycephalosauridae). PLoS ONE 8. https://doi.org/10.1371/journal.pone.0068620

Schott, R.K., Evans, D.C., 2016. Cranial variation and systematics of *Foraminacephale brevis* gen. nov. and the diversity of pachycephalosaurid dinosaurs (Ornithischia: Cerapoda) in the Belly River Group of Alberta, Canada. Zoological Journal of the Linnean Society 179, 865–906. https://doi.org/10.1111/zoj.12465

Williamson, T.E., Brusatte, S.L., 2016. Pachycephalosaurs (Dinosauria: Ornithischia) from the Upper Cretaceous (upper Campanian) of New Mexico: A reassessment of *Stegoceras novomexicanum*. Cretaceous Research 62, 29–43. https://doi.org/10.1016/j.cretres.2016.01.012

Woodruff, D.C., Goodwin, M.B., Lyson, T.R., Evans, D.C., 2021. Ontogeny and variation of the pachycephalosaurine dinosaur *Sphaerotholus buchholtzae*, and its systematics within the genus. Zoological Journal of the Linnean Society 193, 563–601.

Literature Cited

Baird, D., 1979. The dome-headed dinosaur *Tylosteus ornatus* Leidy 1872 (Reptilia: Ornithischia: Pachycephalosauridae). Notulae Naturae 456, 1–11.

Bakker, R.T., Sullivan, R.M., Porter, V., Larson, P., Saulsbury, S.J., 2006. *Dracorex hogwartsia* n. gen., n. so., a spiked, flat-headed pachycphalosaurid dinosaur from the Upper Cretaceous Hell Creek Formation of South Dakota, in: Lucas, S.G., Sullivan, R.M. (Eds.), Late Cretaceous Vertebrates from the Western Interior. New Mexico Museum of Natural History and Science, Bulletin 35, Albuquerque, pp. 331–345.

Bourke, J.M., Porter, W.R., Ridgely, R.C., Lyson, T.R., Schachner, E.R., Bell, P.R., Witmer, L.M., 2014. Breathing life into dinosaurs: tackling challenges of soft-tissue restoration and nasal airflow in extinct species. Anatomical Record 297, 2148–2186. https://doi.org/10.1002/ar.23046

Brown, B., Schlaikjer, E.M., 1943. A study of the troödont dinosaurs with the description of a new genus and four new species. Bulletin of the American Museum of Natural History 82, 115–150.

Brown, C.M., Evans, D.C., Campione, N.E., O'Brien, L.J., Eberth, D.A., 2013. Evidence for taphonomic size bias in the Dinosaur Park Formation (Campanian, Alberta), a model Mesozoic terrestrial alluvial-paralic system. Palaeogeography, Palaeoclimatology, Palaeoecology 372, 108–122. https://doi.org/10.1016/j.palaeo.2012.06.027

Butler, R.J., Zhao, Q., 2009. The small-bodied ornithischian dinosaurs *Micropachycephalosaurus hongtuyanensis* and *Wannanosaurus yansiensis* from the Late Cretaceous of China. Cretaceous Research 30, 63–77. https://doi.org/10.1016/j.cretres.2008.03.002

Carpenter, K., 1997. Agonistic behavior in pachycephalosaurs (Ornithischia: Dinosauria): a new look at head-butting behavior. Contributions to Geology, University of Wyoming 32, 19–25.

Chapman, R.E., Galton, P.M., Sepkoski, J.J., Wall, W.P., 1981. A morphometric study of the cranium of the pachycephalosaurid dinosaur *Stegoceras*. Journal of Paleontology 55, 608–618.

de Pinna, M.G.G., 1991. Concepts and tests of homology in the cladistic paradigm. Cladistics 7, 367–394.

Dieudonné, P.E., Cruzado-Caballero, P., Godefroit, P., Tortosa, T., 2020. A new phylogeny of cerapodan dinosaurs. Historical Biology 33, 2335–2355. https://doi.org/10.1080/08912963.2020.1793979

Dong, Z., 1978. A new genus of Pachycephalosauria from Laiyang, Shantung. Vertebrata PalAsiatica 16, 225–229.

Dyer, A.D., LeBlanc, A.R.H., Doschak, M.R., Currie, P.J., 2021. Taking a crack at the dome: histopathology of a pachycephalosaurid (Dinosauria: Ornithischia) frontoparietal dome. Biosis: Biological Systems 2, 248–270. https://doi.org/10.37819/biosis.002.02.0101

Eberth, D.A., Hamblin, A.P., 1993. Tectonic, stratigraphic, and sedimentologic significance of a regional discontinuity in the upper Judith River Group (Belly River wedge) of southern Alberta, Saskatchewan, and northern Montana. Canadian Journal of Earth Sciences 30, 174–200.

Evans, D.C., Brown, C.M., Ryan, M.J., Tsogtbaatar, K., 2011. Cranial ornamentation and ontogenetic status of *Homalocephale calathocercos* (Ornithischia: Pachycephalosauria) from the Nemegt Formation, Mongolia. Journal of Vertebrate Paleontology 31, 84–92. https://doi.org/10.1080/02724634.2011.546287

Evans, D.C., Brown, C.M., You, H., Campione, N.E., 2021. Description and revised diagnosis of Asia's first recorded pachycephalosaurid, *Sinocephale bexelli* gen. nov., from the Upper Cretaceous of Inner Mongolia, China. Canadian Journal of Earth Sciences 58, 981–992. https://doi.org/10.1139/cjes-2020-0190

Evans, D.C., Hayashi, S., Chiba, K., Watabe, M., Ryan, M.J., Lee, Y.N., Currie, P.J., Tsogtbaatar, K., Barsbold, R., 2018. Morphology and histology of new cranial specimens of

Pachycephalosauridae (Dinosauria: Ornithischia) from the Nemegt Formation, Mongolia. Palaeogeography, Palaeoclimatology, Palaeoecology 494, 121–134. https://doi.org/10.1016/j.palaeo.2017.11.029

Evans, D.C., Schott, R.K., Larson, D.W., Brown, C.M., Ryan, M.J., 2013. The oldest North American pachycephalosaurid and the hidden diversity of small-bodied ornithischian dinosaurs. Nature Communications 4, 1–10. https://doi.org/10.1038/ncomms2749

Fowler, D.W., 2017. Revised geochronology, correlation, and dinosaur stratigraphic ranges of the Santonian-Maastrichtian (Late Cretaceous) formations of the Western Interior of North America. PLoS ONE 12, e0188426. https://doi.org/10.1371/journal.pone.0188426

Galton, P.M., 1971. A primitive dome-headed dinosaur (Ornithischia: Pachycephalosauridae) from the Lower Cretaceous of England and the function of the dome of pachycephalosaurids. Journal of Paleontology 45, 40–47.

Galton, P.M., Sues, H.-D., 1983. New data on pachycephalosaurid dinosaurs (Reptilia: Ornithischia) from North America. Canadian Journal of Earth Sciences 20, 462–472.

Geist, V., 1966. The evolution of horn-like organs. Behaviour 27, 175–214.

Giffin, E.B., 1989a. Pachycephalosaur paleoneurology (Archosauria: Ornithischia). Journal of Vertebrate Paleontology 9, 67–77. https://doi.org/10.1080/02724634.1989.10011739

Giffin, E.B., 1989b. Notes on pachycephalosaurs (Ornithischia). Journal of Paleontology 63, 525–529. https://doi.org/10.1017/S0022336000019739

Giffin, E.B., Gabriel, D.L., Johnson, R.E., 1988. A New Pachycephalosaurid Skull (Ornithischia) from the Cretaceous Hell Creek Formation. Source: Journal of Vertebrate Paleontology 7, 398–407.

Gilmore, C.W., 1931. A new species of Troödont dinosaur from the Lance Formation of Wyoming. Proceedings of the U.S. National Museum 79, 1–6.

Gilmore, C.W., 1924. On *Troodon validus*: an orthopodous dinosaur from the Belly River Cretaceous of Alberta. University of Alberta Department of Geology Bulletin 1, 1–43.

Goloboff, P.A., Catalano, S.A., 2016. TNT version 1.5, including a full implementation of phylogenetic morphometrics. Cladistics 32, 221–238. https://doi.org/10.1111/cla.12160

Goodwin, M.B., 1990. Morphometric landmarks of pachycephalosaurid cranial material from the Judith River Formation of northcentral Montana, in: Carpenter, K., Currie, P.J. (Eds.), Dinosaur Systematics: Approaches and Perspectives. Cambridge University Press, Cambridge, pp. 189–201. https://doi.org/10.1017/cbo9780511608377.017

Goodwin, M.B., Buchholtz, E.A., Johnson, R.E., 1998. Cranial anatomy and diagnosis of *Stygimoloch spinifer* (Ornithischia: Pachycephalosauria) with comments on cranial display structures in agonistic behavior. Journal of Vertebrate Paleontology 18, 363–375. https://doi.org/10.1080/02724634.1998.10011064

Goodwin, M.B., Evans, D.C., 2016. The early expression of squamosal horns and parietal ornamentation confirmed by new end-stage juvenile *Pachycephalosaurus* fossils from the Upper Cretaceous Hell Creek Formation, Montana. Journal of Vertebrate Paleontology 36, e1078343. https://doi.org/10.1080/02724634.2016.1078343

Goodwin, M.B., Horner, J.R., 2004. Cranial histology of pachycephalosaurs (Ornithischia: Marginocephalia) reveals transitory structures inconsistent with head-butting behavior. Paleobiology 30, 253–267. https://doi.org/10.1666/0094-8373(2004)030<0253:chopom>2.0.co;2

Goodwin, M.M., Nirody, J.A., Huynh, T., Horner, J.R., Parkinson, D.Y., Schott, R.C., Evans, D.C., 2016. Mapping and visualizing the complex internal anatomy of pachycephalosaur domes, in: Farke, A., MacKenzie, A., Miller-Camp, J. (Eds.), Society of Vertebrate Paleontology October 2016 Abstracts of Papers 76th Annual Meeting. Society of Vertebrate Paleontology, Salt Lake City, p. 145.

Hammer, Ø., Harper, D.A.T., Ryan, P.D., 2001. Past: paleontological statistics software package for education and data analysis. Palaeontologia Electronica 4, 1–9.

Horner, J.R., Goodwin, M.B., 2009. Extreme cranial ontogeny in the Upper Cretaceous dinosaur *Pachycephalosaurus*. PLoS ONE 4, e7626. https://doi.org/10.1371/journal.pone.0007626

Jasinski, S.E., Sullivan, R.M., 2016. The validity of the Late Cretaceous pachycephalosaurid *Stegoceras novomexicanum* (Dinosauria: Pachycephalosauridae), in: Sullivan, R.M., Lucas, S.G. (Eds.), Fossil Record 5. New Mexico Museum of Natural History and Science, Bulletin 74, Albuquerque, pp. 107–115.

Jasinski, S.E., Sullivan, R.M., 2011. Re-evaluation of pachycephalosaurids from the Fruitland-Kirtland transition (Kirtlandian, Late Campanian), San Juan Basin, New Mexico, with a description of a new species of *Stegoceras* ad a reassessment of *Texacephale langstoni*, in: Sullvian, R.M., Lucas, S.G., Spielmann, J.A. (Eds.), Fossil Record 3. New Mexico Museum of Natural History and Science, Bulletin 53, Albuquerque, pp. 202–215.

Kaiser, H.E., 1960. Untersuchungen zur vergleichenden Osteologie der fossilen und rezenten Pachyostosen. Palaeontographica Abteilung A 114, 113–196.

Lambe, L.M., 1918. The Cretaceous genus *Stegoceras*, typifying a new family referred provisionally to the Stegosauria. Transactions of the Royal Society of Canada 12, 23–36.

Lambe, L.M., 1902. New genera and species from the Belly River series (Mid-Cretaceous). Geological survey of Canada Contributions to Canadian Palaeontology 3, 25–81.

Landry, S.O., 1995. *Stegoceras* not a head-butter. American Zoologist 35, 60A.

Lehman, T.M., 2010. Pachycephalosauridae from the San Carlos and Aguja formations (Upper Cretaceous) of West Texas, and observations of the frontoparietal dome. Journal of Vertebrate Paleontology 30, 786–798. https://doi.org/10.1080/02724631003763532

Leidy, J., 1872. Remarks on some Extinct Vertebrates. Proceedings of the Academy of Natural Sciences of Philadelphia 24, 38–40.

Longrich, N.R., Sankey, J., Tanke, D., 2010. *Texacephale langstoni*, a new genus of pachycephalosaurid (Dinosauria: Ornithischia) from the upper Campanian Aguja Formation, southern Texas, USA. Cretaceous Research 31, 274–284. https://doi.org/10.1016/j.cretres.2009.12.002

Maddison, W.P., Maddison, D.R., 2021. Mesquite: a modular system for evolutionary analysis.

Maidment, S.C.R., Porro, L.B., 2010. Homology of the palpebral and origin of supraorbital ossifications in ornithischian dinosaurs. Lethaia 43, 95–11. https://doi.org/10.1111/j.1502-3931.2009.00172.x

Mallon, J.C., 2017. Recognizing sexual dimorphism in the fossil record: lessons from nonavian dinosaurs. Paleobiology 43, 495–507. https://doi.org/10.5061/dryad.8f6d2

Mallon, J.C., Evans, D.C., Tokaryk, T.T., Currie, M.L., 2015. First pachycephalosaurid (Dinosauria: Ornithischia) from the Frenchman Formation (upper Maastrichtian) of Saskatchewan, Canada. Cretaceous Research 56, 426–431. https://doi.org/10.1016/j.cretres.2015.06.005

Maryańska, T., 1990. Pachycephalosauria, in: Weishampel, D.B., Dodson, P., Osmólska, H. (Eds.), The Dinosauria. University of California Press, Berkley, pp. 564–577.

Maryańska, T., Chapman, R.E., Weishampel, D.B., 2004. Pachycephalosauria, in: Weishampel, D.B., Dodson, P., Osmólska, H. (Eds.), The Dinosauria. University of California Press, Berkley, pp. 464–477.

Maryańska, T., Osmólska, H., 1974. Pachycephalosauria, a new suborder of ornithischian dinosaurs. Palaeontologica Polonica 30, 45–120.

Nelson, G., 1978. Ontogeny, phylogeny, paleontology, and the biogenetic law. Systematic Zoology 19, 324–345.

Owen, R., 1842. Report of British fossil reptiles, Pt II. Report of the British Association for the Advancement of Science 11, 60–204.

Patterson, C., 1982. Morphological characters and homology, in: Joysey, K.A., Friday, A.E. (Eds.), Problems of Phylogenetic Reconstruction. Academic Press, London and New York, pp. 21–74.

Perle, A., Maryańska, T., Osmólska, H., 1982. *Goyocephale lattimorei* gen. et sp. n., a new flat-headed pachycephalosaur (Ornithischia, Dinosauria) from the Upper Cretaceous of Mongolia. Acta Palaeontologica Polonica 27, 8–45.

Peterson, J.E., Dischler, C., Longrich, N.R., 2013. Distributions of cranial pathologies provide evidence for head-butting in dome-headed dinosaurs (Pachycephalosauridae). PLoS ONE 8, e68620. https://doi.org/10.1371/journal.pone.0068620

Peterson, J.E., Vittore, C.P., 2012. Cranial pathologies in a specimen of *Pachycephalosaurus*. PLoS ONE 7, e36227. https://doi.org/10.1371/journal.pone.0036227

Powers, M.J., Sullivan, C., Currie, P.J., 2020. Re-examining ratio based premaxillary and maxillary characters in Eudromaeosauria (Dinosauria: Theropoda): Divergent trends in snout morphology between Asian and North American taxa. Palaeogeography, Palaeoclimatology, Palaeoecology 547, 109704. https://doi.org/10.1016/j.palaeo.2020.109704

Prieto-Márquez, A., 2014. A juvenile *Edmontosaurus* from the late Maastrichtian (Cretaceous) of North America: Implications for ontogeny and phylogenetic inference in saurolophine dinosaurs. Cretaceous Research 50, 282–303. https://doi.org/10.1016/j.cretres.2014.05.003

Rigby, J.K.Jr., Rice, A., Currie, P.J., 1987. Dinosaur thermoregulatory Cretaceous/Tertiary survival strategies. Geological Society of America Abstracts with Programs 19, 820.

Ryan, M.J., Evans, D.C., 2005. Ornithischian dinosaurs, in: Currie, P.J., Koppelhus, E. (Eds.), Dinosaur Provincial Park: A Spectacular Ancient Ecosystem Revealed. Indiana University Press, Bloomington, pp. 313–348.

Schott, R., Evans, D., 2011. New information on pachycephalosaurid dinosaur diversity in the Foremost Formation (Campanian) of Alberta, in: Society of Vertebrate Paleontology Abstracts of Papers Seventy-First Annual Meeting. Society of Vertebrate Paleontology, Las Vegas, p. 189.

Schott, R.K., Evans, D.C., 2016. Cranial variation and systematics of *Foraminacephale brevis* gen. nov. and the diversity of pachycephalosaurid dinosaurs (Ornithischia: Cerapoda) in the Belly River Group of Alberta, Canada. Zoological Journal of the Linnean Society 179, 865–906. https://doi.org/10.1111/zoj.12465

Schott, R.K., Evans, D.C., 2012. Squamosal ontogeny and variation in the pachycephalosaurian dinosaur *Stegoceras validum* Lambe, 1902, from the Dinosaur Park Formation, Alberta. Journal of Vertebrate Palaeontology 32, 903–913.

Schott, R.K., Evans, D.C., Goodwin, M.B., Horner, J.R., Brown, C.M., Longrich, N.R., 2011. Cranial ontogeny in *Stegoceras validum* (Dinosauria: Pachycephalosauria): A quantitative model of pachycephalosaur dome growth and variation. PLoS ONE 6, e21092. https://doi.org/10.1371/journal.pone.0021092

Schott, R.K., Evans, D.C., Williamson, T.E., Carr, T.D., Goodwin, M.B., 2009. The anatomy and systematics of *Colepiocephale lambei* (Dinosauria: Pachycephalosauridae). Journal of Vertebrate Paleontology 29, 771–786. https://doi.org/10.1671/039.029.0329

Seeley, H.G., 1887. On the classification of the fossil animals commonly named Dinosauria. Proceedings of the Royal Society of London 43, 165–171.

Sereno, P.C., 2000. The fossil record, systematics and evolution of pachycephalosaurs and ceratopsians from Asia, in: Benton, M.J., Shishkin, M.A., Unwin, D.M., Kurochkin, E.N. (Eds.), The Age of Dinosaurs in Russia and Mongolia. Cambridge University Press, Cambridge, pp. 480–516.

Sereno, P.C., 1998. A rationale for phylogenetic definitions, with application to the higher-level taxonomy of Dinosauria. Neues Jahrbuch fur Geologie und Palaontologie - Abhandlungen 210, 41–83. https://doi.org/10.1127/njgpa/210/1998/41

Sereno, P.C., 1986. Phylogeny of the bird-hipped dinosaurs (Order Ornithischia). National Geographic Research 2, 234–256.

Simões, T.R., Caldwell, M.W., Palci, A., Nydam, R.L., 2017. Giant taxon-character matrices: quality of character constructions remains critical regardless of size. Cladistics 33, 198–219. https://doi.org/10.1111/cla.12163

Smith, R.J., 2009. Use and misuse of the Reduced Major Axis for line-fitting. American Journal of Physical Anthropology 140, 476–486. https://doi.org/10.1002/ajpa.21090

Snively, E., Cox, A., 2008. Structural mechanics of pachycephalosaur crania permitted head-butting behavior. Palaeontologia Electronica 11, 1–17.

Snively, E., Theodor, J.M., 2011. Common functional correlates of head-strike behavior in the pachycephalosaur *Stegoceras validum* (Ornithischia, Dinosauria) and combative artiodactyls. PLoS ONE 6, e21422. https://doi.org/10.1371/journal.pone.0021422

Sternberg, C.M., 1945. Pachycephalosauridae proposed for dome-headed dinosaurs, *Stegoceras lambei* n. sp., described. Source: Journal of Paleontology 19, 534–538.

Sues, H.-D., 1978. Functional morphology of the dome in pachycephalosaurid dinosaurs. Neues Jahrbuch für Geologie und Paläontologie Monatshefte 8, 489–472.

Sues, H.-D., Galton, P.M., 1987. Anatomy and classification of the North American Pachycephalosauria (Dinosauria: Ornithischia). Paleontographica Abteilung A 198, 1–40.

Sullivan, R.M., 2006. A taxonomic review of the Pachycephalosauridae (Dinosauria: Ornithischia), in: Lucas, S.G., Sullivan, R.M. (Eds.), Late Cretaceous Vertebrates from the Western Interior. New Mexico Museum of Natural History and Science, Bulletin 35, Albuquerque, pp. 347–365.

Sullivan, R.M., 2003. Revision of the dinosaur *Stegoceras* Lambe (Ornithischia, Pachycephalosauridae). Journal of Vertebrate Paleontology 23, 181–207. https://doi.org/10.1671/0272-4634(2003)23[181:ROTDSL]2.0.CO;2

Sullivan, R.M., 2000. *Prenocephale edmontonensis* (Brown and Schlaikjer) new comb. and *P. brevis* (Lambe) new comb. (Dinosauria: Ornithischia: Pachycephalosauria) from the upper Cretaceous of North America, in: Lucas, S.G., Heckert, A.B. (Eds.), Dinosaurs of New Mexico. New Mexico Museum of Natural History and Science, Bulletin 17, Albuquerque, pp. 117–190.

Tsuihiji, T., 2010. Reconstructions of the axial muscle insertions in the occipital region of dinosaurs: Evaluations of past hypotheses on Marginocephalia and Tyrannosauridae using the extant phylogenetic bracket approach. Anatomical Record 293, 1360–1386. https://doi.org/10.1002/ar.21191

Wall, W.P., Galton, P.M., 1979. Notes on pachycephalosaurid dinosaurs (Reptilia: Ornithischia) from North America, with comments on their status as ornithopods. Canadian Journal of Earth Sciences 16, 1176–1186. https://doi.org/10.1139/e79-104

Watabe, M., Tsogtbaatar, K., Sullivan, R.M., 2011. A new pachycephalosaurid from the Baynshire Fromation (Cenomanian-Late Santonian), Gobi Desert, Mongolia, in: Sullivan, R.M., Lucas, S.G., Spielmann, J.A. (Eds.), Fossil Record 3. New Mexico Museum of Natural History and Science, Bulletin 53, Albuquerque, pp. 489–497.

Williamson, T.E., Brusatte, S.L., 2016. Pachycephalosaurs (Dinosauria: Ornithischia) from the Upper Cretaceous (upper Campanian) of New Mexico: A reassessment of *Stegoceras novomexicanum*. Cretaceous Research 62, 29–43. https://doi.org/10.1016/j.cretres.2016.01.012

Williamson, T.E., Carr, T.D., 2002. A new genus of derived pachycephalosaurian from western North America. Journal of Vertebrate Paleontology 22, 779–801. https://doi.org/10.1671/0272-4634(2002)022[0779:ANGODP]2.0.CO;2

Woodruff, D.C., Goodwin, M.B., Lyson, T.R., Evans, D.C., 2021. Ontogeny and variation of the pachycephalosaurine dinosaur *Sphaerotholus buchholtzae*, and its systematics within the genus. Zoological Journal of the Linnean Society 193, 563–601.

Appendix 1

A1.1 Pachycephalosaurid frontoparietal specimens and their linear measurements used in RMA regressions. Measurements are in mm. Estimated values are italicized.

	ROM 2964	TMP2008.045.0001	TMP2016.033.0023	MPC-D 100/1203	CMN 8818	ROM3632	TMP1970.002.0001	TMP1982.046.0001
Taxon	*Acrotholus audeti*	*Acrotholus audeti*	*Acrotholus audeti*	*Amtocephale gobiensis*	*Colepiocephale lambei*	*Colepiocephale lambei*	*Colepiocephale lambei*	*Colepiocephale lambei*
Source	This study	Evans et al. (2013); This study	This study	Watabe et al. (2011)	Schott and Evans (2016)	Schott and Evans (2016)	This study	Schott and Evans (2016)
T:f/p	*59*	59	78.96	19	72	48	*46.18*	63.1
L:fp	*104.7*	106.85						
L:p	*61.87*	67.73		21.83				
L:f	*42.83*	44.2	43.895	11.53	45.2	34.5	*30.615*	44.05
L:po			39.12	31.35	54.2	44.08	*40.98*	52.9
L:pso	*30.4*	25.1	36.87		26.4	21.6	*21.935*	28.3
L:pl	*16.06*	8.6	5.815		15.58	10.56	*16.34*	16.25
L:prf	*28.23*					20.05		
W:post		7.4						
W:po/stf/sq		61.32	*62.28*	31.84	52	43.02	*50.55*	52.6
W:f/p	*85.52*	70.1	92.09	33.68	88.6	70.43	*65.64*	82.3
W:pso/po	*81.46*	76.3	93.36		75.1	60.1	*64.66*	75.1
W:pl/pso	*86.88*	70	75.16	33.16	73.3	52.54	*61.7*	72
W:pfr/pl	*61.34*	63.2	73.29		56.2	38.64	*37.39*	44.9
W:n/pfr	*25.85*	28.5	28.5		31.9	26.26		30.2
H:pso/po	*26.5*	37	*42.075*		13.3	*12.13*	*10.33*	16.5
H:pl/pso	*21.97*	25.6	19.62		13.4	*13.49*	*9.695*	16.7
H:prf/pl	*28.5*	28			18.4	17.04	*14.445*	17.5
H:n/prf	*25.4*	24.47	*20.97*		14.35			14.6
H:n/n	*25.79*	28.2			28.3			25.6

Specimen	TMP1986.146.0001	TMP1986.146.0002	TMP1992.088.0001	TMP2000.057.0001	TMP2010.005.0008	UALVP 349	UALVP 31471	UALVP 52676	UCMP130048
Taxon	*Colepiocephale lambei*	*Colepiocephale lambei*	*Colepiocephale lambei*	*Colepiocephale lambei*	*Colepiocephale lambei*	*Colepiocephale lambei*	*Colepiocephale lambei*	*Colepiocephale lambei*	*Colepiocephale lambei*
T:f/p	67.94	64.81	52	68.4	68.23	67.5	49.41	68.44	40
L:fp									
L:p									
L:f	45.37	45.17	44.3	49.9	50	47.7		54.01	50.48
L:po	39.84	43.49	29.22	38	44.73			40.185	27.8
L:pso	27.86	25.64	22.72	31.6	23.455	28.46	21.63	28.645	24.41
L:pl	21.095	22.83	13.4	24.8	19.755	14.56	14.87	10.335	8.69
L:prf	14.965				19.46	21.93		21.305	
W:post									
W:po/stf/sq	60.98	63.17	54.5	61.6	52.93			54.7	43.83
W:f/p	86.9	88.93	64	96.7	92.08	90.18	68.65	83.05	60.97
W:pso/po	72.46	78.79	59.09	79	72.85	90.99	63.62	75.16	57.9
W:pl/pso	68.33	75.55	56.5	80.27	75.5	80.16	57.67	68.75	57.17
W:pfr/pl	39.08	43.88	34.2	44.88	44.42	61.4	34.86	57.99	46.04
W:n/pfr	23.62		23.77	32.8	23.92	27.74		25.75	25.13
H:pso/po	18.725		14.49	20	15.685	22.01		12.9	10.39
H:pl/pso	11.23	13.61	15.1	15.3	16.995	19.5		10.34	11.23
H:pfr/pl	17.15	9.66	16.74	26.4	17.905	24.875		17.2	12.93
H:n/pfr	*13.6*	*20.12*	*36.5*	*30.2*	*14.035*	*19.505*		*8.17*	*3.29*
H:n/n	*15.56*		*18.5*	*36.5*	*19.5*	*25.15*		*19.01*	*9.56*
Source	This study	This study	Schott and Evans (2016)	Schott and Evans (2016); This study	This study	Schott and Evans (2016)	This study	This study	Schott and Evans (2016)

165

Specimen	YPM-PU-22248	CMN121	CMN193	CMN194	CMN1423	CMN 8819	CMN12351	ROM31616	TMP1967.010.0003
Taxon	*Colepiocephale lambei*	*Foraminacephale brevis*	*Foraminacephale brevis*	*Foraminacephale brevis*	*Foraminacephale brevis*	*Foraminacephale brevis*	*Foraminacephale brevis*	*Foraminacephale brevis*	*Foraminacephale brevis*
T:f/p	46	28.5	25.5	26.7	25.3	34.5	8.5	32.08	28.06
L:fp									
L:p		36		37.3			22		
L:f	35					34.2		33.49	
L:po	32.8	22.1	18.4	19.7	24.3	23.75		20.18	21.97
L:pso	21.85	21.5	19.2	21.95	19.4	19.9		24.92	17.18
L:pl	14.9	11.9	12.7		10.35	12.6		16.15	10.98
L:prf								10.9	
W:post									
W:po/stf/sq	37.4	43.1	48.2		33	54.3	17.2	52.35	42.22
W:f/p	68	47.4	47.4	47.1	41.1	57.6	22.6	54.49	50.34
W:pso/po	59.6	47.1	48.6	47.9	43.3	56.8		56.54	48.4
W:pl/pso	57.4	44.7	44.3	46.5	43.6	51.9		54.48	42.54
W:pfr/pl	37.8	28	26.4		27.8	31.7		32.12	33.6
W:n/pfr	21.3				18.8	20.2		14.96	10.365
H:pso/po	8.5	11.4	14.2	16.8	13.2	18.8		21.37	
H:pl/pso	10.7	7	3.9	5.7	6.2	11.7		9.01	8.3
H:pfr/pl	11.8	9	5.5	8	8	12.4		12.86	5.51
H:prf								6.41	
H:n/prf	11.6	3.8	3.8		10.4	10.4		6.84	
H:n/n						9.7			
Source	Schott and Evans (2016)	Schott and Evans (2016)	Schott and Evans (2016)	Schott and Evans (2016)	Schott and Evans (2016)	Schott and Evans (2016)	Schott and Evans (2016)	Schott and Evans (2016); This study	This study

Specimen	TMP?1970.10.2	TMP1973.008.0223	TMP1974.010.0074	TMP1980.016.0752	TMP1981.016.0145	TMP1981.019.0013	TMP1982.019.0288	TMP1985.036.0292	TMP1985.043.0068
Taxon	*Foraminacephale brevis*	*Foraminacephale brevis*	*Foraminacephale brevis*	*Foraminacephale brevis*	*Foraminacephale brevis*	*Foraminacephale brevis*	*Foraminacephale brevis*	*Foraminacephale brevis*	*Foraminacephale brevis*
T:f/p	46	23.19	27.1	30.58	28.45	9.08		26	12.5
L:fp								66.8	
L:p							29.74	34.6	28.1
L:f	22.9	25.13	32.6	31.51				31.5	
L:po		21.68	22.7	24.8	23.64	12.94		18.3	
L:pso		21.95	20.7					22.7	
L:pl		12.07	9.3	13.86	12.68	5.38		12.8	
L:prf		6.8		5.38					
W:post									13.9
W:po/stf/sq	56	39.6	39.6					47.2	28.6
W:f/p	64.3	45	43.2	48.84	51.24	33.44		49.3	31.8
W:pso/po	64.9	44.97	44.3	59.86	52.61	39.46		50.4	
W:pl/pso		45.68		51.78	47.06	33.48		47.7	
W:pfr/pl		23.82		33.14	27.23	22.74		27.6	
W:n/pfr		12.76	15.6	20.08				16.9	
H:pso/po		12.72	12.9	18.47	13.805	4.59		17.2	
H:pl/pso		6.16	5.6	8	5.58	0.81		7.4	
H:pfr/pl		7.74	8.1	10.71	8.15	2.58		8.5	
H:n:pfr		6.6	7.3	3.48				7.6	
H:n/n		6.81	7	4.87				6.8	
Source	Schott and Evans (2016)	Schott and Evans (2016); This study	Schott and Evans (2016)	This study	This study	This study	This study	This Study	Schott and Evans (2016)

Specimen	TMP1985.056.0121	TMP1986.036.0232	TMP1987.036.0364	TMP1987.050.0029	TMP1991.036.0265	TMP1998.093.0079	TMP1999.055.0122	TMP2000.012.0001	TMP2003.012.0059
Taxon	*Foraminacephale brevis*	*Foraminacephale brevis*	*Foraminacephale brevis*	*Foraminacephale brevis*	*Foraminacephale brevis*	*Foraminacephale brevis*	*Foraminacephale brevis*	*Foraminacephale brevis*	*Foraminacephale brevis*
T:f/p	4.38		34.92	53	27	64.4	24	21.44	
L:fp				95.1	57.1		61.1		
L:p				51.2	29.57		30.1	35.45	
L:f				43.9	27.49		31		
L:po			27.27	28.25	17.31		16.15	21.11	21.9
L:pso			19.64	33.65	17.6	30.97	18	22.63	
L:pl			17.6	17.6	8.94	10.85	10.5	12.64	
L:prf									
W:post				20.5	12.8		10.7		
W:po/stf/sq	23.72		66.03	80.9	38.73		39.7	47.96	42.53
W:f/p	26.7	30.3	67.29	84.1	39.42	86.75	44	47.89	52.02
W:pso/po		34.3	66.19	82.4	38.54	84.52	45.2	50.33	52.34
W:pl/pso				69.9	37.68	72.82	39.7	46.2	
W:pfr/pl				42.8	30.72	60.11	26.3	29.82	
W:n/pfr		12.22		26.5	15.83		15.4	18.03	
H:pso/po		6.1	10.92	27.8	10.99	24.4	12.8	16.09	5.69
H:pl/pso			13.4	16.9	4.84	9.465	5.5	6.73	
H:pfr/pl				22.4	4.8	14.49	6	9.76	
H:n/prf				17.6			4.6		
H:n/n		2.95		22.5	2.06		4.3		
Source	Schott and Evans (2016)	This study	This study	Schott and Evans (2016)	Schott and Evans (2016)	This study	Schott and Evans (2016)	Schott and Evans (2016)	This study

168

Specimen	TMP2003.012.0252	UALVP 5	UALVP 8501	UALVP 8504	UALVP 8508	UALVP 47278	UALVP 57848	UALVP 58027	UALVP 59924
Taxon	*Foraminacephale brevis*	*Foraminacephale brevis*	*Foraminacephale brevis*	*Foraminacephale brevis**	*Foraminacephale brevis*	*Foraminacephale brevis*	*Foraminacephale brevis*	*Foraminacephale brevis*	*Foraminacephale brevis*
T:f/p	22.93	23.41	20.5	48.8	31.6	39.3	25.33	14.01	
L:fp					36.1				
L:p	33.31	26.4			70.3		32.57	25.11	
L:f					34.3	37	34.12		
L:po	15.27	18.74	16.15	18.125	20.3	25.2	17.35		26.76
L:pso					22.8	28.1	19.34		
L:pl					12.3	14	14.95		
L:prf					8.89	8.21	10.06		
W:post	5.98	7.05			14				
W:po/stf/sq	37.44	35.36	34.27	56.49	55.9	58.5	43.54		
W:f/p	39.3	41.25	38.81	52.08	56.4	64.6	45.36	56.76	
W:pso/po	41.51	40.52	39.24	52.38	55.3	62.3	46.31	60.12	
W:pl/pso					48.7	55.1		54.98	
W:pfr/pl					28.7	33.5		27.22	
W:n/pfr					17.5	20.12		23.96	
H:pso/po	11.47	14.22	10.25	7.16	17.4	18.9	10.27	16.55	
H:pl/pso					8.15	6.4		6.99	
H:pfr/pl					10.6	11.3		10.94	
H:n/prf					8.2	11.5		6.34	
H:n/n					7.7	8.28		4.21	
Source	This study	This study	Schott and Evans (2016)	Schott and Evans (2016); This study	Schott and Evans (2016); This study	Schott and Evans (2016); This study	This study	This study	This study

Specimen	MPC-D 100/1501 (photographs)	MPC-D 100/1201	TCMI 2004.17.1	CCM V-87-1 (cast)	ROM 6290 (Photographs)	MPC-D 100/1206	Z. Pal.MgD-I/104	MPC-D 100/1204	MPC-D 100/1207
Taxon	*Goyocephale lattimorei*	*Homalocephale calathocercos*	*Pachycephalosaurus wyomingensis*	*Pachycephalosaurus wyomingensis*	*Pachycephalosaurus wyomingensis*	*Prenocephale prenes*	*Prenocephale prenes*	*Prenocephale prenes*	*Prenocephale prenes*
T:f/p				105.82	133.28	69		120	76
L:fp	118.78	135			160.02		106		
L:p	59.85	64							
L:f	58.93	71		87.36	80.68			71.39	70.27
L:po	22.695	44.77		72.875	83.44		58	68.5	52.34
L:pso	34.095			38.485	57.87		39	62.365	51.93
L:pl	5.355			4.24	10.56		5	13.64	16.71
L:prf	23.41			42.84	38.4				
W:post	14.33	13.22			23.23		10.92		
W:po/stf/sq	61.3	53.53	63.47	113.36	168.7	73.93	93.61	186.98	152.32
W:f/p	59.26	63		111.21	157.17	85	108	174	148.95
W:pso/po	62.48	75		101.3	142.13	82	99	165	149.37
W:pl/pso	67.36	75	70.86	88.41	102.28		86	131	117.65
W:pfr/pl	57.9			82.55	91.66		81	110	86.96
W:n/pfr	18.91	20		27.81	43.96		30	68	45.57
H:pso/po		20		37.34	65.38			70.66	52
H:pl/pso				30.74	37.83			35.395	31
H:pfr/pl		10		30.74	45.18		15	34	31
H:n/prf				17.085	44.59			39	33.89
H:n/n		9		24.32	51.93			43	29
Source	Perle et al. (1982)	Evans et al. (2011); Evans et al. (2018)	Bakker et al. (2006)	This study	This study	Evans et al. (2018); This study	Evans et al. (2018)	Evans et al. (2018); This study	Evans et al. (2018)

Specimen	AMNH 2073	DMNH EPV.97077	LACM 64000 (cast)	ROM 53584	ROM 53585 (cast)	ROM 53667	ROM 75853	TMP 87.113.003 (cast)	UCMP 186026 (cast)
Taxon	*Sinocephale bexelli*	*Sphaerotholus buchholtzae*	*Sphaerotholus buchholtzae*	*Sphaerotholus buchholtzae*	*Sphaerotholus buchholtzae*	*Sphaerotholus buchholtzae*	*Sphaerotholus buchholtzae*	*Sphaerotholus buchholtzae*	*Sphaerotholus buchholtzae*
T:f/p	44	44	41.8	54.6	43	42.4		52.4	34.7
L:fp		107.22	90.47	111.75	97.66			112.27	75.94
L:p		63.09	47.1	57.83		63.1		62	44.08
L:f		42.97	41.94	51.86				56.08	33.41
L:po		39.395	36.03	36.15	34.67	41.27		34	26.56
L:pso		22.65	17.87	22.41	21.6	20.65		21.39	13.9
L:pl		5.44	5.28	6.5	8.89	10.69		10.08	4.98
L:prf		31.155							
W:post	40	22.92	18.41	22.35		20	30.93	22.96	11.15
W:po/stf/sq	80.96	76.2	52.98	83.73	78.23	72.7		78.61	43.01
W:f/p	120	83.54	63.64	93.52	87.92	85.65		83.67	52.84
W:pso/po		84.13	60.7	86.59	86.32	79.77		80.81	48.36
W:pl/pso		72.96	56.38	68.08	66	64.04		60.65	42.75
W:pfr/pl		66.4	51.7	59.56	62.06	54.42		50.12	36.71
W:n/pfr		23.78	14.25	23.6				18.57	13.27
H:pso/po		23.355	19.1	26.66	26.56	24.49		30.02	14.37
H:pl/pso		16.39	12.11	15.22	15.09	12.21		13.14	5.84
H:pfr/pl		16.29	15.24	19.19	20.06	16.46		13.5	8.38
H:n/prf		14.37	14.83	21.52	25.42			29.24	9.31
H:tn/n		18.79	13.18	20.83				15.92	8.42
Source	Evans et al. (2021)	Woodruff et al. (2021)	Woodruff et al. (2021)	Woodruff et al. (2021)	Woodruff et al. (2021)	Woodruff et al. (2021)	Woodruff et al. (2021)	Woodruff et al. (2021)	Woodruff et al. (2021)

Specimen	UWBM 89701	ROM 53668 (cast)	NMMNH P-27403	CMN 8830	AMNH5388 (photographs)	AMNH5450	BMNH-R.-8673	BMNH-R.-8674	CMN138
Taxon	*Sphaerotholus buchholtzae*	*Sphaerotholus buchholtzae*	*Sphaerotholus goodwini*	*Sphaerotholus edmontonensis*	*Stegoceras validum*	*Stegoceras validum*	*Stegoceras validum*	*Stegoceras validum*	*Stegoceras validum*
T:f/p	39.5	49.7	75	37.2	64	20	44.6	38.2	34
L:fp	96.78	104.47	130.5	92.88		82.3			84.2
L:p	53.19	54.45	66.1	54.04	57.98	41			40.9
L:f	47.44	55.28	64.4	41.4		41.3			43.4
L:po	30.48	28.41	60.3	40.4	52.25	24.5			33.9
L:pso	17.52	19.2	34.8	18.2	26.66	15.5			16
L:pl	5.5	9.23	17.9	11.6	21.1	10.1			12.1
L:prf									
W:post	16.98	24.02	6.8	23.7		4.3			6.2
W:po/stf/sq	52.31		77.03	57.73	59.52	35.7			41.2
W:f/p	66.06	88.5	101	66	82	39.2	62.2	53.1	
W:pso/po	64.99	85.63	97.5	64	88.08	45.4			56.6
W:pl/pso	53.7		78.5	53.7	74.45	43.8			55.1
W:pfr/pl	46.29		54.4	38.7	48.38	30.7	44.9		39.4
W:n/pfr	17.45		35.6	19.5	35.65	18.4	21.1		25.8
H:pso/po	17.29	29.44	41.6	18.7	24.38	14.3			14.3
H:pl/pso	10.94	14.58	23.3	10.4	20.89	11.4			8.9
H:pfr/pl	14	16.95	30.2	11.3	29.49	11.7			11.2
H:n/prf	14.22	24.82	30.22	14.6	26.43	9.4			10.1
H:n/n	13.8	20.03	23.7	10.9	33	9.9			15.2
Source	Woodruff et al. (2021)	Woodruff et al. (2021)	Evans et al. (2013); Williamson and Brusatte (2016)	Woodruff et al. (2021)	Brown and Schlaikjer (1943)	Schott and Evans (2016)	Schott and Evans (2016)	Schott and Evans (2016)	Schott and Evans (2016)

Specimen	CMN515	CMN1108A	CMN1594	CMN2379	CMN8816	CMN38428	ROM803	ROM53555	ROM58311
Taxon	Stegoceras validum	Stegoceras validum	Stegoceras validum	Stegoceras validum	Stegoceras validum	Stegoceras validum	Stegoceras validum	Stegoceras validum	Stegoceras validum
T:f/p	35	36	30.6	39	29.5	40		67.66	42.1
L:fp	93.5			84.3		119.1			82.6
L:p	48		51.1	43.7		63.7			54.7
L:f	45.5	41.3		39.5	40.6	55.4		58	41.4
L:po	35.8	29.7		36.1	32	36	34.3	56.46	24
L:pso	20.2	17.1		20.6	16.7	23.1	16.6	28.24	23.3
L:pl	9.4	11.4		15.2	10.5	17.2	9.4	15.65	12.2
L:prf									
W:post	8.4				0				
W:po/stf/sq	44.3	36.4	42.5		32.5	55.6		66.23	
W:f/p	57.5	49.6	57.2	58.2	48.6	70.8	53.4	107.93	69.6
W:pso/po	58.5	55.3		64.1	54.2	67.9	56.7	98	
W:pl/pso	51.8	50			50	66.6	51.7	99.42	60.9
W:pfr/pl	41.9	37.1		42.4	36.4	53.4	39.1	71	47.8
W:n/pfr	26.5	20			15.19	27.3	25.3	41.81	29.4
H:pso/po	14.7	17.1		22	14.2	21	21	26.03	18.5
H:pl/pso	10.2	13.5		14.5	8.5	7.6	8.5	21.19	9.9
H:pfr/pl	15.4	16.3		15.5	11.4	17.2	14.7	22.8	11.4
H:n/prf	16	14.9		19	10.2	16.9		25.29	
H:n/n	16.5	17.4		32.2	11.6	19.4	19.4	27.88	17.3
Source	Schott and Evans (2016)	Brown and Schlaikjer (1943); Schott and Evans (2016)	Schott and Evans (2016)	Schott and Evans (2016)	Schott and Evans (2016)	Schott and Evans (2016)	Schott and Evans (2016)	Schott and Evans (2016); This study	Schott and Evans (2016)

Specimen	TMP1975.011.0005	TMP1978.019.0004	TMP1981.041.0102	TMP1982.020.0189	TMP1983.067.0001	TMP1984.005.0001	TMP1984.067.0020	TMP1984.121.0021	TMP1985.036.0076
Taxon	*Stegoceras validum*	*Stegoceras validum*	*Stegoceras validum*	*Stegoceras validum*	*Stegoceras validum*	*Stegoceras validum*	*Stegoceras validum*	*Stegoceras validum*	*Stegoceras validum*
T:f/p	38.15	16.2	6.8	7.2	47.1	25	15.74	42.7	8.33
L:fp					103.5	85.7			
L:f	36.08	59	36.5	36	45.8	44.5		34.49	
L:p	33.165				57.7	41.2			
L:pso	16.445	21.1	12		21.7	14.9	15.82	20.57	
L:po					36.1	29.2			
L:prf	13.445							13.07	
L:pl	10.38	12.3	5.9		12.5	11.8	9.06	18.51	
W:post						7.3			
W:po/stf/sq	37.27		26.8	34.3	47.4	39.09			
W:f/p	55.41	56.2	37.6		66.8	52.7	36.9	71.08	40.24
W:pso/po	55.37	69.9	45		71.9	56.3	48.48	68.54	49.56
W:pl/pso	50.14	65.4	41		59.7	48.6	43.38	61.19	46.56
W:pfr/pl	37.61	50.3	35		45.3	36.3	31.38	42.73	
W:n/pfr	21.58	20			29.4	21.2		24.8	
H:pso/po	13.31	11.4	6.5		13.6	12.6	6.11	19.76	5.27
H:pl/pso	10.47	7.8	4.1		7.2	7.8	2.44	13.03	
H:pfr/pl	11.68	7.8	3.1		13.1	11.7	4.06	18.89	3.87
H:n:prf	11.67		4.3		14.2	9.21		16.17	
H:n/n	13.78	2.8	2.8		21.2	13.6		21.66	
Source	This study	Schott and Evans (2016)	Schott and Evans (2016)	Schott and Evans (2016)	Schott and Evans (2016)	Schott and Evans (2016); This study	This study	This study	This study

Specimen	TMP1985.053.0004	TMP1985.058.0068	TMP1986.071.0002	TMP1988.116.0049	TMP1989.036.0115	TMP1989.116.0090	TMP1990.066.0002	TMP1992.002.0003	TMP1992.002.0036
Taxon	*Stegoceras validum*	*Stegoceras validum*	*Stegoceras validum*	*Stegoceras validum*	*Stegoceras validum*	*Stegoceras validum*	*Stegoceras validum*	*Stegoceras validum*	*Stegoceras validum*
T:f/p		5.8	18.3	11.6	23.08	16.29	22.71	31.18	31.5
L:f/p								80.2	74
L:fp									
L:p								37.02	38
L:f			44.8	44.8	40.56		38.11	43.18	36
L:po								31.06	23.2
L:pso			15.8		16.46		16.74	15.34	16.7
L:pl	5.95		8.5		11.79		10.5	4.01	10.1
L:prf	13.38				9.87		15.74	11.145	
W:post							40.6	30.69	34.7
W:po/stf/sq									
W:f/p			32.8	40	41.7	35.22	43	46.07	41.7
W:pso/po			36.4		48.12	40.9	53.5	47.82	48.3
W:pl/pso	50.76		37.4		48.04		55.22	39.75	42.5
W:pfr/pl	43.5		30.4		30.84		22.54	33.18	33.3
W:n/pfr	26.62				19.96		11.07	18.52	18.2
H:pso/po			10.3		10.3			12.21	12.9
H:pl/pso	4.64		9.5		9.33		6.56	8.2	7.1
H:pfr/pl	5.34		12.3		11.4		8.05	9.69	10.7
H:n/pfr	4.2				8.72		8.62	10.87	
H:n/prf			11.2						12
H:n/n	4.89				8.09		10.77	11.29	12.3
Source	This study	Schott and Evans (2016)	Schott and Evans (2016)	Schott and Evans (2016)	This study	This study	This study	This Study	Schott and Evans (2016)

Specimen	TMP1992.036.0286	TMP1992.093.0001	TMP1993.036.0257	TMP1995.012.0147	TMP1999.062.0001	TMP2002.012.0057	TMP2002.012.0076	TMP2002.012.0144	TMP2006.012.0241
Taxon	*Stegoceras validum*	*Stegoceras validum*	*Stegoceras validum*	*Stegoceras validum*	*Stegoceras validum*	*Stegoceras validum*	*Stegoceras validum*	*Stegoceras validum*	*Stegoceras validum*
T:f/p	40.2	6.8	7.3	7.8	32.8	16.7	6.25	27.19	18.16
L:fp									
L:p		36.2		46.1	50				
L:f	42					38.8		33.48	31.66
L:po	33.6						15.66		
L:pso	18.5					14	11.74	11.57	12.84
L:pl	15					10.4	7.62	9.19	8.74
L:prf									13.59
W:post									
W:po/stf/sq	42.3		34.8						
W:f/p	56.6	36.8	38.6	39.1	58	36.2	32.08	42.6	36.4
W:pso/po	65.7					44	38.5	48.06	45
W:pl/pso	61					40.4	33.7	47.2	40.86
W:pfr/pl	42.3					29	23.36	31.36	31.32
W:n/pfr	26					17.8		19.68	12.9
H:pso/po	22.1		5.8			8.2	6.92	11.8	7.04
H:pl/pso	17.6					5.7	2.43	9.07	4.33
H:pfr/pl	18.7		3.2			7.1	3.19	11.94	5.91
H:n/prf	14.5					5.5		8.45	3.48
H:n/n	*18.2*					5.8		19.5	5.28
Source	Schott and Evans (2016)	Schott and Evans (2016)	Schott and Evans (2016)	Schott and Evans (2016)	Schott and Evans (2016)	Schott and Evans (2016)	This study	This study	This study

Specimen	TMP2007.020.0003	TMP2009.034.0001	TMP2011.012.0009	TMP2016.012.0106	TMP2019.012.0222	UALVP 2	UALVP 6	UALVP 8502	UALVP 8503
Taxon	*Stegoceras validum*	*Stegoceras validum*	*Stegoceras validum*	*Stegoceras validum*	*Stegoceras validum*	*Stegoceras validum*	*Stegoceras validum*	*Stegoceras validum*	*Stegoceras validum*
T:f/p	27.45	63.3	37.12	28.53	24.91	58.51	40.8	37.6	
L:fp						115.18			
L:p					40	63.16	47	42.4	
L:f	31.45		37.12	30.55		52.02			
L:po			27.92			44.045	33	33	31.3
L:pso	14.54		16.355	16.58		22.145	23.1	18	
L:pl	9.79		12.615	8.65		14.865	13.6	14.2	
L:prf	9.74				12.19	18.22			
W:post					11.56	11.45			
W:po/stf/sq		69.86	43.13		38.92	58.56		41.89	40.58
W:f/p	36.96	*87*	53.43	45.62	44.65	80.98	55.8	56	55.95
W:pso/po	46.54		58.52	54.68		84.55	55.9	62.88	56.92
W:n/pfr	40.5		52.89	49.16		71.85	50.1	58.94	
W:pfr/pl	26.4		34.34	36.12		53.85	33.8	36.15	
W:pl/pso	14.34		20.79	22.36		31.65	21.3	28.9	
H:pso/po	13.38			8.51		18.37		20.2	
H:pl/pso	7.95			4.43		15.875		14.4	
H:pfr/pl	11.4			7.41		19.13		15.9	
H:n/prf	9.64		14.77	5.76		21.555		13.8	
H:n/n	9.03		17.09	9.9		32.95		21.3	
Source	This study	This study	This study	This study	This study	This study	Schott and Evans (2016)	Schott and Evans (2016); This study	This study

Specimen	UALVP 8505	UALVP 8506	UALVP 8507	UALVP 49439	UALVP 49531	UALVP 51156	UALVP 51913	UALVP 60014	UALVP 60421
Taxon	*Stegoceras validum*	*Stegoceras validum*	*Stegoceras validum*	*Stegoceras validum*	*Stegoceras validum*	*Stegoceras validum*	*Stegoceras validum*	*Stegoceras validum*	*Stegoceras validum*
T:f/p	38.86	43.25	39.34	7.37	6.6		7		38.33
L:fp									
L:p					38.6				
L:f	44.48								45.81
L:po	28.97				29.26				32.74
L:pso	16.805		17.3		12.51		11.9		17.06
L:pl	16.03		13.7		8.13		10		10.915
L:prf	15.48		15.15						16.985
W:post					4.57				
W:po/stf/sq	44.31				28.28	52.32			43.91
W:f/p	57.37	58.55	53.64	43.52	32.7	73.85	41.2	65.3	60.87
W:pso/po	62.88		57.62		47.42	77.94	46		60.03
W:pl/pso	58.94		53.08		42.07		43.6		55.7
W:pfr/pl	36.15		39.54		32.1				42.77
W:n/pfr	30.69		17.92			32.8			25.38
H:pso/po	14.18			6.27	5.26		5.9		19.74
H:pl/pso	14.545		8.89		1.94		4.1		8.67
H:pfr/pl	17.9		12.41		3.4		4.3		10.675
H:n/prf	13.18		10.73		14.13				11.36
H:n/n	16.45		9.95		17.82				13.77
Source	This study	This study	This study	This study	Schott and Evans (2016); This study	This study	Schott and Evans (2016)	This study	This study

Specimen	UALVP 60518	UALVP 60987	UCMZ(VP)2008.001	UCMZ(VP)2008.002	UCMZ(VP) unnumbered	CMN192	CMN8817	CMN8945	CMN9148
Taxon	*Stegoceras validum*	*Stegoceras validum*	*Stegoceras validum*	*Stegoceras validum*	*Stegoceras validum*	*Stegoceras validum (Hanssuesia sternbergi)*	*Stegoceras validum (Hanssuesia sternbergi)*	*Stegoceras validum (Hanssuesia sternbergi)*	*Stegoceras validum (Hanssuesia sternbergi)*
T:f/p	33.66	6.53	7.8	6.8	53.2	64.1	63.3	71	71
L:fp									
L:p			36.6	31.2			75	75	
L:f		e37.51	21.74		48.4	53.4	56		55.2
L:po					37.8	52.8	60	58.8	46.7
L:pso	18.67				15.4	25.05	27.7	27.7	29.55
L:pl	12.26	7.44			8.2	22.15	20.3	22.4	23.2
L:prf		12.9							
W:post			0	6.85			79		64.8
W:po/stf/sq			30.38	30.7					
W:f/p	54.54		33.6	30.8	53	91.6	102.5	102.4	97.8
W:pso/po	55.42	e48.4	40.72		57.2	95.5	106	82	102.2
W:pl/pso	48.62	44.86			57.6	83.7	91.8	82	86
W:pfr/pl	37.36	36.24			47.2	52	62.8	61.5	57.5
W:n/pfr		20.3			23.8	35.5	40.1	33.6	40.9
H:pso/po	15.44			6.5	11.8	35.9	30.2	34.5	27.5
H:pl/pso	11.08	2.11			8.1	30.3	24.6	19.2	19
H:pfr/pl	15.02	1.88			10.5	35.1	27.3	23.6	26.3
H:n/prf		3.88			8	38.4	14.8		27.65
H:n/n					15	34	25		37
Source	This study	This study	Schott and Evans (2016)	Schott and Evans (2016); This study	Schott and Evans (2016)	Schott and Evans (2016)	Schott and Evans (2016)	Schott and Evans (2016)	Schott and Evans (2016)

Specimen	CMN38079	TMP1979.014.0853	TMP1987.036.0363	TMP2000.026.0001	TMP2017.012.0019	UALVP 3	TMP1972.027.0001	NMMNH P-33898
Taxon	*Stegoceras validum (Hanssuesia sternbergi)*	*Stegoceras validum (Hanssuesia sternbergi)*	*Stegoceras validum (Hanssuesia sternbergi)*	*Stegoceras validum (Hanssuesia sternbergi)*	*Stegoceras validum (Hanssuesia sternbergi)*	*Stegoceras validum (Hanssuesia sternbergi)*	*Stegoceras validum (Gravitholus albertae)*	*" Stegoceras novomexicanum "*
T:f/p	57	56	57.2	63.8	57.59	60.28	67.87	21.4
L:fp					137.12		121.42	70.7
L:p					84.4		69.8	
L:f	50.25	49	51.8		52.72		51.62	36.45
L:po		51.9	50.1	49.1	49.18		62.805	22.1
L:pso	29.6	24.75	22.95	28.3	21.96	21.48	25.465	14.1
L:pl	19.2	20.9	17.3	22.1	20.43	18.98	17.995	10.6
L:prf							22.58	13.9
W:post					11.32		27.92	
W:po/stf/sq	59	59	61.9		70.79		66.73	28.5
W:f/p	95.7	92.6	88.9	95.3	88.54	98.28	108.99	38.04
W:pso/po	79.9	81.7	77	76.79	87.09	97.75	80.93	40
W:pl/pso	98.8	96	91.7	94.3	85.29	82.93	103.77	43.2
W:pfr/pl		55.8	51.7	47.69	64.19		60.97	30
W:n/pfr		37.5	28	34.4	34.27		43.1	13.3
H:pso/po	27.3	26.3	19.4	24.1	15.1		33.76	8.2
H:pl/pso	18.1	18.7	18	23.8	16.965		23.355	9.7
H:pfr/pl		23.4	14		21.265		26.04	7.1
H:n/prf		25.7	13.4		13.305		30.72	6.94
H:n/n		31	17		24.74		35.13	7.7
Source	Schott and Evans (2016)	Schott and Evans (2016)	Schott and Evans (2016)	Schott and Evans (2016)	This study	This study	This study	Williamson and Brusatte (2016); This study

A1.2 Corrected Measurements

Schott et al. (2011) reported a frontoparietal thickness of 49.6mm for CMN 1108(A) (a cast of the original), whereas Brown and Schlaikjer (1943) reported a frontoparietal thickness of 36 mm from the original specimen. Examination of its published photographs (Brown and Schlaikjer, 1943) suggests that 36mm is the correct frontoparietal thickness. The frontoparietal thickness for CMN1108A reported by Schott et al. (2011) is identical to it's reported frontoparietal width. No other pachycephalosaurid frontoparietal in this dataset is as thick as it is tall, except the unnumbered UCMZ(VP) specimen. Otherwise frontoparietal thickness does not exceed 80% of frontoparietal width. For that reason, UCMZ(VP) was not included in PCA analyses.

Preliminary morphometric results scored CMN 8817 (holotype of "*Hanssuesia sternbergi*") dissimilar from other specimens of *"Hanssuesia sternbergi"* and *Stegoceras validum*. I investigated the variables influencing the placement of CMN 8817, and identified W:po/stf/sq and L:po as strongly influencing the placement of CMN 8817. By examining published photographs of CMN 8817 (Sullivan 2003, Sullivan 2006), it can be concluded that the Po/stf/Sq landmark was misidentified by Schott and Evans (2016). This landmark should be identified much closer to the posterior extent of the specimen and re-measured W:Po/stf/Sq and both L:Po based on published photographs (Sullivan, 2006). PCA incorporating these corrected measurements score CMN 8817 like other *Hanssuesia sternbergi*.

CMN 515 appears to have a damaged endocranial roof along the frontoparietal suture, resulting in an apparent pinching in the endocranial roof along that contact (see photos in Jasinski and Sullivan, 2011). The W:endo has been re-estimated as 14.02 mm from Jasinski and Sullivan's (2011) photographs.

A1.3 Pachycephalosaurid frontoparietal specimens used for PCA.

Specimen	Taxon	H:n/n	H:n/prf	H:pfr/aso	H:aso/pso	H:pso/po	W:n/pfr	W:pfr/aso	W:aso/pso	W:pso/po	W:f/p	W:po/stf/sq	L:aso	L:pso	L:po	L:f	T:f/p
AMNH5388	*Stegoceras validum*	33	26.43	29.49	20.89	24.38	35.65	48.38	74.45	88.08	82	59.52	21.1	26.66	52.25	57.98	64
AMNH5450	*Stegoceras validum*	9.9	9.4	11.7	11.4	14.3	18.4	30.7	43.8	45.4	39.2	35.7	10.1	15.5	24.5	41.3	20
CMN138	*Stegoceras validum*	15.2	10.1	11.2	8.9	14.3	25.8	39.4	55.1	56.6	53.1	41.2	12.1	16	33.9	43.4	34
CMN515	*Stegoceras validum*	16.5	16	15.4	10.2	14.7	26.5	41.9	51.8	58.5	57.5	44.3	9.4	20.2	35.8	45.5	35
CMN1108A	*Stegoceras validum*	17.4	14.9	16.3	13.5	17.1	20	37.1	50	55.3	49.6	36.4	11.4	17.1	29.7	41.3	36
CMN8816	*Stegoceras validum*	11.6	10.2	11.4	8.5	14.2	15.19	36.4	50	54.2	48.6	32.5	10.5	16.7	32	40.6	29.5
CMN38428	*Stegoceras validum*	19.4	16.9	17.2	7.6	21	27.3	53.4	66.6	67.9	70.8	55.6	17.2	23.1	36	55.4	40
ROM53555	*Stegoceras validum*	27.88	25.29	22.8	21.19	26.03	41.81	71	99.42	98	107.93	66.23	15.65	28.24	56.46	58	67.66
TMP1975.011.0005	*Stegoceras validum*	13.78	11.67	11.68	10.47	13.31	21.58	37.61	50.14	55.37	55.41	37.27	10.38	16.445	33.165	36.08	38.15
TMP1983.67.1	*Stegoceras validum*	21.2	14.2	13.1	7.2	13.6	29.4	45.3	59.7	71.9	66.8	47.4	12.5	21.7	36.1	45.8	47.1
TMP1984.005.0001	*Stegoceras validum*	13.6	9.21	11.7	7.8	12.6	39.09	36.3	48.6	56.3	52.7	39.09	11.8	14.9	29.2	44.5	25
TMP1992.2.3	*Stegoceras validum*	11.29	10.87	9.69	8.2	12.21	18.52	33.18	39.75	47.82	46.07	30.69	4.01	15.34	31.06	43.18	31.18
TMP1992.2.36	*Stegoceras validum*	12.3	12	10.7	7.1	12.9	18.2	33.3	42.5	48.3	41.7	34.7	10.1	16.7	23.2	36	31.5
TMP1992.36.286	*Stegoceras validum*	18.2	14.5	18.7	17.6	22.1	26	42.3	61	65.7	56.6	42.3	15	18.5	33.6	42	40.2
UALVP 2	*Stegoceras validum*	32.95	21.555	19.13	15.875	18.37	31.65	53.85	71.85	84.55	80.98	58.56	14.865	22.145	44.045	52.02	58.51
UALVP 8502	*Stegoceras validum*	21.3	13.8	15.9	14.4	20.2	28.9	36.15	58.94	62.88	56	41.89	14.2	18	33	42.4	37.6
UALVP 8505	*Stegoceras validum*	16.45	13.18	17.9	14.545	14.18	30.69	36.15	58.94	62.88	57.37	44.31	16.03	16.805	28.97	44.48	38.86
UALVP 60421	*Stegoceras validum*	13.77	11.36	10.675	8.67	19.74	25.38	42.77	55.7	60.03	60.87	43.91	10.915	17.06	32.74	45.81	38.33
CMN8817	*Hanssuesia sternbergi*	25	14.8	27.3	24.6	30.2	40.1	62.8	91.8	106	102.5	79	20.3	27.7	60	56	63.3
CMN9148	*Hanssuesia sternbergi*	37	27.65	26.3	19	27.5	40.9	57.5	86	102.2	97.8	64.8	23.2	29.55	46.7	55.2	71
TMP1979.14.853	*Hanssuesia sternbergi*	31	25.7	23.4	18.7	26.3	37.5	55.8	81.7	96	92.6	59	20.9	24.75	51.9	49	56
TMP1987.36.363	*Hanssuesia sternbergi*	17	13.4	14	18	19.4	28	51.7	77	91.7	88.9	61.9	17.3	22.95	50.1	51.8	57.2
TMP2017.012.0019	*Hanssuesia sternbergi*	24.74	13.305	21.265	16.965	15.1	34.27	64.19	85.29	87.09	88.54	70.79	20.43	21.96	49.18	52.72	57.59
TMP1972.027.0001	*Gravitholus albertae*	35.13	30.72	26.04	23.355	33.76	43.1	60.97	80.93	103.77	108.99	66.73	17.995	25.465	62.805	51.62	67.87
NMMNH P-33898	*Stegoceras novomexicanum*	7.7	6.94	7.1	9.7	8.2	13.3	30	40	43.2	38.04	28.5	10.6	14.1	22.1	36.45	21.4
CMN 8818	*Colepiocephale lambei*	28.3	14.35	18.4	13.4	13.3	31.9	56.2	73.3	75.1	88.6	52	15.58	26.4	45.2	54.2	72
TMP1982.46.1	*Colepiocephale lambei*	25.6	14.6	17.5	16.7	16.5	30.2	44.9	72	75.1	82.3	52.6	16.25	28.3	44.05	52.9	63.1
TMP2000.057.0001	*Colepiocephale lambei*	36.5	30.2	26.4	15.3	20	32.8	44.88	80.27	79	96.7	61.6	24.8	31.6	38	49.9	68.4
TMP2010.005.0008	*Colepiocephale lambei*	19.5	14.035	17.905	16.995	15.685	23.92	44.42	75.5	72.85	92.08	52.93	19.755	23.455	44.73	50	68.23
UALVP 52676	*Colepiocephale lambei*	19.01	8.17	17.2	10.34	12.9	25.75	57.99	68.75	75.16	83.05	54.7	10.335	28.645	40.185	54.01	68.44
UCMP130048	*Colepiocephale lambei*	9.56	3.29	12.93	11.23	10.39	25.13	46.04	57.17	57.9	60.97	43.83	8.69	24.41	27.8	50.48	40
TMP2008.045.0001	*Acrotholus audeti*	28.2	24.47	28	25.6	37	28.5	63.2	70	76.3	70.1	61.32	8.6	25.1	44.2	51.03	59
NMMNH P-27403	*Sphaerotholus goodwini*	23.7	30.22	30.2	23.3	41.6	35.6	54.4	78.5	97.5	101	77.03	17.9	34.8	60.3	64.4	75
CMN 8819	*Foraminacephale brevis*	9.7	10.4	12.4	11.7	20.2	18.8	31.7	51.9	56.8	57.6	54.3	12.6	19.9	23.75	34.2	34.5
ROM31616	*Foraminacephale brevis*	6.84	6.41	12.86	9.01	21.37	14.96	32.12	54.48	56.54	54.49	52.35	16.15	24.92	20.18	33.49	32.08
TMP1973.008.0223	*Foraminacephale brevis*	6.81	6.6	7.74	6.16	12.72	12.76	23.82	45.68	44.97	45	39.6	12.07	21.95	21.68	25.13	23.19
TMP1985.36.292	*Foraminacephale brevis*	6.8	7.6	8.5	7.4	17.2	16.9	27.6	47.7	50.4	49.3	47.2	12.8	22.7	18.3	31.5	26

TMP1987.50.29	*Foraminacephale brevis*	22.5	17.6	22.4	16.9	27.8	26.5	42.8	69.9	82.4	84.1	80.9	17.6	33.65	28.25	43.9	53
TMP1999.55.122	*Foraminacephale brevis*	4.3	4.6	6	5.5	12.8	15.4	26.3	39.7	45.2	44	39.7	10.5	18	16.15	31	24
UALVP 8508	*Foraminacephale brevis*	7.7	8.2	10.6	8.15	17.4	17.5	28.7	48.7	55.3	56.4	55.9	12.3	22.8	20.3	34.3	31.6
UALVP 47278	*Foraminacephale brevis*	8.28	11.5	11.3	6.4	18.9	20.12	33.5	55.1	62.3	64.6	58.5	14	28.1	25.2	37	39.3
DMNH EPV.97077	*Sphaerotholus buchholtzae*	18.79	14.37	16.29	16.39	23.355	23.78	66.4	72.96	84.13	83.54	76.2	5.44	22.65	39.395	42.97	44
ROM 53584	*Sphaerotholus buchholtzae*	20.83	21.52	19.19	15.22	26.66	23.6	59.56	68.08	86.59	93.52	83.73	6.5	22.41	36.15	51.86	57.83
TMP 87.113.003 (cast)	*Sphaerotholus buchholtzae*	15.92	29.24	13.5	13.14	30.02	18.57	50.12	60.65	80.81	83.67	78.61	10.08	21.39	34	56.08	52.4
LACM 64000 (cast)	*Sphaerotholus buchholtzae*	13.18	14.83	15.24	12.11	19.1	14.25	51.7	56.38	60.7	63.64	52.98	5.28	17.87	36.03	41.94	41.8
UCMP 186026 (cast)	*Sphaerotholus buchholtzae*	8.42	9.31	8.38	5.84	14.37	13.27	36.71	42.75	48.36	52.84	43.01	4.98	13.9	26.56	33.41	34.7
UWBM 89701	*Sphaerotholus buchholtzae*	13.8	14.22	14	10.94	17.29	17.45	46.29	53.7	64.99	66.06	52.31	5.5	17.52	30.48	47.44	53.19
CMN 8830	*Sphaerotholus edmontensis*	10.9	14.6	11.3	10.4	18.7	19.5	38.7	53.7	64	66	50	11.6	18.2	40.4	41.4	37.2
MPC-D 100/1207	*Prenocephale prenes*	29	33.89	31	31	52	45.57	86.96	117.65	149.37	148.95	152.32	16.71	51.93	52.34	70.27	76
MPC-D 100/1204	*Prenocephale prenes*	43	39	34	35.395	70.66	68	110	131	165	174	186.98	13.64	62.365	68.5	71.39	120
CCM V-87-1	*Pachycephalosaurus wyomingensis*	24.32	17.085	30.74	30.74	37.34	27.81	82.55	88.41	101.3	111.21	113.36	4.24	38.485	72.875	87.36	105.82
ROM 68290	*Pachycephalosaurus wyomingensis*	51.93	44.59	45.18	37.83	65.38	43.96	91.66	102.28	142.13	157.17	168.7	10.56	57.87	83.44	80.68	133.28

A1.4 Discontinuous allometry of frontoparietal width vs frontoparietal thickness in
Stegoceras validum. Green – RMA regression with frontoparietals thinner than
TMP1984.005.0001. Orange – RMA regression with frontoparietals thicker than
TMP1984.005.0001.
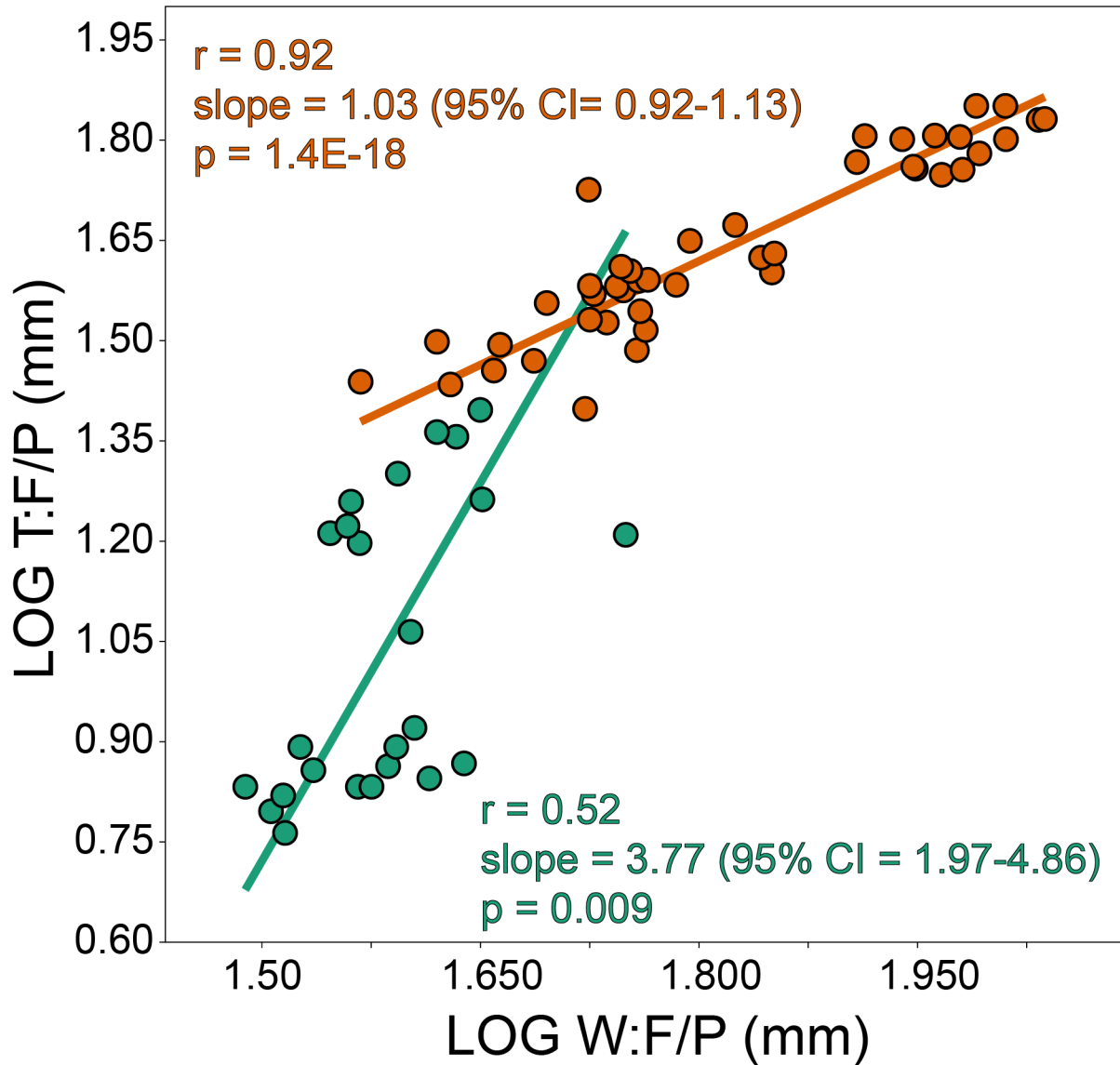
A1.5 Clarifications on pachycephalosaurian Palpebral – Anterior supraorbital

After several interpretations of the number and names of the elements that make up the supraorbital region in pachycephalosaurids (see Sullivan, 2003 for historical interpretations), two supraorbital elements are currently recognised: the anterior supraorbital and posterior supraorbital. Maidment and Porro (2010) explored the homology of various ornithischian supraorbital to the pleisiomorphic palpebral condition. They identified a similar topology between the pachycephalosaurian anterior supraorbital and the pleisiomorphic ornithischian palpebral, where both contact the prefrontal anterolaterally (through posteriorly continuous in pachycephalosaurians), and the lacrimal anteroventrally, and speculated that the anterior supraorbital was a modified palpebral. However, Maidment and Porro stated the absence of basal pachycephalosaurians inhibited a test of primary homology (*sensu* de Pinna, 1991). Primary tests of homology (ie. Test of similarity) can be performed by comparing similarities in topology, development, morphology between two taxa at any taxonomic level. I find no reason that a test of primary homology (similarity) between the ornithischian palpebral and the pachycephalosaurid anterior supraorbital cannot be made or be followed by a test of congruence (secondary homology). The discovery of basal members can inspire further testing of the primary homology. Indeed, the recovery of heterodontosaurids, which retain palpebrals, as basal pachycephalosaurians (Dieudonné et al., 2020) meets this requirement.

Maidment and Porro (2010) perform the test of congruence by mapping the distribution of palpebrals and supraorbitals over phylogenetic trees of the major ornithischian clades, as a test primary homology. This did not test the primary homology assessments that a supraorbital element is homologous with the palpebral, but instead demonstrated the "homology" of nomenclature. They identify character state changes of what is called the palpebral changing into what we call supraorbitals, despite previously demonstrating primary homology in several ornithischian groups. The correct test of congruence of the primary homology would be to assess taxa that possess supraorbitals that are similar (test of similarity) to the palpebral as palpebrals. In which case, all ornithischians possess palpebrals. What Maidment and Porro's (2010) test of congruence actually tests is the state that the palpebral covers the supraorbital region. In this case, they identify several convergences within Ornithischia of the palpebral incorporating with

additional skull roof elements to dorsally close (ossify) the orbit. Pachycephalosaurians represent one of these independent convergent events, where the palpebral participates in closing the dorsal region of the orbit via a contact with the frontal and a *de novo* posterior supraorbital. Therefore, I the pachycephalosaurian "anterior supraorbital" is referred to here as the palpebral.

A1.6 Linear measurement variances for PCA analyses of *Stegoceras validum*. A) non-transformed measurements. B) LOG-transformed measurements. C) L:F proportionate measurements. D) W:F/P proportionate measurements.
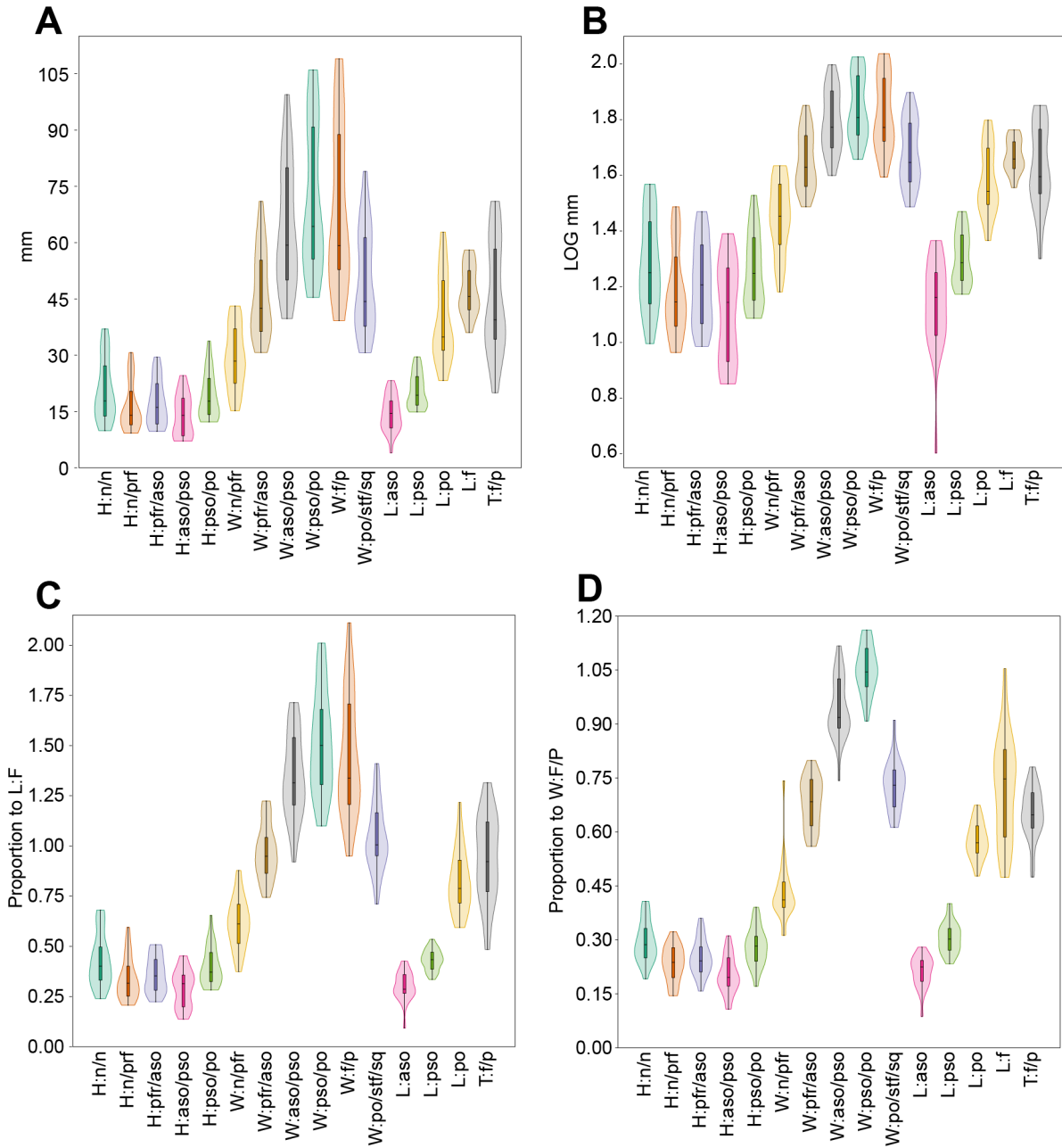
Appendix 2

A2.1 Character state assessments and revisions

Woodruff et al. (2021) character (Wch) 7 (character 7 of this analysis) – "ossified tendons" revised to "ossified caudal myorhabdoi" (Brown and Russell, 2012)

Wch 27 (character 25 of this analysis). "Epaxial muscle attachments" revised to "the main bilateral depression for the insertion area for the atlanto-occipital capsular membrane/ligament (Tsuihiji, 2010); Instinct [0]; positioned lateral to the foramen magnum [1]; positioned dorsal to the foramen magnum [2]. *Homalocephale calathocercos* is reassigned as [1]. *Pachycephalosaurus wyomingensis* is re-assigned as [2].

Wch 28 (character 26 of this analysis). This character is revised to specify its limit to a mature, adult state. *Colepiocephale lambei* re-assigned as [0] as all known *Colepiocephale lambei* specimens retain large supratemporal fenestrae (Schott et al., 2009). *Goyocephale lattimorei, Homalocephale calathocercos,* and *Wannanosaurus yansiensis* are re-assigned [?] due to the immature status of the only known specimens (Butler and Zhao 2009; Evans et al. 2011).

Wch30 (character 28 of this analysis) – This character codes for the presence/absence of grooves separating the frontonasal boss form the supraorbital lobes on the frontal. The dorsal surface of *Tylocephale gilmorei* is damaged, so it is reassigned as [?]. The character is only applicable for a domed state, therefore, *Goyocephale lattimorei* and *Homalocephale calathocercos, Psittacosaurus mongoliensis* and *Yinlong downsi* are reassigned as [?].

Wch 33 (character 31 of this analysis) – As the character states are in reference to a dome (which likely formed throughout ontogeny) *Goyocephale lattimorei*, *Homalocephale calathocercos*, and *Wannanosaurus yansiensis* reassigned as [?] (known solely from likely juvenile specimens; Butler and Zhao 2009; Evans et al. 2011).

Wch 39 (character 36 of this analysis) – This character previously coded for the presence/absence of the primary squamosal node row, as well as the arrangement of the posterior ornamentation (including the primary squamosal node row). This character is herein divided into two characters, one to describe the presence/absent of the primary node row, and another to describe the presence/absence of a dorsal node row (see character 46).

Wch 40 (character 37 in this analysis) – *Goyocephale lattimorei* is reassigned [0/1] as the only known specimen is bilaterally asymmetric (five nodes on left, seven nodes on right; Perle et al. 1982). *Colepiocephale lambei* is assigned [1] (Schott and Evans 2011). *Psittacosaurus mongoliensis* and *Yinlong downsi* reassessed as inapplicable [?] because they do not preserve a primary squamosal node row.

Wch 42 (character 39 in this analysis) – Revised to clarify most medial node of the primary node row: positioned on the squamosal [0], forms a coalescing node along the parietal-squamosal suture [1]. *Goyocephale lattimorei* is reassigned as [0]. *Acrotholus audeti*, *Psittacosaurus mongoliensis*, *Wannanosaurus yansiensis*, and *Yinlong downsi* recoded as inapplicable [?] as they either do not possess primary squamosal node rows, or its presence is unknown.

Wch 43 (character 40 of this analysis) – *Alaskacephale gangloffi* is re-assigned as possessing an enlarged medial node [1] (Gangloff 2005)

Wch character 44 (character 41 of this analysis). This character is revised to code for the presence or absence of enlarged nodes ventral to the primary squamosal node row.

Wch 45 (character 42 of this analysis) – This character is revised to code for the number of nodes ventral to the primary node row: a single node (0); or multiple nodes (1). *Colepiocephale lambei* is assessed as [1]. The "accessory corner nodes" of *Sphaerotholus buchholtzae* (Woodruff et al. 2021) are assessed as [1]. *Alaskacephale gangloffi, Psittacosaurus mongoliensis*, *Stegoceras validum*, *Wannanosaurus yansiensis*, and *Yinlong downsi* are all reassessed as [?] either for missing material or the absence of nodes ventral to the primary node row.

Wch 48 (character 43 of this analysis) – the character states are simplified to specify the absence [0] or presence [1] of rostral nodes. If more species are found to vary in the arrangement of their rostral ornamentation, further characters can be constructed to code those arrangements. *Pachycephalosaurus wyomingensis* is reassigned [1].

Wch 49 (character 44 of this analysis) – *Sphaerotholus buchholtzae* (Woodruff et al. 2021), *Sphaerotholus goodwini* (Williamson and Carr 2002), *Stegoceras validum* (Schott and Evans 2012), and *Tylocephale gilmorei* (Sereno 2000) are all reassigned as [1].

Wch 50 (character 45 of this analysis) – *Sphaerotholus edmontonensis* is reassessed as [?]. Neither the postorbitals nor the squamosals are known (Brown and Schlaikjer, 1943; Sullivan 2000; Woodruff et al. 2021).

Character 46 (New): Row of enlarged nodes, dorsal to the primary squamosal node row: absent (0); present (1).

Alaskacephale gangloffi, *Colepiocephale lambei*, *Goyocephale lattimorei*, and *Pachycephalosaurus wyomingensis* all preserve enlarged nodes dorsal to the primary squamosal node row and are all assessed as [1]. *Foraminacephale brevis*, *Homalocephale calathocercos*, *Prenocephale prenes*; *Sphaerotholus buchholtzae*, *Sphaerotholus goodwini*, and *Stegoceras validum* are all assessed as [0]. *Acrotholus audeti*, *Amtocephale gobiensis*, *Psittacosaurus mongoliensis*, *Sinocephale bexelli*, *Sphaerotholus edmontonensis, Tylocephale gilmorei, Yinlong downsi* assigned as [?] due to either unknown material or the inapplicability of scoring (no primary node row present).

A2.2 Character list used for phylogenetic analysis

1. Posterior sacral rib length: short and subrectangular (0); strap-shaped and elongate (1)

2. Preacetabular process, shape of distal end: tapered and subvertically oriented (0); dorsoventrally flattened and expanded distally (1).

3. Humeral length: more (0), or less than (1); 50% of femoral length

4. Humeral shaft form: straight (0); bowed (1); rudimentary (1).

5. Deltopectoral crest development: strong (0); rudimentary (1).

6. Zygapophyseal articulations, form: flat (0); grooved (1)

7. Ossified caudal myorhabdoi: absent (0); present (1)

8. Sternal shape: plate-like (0); shafted (1).

9. Iliac blade, lateral deflection of preacetabular process: weak (0); marked (1)

10. Iliac blade, position of medial tab: absent (0); above acetabulum (1); on postacetabular process (2).

11. Postacetabular process of ilium: elongate and subrectangular (0); deep and downturned distally, with an arcuate dorsal margin (1)

12. Ischial pubic peduncle, shape: dorsoventrally (0), or transversely (1); flattened

13. Pubic body: substantial (0); reduced, nearly excluded from acetabulum (1).

14. Frontal and parietal thickness: thin (0); thick (1).

15. Arched premaxilla-maxilla diastema: absent (0); present (1).

16. Postorbital-squamosal bar, form: strap-shaped with a narrow dorsal margin (0); broad, flattened (1)

17. Squamosal exposure on occiput: restricted (0); broad (1).

18. Posterior supraorbital: absent (0), present, participates with palpebral in excluding the frontal from the orbital rim (1)

19. Postorbital-jugal bar, position of descending process of postorbital: extends to the ventral margin of the orbit (0); terminates above the ventral margin of the orbit, interdigitate postorbital-jugal contact (1)

20. Parietal septum, form: narrow and smooth (0); broad and rugose, has dorsal ornamentation (1).

21. Infratemporal fenestra size: larger than orbit, lower temporal bar long (0); smaller than orbit, lower temporal bar greatly shortened, jugal and quadrate in close proximity or have a small contact (1).

22. Pterygoquadrate rami, posterior projection of ventral margin: weak, jaw joint at the approximate level of occlusal surface (0); pronounced, jaw joint below occlusal surface (1)

23. Prootic-basisphenoid plate: absent (0); present (1).

24. Quadrate, posterior ramus in lateral view: subvertical or gently curved dorsally (0); sinuous, quadrate strongly inclined dorsally, posterior ramus embayed (1).

25. Main bilateral depressions for the insertion area for the atlanto-occipital capsular membrane/ligament: absent or indistinct (0); positioned lateral to the foramen magnum (1); positioned dorsal to the foramen magnum (2)

26. Supratemporal fenestra if cranial frontoparietal dome formed: open (0); closed (1).

27. Roof of temporal chamber as manifest on parietal in lateral view: absent (0); anterior angle < 22 degrees (ventral landmarks for H:N/N and H:Pso/Po) (1); anterior angle > 26 degrees (2).

28. Grooves in dome on frontal: absent (0); present (1).

29. Frontal nasal contact relative to the length of the frontal-posterior supraorbital contact: tall (0), short (1)

30. Frontal-palpebral contact: absent (0) restricted (1) broad (2)

31. Dorsal margins of postorbital and posterior supraorbital sutural surfaces on dome: postorbital and supraorbital II do not form part of a dome (0); dorsally arched such that there is a distinct diastema between the two (1); both are straight and continuous, diastema absent (2).

32. Doming of the skull roof: Initiates overtop of the frontals (0); initiates overtop of the parietals only (1).

33. Parietosquamosal bar in caudal view (viewed perpendicular to shelf): horizontal or slopes at a shallow ventrolateral angle (0); slopes at a steep ventrolateral angle (1).

34. Parietosquamosal bar beneath the primary node row: absent (0); maintains approximately the same depth or slightly deepens laterally (1); shallows laterally (2).

35. Exposure of posteromedian (intersquamosal) process of the parietal between squamosals: posterolateral wings well developed (0); broad (1); narrowed (2); obliterated, intersquamosal contact (3).

36. Primary parietosquamosal node row: absent (0), present (1)

37. Number of nodes in the primary parietosquamosal node row: 5 or less (0) 6 or more (1).

38. Irregular tuberculate ornamentation on posterior surface of squamosal below the primary node row: absent (0); present (1).

39. A coalescing node with constituents on the parietal and squamosal (i.e., a parietosquamosal node): absent (0); present (1).

40. Most medial nodes in primary parietosquamosal node row, enlarged relative to all other nodes: absent (0); present (1).

41. Enlarged nodes on the posterior surface of the squamosal: absent (0), present, ventral to the primary squamosal node row (1)

42. Arrangement of nodes ventral to the primary squamosal node row: single corner node (0); multiple nodes in a row (1).

43. Nodes posterior to the nares: absent (0); present (1)

44. Postorbital node row: absent (0); present (1).

45. Posterolateral edge of skull formed by squamosal and postorbital in dorsal view: straight (0); convex (1).

46. enlarged nodes on along the dorsal posterior surface of the squamosal: absent (0), present, dorsal to a primary squamosal node row (1)

A2.3 Character-taxon matrix used for phylogenetic analysis

Psittacosaurus_mongoliensis

00000000000000000000000000??00?0000?0??0?0000

Yinlong_downsi

000?100?0000?001001000?0?00??00?0000?0??0?0100

Wannanosaurus_yansiensis

??110????????1?101101???????????0??1?0?????100

Goyocephale_lattimorei

11111111110??1111111??1?1????1??01110/1101111111

Homalocephale_calathocercos

11???111121011?1111111111??????01110111111?110

Tylocephale-gilmorei

?????????????1?11111111??21????1?0121010010?10?

Prenocephale_prenes

11??111?121011111111111121201111012100001101110

Foraminacephale_brevis

?????????????1?111?1?????1111211011/21101010?010

Colepiocephale_lambei

?????????????1?111?1?????0210/1210?1?11???11???1

Stegoceras_validum

?11111110201110111111111110/1110210011/2/31110/110?0100

Pachycephalosaurus_wyomingensis

?????11??????111111111?1212011210?2/310000101101

Alaskacephale_gongloffi

??????????????1?11111?????1??????01?100?1?????1

Sphaerotholus_goodwini

??????????????1?11111??1?211012201221000010?110

Sphaerotholus_buchholtzae

??????????????1?111?1?????12001211211001011?110

Sphaerotholus_edmontonensis

??????????????1??1????????1200221??11??1???????

Acrotholus_audeti

??????????????1?111?1?????1200210??2?4431??????

Amtocephale_gobiensis

??????????????1???1?1?????11???11??1???????????

Sinocephale_bexelli

??????????????1???1?????1?????0??1???????????

A2.4 Allometric relationship of W:Po/stf/Sq (y) to W:F/P (x) amongst pachycephalosaurids.

Taxa	n	r	Slope	ci	Intercept	ci	p	Allometry
Colepiocephale lambei	12	0.68	0.98	0.49 –1.39	-0.13	-0.93 – 1.37	0.016	Isometric
Stegoceras validum	35	0.96	0.81	0.70 – 0.89	0.22	0.07 – 0.40	9.73E-20	-
Foraminacephale brevis	25	0.97	1.15	1.05 – 1.25	-0.29	-0.45 – -0.13	1.75E-16	+
Prenocephale prenes	4	0.99	1.33	1.15 – 1.68	-0.71	-1.39 – -0.32	0.0034	+
Sphaerotholus buchholtzae	8	0.99	1.24	1.01 – 1.34	-0.52	-0.70 – -0.08	4.77E-6	+
Colepiocephale + Stegoceras	47	0.94	0.79	0.69 – 0.87	0.24	0.1 – 0.42	4.13E-22	-
Foraminacephale + Prenocephale + Sphaerotholus buchholtzae	37	0.98	1.08	1.03 – 1.15	-0.17	-0.31 – -0.10	2.87E-28	+
Total	84	0.91	0.96	0.86 – 1.07	-0.02	-0.22 – 0.14	1.01E-33	Isometric

Appendix 3

A3.1 t-test results of the difference in average PC 4 (non-transformed PCA) scores between pathological and non-pathological frontoparietal specimens. Performed on a sample of *Colepiocephale lambei*, *Pachycephalosaurus wyomingensis*, "*Sphaerotholus*" *buchholtzae*, and *Stegoceras validum*.

	n	Average PC 4 scores	Range	Variance
Non-Pathological	29	-3.23	-17.34 – 12.25	50.19
Pathological	9	5.33	-3.55 – 19.03	71.33
		t = 3.03	p = **0.018**	